Title

Ultrasound and Fungi Mediated Degradation of Model Emerging Contaminants: Per- and Polyfluoroalkyl Substances & Nitrotriazolone

Author

Kalra, Shashank Singh

Publication Date

2021

Peer reviewed|Thesis/dissertation

UNIVERSITY OF CALIFORNIA

Los Angeles

Ultrasound and Fungi Mediated Degradation of Model Emerging Contaminants: Per- and Polyfluoroalkyl Substances & Nitrotriazolone

A dissertation submitted in partial satisfaction of the

requirements for the degree Doctor of Philosophy

in Civil Engineering

by

Shashank Singh Kalra

2021

ABSTRACT OF THE DISSERTATION

Ultrasound and Fungi Mediated Remediation of Model Emerging Contaminants: Per- and Polyfluoroalkyl Substances & Nitrotriazolone

by

Shashank Singh Kalra

Doctor of Philosophy in Civil Engineering

University of California, Los Angeles, 2021

Professor Shaily Mahendra, Chair

Water resources are increasingly being impacted by chemicals of emerging concern like per- and polyfluoroalkyl substances (PFASs) and nitrotriazolone (NTO). PFASs can be found in virtually all consumer and industrial applications that require non-stick or fire-resistant properties. Use of aqueous film-forming foams (AFFF) containing PFASs at the fire training sites and munition constituents like NTO at the munition testing ranges can also introduce these chemicals into the environment. Munition constituents and PFASs are also expected to co-occur on military training sites due to the use of AFFF for extinguishing fires caused by munitions use and firefighting training. Physicochemical treatment strategies may be needed for quick degradation

of more recalcitrant chemicals, like PFASs, while biological treatment strategies, being less cost- and energy-intensive, may be more suited for the treatment of large dilute plumes of groundwater and soil at impacted sites. Nevertheless, there is a critical need to develop effective biological as well as abiotic technologies for the degradation of these contaminant classes in various environmental settings. This research investigated the application of ultrasound for the destruction of PFASs as an example of abiotic treatment technology whereas ligninolytic fungi and fungal enzymes were considered representative agents for biodegradation of NTO.

Firstly, a comprehensive review of the treatment of per- and polyfluoroalkyl substances (PFASs) by current wastewater treatment plants was conducted by estimating their detection in treated effluents and surface runoffs throughout the world with respect to water recycling and reuse. This work also discussed the advantages of various destructive technologies for the treatment of PFASs as the current treatment plants were found to be ineffective in PFAS removal. The sorption of PFASs was found to be the determining factor of their fate and transport in the natural environment as well as wastewater treatment plants. A review of current analytical methods for the detection of PFAS along with PFAS toxicity studies was also presented.

Secondly, the treatment of PFASs by high-frequency ultrasound using a custom-built bench-scale reactor was investigated in various matrices and mixtures, including aqueous film-forming foams (AFFF), Investigation derived waste (IDW), and groundwater. Important parameters for designing and operating an ultrasonic reactor for the degradation of PFASs were discussed. The study revealed that salts and surfactants affect the air-water partitioning coefficients of PFASs and their availability at the ultrasonic cavities, thereby affecting the degradation rates. Near-stoichiometric defluorination of hexafluoropropylene oxide dimer acid (HFPO-DA or GenX) and 6:2 fluorotelomer sulfonamidoalkyl betaine (6:2 FTAB) by ultrasound was demonstrated in

laboratory studies. The degradation of PFASs was found to generally follow pseudo-first-order kinetics with degradation rates of sulfonates and short-chain PFASs being lower than those of carboxylates and long-chain PFASs in deionized (DI) water. However, the rates were 30% to 60% higher in groundwater with low total dissolved solids (TDS) than in deionized water, while the rates were generally repressed in the high TDS groundwater. 33 PFASs were degraded by ultrasound in AFFF spiked deionized water and the degradation rates of sulfonates were 40% to 60% higher compared to the 24Mix spiked DI water. The treatment of concentrated, high-TDS IDW resulted in significant mineralization of 41 PFASs, consuming 3 $kWh.g^{-1}$ - 76 $kWh.g^{-1}$. Biological-sonolysis and electrochemical-sonolysis treatment trains are also discussed.

Thirdly, the learnings of the lab-scale study on the destruction of PFASs by ultrasound were leveraged for designing a field-scale reactor and testing it for the treatment of AFFF impacted groundwater. The ultrasonic treatment of high salinity groundwater demonstrated successful degradation of 15 PFASs (>90%) and 11 PFAS precursors, with 11 PFASs and 7 TOPs degraded to < 70 $ng.L^{-1}$. No disinfection byproducts or short-chain intermediates were detected during 8 h ultrasonic treatment in all six tested conditions. The energy consumed during 8 h of sonication was 28.01 ± 0.47 kWh. The E_{EO} estimated was 599.51 ± 52.54 $kWh.m^{-3}.order^{-1}$, 797.25 ± 42.16 $kWh.m^{-3}.order^{-1}$, and 699.43 ± 3.30 $kWh.m^{-3}.order^{-1}$ for the treatment of 54 L, 33 L , and 22 L groundwater, respectively.

Fourthly, packaging of *Trametes versicolor* derived laccase enzyme in vault nanoparticles was performed to investigate the applicability of vault-packaged laccase in bioremediation. Three isozymes were expressed by *T. versicolor* in the Tisma medium out of the five identified isozymes. The activity of the packaged enzyme was retained by using a long Glycine-Serine linker between laccase and INT peptide, along with the addition of 500 µM $CuCl_2$ in the *Spodoptera frugiperda*

(Sf9) insect cell culture expressing the fusion protein. The vault-packaged enzyme (VMLDGI) successfully catalyzed the transformation of 2,2'-azino-bis(3-ethylbenzothiazoline-6-sulfonic acid (ABTS), guaiacol, catechol, 1-naphthol, and 2,6- dichlorohydroquinone. VMLDGI also removed 60% NTO at 5 $U.L^{-1}$ laccase activity in presence of 1-Hydroxybenzotriazole (HBT). In contrast, the degradation of NTO by unpackaged laccase at the same activity was insignificant.

Finally, biotransformation of NTO by ligninolytic fungi, *T. versicolor* and *Phanerochaete chrysosporium*, and their extracellularly secreted enzymes, laccase and manganese peroxidase (MnP), was investigated with implications on stormwater biofilter design. Both fungi demonstrated at least 85% removal of NTO within 96 h in batch reactors. About 40% NTO removal by *P. chrysosporium* was due to biosorption while *T. versicolor* demonstrated no biosorption of NTO. MnP demonstrated no removal of NTO while the laccase + HBT system was able to degrade 90% NTO in 48 h. This implies that only a subset of environmental fungi and their enzymes are capable of biodegrading munition constituents such as NTO.

This research will be important for further developing the ultrasonic treatment technology for industrial applicability in the treatment of various chemicals, including PFASs. This work is also valuable for further developing the technology of ligninolytic fungi-mediated biodegradation of munition constituents and other emerging environmental contaminants.

The dissertation of Shashank Singh Kalra is approved.

Sanjay K. Mohanty

Jennifer Ayla Jay

David Jassby

Shaily Mahendra, Committee Chair

University of California, Los Angeles

2021

ਪਵਣੁ ਗੁਰੂ ਪਾਣੀ ਪਿਤਾ ਮਾਤਾ ਧਰਤਿ ਮਹਤੁ ||

Air is the Guru, Water the Father, and the Earth is the Great Mother.

Table of Contents

List of Figures

based on the 16 identified PFAS species (☆). The experiments were conducted for 240 minutes at 10 °C in Argon saturated environment. The rates were calculated for the first 120 min using the initial rate method. **a.** Sonication of IDW in a 700 kHz - 1040 W closed system (Pd = 1040 $W.L^{-1}$) and 700 kHz - 250 W open system (P_d = 1250 $W.L^{-1}$). The solid black line represents the kinetic model fitting for the experimental data (solid markers) in a 700 kHz - 1040 W closed system (P_d = 1040 $W.L^{-1}$) while the dotted black line represents the kinetic model fitting for the experimental data (empty markers) in a 700 kHz - 250 W open system (P_d = 1250 $W.L^{-1}$). The starting concentration of all PFASs in the IDW mixture is reported in parentheses. Degradation of more PFAS species is reported in Figure A 7. **b.** Defluorination and removal of PFAS moles during sonication of IDW. ■ - Moles of fluoride detected in the closed system, ☆ - moles of fluoride release estimated from 16 identified PFASs in the closed system, ▲ - PFAS mass removed in the closed system, △- PFAS mass removed in the open system. The concentrations ($mg.L^{-1}$) of fluoride, chlorate, and perchlorate are reported in Figure A 6..... 61

Figure 3.3: Destruction of PFASs in AFFF spiked deionized water. The rates of removal for sulfonates in AFFF were significantly higher than those observed for a 24 mix of PFASs; vice versa for carboxylates. The highest rates of short-chained PFAS degradation were observed for the treatment of 24Mix in the low TDS groundwater. All experiments were performed in de-ionized water using a 700 kHz - 250 W open system (P_d = 1250 $W.L^{-1}$) for 240 minutes at 10 °C in Argon saturated environment. The rates were calculated for the first 120 min using the initial rate method. **a.** Pseudo-first-order removal of PFAS in AFFF sample (1:12500 dilution). The starting concentrations of PFASs before ultrasound irradiation are shown in parentheses. The solid black line represents the first-order kinetic model fitting for the experimental data (empty markers). The degradation of more PFAS species is reported in Figure A 8. **b.** Comparison of pseudo-first-order

List of Tables

Acknowledgments

First, I would like to express my heartfelt gratitude and sincerest appreciation to my advisor and committee chair, Professor Shaily Mahendra. She has always remained caring and generous towards all her students and strived to ensure their holistic wellbeing, along with the commitment to producing good science. Her mentorship has been indispensable to me and has allowed me to complete all endeavors during my doctoral studies at UCLA. Professor Mahendra has provided many resources and opportunities, including proposal writing, manuscript peer review, conference attendance, and research collaborations, and supported my professional development. Her invaluable support has allowed me to develop as a scholar, an engineer, a mentor, a teacher, a researcher, and an overall better individual. I promise to take these learnings forward and sincerely believe that they will keep pushing me to evolve and progress. She has remained steadfast in the face of challenges and persevered in doing everything possible to elevate her students' scholarly spirit and professionalism. My time as a Ph.D. student at UCLA would not have been nearly as successful without her continued support and guidance.

I would like to thank my committee members, Professor Sanjay K. Mohanty, Professor David Jassby, and Professor Jennifer Ayla Jay, for providing valuable insights, resources, and guidance towards my research and professional development.

I would like to thank Professor Jens Blotevogel from the Colorado State University, Fort Collins, and his colleagues Dr. Nasim Pica, Dr. Andrea Hanson, Professor Gregory Dooley, Dr. Brian Cranmer for conducting the analytical investigation of per- and polyfluoroalkyl substances

for the work featured in Chapters 3-5 of this dissertation. I would also like to give a special thanks to Professor Jens Blotevogel for all the guidance, training, and advice throughout this journey. I learned a lot from him about PFAS analysis and a good chunk of the work presented in this dissertation would not have been possible without his collaboration and dedication to conducting good science.

I would also like to thank Professor Daniel L. McCurry from the University of Southern California, Los Angeles, and his students for helping me perform the analytical investigation of nitrotriazolone for the work featured in Chapters 6 of this dissertation.

I would like to thank Prof. Leonard H. Rome and Dr. Valarie Kickhoefer, and Hedi Roseboro, for letting me work on vaults in the Rome lab, providing guidance, and training me for different experimental procedures and equipment handling. The work presented in this dissertation would not have been possible without their collaboration.

I would like to thank Drs. David Adamson, Stephen Richardson, Blossom Nwedo Nzeribe and Poonam Kulkarni of GSI Environmental Inc., Sharyl Maraviov from PCT systems Inc., and Drs. Jovan Popovic, Anthony Danko, John J. Kornuc, and Arun R. Gavaskar of the US Navy for providing me the opportunity and guidance to work on the research included in Chapters 3 and 4 of this dissertation.

I would like to especially thank my wife, Anjali G. Lothe, who has been a constant source of moral and emotional support during this journey and has helped me with lab work, experimental design, professional development, and overall learning. I would like to thank all the undergraduate students who have assisted in my research over the years and contributed to the laboratory work or data analysis at various stages including Kshitija Shah, Kelly Hollman, and Allison Bell.

Additionally, I would like to thank Dr. Phillip Gedalanga, Alexandra Polasko, Dr. Nicholas Wade Johnson, Dr. Yu Miao, who provided invaluable time, discussion, and insights for addressing research challenges as they emerged. I would also like to extend my deepest gratitude to the members of Mahendra Lab, Mohanty Lab, Jay Lab, and Jassby Lab for offering their invaluable time and support at various stages of this dissertation.

I would like to thank the staff of the Department of Civil and Environmental Engineering who have helped me with all the crucial administrative tasks necessary for conducting research at UCLA as a graduate student: Jesse Dieker, Dr. Vanessa Thulsiraj, Stacey Tran Fong, Mimi Baik, Diana de los Santos, Reba Glover, Dr. Eric Ahlberg, Dr. Ben Rossi, Helen Weary, Dylan Giron, and Paula Columbia.

This research was funded by contracts from the United States Naval Facilities Engineering and Expeditionary Warfare Center (NAVFAC EXWC) [N3943018C2076], Strategic Environmental Research and Development Program [ER-2422 and ER-2718], Dow Chemical Company [244633], DuPont/Corteva Remediation Group [MA-03653-13], and City of Los Angeles Department of Water and Power [20204613]. Support from the National Science Foundation CAREER award [1255021], the 2015 Henry Samueli fellowship and, the 2017 Paul L. Busch award to Dr. Mahendra are also acknowledged. We thank Dr. Paul Hatzinger of APTIM Corp. for providing the AFFF sample and Dr. Jovan Popovic for the IDW sample used in this study.

Finally, I would like to thank my parents, Narendra and Sukhvinder, my brother Harshvardhan, and my wife, Anjali G. Lothe, for the endless love, faith, and confidence in me.

Their support has always motivated me to extend my limits and take on the seemingly daunting challenges head-on.

Vita

Education

M.S., Civil & Environmental Engineering, University of California, Los Angeles	2018
Post Graduate Diploma, Urban Environmental Management and Law, Nation Law University, New Delhi	2013
B. Tech., Environmental Engineering, Indian Institute of Technology (Indian School of Mines), Dhanbad	2012

Professional Experience

Environmental Engineer, Jindal Steel, and Power Limited July 2012 - Sep. 2015

Publications

1. Kalra, S.; Cranmer, B.; Dooley, G.; Hanson, A. J.; Maraviov, S.; Mohanty, S.; Blotevogel, J.; Mahendra, S.; (2021). Sonolytic Destruction of Per- and Polyfluoroalkyl Substances in Mixtures, Groundwater, and Investigation Derived Waste. In Review (Chemical Engineering Journal).
2. Kalra, S.; Gao, Y.; Lothe, A., G; Shah, K.; Bell, A.; Kickhoefer, V., A.; Rome, L., H.; Mahendra, S.; (2021). Synthesis of Vault Packaged Laccase and Detection of Laccase Isozymes from *Trametes versicolor*. In Preparation.
3. Kalra, S.; Valenca, R.; Lothe, A.; McCurry, D.; Mahendra, S.; Mohanty, S.; (2021). Fungal-mediated degradation of Nitrotriazolone. In Preparation.
4. Kalra, S.; Ramos, P.; Polasko, A,; Tsai K.; Jay J.; Mahendra, S.; (2021). PFASs in Treatment Plant Effluents and Recycled Water: A Review (Environmental Science and Technology – Water) – In Preparation
5. Kulkarni, P.; Nzeribe, B.; Adamson, D.; Richardson, S.; Kalra, S.; Mahendra, S.; Maraviov, S.; Popovic, J.; Kornuc. J.; (2021). Field Demonstration of Pilot-Scale Treatment System Using Novel Sorbents and Sonolysis Reactor for PFAS Removal. In Preparation.
6. Ramos, P.; Kalra, S.; Johnson, N.; Khor, C.; Borthakur, A.; Cranmer, B.; Dooley, G.; Mohanty, S.; Jassby, D.; Blotevogel, J.; Mahendra, S.; (2021). Enhanced Removal of Anionic Per- and Polyfluoroalkyl Substances in Complex Matrices by Optimized polyDADMAC-Stabilized Granular Activated Carbon. (Chemical Engineering Journal) – In Preparation

7. Lothe, A.G.; Kalra, S..; Wang, M.; Mack, E.E.; Walecka-Hutchison, C.; Kickhoefer, V.A.; Rome, L.H.; Mahendra, S.; (2020). Vault Packaged Enzyme-Mediated Degradation of Amino-Aromatic Energetic Compounds. Chemosphere. 242, 125117.

Presentations

1. Kalra, S.; Cranmer, B.; Dooley, G.; Hanson, A. J.; Maraviov, S.; Mohanty, S.; Blotevogel, J.; Mahendra, S.; (2021). Destruction of various Per- and Polyfluoroalkyl substances mixtures in groundwater by ultrasound. American Chemical Society 260th National Meeting & Exposition. Virtual.
2. Kalra, S.; Lothe A.; Wang M.; Chen Y; Kickhoefer V; Rome L; Allard P; Mahendra S.; (2019). Vault Packaged Ligninolytic Enzymes as Nanoscale Environmental Bioremediation Agents. American Chemical Society 257th National Meeting & Exposition. Orlando, FL.
3. Ramos, P.; Kalra, S.; Johnson, N.; Khor, C.; Borthakur, A.; Cranmer, B.; Dooley, G.; Mohanty, S.; Jassby, D.; Blotevogel, J.; Mahendra, S.; (2021). Enhanced Removal of Anionic Per- and Polyfluoroalkyl Substances in Complex Matrices by Optimized polyDADMAC-Stabilized Granular Activated Carbon. American Chemical Society 260th National Meeting & Exposition. Virtual.
4. Blotevogel J.; Pica, N.; Young, R.; Kalra, S.; Miao, Y; Chen, H.; McKenna, A.M.; Borch, T.; Mahendra, S.; (2019). Bioelectrochemical oxidation of per- and polyfluoroalkyl substances and non-fluorinated co-contaminants in aqueous film-forming foam. American Chemical Society 257th National Meeting & Exposition. Orlando, FL.
5. Kalra, S.; Valenca, R.; Lothe, A.; Mahendra, S.; Mohanty, S.; (2018). Fungi-augmented biofilters for the removal of energetic compounds from stormwater runoff and groundwater. American Chemical Society 256th National Meeting & Exposition. Washington, DC.
6. Lothe, A. G.; Kalra, S.; Sinha, A.; (2015) “A comparative study on biodiesel production from waste cooking oil”, Int. Conf. on Recent Advances in Civil Engg., Arch., Env. Engg for Sustainable Development (CEAESD) vol 9.
7. Kalra, S.; Mohan, S.; Sinha, A.; and Singh, G.; (2011). Advanced oxidation processes for treatment of textile and dye wastewater: A review. In 2nd International conference on environmental science and development (Vol. 4, pp. 271-5). IACSIT Press Singapore.
8. Kalra, S.; Mohan, S.; Paul, B.; (2010). Methane Hydrate Development in India – A Challenge. Proceedings of National Conference on Green Chemistry (NCGC), pg. 233-237.
9. Mohan S., Kalra, S.; Sinha, A.; and Singh, G.; (2010). Prospects of CBM and its Potential in India. Proceedings of National Conference on Green Chemistry (NCGC), pg. 161-164.

Chapter 1

Introduction and Objectives

1.1 Objective and Scope

The ever-growing requirement of manufacturing better materials also adds to the list of chemicals of emerging concern. Per- and polyfluoroalkyl substances (PFASs) and nitrotriazolone (NTO) are two such emerging chemicals with a critical need for enhanced treatment alternatives. PFASs have been manufactured since 1949, but it was not until very recently that adverse health effects associated with PFAS exposure have been studied. They are used in the manufacture of non-stick coatings on virtually all consumer and industrial products required to be water or oil repellent. The surfactant and fire-retardant nature of PFASs also make them ideal for firefighting and fire-resistant coating. Their versatility had led to their detection in environmental matrices, and their inertness also makes them resistant to most treatment technologies. Similarly, NTO was developed as an insensitive alternate to the legacy munitions tending to explode spontaneously. The NTO toxicology has only been studied in recent years, and the evidence for its toxicity is still being gathered. However, the high solubility (12000 $mg.L^{-1}$) of NTO makes it an environmental exposure risk. Fungal and ligninolytic enzyme-mediated biodegradation is being increasingly investigated for the removal of various chemicals of emerging concern due to the ubiquity and synergic role of fungi in the environment. The ligninolytic fungi and enzymes are ideal candidates for the biodegradation of PFASs due to their ability to degrade the toughest biological macromolecules like lignin and cellulose. Packaging and immobilization of enzymes are also increasingly investigated to prevent their deactivation in the reaction and increase their applicability in environmental remediation. However, the inertness of PFASs leads to long treatment times for biodegradation. As a result, quicker degradation alternatives like high-frequency ultrasound, which can mineralize PFASs without producing harmful byproducts, are also being studied. The overall objective of this work was to explore the ultrasonic degradation of

per- and polyfluoroalkyl substances (PFASs) in complex mixtures and real waters along with biodegradation of PFASs and munition constituents using fungi, unmodified ligninolytic enzymes, and vault-packaged ligninolytic enzymes.

Objective 1: To explore and optimize the degradation of per- and polyfluoroalkyl substances (PFASs) in different matrices like groundwater, Aqueous Film Forming Foam (AFFF), and Investigation Derived Wastes (IDW) by high-frequency ultrasound using custom-built lab-scale and field-scale reactors.

Objective 2: To engineer and package laccase derived from *Trametes versicolor* into vault nanoparticles and evaluate degradation of NTO by vault-packaged laccase.

Objective 3: To evaluate the ability of wood-rotting fungi *Trametes versicolor* or *Phanerochaete chrysosporium* and their ligninolytic enzymes like laccase and manganese peroxidase, to degrade munition analogs like amino-nitrotoluene (ANT) and nitrotriazolone (NTO).

1.2 Dissertation Overview

This dissertation is organized into seven chapters. A summary and research objectives of the current dissertation are outlined in Chapter 1. Chapter 2 contains a review of current literature on per- and polyfluoroalkyl substances (PFASs) with emphasis on detection in treated wastewater and surface runoff. The toxicological effects of PFASs, destructive treatment technologies for remediation of PFASs, and current analytical methods for PFAS detection are also briefly presented in this chapter. The degradation of various PFASs in various matrices like high and low salinity groundwater, deionized water, diluted AFFF, and concentrated investigation derived waste (IDW) by high-frequency ultrasound in a custom-built lab-scale reactor is described in Chapter 3.

The work presented in Chapter 3 discusses the effect of operational conditions and matrix constituents on the degradation kinetics of PFASs and informs the design of the subsequent field-scale ultrasonic reactor used in Chapter 4. Consequently, Chapter 4 reports the degradation of PFAS by ultrasonic treatment of AFFF impacted groundwater during the field demonstration conducted by GSI Environmental Inc. at a site in California. Chapter 5 describes the detection of several laccase isozymes produced by *Trametes versicolor* in ligninolytic culture conditions and engineering of laccase to produce laccase-peptide fusion enabling the packaging of laccase into vault nanoparticle with prolonged retention of activity. The degradation of NTO by vault-packaged laccase and natural laccase are also compared in Chapter 5. Degradation of munition constituents, like NTO, by wood-rotting fungi *Trametes versicolor* and *Phanerochaete chrysosporium* and their ligninolytic enzymes, manganese peroxidase and laccase, are presented in Chapter 6 with emphasis on stormwater remediation. A summary of the results and significance to the field of environmental science and engineering along with suggestions for future research directions is presented in Chapter 7. Supporting information for Chapters 3, 5, and 6 are included in Appendices A, B, and C.

Chapter 2

Per- and polyfluoroalkyl substances (PFASs): Literature Review.

Abstract

Per- and poly-fluoroalkyl substances (PFASs) are a large class of synthetic chemicals used in a variety of industrial processes and consumer goods. The carbon-fluorine chain in PFASs makes them oleophilic and resistant to chemical or biological degradation. PFASs and their potential health effects have more recently been receiving a great deal of state, national, and public attention. This class of more than 9000 chemicals is highly resistant to environmental degradation and persistent in the environment. The current EPA guidelines only address perfluorooctanoic acid (PFOA) and perfluorooctane sulfonic acid (PFOS) which are rapidly being replaced in manufacturing by other PFAS. Greater knowledge of levels of these contaminants in unregulated sources is needed to effectively address public health concerns. This study aims to review the levels of PFAS in surface runoff and effluents of water treatment plants around the world in relation to the current PFAS standards and factors affecting their fate and transport in the environment. The advantages and disadvantages of various destructive treatment technologies for the removal of PFASs are also discussed along with the various analytical methods for the detection of PFASs and toxicity of PFASs.

2.1 Introduction

Per- and polyfluoroalkyl substances (PFASs) play a central role in the modern world, owing to their properties like high thermal stability, lubrication and friction resistance, surfactant, and insulating behavior. PFASs are ubiquitously used as flame retardants in AFFF, coatings on paper for food packaging, coatings on carpets, furniture, outdoor clothing, leather impregnation, constituents in polish, ink, paint, varnish, etc., nonstick-coatings on metals and plastic, coatings on the photographic printing plate, films and paper, manufacturing of semiconductors, constituents of biocides and pesticides, as surfactants in oil and mining industry, (co)monomer for polymerization, etc. [1, 2]. Due to their detection in virtually all environmental matrices, PFASs are rapidly gaining attention in the field of environmental remediation. PFAS compounds include 5000 to 10000 different chemicals [3], by recent estimates, out of which 4700 chemicals are in use globally [4, 5]. Polytetrafluoroethylene (PTFE) was the first PFAS invented by DuPont in 1938 and was synthesized by compression of tetrafluoroethylene; a gaseous coolant, and is hailed as the most slippery material [5, 6]. PTFE was first sold commercially in 1946, followed by 3M company's commercial production of PFASs in 1949 [6-8]. The PFAS based Aqueous Film Forming Foam (AFFF) was developed in 1964 by the United States Navy and the 3M company to fight class B fuel fires. Since 1967, it has been mandatory to carry AFFF aboard naval ships [9, 10]. Until 2000, the manufacturing of PFASs was done using the electrochemical fluorination (ECF) technique. However, since then, telomerization (TM) is the dominant production technique, while the ECF process is being used to make smaller chain PFASs. The ECF process involves electrolysis of alkyl sulfonyl fluoride or alkyl carbonyl fluoride in hydrofluoric acid, resulting in free radical generation leading to the replacement of hydrogen atoms by fluorine atoms in the carbon chain. In the TM technique, perfluoroalkyl iodide (termed as telogen) and

tetrafluoroethylene (termed as taxogen) are used as reactants to produce a mixture of longer perfluoroalkyl iodides (termed as telomer A). Telomer A mixture is then reacted with ethylene resulting in the formation of fluorotelomer iodide (termed as telomer B). Telomer A and Telomer B are used as reactants to synthesize other PFASs. The ECF process produces a mix of branched and linear chain PFASs while the TM technique produces linear compounds with even chain length [2, 11-13].

Recycled water offers numerous and far-reaching benefits such as reducing water pollution, increasing water supply, minimizing stress on ecosystems, mitigating seawater intrusion, and decreasing water transportation costs. The Los Angeles Sustainable City Plan aims to source 70% of the water locally by 2035 [14]. Recycled water will be a significant share of this locally sourced water by implementing indirect potable reuse, i.e., purifying recycled water and conveying it into the groundwater basin for future use as drinking water. USEPA has also launched a nationwide Water Reuse Action Plan in February 2020, which details 37 actions for various water partners to support water reuse [15]. The LA sustainable city plan also aims to capture 150,000 acre.ft/yr stormwater by 2035 [14]. Recent studies have reported that PFASs have a high tendency to be sequestered in the vadose zone [16-20]. Inevitably, the stormwater coming from the PFAS-impacted soils will contain the PFASs, and as a result, end up in the water reuse reservoirs [21]. The emerging reports of the inadequacy of traditional water treatment plants in removing PFASs [22] and the risk posed by PFASs to public health may lead to the regulation of PFASs present in wastewater treatment plant effluent. With current advisories only focusing on a few specific PFASs, industries could adapt by switching to novel PFASs, which may be harmful to public health. Inarguably, a detailed study of PFASs present in the water reuse sources is necessary to inform the safe application of recycled water.

The water agencies will need to make informed decisions, from both economic and public health perspectives, to address emerging concerns of PFASs in drinking water. Consequently, it is crucial to identify PFASs of interest, especially the PFAS precursors, short-chain PFASs, and the species not yet regulated by the current monitoring advisories. The objective of this work is to review the levels PFASs reported in wastewater treatment plant effluents and surface water runoff. Furthermore, the interaction of PFASs with current treatment processes, current PFAS regulations/advisories, destructive PFAS treatment technologies, and precise PFAS detection methodologies will be discussed. The toxicological, ecological, and health effects of PFASs and their treatment byproducts must be evaluated to ensure safe water reuse.

2.2 Toxicology of PFAS

The steadily growing body of evidence on PFAS toxicity and bioaccumulation has shown that the PFASs are terminally stable in living organisms. They can persist for long intervals in marine life, drinking water supplies, surface waters, and groundwaters. As a result, the ingestion of PFASs is the principal pathway for human exposure to PFAS [9, 23, 24]. Recently, among the five tested marine endpoints, higher toxicity was reported for PFOS, followed by PFOA [25]. Similarly, a study conducted in Brazil on the bioaccumulation of PFASs in tropical mangrove food web reported bioaccumulation of PFNA, PFOS, and EtFOSA in the food web [26]. A detailed review of studies on human health effects of PFASs has been published by Sunderland et al. [23], and the ecotoxicology of PFASs was recently reviewed by Ankely et al. [27], Conder et al. [28], and Leeson et al. [29]. The Interstate Technology & Regulatory Council (ITRC) has also published a detailed review of PFAS toxicity and bioaccumulation in humans and animals [9]. In summary, studies have shown a positive correlation with PFASs causing endocrine effects, cardiovascular

effects, immunotoxicity, kidney and testicular cancer at high exposure concentrations, and dyslipidemia (elevated fat levels in the blood). The human health effects of PFASs have been primarily studied for legacy PFASs like PFOA and PFOS. Moreover, only PFOA, but not PFOS, has been classified as a probable human carcinogen by The International Agency for Research on Cancer (IARC). USEPA reports PFOS, PFOA, and HFPO-DA to have suggestive evidence of human carcinogenicity. The living organisms that are acutely exposed to the PFAS-impacted water demonstrate severe bioaccumulation and toxicity effects compared to the chronically exposed organisms. Shorter chain PFASs ($C < 8$) are reported to be more persistent in plants, while longer chain PFASs ($C > 8$) are more persistent in animal species [9]. There is a critical need for assessing the effects of target/non-target novel PFASs and mixtures of PFASs however, the hazardous nature of tested PFASs has already been established. Recently, a notice of intent was issued by the California Office of Environmental Health Hazard Assessment to include PFOA as a known carcinogen under the Safe Drinking Water and Toxic Enforcement Act of 1986 [30].

2.3 PFAS in Wastewater and Surface Runoff

PFASs are present in the effluents of wastewater treatment plants and stormwater runoffs throughout the world, including the USA, Australia, Europe, and Japan [21, 31-34]. The analysis of hydrologic units in the USA revealed a correlation between the increase in PFOA and PFOS concentration with an increase in the abundance of wastewater treatment plants [35]. PFASs have been detected in the effluents of many wastewater treatment plants in the USA. The samples collected in California from 8 different wastewater treatment plants in 2009 and 2014 had significant PFAS concentrations in all samples. In January 2020, the Vermont Department of Environmental Conservation published the report on PFASs detected in the influent, effluent, and

sludge of the wastewater treatment plants and landfill leachate [36, 37]. The amount of novel PFAS species, including PFAS precursors and short-chain PFASs, has been reported to be higher than the legacy PFASs and longer chain PFASs [36-38]. The treatment plants were found to be inefficient in the removal of PFAS and the reduction in concentration between influent and effluent was attributed to their sorption on the sludge. Successively, The California Water Resource Control Board has issued a statewide order on 9th July 2020 to monitor PFASs in the discharges of public water treatment facilities [37]. The order delineates 42 PFASs to be monitored in the wastewater effluent discharged in surface waters and/or percolation basins, biosolids, and reverse osmosis concentrate/retentate. The Michigan Department of Environment, Great Lakes, and Energy (EGLE) published the findings of the Industrial Pretreatment Program in June 2020 [39]. The report states that the discharge from 57% of the treatment plants which had PFOSs in the influent streams, does not meet the water quality standard. Subsequently, The EGLE plans to update the National Pollutant Discharge Elimination System (NPDES) permits to incorporates effluent limits with schedules for PFASs [40]. Similarly, The Connecticut Department of Public Health and the Department of Energy Environmental Protection have published PFAS Action Plan in November 2019 [41]. One of the objectives of the plan is to evaluate the levels of PFAS in wastewater treatment plants, biosolids, and compost. North Carolina Division of Water Resources has also detected significant PFAS concentrations in the Cape Fear River Basin. Elevated concentrations of PFASs were detected in 25 treatment plants one of which, the Sanford sewage treatment plant was found to have a PFOS influent concentration of 1000 ng/L along with other PFASs detected at low ng/L concentrations [42]. Minnesota Pollution Control Agency also detected PFASs in the influent streams of 28 wastewater treatment plants, in landfills, and groundwater as of 2009 [43]. The PFAS contamination of wastewater treatment plant influent was

attributed to the waste disposal sites and the effluent of the chrome plating industry [44]. Currently, USEPA is working on re-proposing the Fifth Unregulated Contaminant Monitoring Rule (UCMR 5) and reissuing the final regulatory determinations for PFOA and PFOS with an assurance to implement drinking water regulations [45]. The current PFAS Regulatory Standards in the United States of America are listed in Table 2.1 and are also reviewed by Fiedler et al. [46].

Table 2.1: Current regulatory levels of various PFASs in the United States. Combined levels relate to the combined threshold concentration of PFAS species.

Authorities	Concentration ($ng.L^{-1}$)	Compound	Regulation Type
EPA	70	PFOA	Combined Health Advisory
		PFOS	
ATSDR	78	PFOA	Minimal Risk Levels
	52	PFOS	
	517	PFHxA	
	78	PFNA	
Alaska	70	PFOA	Combined Action Level
		PFOS	
Colorado	70	PFOA	Combined Site-specific Standard
		PFOS	
California	5.1	PFOA	Notification Levels
	5.1	PFOS	
Connecticut	70	PFOA	Combined Action Level
		PFOS	
		PFNA	
		PFHxS	
		PFHpA	
Illinois	140000	PFBS	Health Advisory
	140	PFHxS	
	2	PFOA	
	560000	PFHxA	
Maine	400	PFOA	Remedial Action Guidelines
	400	PFOS	
	400000	PFBS	
Massachusetts	20	PFOA	Combined Maximum Contaminant Level
		PFOS	
		PFHxS	
		PFHpA	
		PFDA	
		PFNA	
Michigan	6	PFNA	Maximum Contaminant Level
	8	PFOA	
	370	HFPO-DA	
	420	PFBS	
	51	PFHxS	
	400,000	PFHxA	
	16	PFOS	
New Hampshire	12	PFOA	Maximum Contaminant Level
	15	PFOS	
	18	PFHxS	
	11	PFNA	
New Jersey	13	PFNA	Maximum Contaminant Level
	14	PFOA	
	13	PFOS	

Authorities	Concentration ($ng.L^{-1}$)	Compound	Regulation Type
Texas	560	PFOS	Protective Concentration Levels
	290	PFOA	
	290	PFNA	
	93	PFHxS	
	560	PFHpA	
	34000	PFBS	
	370	PFDA	
	290	PFDoA	
	93	PFHxA	
	290	PFTeA	
	290	PFTrDA	
	290	PFUnA	
	71000	PFBA	
	290	PFDS	
	290	PFOSA	
	93	PFPeA	
Vermont	20	PFOA	Combined Maximum Contaminant Level
		PFOS	
		PFHxS	
		PFHpA	
		PFNA	
Delaware	70	PFOA	Combined Health Advisory
		PFOS	
Montana	70	PFOA	Combined Health Advisory
		PFOS	
Rhode Island	70	PFOA	Combined Health Advisory
		PFOS	
Ohio	21	PFNA	Action Levels
	70	PFOA	
	70	PFOS	
	700	GenX	
	140000	PFBS	
	140	PFHxS	
Minnesota	15	PFOS	Health-Based Values
	35	PFOA	
	47	PFHxS	
	2000	PFBS	
	7000	PFBA	
New York	10	PFOA	Maximum Contaminant Level
	10	PFOS	
North Carolina	140	GenX	Health Goal
Nevada	667	PFOA	Basic Comparison Levels
	667	PFOS	
	667000	PFBS	

Detection of PFASs in drinking water, in the USA and globally [24, 35, 47-50], is evidence that the traditional treatment processes are ineffective in treating PFASs, and as a result, PFASs are also expected to be found in recycled water [21, 24, 48, 51, 52]. The effluent concentrations of PFASs from wastewater treatment plants around the world are reported in Table 2.2 and also reviewed by Phong et al. [50] and Page et al. [21]. In summary, a median of 27 $ng.L^{-1}$ PFOA was detected in wastewater treatment plant (WWTP) effluents around the world [21]. The short-chain PFASs were detected to be at least 50-fold higher than long-chain PFASs. In general, a higher concentration of short-chain PFASs has been observed in the environment, partly due to the increased use of short-chain PFASs as alternatives to the long-chain PFASs [53]. Higher mobility and concentrations observed for short-chain PFASs, in water, wastewater, and soil, are also attributed to their lower sorption and hydrophobicity, as compared to those of longer chain PFASs [50, 53, 54]. In a recent publication, Kibambe et al. report seven out of sixteen screened PFASs detected in the influents and effluents of three wastewater treatment plants in South Africa [55]. The effectiveness of current wastewater treatment technology was also investigated and the removal of PFASs by different unit processes are reported to vary with PFAS type and treatment plant design. For most samples analyzed, the concentration of PFBA, PFHxA PFDA increased or remained steady in the effluent. Most decreases in PFASs concentrations were observed in the aerobic pond for Phola WWTP, 50% decrease in PFPeA, 65% decrease in PFHxA, 63% decrease in PFHxS, 65% decrease in PFOA, and a 35% decrease in PFOS. The nominal decrease was observed in 5 studied PFASs in the activated sludge based Daspoort WWTP except 85% concentration decrease for PFOS in the secondary settling tank. The highest decrease in the PFOS concentration (94%) is reported in the effluent of the activated sludge based Zeekoegat WWTP. The concentration of PFOA, PFHxS, and PFBA in the effluent of Zeekoegat WWTP also

decreased by 63%, 78%, and 45% respectively. The decrease in concentration has been attributed to the adsorption of PFASs to sludge or particulate matter, no evidence of biodegradation was reported. Similar observations are reported in a review of PFAS environmental cycling by Hamid et al. [51]. Up to 520 $ng.L^{-1}$ of cumulative PFAS concentration (21 species) have been reported in the effluents collected from 19 wastewater treatment plants in Australia [34]. Treatment processes around the world are reported to show zero or negative PFAS removal efficiency with short-chain PFASs forming the majority of effluent PFAS mass. The increase in effluent PFAS concentration is attributed to the biological transformation of PFAS precursors to the terminal PFASs like PFOA and PFOS [22]. The PFAS-containing wastewater effluents are implicated as the major source of surface water contamination. An updated PFAS environmental release and exposure pathway is reported in a recent study published by Meegoda et al. [52]. High amounts of PFASs (12 of 25 investigated), including HFPO-DA (0.15 $\mu g.L^{-1}$) and PFBS (8 $\mu g.L^{-1}$), were detected in the treated effluents collected from the electronic fabrication industry. The effluent from these facilities was discharged into a stream or was influent to the public wastewater treatment facilities [56].

The detection of PFASs in stormwater runoff around the world has been reviewed by Page et al. [21]. PFASs were detected in all runoff samples collected from 7 storm events in the USA. The PFAS concentrations were higher in the runoff in comparison to those identified in the WWTP effluents in the Tsurumi River basin, Japan. The 33 runoff samples collected from San Francisco Bay (CA, USA) also demonstrated the presence of 8.6 – 77 $ng.L^{-1}$ PFASs, including PFAS precursors. PFASs have also been detected in runoff samples collected from Tokyo, New York, Albany, Zurich, and Toronto [57]. Similarly, AFFF use and partially treated wastewater, discharged into the Saudi Arabian Red Sea, was responsible for the high concentration of PFASs (< 956 $ng.L^{-1}$) detected in the marine samples, with 6:2 FTS, PFHxS, and PFHxA as the most

abundant [58]. In a recent publication, all samples collected from the fire training site in France were reported to have high concentrations of 50 PFASs investigated by Dauchy et al. [59]. The samples were collected from the drainage of the fire training area, wastewater treatment plant effluents, runoff water, and lagoon water. Specifically, the WWTP is reported to be largely ineffective for PFAS treatment, with some removal of PFSAs observed. However, 6:2FTAB was reported to not biodegrade in WWTP. The PFAS profile for WWTP and the runoff samples were similar, with fluorotelomer alcohols being most abundant, followed by PFSAs and PFCAs. Surface runoff and wastewater were also implicated as major sources of PFAS contamination for surface waters in Jiaozhou Bay, China, with PFOA and PFOS being the majority constituents out of the 14 investigated PFASs. Interestingly, the water samples collected from the surface of the yellow sea had a prominently high concentration of PFUnDA, which was not observed in freshwater samples [60]. A recently published study by Bia et al. also implicates wastewater, snowmelt, and surface runoff for major PFAS pollution in the Las Vegas and Reno watershed of Nevada [61]. The study conducted in Japan reports up to 100 $ng.L^{-1}$ PFASs concentration in the first flush runoff after rainfall [62]. PFASs were also detected in the samples collected from Lakes (< 36 $ng.L^{-1}$), Snow (< 24 $ng.L^{-1}$), Rainwater (< 13.2 $ng.L^{-1}$), Surface runoff (< 15 $ng.L^{-1}$) in rural and urban Albany, New York [63]. Canadian cities have also reported up to 16 $ng.L^{-1}$ PFAS in snowmelt and surface runoff [64].

Table 2.2: Presence of PFASs in WWTP effluents around the world.

Location	Number of WWTPs	Influent Type	National PFAS Standards ($ng.L^{-1}$)	PFASs Detected	Average Concentration in Effluent ($ng.L^{-1}$)	References
New York, USA	6	Domestic,	Combined PFOA	Σ_8 PFASs	83-719	Sinclair and Kannan, 2006
Kentucky, USA	1	Commercial &	and PFOS – 70	Σ_8 PFASs	146.74-206.7	[65]
Georgia, USA	1	Industrial		Σ_8 PFASs	19.4-143.7	Loganathan et al., 2007 [66]
USA	10			Σ_{11} PFASs	22.9-569.5	
Iowa, USA	1			Σ_8 PFASs	43.7-55.9	Schultz et al.,2006 [67]
USA	3	Electronics fabrications		Σ_{25} PFASs	376-623	Boulanger et al., 2005 [68] Jacobs et al., 2021 [56]
European Union	90	Domestic & Industrial		PFNA PFOS PFHpA PFOA PFDA PFHxA PFHxS	35100 62.5 82.9 255 23.9 304 48.6	Loos et al., 2013 [69]
Japan	5	Domestic & Industrial		PFOA PFOS	10-68 42-635	Murakami et al., 2009 [31]
Germany	9	Domestic & Industrial	PFOA, PFOS – 100	PFOA PFOS Σ_{15} PFASs	12.3-77.6 N.D. -82.2 17.46-99.8	Ahrens et al., 2009 [70] Llorca et al., 2012 [71]
Sweden	3	Medical and Industrial	PFOA, PFOS, PFHxA, PFBS, PFBA – 90	ΣPFASs	29.8-77.0	Eriksson et al., 2017 [22]
Denmark	10	Domestic & Industrial	PFOA, PFOS, PFHxA, PFBS, PFBA – 100	Σ_7 PFASs	12.7-809.9	Bossi et al., 2008 [72]
Australia	14	Domestic &	PFOA – 560	Σ_9 PFASs	21-560	Gallen et al., 2018 [33]
	19	Industrial	PFOS – 70	Σ_{21} PFASs	9.3-520	Coggan et al., 2019 [34]
	2			Σ_{11} PFASs	31-142	Nguyen et al., 2019 [73]
China	12	Domestic & Industrial		PFOA PFOS	2.8-160000 1.1-74.8	Chen et al., 2012 [74]
	2			Σ_{14} PFASs	120-170	Han et al., 2020 [60]
	2			Σ_{14} PFASs	1070-1589	Zhang et al., 2015 [75]
China (Taiwan)	3			Σ_{10} PFASs	379.5-18156.5	Lin et al. 2010 [76]
Hong Kong	4	Domestic		Σ_6 PFASs	19.7-67.2	Ma and Shih., 2010 [77]
South Korea	22	Domestic &		Σ_{10} PFASs	N.D.-598.7	Guo et al., 2010 [78]
	15	Industrial		Σ_{13} PFASs	18-270	Kim et al., 2012 [79]
	81			Σ_{13} PFASs	269-561	Kwon et a.,2017 [80]
	25			Σ_{11} PFASs	2.29-1375	Kim et al.,2016 [81]
	77			Σ_{28} PFASs	1040-5180	Kim et al., 2021 [82]
Kenya	6	Hospital, Domestic, & Industrial		Σ_{10} PFASs	29.24-77.1	Chirikona et al., 2015 [83]
Singapore	13	Domestic & Industrial		PFOA PFOS	16-1057 7.3-462	Yu et al., 2009b [84]
Greece	2	Domestic & Industrial		Σ_{18} PFASs	70.47-162.7	Arvaniti et al., 2012 [85]
Canada	4	Domestic Lagoons and Lake	PFOA – 200 PFOS – 600 PFHxA – 200 PFBA – 30000 PFBS – 15000	Σ_5 PFASs	83.5-248	Stroski et al., 2020 [86]
Thailand	2	Industrial		Σ_{10} PFASs	661.8-1143.4	Kunacheva et al., 2011 [87]
France	1	PFAS Manufacturing Fire Fighting Training		Σ_{51} PFASs Σ_{50} PFASs	2381300-7838400 3600000-13000000	Dauchy et al., 2017 [88] Dauchy et al., 2019 [59]
Uganda	1	-		Σ_{26}PFASs	5.6-9.1	Dalahmeh et al., 2018 [89]
Spain	16	Domestic &		Σ_{21} PFASs	195-567	Campo et al., 2014 [90]
	8	Industrial		Σ_5 PFASs	3.5-132	Sanchez-Avila et al., 2010
	3			Σ_{12} PFASs	12.46-601.3	[91] Llorca et al., 2012 [71]
South Africa	3	-		Σ_7 PFASs	35.8-224.4	Kibambe et al., 2020 [55]

2.4 Destructive PFAS Treatment Technologies

Various treatment technologies are being developed for the remediation of PFAS-impacted water. Currently, the widely adopted treatment method for PFASs impacted water is separation using carbon-based sorbents, ion exchange sorbents, mineral-based sorbents, polymers sorbents, sorption on biomaterials [92]. Similar separation-based technologies like using membrane filtration and Surface activation foam fractionation are also being tested for field applications [9]. However, separation-based technologies have the drawback of creating concentrated waste and spent sorbents. Alternate treatment techniques include destructive treatment methodologies like biotransformation, ultrasound, eBeam, plasma, electro-chemical, hydrothermal, photo-catalysis, and activated persulfate. Table 2.3 summarizes the key difference in destructive technologies for the removal of PFAS. Biotransformation can be a cost-effective long-term treatment alternative but the inertness of PFASs make them resistant to biodegradation. The applicability of current biodegradation techniques for PFASs remains elusive. A few lab-scale studies have demonstrated the ability of organisms, including fungi [93-95], bacteria [96-99], and some fungal enzymes [100-103] to biodegrade PFAS precursors, and a few PFASs. Some evidence of biotransformation of PFASs in mixed cultures is also available [104-107]. The photocatalytic and activated persulfate-based treatment of PFASs has been successful for the treatment of carboxylates but ineffective towards sulfonates. These technologies can have high energy demand and long treatment times. Hydrothermal treatment and activated persulfate treatment also require high temperature/pressure, and therefore the energy consumption is also considerably large. Ineffective degradation of short-chain PFSAs and generation of shorter-chain intermediates or byproducts like chlorate/perchlorate is also a drawback of most PFAS destruction technologies including ebeam, electrochemical, and plasma-based treatment except for ultrasonic and hydrothermal treatment methods. Plasma-based

treatment and ultrasonic treatment technologies are ahead in terms of large-scale applicability and have been successfully tested in the field for the treatment of AFFF-impacted groundwater and IDW. Various reviews of PFAS treatment technologies have been published in recent years [108-115].

Table 2.3: Comparison of PFAS Destructive Treatment Technologies. [a]The findings of this dissertation are included.

Type	PFAS Species and Matrices Studied	Field Testing	PFAS Load Reduction	Limitations	Advantage	Removal Mechanism
Biotransformation [93, 94, 96-104, 106, 107, 113, 116-120]	Various PFASs and PFAS precursors tested, Pure culture, mix culture, Fungi, Bacteria, Enzymes, wastewater, landfill leachate-sediment	No	Low	Highly dependent on microorganisms and associated reaction environment, chemical additives needed, long retention times, ineffective for short-chain PFSAs, generation of shorter-chain intermediates, tested for higher concentrations than environmentally relevant.	Low cost and energy requirements, suitable for precursor degradation	Microbes mediated degradation
Ultrasound [121-142]	AFFF[a], IDW[a], short-chain including PFPrA[a] and PFBA[a], HFPO-DA[a], 24 mixes of PFASs[a], precursors, high salinity groundwater, low salinity groundwater, ultrapure water/deionized water, and landfill leachate.	Yes[a]	High	High energy consumption for the treatment of low PFAS load matrices	Mineralization of tested PFASs with no short-chain byproducts or other toxic byproducts. No pretreatment is needed.	Pyrolysis in acoustic cavities
eBeam [143-147]	PFOS, PFOA ultrapure water/deionized water, Synthetic water	No	Low	Specialized equipment, Generation of short-chain and polyfluorinated ether byproducts or other toxic byproducts, long treatment times	-	Reduction by hydrated electrons generated through Gamma-ray irradiation
Plasma [148-151]	IDW, groundwater, landfill leachate, ultrapure water/deionized water	Yes	High	Generation of short-chain byproducts or other toxic byproducts, Energy requirements, and treatment times increase with increasing concentration and complexity of the matrix.	Mineralization. Shorter residence time for treatment of low PFAS load matrix	Reduction by hydrated electrons and radical species generated through high voltage electric discharge
Electro-Chemical [152-159]	Groundwater, ultrapure water/deionized water, PFCAs, PFAA Precursors, PFOS.	No	High	Generation of short-chain and polyfluorinated ether byproducts or other toxic byproducts. Passivation of expensive electrodes, high energy consumption for high salinity matrix, Ineffective for short-chain PFSAs,	-	Direct Electron Transfer at the anode surface
Hydrothermal [160-165]	PFOA, PFOS, PFHxS, AFFF, ultrapure water/deionized water, wastewater	No	High	Caustic brine generation, high temperature, pressure, and energy requirement additives like NaOH or zerovalent metals are required.	Mineralization with no short-chain byproducts or other toxic byproducts. No pretreatment is needed.	The reactive environment in subcritical water.
Activated Persulfate [166-176]	PFOA, PFOS, AFFF, PFCAs, ultrapure water/deionized water	No	Medium	Generation of short-chain byproducts or other toxic byproducts, Ineffective for sulfonates and short-chain PFASs, matrix acidification, long treatment/residence times, high energy demand.	-	Persulfate ion
Photo-catalysis [109, 110, 171, 172, 174, 177-212]	PFOA, PFOS, collection of 34 PFAS, PFECA ultrapure water/deionized water, treated wastewater	No	Low	Highly dependent on matrix constituents, specialized photo-catalyst and chemical additives needed can have long retention times, ineffective for short-chain PFSAs, generation of shorter-chain intermediates and other toxic byproducts, tested for higher concentrations than environmentally relevant, low degradation rates in presence of radical scavenging constituents, high energy demand.	Mineralization of tested PFCAs and fluorotelomer carboxylic acids	Radical species like hydroxyl radical, persulfate ion, sulfate radicals, carbonate radicals, iodate radicals, hydrated electrons, direct electron transfer from nano catalysts induced bulk reactions by light irradiation

2.5 PFAS Detection Methods

PFAS detection techniques are mainly based on liquid chromatography (LC-MS/MS) for soluble PFASs or gas chromatography (GC-MS/MS) for volatile PFASs, coupled with mass spectroscopy (MS) using a method like USEPA Method 533 [213], 537.1 [214] or 8327 [215]. In LC-MS/MS the mass spectroscopy can be a single or triple quadrupole MS, ion-trap MS, time-of-flight MS, or quadrupole time-of-flight MS while GC-MS/MS can be a double or triple quadrupole MS with electron ionization (EI), positive chemical ionization (PCI), negative chemical ionization (NCI), or flame ionization detector (FID). A non-specific precursor quantification can be performed using a total oxidizable precursors assay (TOP assay) and analyzing the concentration of terminal PFASs in the samples before and after the TOP assay using an LC-MS/MS. The TOP assay uses heat-activated persulfate to oxidize all precursors to their terminal PFASs [57]. Similarly, total fluorine (TF) detection methods like particle-induced gamma-ray emission (PIGE) [216] and inductively coupled plasma mass spectrometer (ICP-MS/MS) [217] have been developed for quantification of total fluorine in samples, and by extension, PFAS mass. Combustion ion chromatography (CIC) has also been utilized to detect TF and total organic fluorine or total extractable organic fluorine (TOF/TOEF) in rat blood samples containing PFOA [218]. Other methods for TF and TOF/TOEF detection include detection ^{19}F-NMR [219], and XPS [220]. The sample preparation/extraction is needed before the analysis of PFASs using the above methods. The extraction methods generally involve solid-phase extraction (SPE), liquid-liquid extraction (LLE), solid-liquid extraction (SLE), solid-phase microextraction (SPME), and dispersive liquid-liquid microextraction (DLLME). The SLE is used for the extraction of PFASs from solids by acidic and/or basic methanol. A detailed review of PFAS analytical methods was also published recently [46, 221].

2.6 Conclusion

PFASs can bioaccumulate in various ecosystems and are ubiquitous in treated wastewater effluents throughout the world as traditional treatment methods are ineffective towards PFAS removal. Therefore, to ensure safe reuse and recycling of water, the effective treatment of PFAS impacted wastewater and runoff is critical. This review discusses the current PFAS regulatory standards in the USA, the fate of PFASs in current water treatment systems, current analytical methods for detection of PFASs, and the emerging destructive treatment methods for PFAS removal. The findings of similar recent reviews and recent studies summarized in this report demonstrate that both the novel PFASs, like short-chain PFASs, and legacy PFASs have been detected in the runoff and wastewater effluents. The sorption of PFASs and PFAS precursors on organic matter/solids is the primary influencer of the fate and transport of PFAS in the environment and water treatment plants. The analysis of PFASs requires expensive machinery and technical expertise. However, analysis of precursors and novel PFASs remains challenging. The ultrasonic treatment of PFASs and plasma-based treatment of PFASs are the only two destructive technologies that are promising for industrial application and have been tested at field-scale, while bioremediation remains an elusive but promising low cost-energy demanding alternative remediation technology.

References

1. OECD/UNEP, *Synthesis Paper on Per- And Polyfluorinated Chemicals (PFCS)*. 2013.
2. Concawe, *Environmental fate and effects of polyand perfluoroalkyl substances (PFAS)*. 2016, Concawe: Brussels.
3. USEPA. *PFAS Master List of PFAS Substances (Version 2)*. 2020 [cited 2021 03/09/2021]; Available from: https://comptox.epa.gov/dashboard/chemical_lists/pfasmaster.
4. Administration, U.S.F.D. *Per and Polyfluoroalkyl Substances (PFAS)*. [Website] 2019 14 October 2019]; Available from: https://www.fda.gov/food/chemicals/and-polyfluoroalkyl-substances-pfas#targetText=There%20are%20nearly%205%2C000%20types,used%20and%20studied%20than%20others.
5. Council, I.T.R. *History and Use of Per- and Polyfluoroalkyl Substances (PFAS)*. 2020 [cited 2020 08/11/2020].
6. Chemours. *The History of Teflon Fluoropolymers*. 2020 08/11/2020].
7. Paul, A.G., K.C. Jones, and A.J. Sweetman, *A First Global Production, Emission, And Environmental Inventory For Perfluorooctane Sulfonate.* Environmental Science & Technology, 2009. **43**(2): p. 386-392.
8. Lindstrom, A.B., M.J. Strynar, and E.L. Libelo, *Polyfluorinated Compounds: Past, Present, and Future.* Environmental Science & Technology, 2011. **45**(19): p. 7954-7961.
9. Council, T.I.T.R., *Technical and Regulatory Guidance on Per- and Polyfluoroalkyl Substances (PFAS)*. 2020.
10. 3M. *PFAS History*. 2020 [cited 2020 08/11/2020].
11. Buck, R.C., J. Franklin, U. Berger, J.M. Conder, I.T. Cousins, P. de Voogt, A.A. Jensen, K. Kannan, S.A. Mabury, and S.P.J. van Leeuwen, *Perfluoroalkyl and polyfluoroalkyl substances in the environment: Terminology, classification, and origins.* Integrated Environmental Assessment and Management, 2011. **7**(4): p. 513-541.
12. Dorrance, L.R., S. Kellogg, and A.H. Love, *What You Should Know About Per- and Polyfluoroalkyl Substances (PFAS) for Environmental Claims.* Environmental Claims Journal, 2017. **29**(4): p. 290-304.
13. Hill, P.J., M. Taylor, P. Goswami, and R.S. Blackburn, *Substitution of PFAS chemistry in outdoor apparel and the impact on repellency performance.* Chemosphere, 2017. **181**: p. 500-507.
14. Garcetti, M.E. *L.A.'s Green New Deal Sustainable City Plan*. 2019 08/12/2020].
15. Agency, U.S.E.P. *National Water Reuse Action Plan: Collaborative Implementation*. 2020 08/12/2020].
16. Silva, J.A.K., W.A. Martin, J.L. Johnson, and J.E. McCray, *Evaluating air-water and NAPL-water interfacial adsorption and retention of Perfluorocarboxylic acids within the Vadose zone.* Journal of Contaminant Hydrology, 2019. **223**: p. 103472.
17. Brusseau, M.L., *Assessing the potential contributions of additional retention processes to PFAS retardation in the subsurface.* Science of The Total Environment, 2018. **613-614**: p. 176-185.
18. Brusseau, M.L., R.H. Anderson, and B. Guo, *PFAS concentrations in soils: Background levels versus contaminated sites.* Science of The Total Environment, 2020. **740**.

19. Guo, B., J. Zeng, and M.L. Brusseau, *A Mathematical Model for the Release, Transport, and Retention of Per- and Polyfluoroalkyl Substances (PFAS) in the Vadose Zone.* Water Resources Research, 2020. **56**(2): p. e2019WR026667.
20. Sharifan, H., M. Bagheri, D. Wang, J.G. Burken, C.P. Higgins, Y. Liang, J. Liu, C.E. Schaefer, and J. Blotevogel, *Fate and transport of per- and polyfluoroalkyl substances (PFASs) in the vadose zone.* Science of The Total Environment, 2021. **771**: p. 145427.
21. Page, D., J. Vanderzalm, A. Kumar, K.Y. Cheng, A.H. Kaksonen, and S. Simpson, *Risks of Perfluoroalkyl and Polyfluoroalkyl Substances (PFAS) for Sustainable Water Recycling via Aquifers.* Water, 2019. **11**(8).
22. Eriksson, U., P. Haglund, and A. Karrman, *Contribution of precursor compounds to the release of per- and polyfluoroalkyl substances (PFASs) from waste water treatment plants (WWTPs).* Journal of Environmental Sciences (China), 2017. **61**: p. 80-90.
23. Sunderland, E.M., X.C. Hu, C. Dassuncao, A.K. Tokranov, C.C. Wagner, and J.G. Allen, *A review of the pathways of human exposure to poly- and perfluoroalkyl substances (PFASs) and present understanding of health effects.* Journal of Exposure Science and Environmental Epidemiology, 2019. **29**(2): p. 131-147.
24. Domingo, J.L. and M. Nadal, *Human exposure to per- and polyfluoroalkyl substances (PFAS) through drinking water: A review of the recent scientific literature.* Environmental Research, 2019. **177**: p. 108648.
25. Hayman, N.T., G. Rosen, M.A. Colvin, J. Conder, and J.A. Arblaster, *Aquatic toxicity evaluations of PFOS and PFOA for five standard marine endpoints.* Chemosphere, 2021. **273**: p. 129699.
26. Miranda, D.A., J.P. Benskin, R. Awad, G. Lepoint, J. Leonel, and V. Hatje, *Bioaccumulation of Per- and polyfluoroalkyl substances (PFASs) in a tropical estuarine food web.* Science of The Total Environment, 2021. **754**: p. 142146.
27. Ankley, G.T., P. Cureton, R.A. Hoke, M. Houde, A. Kumar, J. Kurias, R. Lanno, C. McCarthy, J. Newsted, C.J. Salice, B.E. Sample, M.S. Sepulveda, J. Steevens, and S. Valsecchi, *Assessing the Ecological Risks of Per- and Polyfluoroalkyl Substances: Current State-of-the Science and a Proposed Path Forward.* Environmental Toxicology and Chemistry, 2021. **40**(3): p. 564-605.
28. Conder, J., J. Arblaster, E. Larson, J. Brown, and C. Higgins, *Guidance for Assessing the Ecological Risks of PFASs to Threatened and Endangered Species at Aqueous Film Forming Foam-Impacted Sites*. 2019, Geosyntec Consultants Huntington Beach United States.
29. Leeson, A., T. Thompson, H.F. Stroo, R.H. Anderson, J. Speicher, M.A. Mills, J. Willey, C. Coyle, R. Ghosh, C. Lebron, and C. Patton, *Identifying and Managing Aqueous Film-Forming Foam-Derived Per- and Polyfluoroalkyl Substances in the Environment.* Environmental Toxicology and Chemistry, 2021. **40**(1): p. 24-36.
30. COEHHA, *Notice Of Intent To List Chemical By The Authoritative Bodies Mechanism: Perfluorooctanoic Acid*, C.E.P.A.s.O.o.E.H.H. Assessment, Editor. 2021.
31. Murakami, M., H. Shinohara, and H. Takada, *Evaluation of wastewater and street runoff as sources of perfluorinated surfactants (PFSs).* Chemosphere, 2009. **74**(4): p. 487-493.
32. Xiao, F., M.F. Simcik, and J.S. Gulliver, *Perfluoroalkyl acids in urban stormwater runoff: Influence of land use.* Water Research, 2012. **46**(20): p. 6601-6608.

33. Gallen, C., G. Eaglesham, D. Drage, T.H. Nguyen, and J.F. Mueller, *A mass estimate of perfluoroalkyl substance (PFAS) release from Australian wastewater treatment plants.* Chemosphere, 2018. **208**: p. 975-983.
34. Coggan, T.L., D. Moodie, A. Kolobaric, D. Szabo, J. Shimeta, N.D. Crosbie, E. Lee, M. Fernandes, and B.O. Clarke, *An investigation into per- and polyfluoroalkyl substances (PFAS) in nineteen Australian wastewater treatment plants (WWTPs).* Heliyon, 2019. **5**(8): p. e02316.
35. Hu, X.C., D.Q. Andrews, A.B. Lindstrom, T.A. Bruton, L.A. Schaider, P. Grandjean, R. Lohmann, C.C. Carignan, A. Blum, S.A. Balan, C.P. Higgins, and E.M. Sunderland, *Detection of Poly- and Perfluoroalkyl Substances (PFASs) in U.S. Drinking Water Linked to Industrial Sites, Military Fire Training Areas, and Wastewater Treatment Plants.* Environmental Science & Technology Letters, 2016. **3**(10): p. 344-350.
36. Weston and Sampson Engineers, I., *Poly- and Perfluoroalkyl Substances at Wastewater Treatment Facilities and Landfill Leachate*. 2020, Vermont Department of Environmental Conservation (VTDEC).
37. Board, C.W.R.C., *Water Code Sections 13267 And 13383 Order for The Determination of The Presence Of Per- And Polyfluoroalkyl Substances At Publicly Owned Treatment Works*. 2020.
38. Xu, C., Z. Liu, X. Song, X. Ding, and D. Ding, *Legacy and emerging per- and polyfluoroalkyl substances (PFASs) in multi-media around a landfill in China: Implications for the usage of PFASs alternatives.* Science of The Total Environment, 2021. **751**: p. 141767.
39. The Michigan Department of Environment, G.L., and Energy *SUMMARY REPORT: Initiatives to Evaluate the Presence of PFAS in Municipal Wastewater and Associated Residuals (Sludge/Biosolids) in Michigan*. 2020.
40. The Michigan Department of Environment, G.L., and Energy *Municipal NPDES Permitting Strategy for PFOS And PFOA Water Resources Guidance*. 2020.
41. protection, C.D.o.P.H.a.D.o.e.e., *PFAS Action Plan*. 2019.
42. Resources, N.C.D.o.W. *Managing Emerging Compounds in Water*. 2020 [cited 2020; Available from: https://deq.nc.gov/news/key-issues/emerging-compounds/managing-emerging-compounds-water#management-strategy-for-industrial-dischargers-and-pretreatment-facilities.
43. Agency, M.P.C., *Investigating PFCs in Minnesota: Current Status (March 2009)* 2009.
44. Agency, M.P.C., *PFCs in Minnesota's Ambient Environment:2008 Progress Report*. 2008.
45. USEPA, *EPA Takes Action to Address PFAS in Drinking Water.* 2021.
46. Fiedler, H., T. Kennedy, and B.J. Henry, *A Critical Review of a Recommended Analytical and Classification Approach for Organic Fluorinated Compounds with an Emphasis on Per- and Polyfluoroalkyl Substances.* Integrated Environmental Assessment and Management, 2021. **17**(2): p. 331-351.
47. Guardian, M.G.E., E.G. Boongaling, V.R.R. Bernardo-Boongaling, J. Gamonchuang, T. Boontongto, R. Burakham, P. Arnnok, and D.S. Aga, *Prevalence of per- and polyfluoroalkyl substances (PFASs) in drinking and source water from two Asian countries.* Chemosphere, 2020. **256**: p. 127115.
48. Stoiber, T., S. Evans, A.M. Temkin, D.Q. Andrews, and O.V. Naidenko, *PFAS in drinking water: an emergent water quality threat*. 2020, Water Solutions.

49. Guelfo, J.L., T. Marlow, D.M. Klein, D.A. Savitz, S. Frickel, M. Crimi, and E.M. Suuberg, *Evaluation and Management Strategies for Per- and Polyfluoroalkyl Substances (PFASs) in Drinking Water Aquifers: Perspectives from Impacted U.S. Northeast Communities.* Environ Health Perspect, 2018. **126**(6): p. 065001.
50. Phong Vo, H.N., H.H. Ngo, W. Guo, T.M. Hong Nguyen, J. Li, H. Liang, L. Deng, Z. Chen, and T.A. Hang Nguyen, *Poly-and perfluoroalkyl substances in water and wastewater: A comprehensive review from sources to remediation.* Journal of Water Process Engineering, 2020. **36**.
51. Hamid, H. and L. Li, *Role of wastewater treatment plant (WWTP) in environmental cycling of poly- and perfluoroalkyl (PFAS) compounds.* Ecocycles, 2016. **2**(2).
52. Meegoda, J.N., J.A. Kewalramani, B. Li, and R.W. Marsh, *A Review of the Applications, Environmental Release, and Remediation Technologies of Per- and Polyfluoroalkyl Substances.* International Journal of Environmental Research and Public Health, 2020. **17**(21).
53. Ateia, M., A. Maroli, N. Tharayil, and T. Karanfil, *The overlooked short- and ultrashort-chain poly- and perfluorinated substances: A review.* Chemosphere, 2019. **220**: p. 866-882.
54. Li, F., J. Duan, S. Tian, H. Ji, Y. Zhu, Z. Wei, and D. Zhao, *Short-chain per- and polyfluoroalkyl substances in aquatic systems: Occurrence, impacts and treatment.* Chemical Engineering Journal, 2020. **380**.
55. Kibambe, M.G., M.N.B. Momba, A.P. Daso, and M.A.A. Coetzee, *Evaluation of the efficiency of selected wastewater treatment processes in removing selected perfluoroalkyl substances (PFASs).* Journal of Environmental Management, 2020. **255**: p. 109945.
56. Jacob, P., K.A. Barzen-Hanson, and D.E. Helbling, *Target and Nontarget Analysis of Per- and Polyfluoralkyl Substances in Wastewater from Electronics Fabrication Facilities.* Environmental Science & Technology, 2021. **55**(4): p. 2346-2356.
57. Houtz, E.F. and D.L. Sedlak, *Oxidative Conversion as a Means of Detecting Precursors to Perfluoroalkyl Acids in Urban Runoff.* Environmental Science & Technology, 2012. **46**(17): p. 9342-9349.
58. Ali, A.M., C.P. Higgins, W.M. Alarif, S.S. Al-Lihaibi, M. Ghandourah, and R. Kallenborn, *Per- and polyfluoroalkyl substances (PFASs) in contaminated coastal marine waters of the Saudi Arabian Red Sea: a baseline study.* Environmental Science and Pollution Research, 2021. **28**(3): p. 2791-2803.
59. Dauchy, X., V. Boiteux, A. Colin, C. Bach, C. Rosin, and J.F. Munoz, *Poly- and Perfluoroalkyl Substances in Runoff Water and Wastewater Sampled at a Firefighter Training Area.* Archives of Environmental Contamination and Toxicology, 2019. **76**(2): p. 206-215.
60. Han, T., L. Gao, J. Chen, X. He, and B. Wang, *Spatiotemporal variations, sources and health risk assessment of perfluoroalkyl substances in a temperate bay adjacent to metropolis, North China.* Environmental Pollution, 2020. **265**(Pt A): p. 115011.
61. Bai, X. and Y. Son, *Perfluoroalkyl substances (PFAS) in surface water and sediments from two urban watersheds in Nevada, USA.* Science of The Total Environment, 2021. **751**: p. 141622.
62. Zushi, Y. and S. Masunaga, *First-flush loads of perfluorinated compounds in stormwater runoff from Hayabuchi River basin, Japan served by separated sewerage system.* Chemosphere, 2009. **76**(6): p. 833-40.

63. Kim, S.-K. and K. Kannan, *Perfluorinated Acids in Air, Rain, Snow, Surface Runoff, and Lakes: Relative Importance of Pathways to Contamination of Urban Lakes.* Environmental Science & Technology, 2007. **41**(24): p. 8328-8334.
64. Codling, G., H. Yuan, P.D. Jones, J.P. Giesy, and M. Hecker, *Metals and PFAS in stormwater and surface runoff in a semi-arid Canadian city subject to large variations in temperature among seasons.* Environmental Science and Pollution Research, 2020. **27**(15): p. 18232-18241.
65. Sinclair, E. and K. Kannan, *Mass Loading and Fate of Perfluoroalkyl Surfactants in Wastewater Treatment Plants.* Environmental Science & Technology, 2006. **40**(5): p. 1408-1414.
66. Loganathan, B.G., K.S. Sajwan, E. Sinclair, K. Senthil Kumar, and K. Kannan, *Perfluoroalkyl sulfonates and perfluorocarboxylates in two wastewater treatment facilities in Kentucky and Georgia.* Water Research, 2007. **41**(20): p. 4611-20.
67. Schultz, M.M., D.F. Barofsky, and J.A. Field, *Quantitative Determination of Fluorinated Alkyl Substances by Large-Volume-Injection Liquid Chromatography Tandem Mass SpectrometryCharacterization of Municipal Wastewaters.* Environmental Science & Technology, 2006. **40**(1): p. 289-295.
68. Boulanger, B., J.D. Vargo, J.L. Schnoor, and K.C. Hornbuckle, *Evaluation of Perfluorooctane Surfactants in a Wastewater Treatment System and in a Commercial Surface Protection Product.* Environmental Science & Technology, 2005. **39**(15): p. 5524-5530.
69. Loos, R., R. Carvalho, D.C. Antonio, S. Comero, G. Locoro, S. Tavazzi, B. Paracchini, M. Ghiani, T. Lettieri, L. Blaha, B. Jarosova, S. Voorspoels, K. Servaes, P. Haglund, J. Fick, R.H. Lindberg, D. Schwesig, and B.M. Gawlik, *EU-wide monitoring survey on emerging polar organic contaminants in wastewater treatment plant effluents.* Water Research, 2013. **47**(17): p. 6475-87.
70. Moller, A., L. Ahrens, R. Surm, J. Westerveld, F. van der Wielen, R. Ebinghaus, and P. de Voogt, *Distribution and sources of polyfluoroalkyl substances (PFAS) in the River Rhine watershed.* Environmental Pollution, 2010. **158**(10): p. 3243-50.
71. Llorca, M., M. Farre, Y. Pico, J. Muller, T.P. Knepper, and D. Barcelo, *Analysis of perfluoroalkyl substances in waters from Germany and Spain.* Science of The Total Environment, 2012. **431**: p. 139-50.
72. Bossi, R., J. Strand, O. Sortkjaer, and M.M. Larsen, *Perfluoroalkyl compounds in Danish wastewater treatment plants and aquatic environments.* Environment International, 2008. **34**(4): p. 443-50.
73. Nguyen, H.T., S.L. Kaserzon, P.K. Thai, S. Vijayasarathy, J. Bräunig, N.D. Crosbie, A. Bignert, and J.F. Mueller, *Temporal trends of per- and polyfluoroalkyl substances (PFAS) in the influent of two of the largest wastewater treatment plants in Australia.* Emerging Contaminants, 2019. **5**: p. 211-218.
74. Chen, H., C. Zhang, J. Han, Y. Yu, and P. Zhang, *PFOS and PFOA in influents, effluents, and biosolids of Chinese wastewater treatment plants and effluent-receiving marine environments.* Environmental Pollution, 2012. **170**: p. 26-31.
75. Zhang, C., H. Yan, F. Li, and Q. Zhou, *Occurrence and fate of perfluorinated acids in two wastewater treatment plants in Shanghai, China.* Environmental Science and Pollution Research, 2015. **22**(3): p. 1804-11.

76. Lin, A.Y., S.C. Panchangam, and P.S. Ciou, *High levels of perfluorochemicals in Taiwan's wastewater treatment plants and downstream rivers pose great risk to local aquatic ecosystems.* Chemosphere, 2010. **80**(10): p. 1167-74.
77. Ma, R. and K. Shih, *Perfluorochemicals in wastewater treatment plants and sediments in Hong Kong.* Environmental Pollution, 2010. **158**(5): p. 1354-62.
78. Guo, R., W.J. Sim, E.S. Lee, J.H. Lee, and J.E. Oh, *Evaluation of the fate of perfluoroalkyl compounds in wastewater treatment plants.* Water Research, 2010. **44**(11): p. 3476-86.
79. Kim, S.K., J.K. Im, Y.M. Kang, S.Y. Jung, Y.L. Kho, and K.D. Zoh, *Wastewater treatment plants (WWTPs)-derived national discharge loads of perfluorinated compounds (PFCs).* Journal of Hazardous Materials, 2012. **201-202**: p. 82-91.
80. Kwon, H.O., H.Y. Kim, Y.M. Park, K.S. Seok, J.E. Oh, and S.D. Choi, *Updated national emission of perfluoroalkyl substances (PFASs) from wastewater treatment plants in South Korea.* Environmental Pollution, 2017. **220**(Pt A): p. 298-306.
81. Kim, H.Y., H.W. Seok, H.O. Kwon, S.D. Choi, K.S. Seok, and J.E. Oh, *A national discharge load of perfluoroalkyl acids derived from industrial wastewater treatment plants in Korea.* Science of The Total Environment, 2016. **563-564**: p. 530-7.
82. Kim, K.Y., M. Ndabambi, S. Choi, and J.E. Oh, *Legacy and novel perfluoroalkyl and polyfluoroalkyl substances in industrial wastewater and the receiving river water: Temporal changes in relative abundances of regulated compounds and alternatives.* Water Research, 2021. **191**: p. 116830.
83. Chirikona, F., M. Filipovic, S. Ooko, and F. Orata, *Perfluoroalkyl acids in selected wastewater treatment plants and their discharge load within the Lake Victoria basin in Kenya.* Environmental Monitoring and Assessment, 2015. **187**(5): p. 238.
84. Yu, J., J. Hu, S. Tanaka, and S. Fujii, *Perfluorooctane sulfonate (PFOS) and perfluorooctanoic acid (PFOA) in sewage treatment plants.* Water Research, 2009. **43**(9): p. 2399-408.
85. Arvaniti, O.S., E.I. Ventouri, A.S. Stasinakis, and N.S. Thomaidis, *Occurrence of different classes of perfluorinated compounds in Greek wastewater treatment plants and determination of their solid-water distribution coefficients.* Journal of Hazardous Materials, 2012. **239-240**: p. 24-31.
86. Stroski, K.M., K.H. Luong, J.K. Challis, L.G. Chaves-Barquero, M.L. Hanson, and C.S. Wong, *Wastewater sources of per- and polyfluorinated alkyl substances (PFAS) and pharmaceuticals in four Canadian Arctic communities.* Science of The Total Environment, 2020. **708**: p. 134494.
87. Kunacheva, C., S. Tanaka, S. Fujii, S.K. Boontanon, C. Musirat, T. Wongwattana, and B.R. Shivakoti, *Mass flows of perfluorinated compounds (PFCs) in central wastewater treatment plants of industrial zones in Thailand.* Chemosphere, 2011. **83**(6): p. 737-44.
88. Dauchy, X., V. Boiteux, C. Bach, A. Colin, J. Hemard, C. Rosin, and J.F. Munoz, *Mass flows and fate of per- and polyfluoroalkyl substances (PFASs) in the wastewater treatment plant of a fluorochemical manufacturing facility.* Science of The Total Environment, 2017. **576**: p. 549-558.
89. Dalahmeh, S., S. Tirgani, A.J. Komakech, C.B. Niwagaba, and L. Ahrens, *Per- and polyfluoroalkyl substances (PFASs) in water, soil and plants in wetlands and agricultural areas in Kampala, Uganda.* Science of The Total Environment, 2018. **631-632**: p. 660-667.

90. Campo, J., A. Masia, Y. Pico, M. Farre, and D. Barcelo, *Distribution and fate of perfluoroalkyl substances in Mediterranean Spanish sewage treatment plants.* Science of The Total Environment, 2014. **472**: p. 912-22.
91. Sanchez-Avila, J., J. Meyer, and S. Lacorte, *Spatial distribution and sources of perfluorochemicals in the NW Mediterranean coastal waters (Catalonia, Spain).* Environmental Pollution, 2010. **158**(9): p. 2833-40.
92. Vu, C.T. and T. Wu, *Recent progress in adsorptive removal of per- and poly-fluoroalkyl substances (PFAS) from water/wastewater.* Critical Reviews in Environmental Science and Technology, 2020: p. 1-40.
93. Tseng, N.S.-l., *Feasibility of Biodegradation of Polyfluoroalkyl and Perfluoroalkyl Substances.* 2012.
94. Tseng, N., N. Wang, B. Szostek, and S. Mahendra, *Biotransformation of 6:2 Fluorotelomer Alcohol (6:2 FTOH) by a Wood-rotting Fungus.* Environmental Science & Technology, 2014. **48**(7): p. 4012-4020.
95. Merino, N., M. Wang, R. Ambrocio, K. Mak, E. O'Connor, A. Gao, E.L. Hawley, R.A. Deeb, L.Y. Tseng, and S. Mahendra, *Fungal biotransformation of 6:2 fluorotelomer alcohol.* Remediation Journal, 2018. **28**(2): p. 59-70.
96. Kwon, B.G., H.J. Lim, S.H. Na, B.I. Choi, D.S. Shin, and S.Y. Chung, *Biodegradation of perfluorooctanesulfonate (PFOS) as an emerging contaminant.* Chemosphere, 2014. **109**: p. 221-5.
97. Yi, L.B., L.Y. Chai, Y. Xie, Q.J. Peng, and Q.Z. Peng, *Isolation, identification, and degradation performance of a PFOA-degrading strain.* Genetics and Molecular Research, 2016. **15**(2).
98. Chetverikov, S.P., D.A. Sharipov, T.Y. Korshunova, and O.N. Loginov, *Degradation of perfluorooctanyl sulfonate by strain Pseudomonas plecoglossicida 2.4-D.* Applied Biochemistry and Microbiology, 2017. **53**(5): p. 533-538.
99. Huang, S. and P.R. Jaffe, *Defluorination of Perfluorooctanoic Acid (PFOA) and Perfluorooctane Sulfonate (PFOS) by Acidimicrobium sp. Strain A6.* Environmental Science & Technology, 2019. **53**(19): p. 11410-11419.
100. Luo, Q., J. Lu, H. Zhang, Z. Wang, M. Feng, S.-Y.D. Chiang, D. Woodward, and Q. Huang, *Laccase-Catalyzed Degradation of Perfluorooctanoic Acid.* Environmental Science & Technology Letters, 2015. **2**(7): p. 198-203.
101. Luo, Q., Z. Wang, M. Feng, D. Chiang, D. Woodward, S. Liang, J. Lu, and Q. Huang, *Factors controlling the rate of perfluorooctanoic acid degradation in laccase-mediator systems: The impact of metal ions.* Environmental Pollution, 2017. **224**: p. 649-657.
102. Luo, Q., X. Yan, J. Lu, and Q. Huang, *Perfluorooctanesulfonate Degrades in a Laccase-Mediator System.* Environmental Science & Technology, 2018. **52**(18): p. 10617-10626.
103. Luo, Q., S. Liang, and Q. Huang, *Laccase induced degradation of perfluorooctanoic acid in a soil slurry.* Journal of Hazardous Materials, 2018. **359**: p. 241-247.
104. Harding-Marjanovic, K.C., E.F. Houtz, S. Yi, J.A. Field, D.L. Sedlak, and L. Alvarez-Cohen, *Aerobic Biotransformation of Fluorotelomer Thioether Amido Sulfonate (Lodyne) in AFFF-Amended Microcosms.* Environmental Science & Technology, 2015. **49**(13): p. 7666-7674.
105. Hamid, H., L.Y. Li, and J.R. Grace, *Aerobic biotransformation of fluorotelomer compounds in landfill leachate-sediment.* Science of The Total Environment, 2020. **713**: p. 136547.

106. Lange, C.C., *Anaerobic biotransformation of N-methyl perfluorobutanesulfonamido ethanol and N-ethyl perfluorooctanesulfonamido ethanol.* Environmental Toxicology and Chemistry, 2018. **37**(3): p. 768-779.
107. Liu, J., N. Wang, B. Szostek, R.C. Buck, P.K. Panciroli, P.W. Folsom, L.M. Sulecki, and C.A. Bellin, *6-2 Fluorotelomer alcohol aerobic biodegradation in soil and mixed bacterial culture.* Chemosphere, 2010. **78**(4): p. 437-44.
108. Nzeribe, B.N., M. Crimi, S. Mededovic Thagard, and T.M. Holsen, *Physico-Chemical Processes for the Treatment of Per- And Polyfluoroalkyl Substances (PFAS): A review.* Critical Reviews in Environmental Science and Technology, 2019. **49**(10): p. 866-915.
109. Cui, J., P. Gao, and Y. Deng, *Destruction of Per- and Polyfluoroalkyl Substances (PFAS) with Advanced Reduction Processes (ARPs): A Critical Review.* Environmental Science & Technology, 2020. **54**(7): p. 3752-3766.
110. Trojanowicz, M., A. Bojanowska-Czajka, I. Bartosiewicz, and K. Kulisa, *Advanced Oxidation/Reduction Processes treatment for aqueous perfluorooctanoate (PFOA) and perfluorooctanesulfonate (PFOS) – A review of recent advances.* Chemical Engineering Journal, 2018. **336**: p. 170-199.
111. Dombrowski, P.M., P. Kakarla, W. Caldicott, Y. Chin, V. Sadeghi, D. Bogdan, F. Barajas-Rodriguez, and S.-Y.D. Chiang, *Technology review and evaluation of different chemical oxidation conditions on treatability of PFAS.* Remediation Journal, 2018. **28**(2): p. 135-150.
112. Kucharzyk, K.H., R. Darlington, M. Benotti, R. Deeb, and E. Hawley, *Novel treatment technologies for PFAS compounds: A critical review.* Journal of Environmental Management, 2017. **204**(Pt 2): p. 757-764.
113. Butt, C.M., D.C.G. Muir, and S.A. Mabury, *Biotransformation pathways of fluorotelomer-based polyfluoroalkyl substances: A review.* Environmental Toxicology and Chemistry, 2014. **33**(2): p. 243-267.
114. Merino, N., Y. Qu, R.A. Deeb, E.L. Hawley, M.R. Hoffmann, and S. Mahendra, *Degradation and Removal Methods for Perfluoroalkyl and Polyfluoroalkyl Substances in Water.* Environmental Engineering Science, 2016. **33**(9): p. 615-649.
115. Wanninayake, D.M., *Comparison of currently available PFAS remediation technologies in water: A review.* Journal of Environmental Management, 2021. **283**: p. 111977.
116. Yu, J., C. He, X. Liu, J. Wu, Y. Hu, and Y. Zhang, *Removal of perfluorinated compounds by membrane bioreactor with powdered activated carbon (PAC): Adsorption onto sludge and PAC.* Desalination, 2014. **334**(1): p. 23-28.
117. Rankin, K., H. Lee, P.J. Tseng, and S.A. Mabury, *Investigating the biodegradability of a fluorotelomer-based acrylate polymer in a soil-plant microcosm by indirect and direct analysis.* Environmental Science & Technology, 2014. **48**(21): p. 12783-12790.
118. Wang, N., R.C. Buck, B. Szostek, L.M. Sulecki, and B.W. Wolstenholme, *5:3 Polyfluorinated acid aerobic biotransformation in activated sludge via novel "one-carbon removal pathways".* Chemosphere, 2012. **87**(5): p. 527-534.
119. Lim, X. *Can Microbes Save Us from PFAS?* 2021 Jan 27 [cited 7 1]; 2021/02/04:[3-6]. Available from: https://www.ncbi.nlm.nih.gov/pubmed/33532561.
120. Ochoa-Herrera, V., J.A. Field, A. Luna-Velasco, and R. Sierra-Alvarez, *Microbial toxicity and biodegradability of perfluorooctane sulfonate (PFOS) and shorter chain perfluoroalkyl and polyfluoroalkyl substances (PFASs).* Environmental Sciences: Processes and Impacts, 2016. **18**(9): p. 1236-1246.

121. Shende, T., G. Andaluri, and R. Suri, *Frequency-dependent sonochemical degradation of perfluoroalkyl substances and numerical analysis of cavity dynamics.* Separation and Purification Technology, 2021. **261**.
122. James Wood, R., T. Sidnell, I. Ross, J. McDonough, J. Lee, and M.J. Bussemaker, *Ultrasonic degradation of perfluorooctane sulfonic acid (PFOS) correlated with sonochemical and sonoluminescence characterisation.* Ultrasonics Sonochemistry, 2020. **68**: p. 105196.
123. Cao, H., W. Zhang, C. Wang, and Y. Liang, *Sonochemical degradation of poly- and perfluoroalkyl substances - A review.* Ultrasonics Sonochemistry, 2020. **69**: p. 105245.
124. Shende, T., G. Andaluri, and R.P.S. Suri, *Kinetic model for sonolytic degradation of non-volatile surfactants: Perfluoroalkyl substances.* Ultrasonics Sonochemistry, 2019. **51**(September 2018): p. 359-368.
125. Waldo, N.B. and C.D. Vecitis, *Combined effects of phase-shift and power distribution on efficiency of dual-high-frequency sonochemistry.* Ultrasonics Sonochemistry, 2018. **41**: p. 100-108.
126. Hu, Y.B., S.L. Lo, Y.F. Li, Y.C. Lee, M.J. Chen, and J.C. Lin, *Autocatalytic degradation of perfluorooctanoic acid in a permanganate-ultrasonic system.* Water Research, 2018. **140**: p. 148-157.
127. Gole, V.L., R. Sierra-Alvarez, H. Peng, J.P. Giesy, P. Deymier, and M. Keswani, *Sono-chemical treatment of per- and poly-fluoroalkyl compounds in aqueous film-forming foams by use of a large-scale multi-transducer dual-frequency based acoustic reactor.* Ultrasonics Sonochemistry, 2018. **45**: p. 213-222.
128. Gole, V.L., A. Fishgold, R. Sierra-Alvarez, P. Deymier, and M. Keswani, *Treatment of perfluorooctane sulfonic acid (PFOS) using a large-scale sonochemical reactor.* Separation and Purification Technology, 2018. **194**: p. 104-110.
129. Rodriguez-Freire, L., N. Abad-Fernandez, R. Sierra-Alvarez, C. Hoppe-Jones, H. Peng, J.P. Giesy, S. Snyder, and M. Keswani, *Sonochemical degradation of perfluorinated chemicals in aqueous film-forming foams.* Journal ofHazardous Materials, 2016. **317**: p. 275-283.
130. Lin, J.C., C.Y. Hu, and S.L. Lo, *Effect of surfactants on the degradation of perfluorooctanoic acid (PFOA) by ultrasonic (US) treatment.* Ultrasonics Sonochemistry, 2016. **28**: p. 130-135.
131. Fernandez, N.A., L. Rodriguez-Freire, M. Keswani, and R. Sierra-Alvarez, *Effect of chemical structure on the sonochemical degradation of perfluoroalkyl and polyfluoroalkyl substances (PFASs).* Environmental Science: Water Research & Technology, 2016. **2**(6): p. 975-983.
132. Lin, J.C., S.L. Lo, C.Y. Hu, Y.C. Lee, and J. Kuo, *Enhanced sonochemical degradation of perfluorooctanoic acid by sulfate ions.* Ultrasonics Sonochemistry, 2015. **22**: p. 542-7.
133. Campbell, T. and M.R. Hoffmann, *Sonochemical degradation of perfluorinated surfactants: Power and multiple frequency effects.* Separation and Purification Technology, 2015. **156**(April): p. 1019-1027.
134. Phan Thi, L.A., H.T. Do, and S.L. Lo, *Enhancing decomposition rate of perfluorooctanoic acid by carbonate radical assisted sonochemical treatment.* Ultrasonics Sonochemistry, 2014. **21**(5): p. 1875-80.

135. Hori, H., Y. Nagano, M. Murayama, K. Koike, and S. Kutsuna, *Efficient decomposition of perfluoroether carboxylic acids in water with a combination of persulfate oxidant and ultrasonic irradiation.* Journal of Fluorine Chemistry, 2012. **141**: p. 5-10.
136. Zhao, D., C. Ding, X. Xu, and M.R. Hoffmann, *Kinetics of perfluorooctane sulfonate and perfluorooctanoate degradation by ultrasound irradiation.* CIESC Journal, 2011.
137. Vecitis, C.D., Y. Wang, J. Cheng, H. Park, B.T. Mader, and M.R. Hoffmann, *Sonochemical degradation of perfluorooctanesulfonate in aqueous film-forming foams.* Environmental Science & Technology, 2010. **44**(1): p. 432-8.
138. Cheng, J., C.D. Vecitis, H. Park, B.T. Mader, and M.R. Hoffmann, *Sonochemical degradation of perfluorooctane sulfonate (PFOS) and perfluorooctanoate (PFOA) in groundwater: kinetic effects of matrix inorganics.* Environmental Science & Technology, 2010. **44**(1): p. 445-50.
139. Vecitis, C.D., H. Park, J. Cheng, B.T. Mader, and M.R. Hoffmann, *Enhancement of Perfluorooctanoate and Perfluorooctanesulfonate Activity at Acoustic Cavitation Bubble Interfaces.* Journal of Physical Chemistry C, 2008. **112**(43): p. 16850-16857.
140. Vecitis, C.D., H. Park, J. Cheng, B.T. Mader, and M.R. Hoffmann, *Kinetics and mechanism of the sonolytic conversion of the aqueous perfluorinated surfactants, perfluorooctanoate (PFOA), and perfluorooctane sulfonate (PFOS) into inorganic products.* The Journal of Physical Chemistry A, 2008. **112**(18): p. 4261-70.
141. Cheng, J., C.D. Vecitis, H. Park, B.T. Mader, and M.R. Hoffmann, *Sonochemical degradation of peerfluorooctane sulfonate (PFOS) and perfluorooctanoate (PFOA) in landfill groundwater: environmental matrix effects.* Environmental Science & Technology, 2008. **42**(21): p. 8057-63.
142. Moriwaki, H., Y. Takagi, M. Tanaka, K. Tsuruho, K. Okitsu, and Y. Maeda, *Sonochemical decomposition of perfluorooctane sulfonate and perfluorooctanoic acid.* Environmental Science & Technology, 2005. **39**(9): p. 3388-92.
143. Kim, T.-H., S.-H. Lee, H.Y. Kim, K. Doudrick, S. Yu, and S.D. Kim, *Decomposition of perfluorooctane sulfonate (PFOS) using a hybrid process with electron beam and chemical oxidants.* Chemical Engineering Journal, 2019. **361**: p. 1363-1370.
144. Kim, T.H., S. Yu, Y. Choi, T.Y. Jeong, and S.D. Kim, *Profiling the decomposition products of perfluorooctane sulfonate (PFOS) irradiated using an electron beam.* Science of The Total Environment, 2018. **631-632**: p. 1295-1303.
145. Wang, L., B. Batchelor, S.D. Pillai, and V.S.V. Botlaguduru, *Electron beam treatment for potable water reuse: Removal of bromate and perfluorooctanoic acid.* Chemical Engineering Journal, 2016. **302**: p. 58-68.
146. Horst, J., J. McDonough, I. Ross, and E. Houtz, *Understanding and Managing the Potential By-Products of PFAS Destruction.* Groundwater Monitoring and Remediation, 2020. **40**(2): p. 17-27.
147. Horst, J., J. McDonough, I. Ross, M. Dickson, J. Miles, J. Hurst, and P. Storch, *Water treatment technologies for PFAS: the next generation.* Groundwater Monitoring Remediation, 2018. **38**(2): p. 13-23.
148. Stratton, G.R., F. Dai, C.L. Bellona, T.M. Holsen, E.R. Dickenson, and S. Mededovic Thagard, *Plasma-Based Water Treatment: Efficient Transformation of Perfluoroalkyl Substances in Prepared Solutions and Contaminated Groundwater.* Environmental Science & Technology, 2017. **51**(3): p. 1643-1648.

149. Singh, R.K., E. Brown, S. Mededovic Thagard, and T.M. Holsen, *Treatment of PFAS-containing landfill leachate using an enhanced contact plasma reactor.* Journal of Hazardous Materials, 2021. **408**: p. 124452.
150. Singh, R.K., N. Multari, C. Nau-Hix, R.H. Anderson, S.D. Richardson, T.M. Holsen, and S. Mededovic Thagard, *Rapid Removal of Poly- and Perfluorinated Compounds from Investigation-Derived Waste (IDW) in a Pilot-Scale Plasma Reactor.* Environmental Science & Technology, 2019. **53**(19): p. 11375-11382.
151. Nau-Hix, C., N. Multari, R.K. Singh, S. Richardson, P. Kulkarni, R.H. Anderson, T.M. Holsen, and S. Mededovic Thagard, *Field Demonstration of a Pilot-Scale Plasma Reactor for the Rapid Removal of Poly- and Perfluoroalkyl Substances in Groundwater.* ACS ES&T Water, 2021.
152. Pica, N.E., J. Funkhouser, Y. Yin, Z. Zhang, D.M. Ceres, T. Tong, and J. Blotevogel, *Electrochemical Oxidation of Hexafluoropropylene Oxide Dimer Acid (GenX): Mechanistic Insights and Efficient Treatment Train with Nanofiltration.* Environmental Science & Technology, 2019. **53**(21): p. 12602-12609.
153. Schaefer, C.E., S. Choyke, P.L. Ferguson, C. Andaya, A. Burant, A. Maizel, T.J. Strathmann, and C.P. Higgins, *Electrochemical Transformations of Perfluoroalkyl Acid (PFAA) Precursors and PFAAs in Groundwater Impacted with Aqueous Film Forming Foams.* Environmental Science & Technology, 2018. **52**(18): p. 10689-10697.
154. Schaefer, C.E., C. Andaya, A. Burant, C.W. Condee, A. Urtiaga, T.J. Strathmann, and C.P. Higgins, *Electrochemical treatment of perfluorooctanoic acid and perfluorooctane sulfonate: Insights into mechanisms and application to groundwater treatment.* Chemical Engineering Journal, 2017. **317**: p. 424-432.
155. Urtiaga, A., C. Fernandez-Gonzalez, S. Gomez-Lavin, and I. Ortiz, *Kinetics of the electrochemical mineralization of perfluorooctanoic acid on ultrananocrystalline boron doped conductive diamond electrodes.* Chemosphere, 2015. **129**: p. 20-26.
156. Schaefer, C.E., C. Andaya, A. Urtiaga, E.R. McKenzie, and C.P. Higgins, *Electrochemical treatment of perfluorooctanoic acid (PFOA) and perfluorooctane sulfonic acid (PFOS) in groundwater impacted by aqueous film forming foams (AFFFs).* Journal of Hazardous Materials, 2015. **295**: p. 170-175.
157. Niu, J., H. Lin, J. Xu, H. Wu, and Y. Li, *Electrochemical mineralization of perfluorocarboxylic acids (PFCAs) by ce-doped modified porous nanocrystalline PbO2 film electrode.* Environmental Science & Technology, 2012. **46**(18): p. 10191-8.
158. Lin, H., J. Niu, S. Ding, and L. Zhang, *Electrochemical degradation of perfluorooctanoic acid (PFOA) by Ti/SnO2-Sb, Ti/SnO2-Sb/PbO2 and Ti/SnO2-Sb/MnO2 anodes.* Water Research, 2012. **46**(7): p. 2281-9.
159. Zhuo, Q., S. Deng, B. Yang, J. Huang, and G. Yu, *Efficient electrochemical oxidation of perfluorooctanoate using a Ti/SnO2-Sb-Bi anode.* Environmental Science & Technology, 2011. **45**(7): p. 2973-9.
160. Hao, S., Y.J. Choi, B. Wu, C.P. Higgins, R. Deeb, and T.J. Strathmann, *Hydrothermal Alkaline Treatment for Destruction of Per- and Polyfluoroalkyl Substances in Aqueous Film-Forming Foam.* Environmental Science & Technology, 2021. **55**(5): p. 3283-3295.
161. Wu, B., S. Hao, Y. Choi, C.P. Higgins, R. Deeb, and T.J. Strathmann, *Rapid Destruction and Defluorination of Perfluorooctanesulfonate by Alkaline Hydrothermal Reaction.* Environmental Science & Technology Letters, 2019. **6**(10): p. 630-636.

162. Hori, H., Y. Nagaoka, M. Murayama, and S. Kutsuna, *Efficient decomposition of perfluorocarboxylic acids and alternative fluorochemical surfactants in hot water.* Environmental Science & Technology, 2008. **42**(19): p. 7438-7443.
163. Hori, H., Y. Nagaoka, T. Sano, and S. Kutsuna, *Iron-induced decomposition of perfluorohexanesulfonate in sub- and supercritical water.* Chemosphere, 2008. **70**(5): p. 800-806.
164. Hori, H., Y. Noda, A. Takahashi, and T. Sakamoto, *Decomposition of Perfluorinated Ionic Liquid Anions to Fluoride Ions in Subcritical and Supercritical Water with Iron-Based Reducing Agents.* Industrial & Engineering Chemistry Research, 2013. **52**(38): p. 13622-13628.
165. Hori, H., H. Saito, H. Sakai, T. Kitahara, and T. Sakamoto, *Efficient decomposition of a new fluorochemical surfactant: perfluoroalkane disulfonate to fluoride ions in subcritical and supercritical water.* Chemosphere, 2015. **129**: p. 27-32.
166. Liu, C.S., C.P. Higgins, F. Wang, and K. Shih, *Effect of temperature on oxidative transformation of perfluorooctanoic acid (PFOA) by persulfate activation in water.* Separation and Purification Technology, 2012. **91**: p. 46-51.
167. Lee, Y.C., S.L. Lo, J. Kuo, and Y.L. Lin, *Persulfate oxidation of perfluorooctanoic acid under the temperatures of 20–40°C.* Chemical Engineering Journal, 2012. **198–199**: p. 27-32.
168. Lee, Y.C., S.L. Lo, P.T. Chiueh, Y.H. Liou, and M.L. Chen, *Microwave-hydrothermal decomposition of perfluorooctanoic acid in water by iron-activated persulfate oxidation.* Water Research, 2010. **44**(3): p. 886-892.
169. Lee, Y.C., S.L. Lo, P.T. Chiueh, and D.G. Chang, *Efficient decomposition of perfluorocarboxylic acids in aqueous solution using microwave-induced persulfate.* Water Research, 2009. **43**(11): p. 2811-2816.
170. Lee, Y., S. Lo, J. Kuo, and C. Hsieh, *Decomposition of perfluorooctanoic acid by microwave activated persulfate: Effects of temperature, pH, and chloride ions.* Frontiers of Environmental Science & Engineering, 2012. **6**(1): p. 17-25.
171. Hori, H., A. Yamamoto, K. Koike, S. Kutsuna, I. Osaka, and R. Arakawa, *Persulfate-induced photochemical decomposition of a fluorotelomer unsaturated carboxylic acid in water.* Water Research, 2007. **41**(13): p. 2962-2968.
172. Hori, H., A. Yamamoto, E. Hayakawa, S. Taniyasu, N. Yamashita, S. Kutsuna, H. Kiatagawa, and R. Arakawa, *Efficient Decomposition of Environmentally Persistent Perfluorocarboxylic Acids by Use of Persulfate as a Photochemical Oxidant.* Environmental Science & Technology, 2005. **39**(7): p. 2383-2388.
173. Hori, H., A. Ishiguro, K. Nakajima, T. Sano, S. Kutsuna, and K. Koike, *Visible light-induced decomposition of a fluorotelomer unsaturated carboxylic acid in water with a combination of tungsten trioxide and persulfate.* Chemosphere, 2013. **93**(11): p. 2732-2737.
174. Chen, J. and P. Zhang, *Photodegradation of perfluorooctanoic acid in water under irradiation of 254 nm and 185 nm light by use of persulfate.* Water Science and Technology, 2006. **54**(11-12): p. 317-325.
175. Bruton, T.A. and D.L. Sedlak, *Treatment of Aqueous Film-Forming Foam by Heat-Activated Persulfate Under Conditions Representative of In Situ Chemical Oxidation.* Environmental Science & Technology, 2017. **51**(23): p. 13878-13885.

176. Bruton, T.A. and D.L. Sedlak, *Treatment of perfluoroalkyl acids by heat-activated persulfate under conditions representative of in situ chemical oxidation.* Chemosphere, 2018. **206**: p. 457-464.
177. Bentel, M.J., Y. Yu, L. Xu, H. Kwon, Z. Li, B.M. Wong, Y. Men, and J. Liu, *Degradation of Perfluoroalkyl Ether Carboxylic Acids with Hydrated Electrons: Structure-Reactivity Relationships and Environmental Implications.* Environmental Science & Technology, 2020. **54**(4): p. 2489-2499.
178. Wang, S.N., Q. Yang, F. Chen, J. Sun, K. Luo, F.B. Yao, X.L. Wang, D.B. Wang, X.M. Li, and G.M. Zeng, *Photocatalytic degradation of perfluorooctanoic acid and perfluorooctane sulfonate in water: A critical review.* Chemical Engineering Journal, 2017. **328**: p. 927-942.
179. Bentel, M.J., Y. Yu, L. Xu, Z. Li, B.M. Wong, Y. Men, and J. Liu, *Defluorination of Per- and Polyfluoroalkyl Substances (PFASs) with Hydrated Electrons: Structural Dependence and Implications to PFAS Remediation and Management.* Environmental Science & Technology, 2019. **53**(7): p. 3718-3728.
180. Jin, L., P. Zhang, and T. Shao, *Factors Influencing the Ferric Ion-mediated Photochemical Decomposition of Perfluorooctane Sulfonate (PFOS) in Water.* Journal of Advanced Oxidation Technologies, 2015. **18**(1): p. 147-154.
181. Jin, L. and P.Y. Zhang, *Photochemical decomposition of perfluorooctane sulfonate (PFOS) in an anoxic alkaline solution by 185 nm vacuum ultraviolet.* Chemical Engineering Journal, 2015. **280**: p. 241-247.
182. Gatto, S., M. Sansotera, F. Persico, M. Gola, C. Pirola, W. Panzeri, W. Navarrini, and C.L. Bianchi, *Surface fluorination on TiO_2 catalyst induced by photodegradation of perfluorooctanoic acid.* Catalysis Today, 2015. **241, Part A**: p. 8-14.
183. Chen, M.J., S.L. Lo, Y.C. Lee, and C.C. Huang, *Photocatalytic decomposition of perfluorooctanoic acid by transition-metal modified titanium dioxide.* Journal of Hazardous Materials, 2015. **288**: p. 168-175.
184. Zhang, C., Y. Qu, X. Zhao, and Q. Zhou, *Photoinduced Reductive Decomposition of Perflurooctanoic Acid in Water: Effect of Temperature and Ionic Strength.* CLEAN – Soil, Air, Water, 2014. **43**: p. 223-228.
185. Sansotera, M., F. Persico, C. Pirola, W. Navarrini, A. Di Michele, and C.L. Bianchi, *Decomposition of perfluorooctanoic acid photocatalyzed by titanium dioxide: Chemical modification of the catalyst surface induced by fluoride ions.* Applied Catalysis B: Environmental, 2014. **148–149**: p. 29-35.
186. Qu, Y., C.J. Zhang, P. Chen, Q. Zhou, and W.X. Zhang, *Effect of initial solution pH on photo-induced reductive decomposition of perfluorooctanoic acid.* Chemosphere, 2014. **107**: p. 218-223.
187. Jin, L., P. Zhang, T. Shao, and S. Zhao, *Ferric ion mediated photodecomposition of aqueous perfluorooctane sulfonate (PFOS) under UV irradiation and its mechanism.* Journal of Hazardous Materials, 2014. **271**: p. 9-15.
188. Cheng, J.h., X.y. Liang, S.w. Yang, and Y.y. Hu, *Photochemical defluorination of aqueous perfluorooctanoic acid (PFOA) by VUV/Fe^{3+} system.* Chemical Engineering Journal, 2014. **239**: p. 242-249.
189. Song, Z., H. Tang, N. Wang, and L. Zhu, *Reductive defluorination of perfluorooctanoic acid by hydrated electrons in a sulfite-mediated UV photochemical system.* Journal of Hazardous Materials, 2013. **262**: p. 332-338.

190. Shao, T., P. Zhang, L. Jin, and Z. Li, *Photocatalytic decomposition of perfluorooctanoic acid in pure water and sewage water by nanostructured gallium oxide.* Applied Catalysis B: Environmental, 2013. **142–143**: p. 654-661.
191. Phan Thi, L.A., H.T. Do, Y.C. Lee, and S.L. Lo, *Photochemical decomposition of perfluorooctanoic acids in aqueous carbonate solution with UV irradiation.* Chemical Engineering Journal, 2013. **221**: p. 258-263.
192. Zhao, B., M. Lv, and L. Zhou, *Photocatalytic degradation of perfluorooctanoic acid with β-Ga2O3 in anoxic aqueous solution.* Journal of Environmental Sciences, 2012. **24**(4): p. 774-780.
193. Song, C., P. Chen, C. Wang, and L. Zhu, *Photodegradation of perfluorooctanoic acid by synthesized TiO_2–MWCNT composites under 365 nm UV irradiation.* Chemosphere, 2012. **86**(8): p. 853-859.
194. Li, X., P. Zhang, L. Jin, T. Shao, Z. Li, and J. Cao, *Efficient Photocatalytic Decomposition of Perfluorooctanoic Acid by Indium Oxide and Its Mechanism.* Environmental Science & Technology, 2012. **46**(10): p. 5528-5534.
195. Giri, R.R., H. Ozaki, T. Okada, S. Taniguchi, and R. Takanami, *Factors influencing UV photodecomposition of perfluorooctanoic acid in water.* Chemical Engineering Journal, 2012. **180**: p. 197-203.
196. Park, H., C.D. Vecitis, J. Cheng, N.F. Dalleska, B.T. Mader, and M.R. Hoffmann, *Reductive degradation of perfluoroalkyl compounds with aquated electrons generated from iodide photolysis at 254 nm.* Photochemical & Photobiological Sciences, 2011. **10**(12): p. 1945-1953.
197. Ochiai, T., Y. Iizuka, K. Nakata, T. Murakami, D.A. Tryk, Y. Koide, Y. Morito, and A. Fujishima, *Efficient Decomposition of Perfluorocarboxylic Acids in Aqueous Suspensions of a TiO_2 Photocatalyst with Medium-Pressure Ultraviolet Lamp Irradiation under Atmospheric Pressure.* Industrial & Engineering Chemistry Research, 2011. **50**(19): p. 10943-10947.
198. Giri, R.R., H. Ozaki, T. Morigaki, S. Taniguchi, and R. Takanami, *UV photolysis of perfluorooctanoic acid (PFOA) in dilute aqueous solution.* Water Science and Technology, 2011. **63**(2): p. 276-282.
199. Wang, B.B., M.H. Cao, Z.J. Tan, L.L. Wang, S.H. Yuan, and J. Chen, *Photochemical decomposition of perfluorodecanoic acid in aqueous solution with VUV light irradiation.* Journal of Hazardous Materials, 2010. **181**(1–3): p. 187-192.
200. Qu, Y., C. Zhang, F. Li, J. Chen, and Q. Zhou, *Photo-reductive defluorination of perfluorooctanoic acid in water.* Water Research, 2010. **44**(9): p. 2939-2947.
201. Estrellan, C.R., C. Salim, and H. Hinode, *Photocatalytic decomposition of perfluorooctanoic acid by iron and niobium co-doped titanium dioxide.* Journal of Hazardous Materials, 2010. **179**(1–3): p. 79-83.
202. Cao, M.H., B.B. Wang, H.S. Yu, L.L. Wang, S.H. Yuan, and J. Chen, *Photochemical decomposition of perfluorooctanoic acid in aqueous periodate with VUV and UV light irradiation.* Journal of Hazardous Materials, 2010. **179**(1–3): p. 1143-1146.
203. Panchangam, S.C., A.Y.C. Lin, K.L. Shaik, and C.F. Lin, *Decomposition of perfluorocarboxylic acids (PFCAs) by heterogeneous photocatalysis in acidic aqueous medium.* Chemosphere, 2009. **77**(2): p. 242-248.

204. Wang, Y., P.Y. Zhang, G. Pan, and H. Chen, *Photochemical degradation of environmentally persistent perfluorooctanoic acid (PFOA) in the presence of Fe(III).* Chinese Chemical Letters, 2008. **19**(3): p. 371-374.
205. Wang, Y., P. Zhang, G. Pan, and H. Chen, *Ferric ion mediated photochemical decomposition of perfluorooctanoic acid (PFOA) by 254 nm UV light.* Journal of Hazardous Materials, 2008. **160**(1): p. 181-186.
206. Yamamoto, T., Y. Noma, S.I. Sakai, and Y. Shibata, *Photodegradation of Perfluorooctane Sulfonate by UV Irradiation in Water and Alkaline 2-Propanol.* Environmental Science & Technology, 2007. **41**(16): p. 5660-5665.
207. Huang, L., W. Dong, and H. Hou, *Investigation of the reactivity of hydrated electron toward perfluorinated carboxylates by laser flash photolysis.* Chemical Physics Letters, 2007. **436**(1–3): p. 124-128.
208. Hori, H., A. Yamamoto, K. Koike, S. Kutsuna, I. Osaka, and R. Arakawa, *Photochemical decomposition of environmentally persistent short-chain perfluorocarboxylic acids in water mediated by iron(II)/(III) redox reactions.* Chemosphere, 2007. **68**(3): p. 572-578.
209. Chen, J., P.-Y. Zhang, and J. Liu, *Photodegradation of perfluorooctanoic acid by 185 nm vacuum ultraviolet light.* Journal of Environmental Sciences (China), 2007. **19**(4): p. 387-390.
210. Chen, J., P. Zhang, and L. Zhang, *Photocatalytic Decomposition of Environmentally Persistent Perfluorooctanoic Acid.* Chemistry Letters, 2006. **35**(2): p. 230-231.
211. Hori, H., A. Yamamoto, and S. Kutsuna, *Efficient Photochemical Decomposition of Long-Chain Perfluorocarboxylic Acids by Means of an Aqueous/Liquid CO_2 Biphasic System.* Environmental Science & Technology, 2005. **39**(19): p. 7692-7697.
212. Hori, H., E. Hayakawa, H. Einaga, S. Kutsuna, K. Koike, T. Ibusuki, H. Kiatagawa, and R. Arakawa, *Decomposition of Environmentally Persistent Perfluorooctanoic Acid in Water by Photochemical Approaches.* Environmental Science & Technology, 2004. **38**(22): p. 6118-6124.
213. USEPA, *Method 533: Determination of Per- and Polyfluoroalkyl Substances in Drinking Water by Isotope Dilution Anion Exchange Solid Phase Extraction and Liquid Chromatography/Tandem Mass Spectrometry*. 2019.
214. Shoemaker, J. and T. D., *Method 537.1 Determination of Selected Per- and Polyflourinated Alkyl Substances in Drinking Water by Solid Phase Extraction and Liquid Chromatography/Tandem Mass Spectrometry (LC/MS/MS).* USEPA, Editor. 2020.
215. USEPA, *Validated Test Method 8327: Per-and Polyfluoroalkyl Substances (PFAS) Using External Standard Calibration and Multiple Reaction Monitoring (MRM) Liquid Chromatography/Tandem Mass Spectrometry (LC/MS/MS).* 2019.
216. Ritter, E.E., M.E. Dickinson, J.P. Harron, D.M. Lunderberg, P.A. DeYoung, A.E. Robel, J.A. Field, and G.F. Peaslee, *PIGE as a screening tool for Per- and polyfluorinated substances in papers and textiles.* Nuclear Instruments and Methods in Physics Research Section B: Beam Interactions with Materials and Atoms, 2017. **407**: p. 47-54.
217. Jamari, N.L.A., J.F. Dohmann, A. Raab, E.M. Krupp, and J. Feldmann, *Novel non-target analysis of fluorine compounds using ICPMS/MS and HPLC-ICPMS/MS.* Journal of Analytical Atomic Spectrometry, 2017. **32**(5): p. 942-950.
218. Yeung, L.W., Y. Miyake, P. Li, S. Taniyasu, K. Kannan, K.S. Guruge, P.K. Lam, and N. Yamashita, *Comparison of total fluorine, extractable organic fluorine and perfluorinated compounds in the blood of wild and pefluorooctanoate (PFOA)-exposed rats: evidence for*

the presence of other organofluorine compounds. Analytica Chimica Acta, 2009. **635**(1): p. 108-14.
219. Okaru, A.O., T.S. Brunner, S.M. Ackermann, T. Kuballa, S.G. Walch, M. Kohl-Himmelseher, and D.W. Lachenmeier, *Application of (19)F NMR Spectroscopy for Content Determination of Fluorinated Pharmaceuticals.* Journal of Analytical Methods in Chemistry, 2017. **2017**: p. 9206297.
220. Boča, M., P. Barborík, M. Mičušík, and M. Omastová, *X-ray photoelectron spectroscopy as detection tool for coordinated or uncoordinated fluorine atoms demonstrated on fluoride systems NaF, K2TaF7, K3TaF8, K2ZrF6, Na7Zr6F31 and K3ZrF7.* Solid State Sciences, 2012. **14**(7): p. 828-832.
221. Al Amin, M., Z. Sobhani, Y. Liu, R. Dharmaraja, S. Chadalavada, R. Naidu, J.M. Chalker, and C. Fang, *Recent advances in the analysis of per- and polyfluoroalkyl substances (PFAS)—A review.* Environmental Technology & Innovation, 2020. **19**.

Chapter 3

Acoustic Destruction of Per- and Polyfluoroalkyl Substances (PFASs): Mixtures, Ground-water and Investigation Derived Waste

Abstract

We tested the destruction of 7 individual per- and polyfluoroalkyl substances (PFASs), a mix of 24 native PFASs (24Mix), AFFF, and concentrated Investigation derived waste (IDW) in deionized water, groundwater containing low total dissolved solids (TDS) (388 $mg.L^{-1}$), and high TDS groundwater (10.2 $g.L^{-1}$) by high-frequency ultrasound (700 kHz). This study demonstrated the mineralization of hexafluoropropylene oxide dimer acid (HFPO-DA) and 6:2 fluorotelomer sulfonamidoalkyl betaine (6:2 FTAB) with near-stoichiometric fluoride release. The degradation rates of sulfonates and short-chain PFASs were 30% to 60% higher in low TDS groundwater than in deionized water, while the rates were repressed in high TDS groundwater. The degradation rates of sulfonates in AFFF were 40% to 60% higher compared to the 24Mix. The salts and surfactants affect the air-water partitioning coefficients of PFASs and their availability at the ultrasonic cavity, thereby affecting the degradation rates. The treatment of concentrated, high-TDS IDW resulted in significant mineralization of 41 PFASs, consuming 3 $kWh.g^{-1}$ - 76 $kWh.g^{-1}$ whereas, dilute AFFF degradation utilized 5900 $kWh.g^{-1}$. Important parameters for designing and operating an ultrasonic reactor for the degradation of PFASs are also discussed. Our results imply that sonolysis utilized for the treatment of concentrated PFAS mixtures and AFFF IDWs can mineralize PFASs without the production of disinfection by-products.

3.1 Introduction

There are more than 5000 different compounds identified as per- and polyfluoroalkyl substances (PFASs) and more are being synthesized as safer alternatives to the legacy compounds like perfluorooctanoic acid (PFOA) and perfluorooctanesulfonic acid (PFOS) [1]. These chemicals are designed to be flame retardants and have amphipathic properties because of the oleophilic C-F chains and hydrophilic headgroups. These properties have led to their widespread use in domestic and commercial products for more than 60 years and consequently, PFASs have impacted various environments [2-4]. PFAS are being called 'forever chemicals' because of their ubiquitous presence in the environment and recalcitrance towards traditional remediation approaches. Presently, the treatment of PFAS impacted water is primarily based on using separation agents like activated carbon or ion exchange resins, followed by their landfilling or incineration [5-8]. Largely, the existing PFAS degradation technologies have had limited success because of the varying properties of different compounds, the inability of the hydroxyl radicals to react with PFASs [9], and the production of harmful degradation byproducts [5, 10, 11]. Moreover, most of the studies were performed in pure water at high concentrations instead of the environmental samples and relevant concentrations [11]. In general, physicochemical treatment processes available to treat PFAS impacted water have some limitations. For example, photochemical processes and heat-activated persulfate treatment have been unsuccessful for the treatment of PFSAs, and PFASs in real waters, electrochemical treatment requires expensive electrode synthesis, and mineral precipitation can cause electrode passivation leading to the formation of toxic byproducts. The reductive processes like eBeam and plasma utilizing hydrated electrons generated by water splitting are in the early stages of development and may produce recalcitrant polyfluorinated ether byproducts from the treatment of novel PFASs like HFPO-DA.

These treatment technologies may produce shorter chain intermediates that can be even more recalcitrant than the parent compounds [9, 12-19].

The treatment technologies capable of mineralizing PFASs are but a few; one such technology is the destruction of PFASs by ultrasonic cavities. Ultrasonic treatment technology employs high-energy ultrasound (> 20 kHz) producing nano - microscale cavities that implode, raising the temperature in the nano environment up to 5000 K. The high temperatures and pressures in these cavities have been shown to pyrolyze the chemical bonds thereby mineralizing PFASs [20-25]. Ultrasound of 20-40 kHz produces shockwaves and is used regularly in medicine for cleaning and sterilization [26, 27], medical treatments like liposuction, and Extracorporeal Shock Wave Lithotripsy (ESWL) to treat kidney stones [28]. Ultrasonic humidification [29] and medical diagnostic imaging [30] utilize frequencies greater than 1 MHz that cause weaker cavitations [31]. The ultrasonic frequency range of 100 kHz – 1 MHz generates smaller size and high-temperature cavitation [21] and therefore is best suited for environmental remediation applications. Energy requirements for ultrasonic treatment are higher than other technologies [9, 32], however, the ability of ultrasound to mineralize PFASs without producing shorter chain intermediates makes it advantageous for destruction of PFASs [33].

Utilizing ultrasound as a primary treatment or post-treatment block in a treatment train for the degradation of high PFAS load mixtures might prove more efficient. Sonication can also be a point-of-use under-the-sink technology for the treatment of impacted water, as minimal technical know-how is needed for the operation of the reactor. Little information is available regarding the optimal operating conditions of an ultrasonic reactor to achieve higher PFASs degradation rates. Furthermore, the matrix constituents like salt and surfactants have been reported to affect the surface tension and consequently change the ultrasonic degradation kinetics of PFASs [34-37].

The decrease in the surface tension increases the separation of PFASs to the air-water interface creating a PFAS-LNAPL and decreasing their availability in the reaction [35, 36]. The ultrasonic destruction of Investigation Derived Waste (IDW) has hitherto remained untested. The destruction of PFAS IDWs has only been demonstrated by Singh et al. using a bench-scale plasma-based reactor [32]. There is a critical need to develop a better understanding of the effects of matrix constituents on ultrasonic degradation kinetics, specifically for the treatment of environmental waters and complex PFAS mixtures.

The objective of this study was to explore the ability of high-frequency ultrasound to degrade individual PFASs, PFAS mixtures, high concentration IDW, and PFASs in diluted AFFF using a custom-built bench-scale reactor. This paper presents the first account of ultrasonic mineralization of HFPO-DA, zwitterionic compounds like 6:2 FTAB, and high TDS concentrated IDW by ultrasound. We also investigated the extent of mineralization and potential generation of disinfection byproducts.

3.2 Materials and Methods

3.2.1 PFAS Sample Preparation

The acoustic degradation of 7 individual PFASs, a 24 mix of PFAS, diluted AFFF, and PFAS IDW was tested in different matrices to examine the effect of matrix constituents and system conditions on the degradation kinetics. 7 individual PFASs, 24Mix of standard PFASs, and the respective labeled compounds for internal standards (Table 3.1) were obtained from Wellington Labs (Guelph, Ontario, Canada). The AFFF mixture was donated by Dr. Paul Hatzinger, APTIM, and 2,3,3,3-tetrafluoro-2-(heptafluoropropoxy)propanoic acid (HFPO-DA 97%) was purchased

from Matrix Scientific, Columbia, SC. Respective mass-labeled internal standards were provided by Wellington Labs (Guelph, Ontario, Canada). The IDW was derived from an undisclosed location in Los Angeles metropolitan area. The groundwater (Table 3.2) was obtained from two AFFF-impacted sites and was stored in sealed polypropylene containers in dark at 4 °C.

Table 3.1: List of PFASs tested for degradation by ultrasound. The PFASs and their respective internal standards were obtained from Wellington Labs (Guelph, Ontario, Canada). #d-N-EtFOSAM was used as an internal standard for 6:2FTAB.

Name of Compound	Abbreviations
perfluoro-n-octanoic acid	PFOA
sodium perfluoro-1-octanesulfonate	PFOS
potassium perfluoro-1-butanesulfonate	PFBS
sodium 1H,1H,2H,2H-perfluorooctane sulfonate	6:2FTS
perfluoro -1-octanesulfonamide	FOSA
N-(carboxymethyl)N,N-dimethyl-N-[3-(1H,1H,2H,2H-perfluoro-1-octanesulfonamido)propan-1-yl] ammonium	6:2FTAB#
Mix of 24 standard PFASs (24 components)	24Mix
Internal Standards	
perfluoro-n-[1,2,3,4-13C4] octanoic acid	MPFOA
sodium perfluoro-1-[1,2,3,4-$^{13}C_4$] octanesulfonate	MPFOS
sodium perfluoro-1-[2,3,4-$^{13}C_3$]- butanesulfonate	M3PFBS
sodium 1H,1H,2H,2H-perfluoro-1-[1,2-$^{13}C_4$]-octane sulfonate	M2-6:2FTS
perfluoro-1-[$^{13}C_8$] octanesulfonamide	M8FOSA
N-ethyl-d5-perfluoro-1-octanesulfonamide	d-N-EtFOSAM
2,3,3,3-Tetrafluoro-2-(1,1,2,2,3,3,3-heptafluoropropoxy)-$^{13}C_3$-propanoic acid	M3HFPO-DA
Labeled PFAS standards for 24Mix (19 components)	MPFAC-24ES

Table 3.2: Groundwater Characteristics. The groundwater was collected from two different sites in the USA. High concentrations of ions are indicated in grey-shaded cells.

Characteristic	High TDS Groundwater	Low TDS Groundwater
Fluoride (mg.L^{-1})	N.D.	3.3
Chloride (mg.L^{-1})	5283.7	55.5
Nitrite (mg.L^{-1})	15.4	N.D.
Bromide (mg.L^{-1})	17.4	N.D.
Nitrate (mg.L^{-1})	11.0	4.0
Sulfate (mg.L^{-1})	1955.5	19.7
Sodium (mg.L^{-1})	3203.0	25.1
Aluminum (mg.L^{-1})	N.D.	N.D.
Magnesium (mg.L^{-1})	581.6	13.4
Calcium (mg.L^{-1})	1145.0	96.1
Manganese (mg.L^{-1})	1.7	0.02
Iron (mg.L^{-1})	0.05	N.D.
TDS (mg.L^{-1})	10200	388
pH	6.70	6.70
Specific Conductance (µS.cm^{-1})	16000	610
TOC (mg.L^{-1})	6.43	4.45

3.2.2 Reactor Design and Operation

The PFAS spiked or impacted deionized water, impacted groundwater, or IDW was treated using high-frequency ultrasound in a custom-built bench-scale reactor supplied by PCT Systems, Inc. (San Jose, California). The reactor body with 2000 mL maximum working volume was made of polypropylene with a polypropylene air-tight lid (Figure A 1). It was equipped with ports for sample collection and gas circulation, and high-density polyethylene (HDPE) or stainless-steel cooling coils. The ultrasonic energy was produced by an array of piezoelectric transducers under the stainless-steel plate forming the base of the reaction vessel (Figure A 1). The experiments were performed either using a 700 kHz - 250 W system or 700 kHz - 1040 W system or 900 kHz - 572 W system for four hours in a high purity Argon (99.999%) atmosphere. The different frequencies were tested to observe their effect on PFAS degradation kinetics [31, 38, 39]. The appropriate volume of PFAS impacted water (deionized or groundwater), IDW, and AFFF were prepared in polypropylene bottles. The PFAS or AFFF impacted deionized water or groundwater were prepared by spiking the water with individual compounds or mixtures of PFASs as needed. The IDW was centrifuged at 7000 × g to remove the suspended material and the clear supernatant was then sonicated. The impacted water or IDW supernatant was then added into the reactor vessel, followed by 30 minutes of Argon sparging at 5.7×10^{-2} $m^3.h^{-1}$ to allow for an argon saturated reaction environment. The flow of argon was monitored using an inline flow meter. In open system experimental conditions, the gas could continuously escape the reactor for the period of the experiment while the gas inflow was maintained at 5.7×10^{-2} $m^3.h^{-1}$. However, in closed system experimental conditions, after the first 30 min of argon sparging the reactor was maintained completely airtight for the period of the sonication experiment. The power density (P_d) was varied by varying the treatment volume (200 mL, 500 mL, 1000 mL, 1500 mL, and 2000 mL). A sample

(5 mL) was collected every 30 min using a sterile 1 mL polypropylene syringe and stored in 15 mL polypropylene tubes at 4 °C till needed for analysis. For all experiments, the reactor was maintained at 10 °C using a recirculating water bath, for the period of the sonication experiment.

3.2.3 Degradation of AFFF components by Bio – Sono Treatment Train

To evaluate the treatment of AFFF components by laccase derived from *T. versicolor,* 400 mL, 0.2 M bi-phosphate buffer (pH 6) was spiked with AFFF to achieve a final concentration of 80 µL/L. The reactions were initiated by adding 1 $U.mL^{-1}$ laccase and 20 mM 1-hydroxybenzotriazole (HBT). The 1 $U.mL^{-1}$ laccase and 20 mM HBT were supplemented every 6 days. All experiments were performed in 2000 mL baffled flasks equipped with 0.2 µm air filters at 30 °C and 150 rpm. The flasks were kept open to air for 30 min every day to ensure aerobic conditions. The 0 h samples (200 µL) were collected immediately after the addition of the AFFF and 200 µL samples were collected after 30 days of adding AFFF. The collected samples were quenched by adding an equal volume of methanol. The samples were then filtration through a 0.2 µm polyethersulfone (PES) filter to remove suspended particulates and stored at -20 °C, till needed for analysis. All reactions were kept in similar conditions and conducted in triplicate to ensure the statistical significance of the data.

Following the degradation of AFFF spiked phosphate buffer (0.2M, pH 6) by laccase HBT system, the triplicate laccase treated solutions were pooled together to obtain a 200 mL solution and centrifuged at 7000 × g for 15 min to remove any suspended particulate matter. The solution was then treated using 700 kHz ultrasound for 4 h in a 250 W open system (P_d = 1250 $W.L^{-1}$). 5 mL samples were collected every 30 min and stored at -20 °C, till needed for analysis.

3.2.4 Electro - Sono Treatment Train

Post-treatment in the electrochemical reactor for 15 min, 200 mL AFFF spiked deionized (1:12500) water containing 1.6 g.L^{-1} KH_2PO_4, 0.4 g.L^{-1} Na_2HPO_4, 0.057 g.L^{-1} $CaCl_2 \cdot 2H_2O$, and 0.5 g.L^{-1} $MgSO_4 \cdot 7H_2O$ was treated using 700 kHz ultrasound for 4 h in a 250 W open system (P_d = 1250 W.L^{-1}). 5 mL samples were collected every 30 min and stored at -20 °C till needed for analysis.

The electrochemical flow cell (Advanced Diamond Technologies Inc., Romeoville, IL) held a stainless-steel cathode and a boron-doped diamond (BDD) anode with an active surface area of 44 cm^2. An electrolyte containing 1.6 g/L of KH_2PO_4 and 0.4 g/L of Na_2HPO_4 were chosen based on the treatment medium. The electrolyte solution was then spiked with a 1:12500 dilution of aqueous film-forming foam (AFFF) was recirculated from a polypropylene container at a flow rate of 3 L/min and a current density of 90 to 125 mA/cm^2.

3.2.5 Performance Metrics

PFAS removal percentage was calculated by (equation 3.1)

$$\text{PFAS removal (\%)} = \frac{C_o - C}{C_o} \times 100 \qquad (3.1)$$

where C_o is the initial PFAS concentration and C is the final PFAS concentration. Fluoride mass balance was performed by calculating the fluoride concentration corresponding to the PFAS concentration detected by LC-MS/MS (equation 3.2).

$$C_F = \frac{C_{PFAS} \times N \times M_F}{M_{PFAS}} \qquad (3.2)$$

where C_{PFAS} is the concentration of PFAS, N is the number of fluorine atoms in the PFAS compound, M_F is the molecular weight of fluorine, and M_{PFAS} is the molecular weight of the PFAS compound. This estimate was then compared with the fluoride concentration detected by the IC. The pseudo-first-order rates were calculated using the initial rate method [40] and the kinetics were modeled as (equation 3.3)

$$\frac{dC_{PFAS}}{dt} = -k \times C_{PFAS} \quad (3.3)$$

The energy consumption for PFAS degradation by ultrasound was calculated as the energy consumed for total mass removed (equation 3.4) or as the energy consumed per order of magnitude removal (equation 3.5).

$$E_{EM} = \frac{P \times t \times 10^3}{V(C_i - C_f)} \quad (3.4)$$

$$E_{EO} = \frac{P \times t \times 10^3}{V \times \log(C_i/C_f)} \quad (3.5)$$

where E_{EM} is the energy consumed per mass removed ($kWh.g^{-1}$), E_{EO} is the energy consumed per order of magnitude removal ($kWh.m^{-3}.order^{-1}$), P is the rated power (kW), t is time (h), V is the volume (L), C_i is the initial cumulative PFAS concentration ($mg.L^{-1}$), and C_f is the final cumulative PFAS concentration ($mg.L^{-1}$). The power density was calculated as (equation 3.6)

$$\text{PowerDensity } (P_d)\left(\frac{W}{L}\right) = \frac{I \times v}{V} \quad (3.6)$$

where I is the current drawn for acoustics (A), v is the voltage (V), V is the volume of water treated (L). The calorimetric power density is 62.2% of the electrical power and can be calculated as described by Laugier et al.[41]

3.2.6 Analytical Methods

For all PFAS analyses, an aliquot (1000 µL) was taken from the 5 mL samples collected at different time points and centrifuged at 20000 × g for 5 min. The supernatant (500 µL) of the centrifuged samples was then transferred to a fresh 2 mL polypropylene tube followed by dilution in 500 µL methanol. Respective internal standards were added immediately at a concentration of 50 $\mu g.L^{-1}$ each. Samples were stored at -20 °C and shipped overnight in cold packaging to Colorado State University and analyzed within ≤3 days of sample shipment.

Analyses of PFASs in the mixture and pure compound-spiked solutions were performed on an Agilent 1290 liquid chromatograph coupled to an Agilent 6460 triple quadrupole mass spectrometer (LC/QqQ-MS), which was equipped with an electrospray ionization (ESI) source using Agilent Jet Stream Technology (Agilent, Santa Clara, CA). Analytes were separated on an Agilent Poroshell C18 column (2.1 mm x 100 mm, 2.7 µm particle size) at 40 °C. A sample volume of 15 µL was injected into a binary mixture of 5 mM ammonium acetate in water (A) and 5 mM ammonium acetate in methanol (B) at a flow rate of 0.4 $mL.min^{-1}$. The gradient used was 20% of solution B for 1 minute, increasing to 45% of solution B at 2 min, and finally increased to 100% of solution B at 5 min. The ionization source conditions used were as follows: negative polarity, nebulizer of 15 psi, gas flow of 4 $L.min^{-1}$ at 230°C, sheath gas flow of 12 $L.min^{-1}$ at 350 °C, nozzle voltage of 500 V, and capillary voltage at 3500 V. Analytes were identified by comparison of retention times with analytical standards, individual MRM mass transitions, and with MS/MS ion ratios. Peaks matching retention within 5% and with ion ratios at 20% of the standard ratio were considered acceptable for identification. The data collection and processing were performed by using Agilent MassHunter Quantitative software (v B.07.01). Quantitation was performed with

linear regression using calibration curves from 0.01-250 ng.mL^{-1}. Several steps were taken to minimize system-related interferences or background. An Agilent Eclipse Plus C18 column (4.6 mm x 50 mm, 5 μm particle size) was installed immediately after the binary pump and prior to the injection port to perform as a delay column. The mobile phase degasser was bypassed allowing the mobile phase to enter the binary pump directly and avoiding contact with plastic filters. All plastic tubing in the LC-MS/MS system was replaced with PEEK tubing and plastic frits were replaced with stainless steel. All sample vials were polypropylene with polypropylene caps. Five injections of pure methanol were made prior to sample analysis to determine if any system background analyte levels were present. With these system changes, background levels for each analyte were not detected in blank samples.

Analysis of PFASs in AFFF-spiked solutions and in IDW was performed on an Agilent 1290 Liquid Chromatograph paired with an Agilent 6530 Quadrupole Time-of-Flight Mass Spectrometer (LC/QToF-MS) in both negative and positive ESI modes. Liquid chromatography was performed with a 2.1 x 150 mm, 5 μm Atlantis dC18 column (Waters), a 2.1 mm x 5 mm, 5 μm Atlantis dC18 VanGuard guard column (Waters), and a mobile phase consisting of 5 mM ammonium acetate in water (A) and 5 mM ammonium acetate in methanol (B) at a flow rate of 0.5 mL.min^{-1}. A gradient method was used at 30 °C, starting at 55% of solution B for 2.5 minutes, then constantly increasing to 60% of solution B by 7 minutes and 80% of solution B by 12 minutes, and held at 80% of solution B until 30 minutes. Negative ESI mode was performed with a capillary voltage of 3500 V, a fragmentor voltage of 150, a gas temperature of 350 °C, and the two reference masses 119.036320 and 980.016375. Positive ESI mode was performed with the same settings and the two reference masses 121.050873 and 922.009798. Nitrogen (>99.999% purity, Airgas) was used as the nebulizer and drying gas with flow rates of 9 and 11 L.min^{-1}, respectively. High-

resolution accurate mass spectra were recorded across the range *m/z* 50 - 1500. The identities of all PFAS species reported here were validated by comparison to analytical standards. The changes in concentrations for the incubation (24 h, 48h, and 8 days) of 25 PFASs in 50:50 methanol:water can be found in Table 3.3.

Table 3.3: Change in concentrations observed for incubation of 20 µg.L^{-1} PFASs in 50:50 methanol:water. The samples were incubated at room temperature for 24 h, 48 h, and 8 days in 200 µL polypropylene HPLC injection vials. *MFOSA was used as an internal standard for PFDS. ^MPFDoA was used as an internal standard for PFTrDA. #d-N-EtFOSAM was used as an internal standard for 6:2FTAB.

Compounds	Change in Concentration (%)			Detection Limit (µg.L^{-1})
	24 h	48 h	8 days	
PFBA	-0.53%	-0.33%	-0.85%	0.05
PFPeA	-2%	-2%	-0.80%	0.03
PFBS	0.85%	0.86%	1.96%	0.02
4:2FTS	1.81%	0.36%	0.44%	0.06
PFHxA	3.88%	1.90%	2.50%	0.03
PFPeS	9.10%	7.98%	7.62%	0.02
PFHpA	1.10%	1.11%	2.92%	0.02
PFHxSK	2.40%	2.34%	0.33%	0.03
6:2 FTS	1.06%	-2.13%	2.11%	0.05
PFOA	-6.33%	-1.00%	-6.95%	0.01
PFHpS	5.37%	2.37%	8.62%	0.04
PFOS	-4.89%	-2.32%	-12.72%	0.04
PFNA	3.89%	3.09%	14.85%	0.04
PFNS	-0.02%	-1.77%	0.00%	0.07
PFDA	-3.36%	-4.70%	-0.54%	0.02
8:2 FTS	-11.74%	-8.30%	-6.22%	0.07
N-MeFOSAA	3.29%	-1.60%	-4.00%	0.03
FOSA	-1.19%	-0.66%	-1.61%	0.02
PFDS*	-5.42%	-24.63%	-18.97%	0.04
PFUdA	-0.62%	-1.45%	-1.35%	0.02
N-EtFOSSA	1.02%	-5.92%	-4.72%	0.04
PFDoA	3.11%	1.73%	4.34%	0.03
PFTrDA^	-43.90%	-77.81%	-71.88%	0.02
PFTeDA	-0.95%	-1.22%	-1.29%	0.02
6:2FTAB#	-	-	-	0.03

For the quantification of fluoride, chlorate, and perchlorate, filtered samples (0.22 µm-filtered) were injected onto an ion chromatograph (Dionex Integrion HPIC, Thermo Fisher Scientific) equipped with an IonPac™ AG16 Guard Column (4 x 50 mm) and Dionex™ IonPac™ AS16 Analytical Column (250 m x 4.0 mm ID) operated at 30 °C. Chromatographic separation of anions was achieved by running a gradient of aqueous hydroxide mobile phase ramping from 0.5

mM to 55 mM at a flow rate of 1 $mL.min^{-1}$ for a total run time of 35 min. Anions were detected using a conductivity detector with elution patterns confirmed by standards; the detection limit for all three anions was 0.007 $mg.L^{-1}$.

3.3 Results and Discussion

3.3.1 Sonolysis of PFASs in Deionized water and Groundwater

The acoustic irradiation of PFASs in deionized water and the two groundwater samples demonstrated similar pseudo-first-order kinetics at the tested concentrations with more than 98% degradation of most species in 120 min, except in the high TDS groundwater. The acoustic degradation of 6:2 FTAB and HFPO-DA-spiked deionized water, when performed independently in a 700 kHz - 1040 W closed system (P_d = 1040 $W.L^{-1}$), followed pseudo-first-order kinetics. 94% of 6:2 FTAB (4 $mg.L^{-1}$ to 237 $\mu g.L^{-1}$) was destroyed at a rate constant of 0.025 ± 0.0012 min^{-1} and 99% HFPO-DA (23 $mg.L^{-1}$ to 232 $\mu g.L^{-1}$) was destroyed at a rate of 0.010 ± 0.0008 min^{-1}. Aqueous fluoride concentration was found to increase during ultrasound irradiation with an observed defluorination efficiency of 98% for 6:2 FTAB and 99% for HFPO-DA (Figure 3.1b). Complete fluoride recovery during the ultrasonic degradation of HFPO-DA and 6:2 FTAB suggests a low potential for the generation of intermediates. A linear increase in aqueous fluoride concentration suggests the direct mineralization of HFPO-DA. However, a delayed increase in fluoride for the ultrasonic degradation of 6:2 FTAB indicates the generation of short-lived fluorocarbon intermediates followed by the eventual complete mineralization of the zwitterion. Degradation of HFPO-DA in deionized water (900 $\mu g.L^{-1}$ and 27 $mg.L^{-1}$) was also tested in the 700 kHz - 250 W open system (P_d = 1250 $W.L^{-1}$) for 240 min at 10 °C. 96% HFPO-DA was removed for the starting

concentration of 867 µg.L^{-1} at a rate of 0.032 ± 0.0030 min^{-1} while for the starting concentration of 27 mg.L^{-1} 85% HFPO-DA was removed at a rate of 0.012 ± 0.00027 min^{-1} (Figure A 2). The degradation kinetics of HFPO-DA at higher concentrations (27 mg.L^{-1} and 23 mg.L^{-1}) was closer to zero-order, while at lower concentrations (900 µg.L^{-1}), the degradation was pseudo-first-order. Similarly, degradation of PFOA, when treated in the 700 kHz - 250 W open system (P_d = 1250 W.L^{-1}), also followed pseudo-first-order kinetics (Figure A 2). The degradation rates were statistically similar across three orders of magnitude in PFOA concentrations (10 µg.L^{-1}, 180 µg.L^{-1}, and 1200 µg.L^{-1}). Other studies have also reported that at lower starting concentrations, the sonolysis of PFASs follows pseudo-first-order kinetics. However, at PFAS concentrations higher than the kinetics transition concentration, the acoustic degradation kinetics were zero-order. At high starting concentrations, the availability of PFASs is limited by their diffusion to the cavity from the aqueous bulk solution [20, 33, 42].

The sonication of low TDS groundwater spiked with individual compounds using a 700 kHz - 250 W open system (P_d = 1250 W.L^{-1}) demonstrated pseudo-first-order kinetics with higher than 90% degradation of PFBS and more than 97% degradation of PFOA, PFOS, 6:2 FTS, FOSA, and 6:2 FTAB. The sonication of deionized water spiked with the same compounds in individual experiments demonstrated similar pseudo-first-order kinetics (Figure A 3). In deionized water the concentration was reduced by 99% for PFOA, 98% for PFOS, 98% for 6:2 FTAB, 100% for FOSA, 90% for PFBS, and 97% for 6:2 FTS. In low TDS groundwater, the ultrasound removed 90% PFOA, 30% PFOS, 100% 6:2 FTAB, 88% FOSA, 97% PFBS, and 95% 6:2 FTS. In agreement with previously published studies, for the same chain length, the observed rate constants for sulfonates were lower than those of carboxylates whereas, for the same functional group, the degradation rates were lower for shorter-chain PFASs [31, 43]. The observed rate constants were

higher in deionized water than low TDS groundwater except for PFBS and 6:2 FTS. The rate constants in low TDS groundwater were 55% and 41% higher for PFBS and 6:2 FTS, respectively Table 3.4.

Table 3.4: Pseudo-first-order removal rates (k), initial (C_i), and final concentrations (C_f) of different PFASs in independent experiments. The experiments were performed in a 700 kHz - 250 W open system (P_d = 1250 $W.L^{-1}$). The error represents the standard deviation of the samples. Supplemental information can be found in Figure A 3.

Compounds	Deionized Water			Low TDS Groundwater		
	C_i ($\mu g.L^{-1}$)	C_f ($\mu g.L^{-1}$)	$k \times 10^{-3}$ (min^{-1})	C_i ($\mu g.L^{-1}$)	C_f ($\mu g.L^{-1}$)	$k \times 10^{-3}$ (min^{-1})
PFOA	140.26 ± 0.38	1.23 ± 0.0017	37 ± 1.92	5.04 ± 0.06	0.52 ± 0.14	29 ± 4.19
PFOS	2.89 ± 0.11	0.06 ± 0.009	16 ± 0.78	10.41 ± 0.72	7.20 ± 0.38	4.7 ± 0.95
PFBS	10.53 ± 0.14	1.06 ± 0.007	10 ± 0.64	7.52 ± 0.12	0.24 ± 0.005	21 ± 2.36
6:2 FTS	5.04 ± 0.13	0.16 ± 0.028	18 ± 0.32	6.14 ± 0.08	0.33 ± 0.003	32 ± 0.24
FOSA	0.2 ± 0.008	ND	15 ± 4.61	2.32 ± 0.03	0.27 ± 0.003	18 ± 0.77
6:2 FTAB	7.2 ± 1.06	0.15 ± 0.02	27 ± 0.94	0.24 ± 0.008	ND	16 ± 6.81

The ultrasonic irradiation of low TDS groundwater, high TDS groundwater, and deionized water, spiked with a mix of 24 PFASs (24Mix), followed pseudo-first-order kinetics in 700 kHz - 250 W open system and 700 kHz - 1040 W closed system (Figure 3.1a). The acoustic treatment of 24Mix in low TDS groundwater demonstrated 90% removal of PFBA (11 $\mu g.L^{-1}$ to 1 $\mu g.L^{-1}$), 99% removal of PFBS (12 $\mu g.L^{-1}$ to 140 $ng.L^{-1}$), 98% degradation of PFOA (10 $\mu g.L^{-1}$ to 230 $ng.L^{-1}$) and PFOS (4 $\mu g.L^{-1}$ to 370 $ng.L^{-1}$). The acoustic treatment of 24Mix in deionized water degraded 91% of PFOA (13 $\mu g.L^{-1}$ to 1 $\mu g.L^{-1}$), 98% of PFOS (10 $\mu g.L^{-1}$ to 200 $ng.L^{-1}$), greater than 70% of PFBA (12 $\mu g.L^{-1}$ to 3.5 $\mu g.L^{-1}$) and PFBS (13 $\mu g.L^{-1}$ to 3 $\mu g.L^{-1}$). The mass removal of PFASs and the degradation rates were lower in high TDS groundwater compared to those in low TDS groundwater as well as deionized water. The ultrasonic degradation of the 24Mix spiked high TDS

groundwater was also tested in a 700 kHz - 1040 W closed system (P_d = 1040 W.L^{-1}). Despite the larger volume of treatment/lower power density, the degradation rates were higher than those observed in the open system experiment for the high TDS groundwater (Figure A 4b). Estimation of Henry's Law constant or the air-water partition constant (Kaw) of PFASs can be challenging because of their rapid ionization in water. However, higher Kaw of long-chain PFASs, as compared to the short-chain PFASs[4, 36, 44, 45] indicates higher availability of long-chain PFASs at the cavity interface leading to higher degradation rates during sonication The high TDS groundwater had high concentrations of chloride (5.28 g.L^{-1}), sodium (3.20 g.L^{-1}), calcium (1.14 g.L^{-1}), and sulfate (1.95 g.L^{-1}) along with high specific conductance (16 mS.cm^{-1}). Studies on sonication of PFASs in groundwater are limited to two studies that tested the gradation of PFOS and PFOA in individual experiments [46, 47]. These studies have reported that the rates of removal in groundwater were lower than that observed in Milli- Q water and increasing sulfate concentration (1-10 mM) in the mixture was detrimental to removal kinetics. In this study, we tested the degradation of a mixture of 24 PFASs (24Mix) in groundwater from two different locations and compared it to the degradation in deionized water. Interestingly, the removal kinetics of short-chain PFASs (C < 8) and the removal kinetics of sulfonates were enhanced in low TDS groundwater when compared to the kinetics in deionized water. However, removal rates for long-chain compounds (C ≥ 8) were higher in deionized water as compared to the low TDS groundwater. The degradation of shorter chain PFASs by sonication is generally slower than

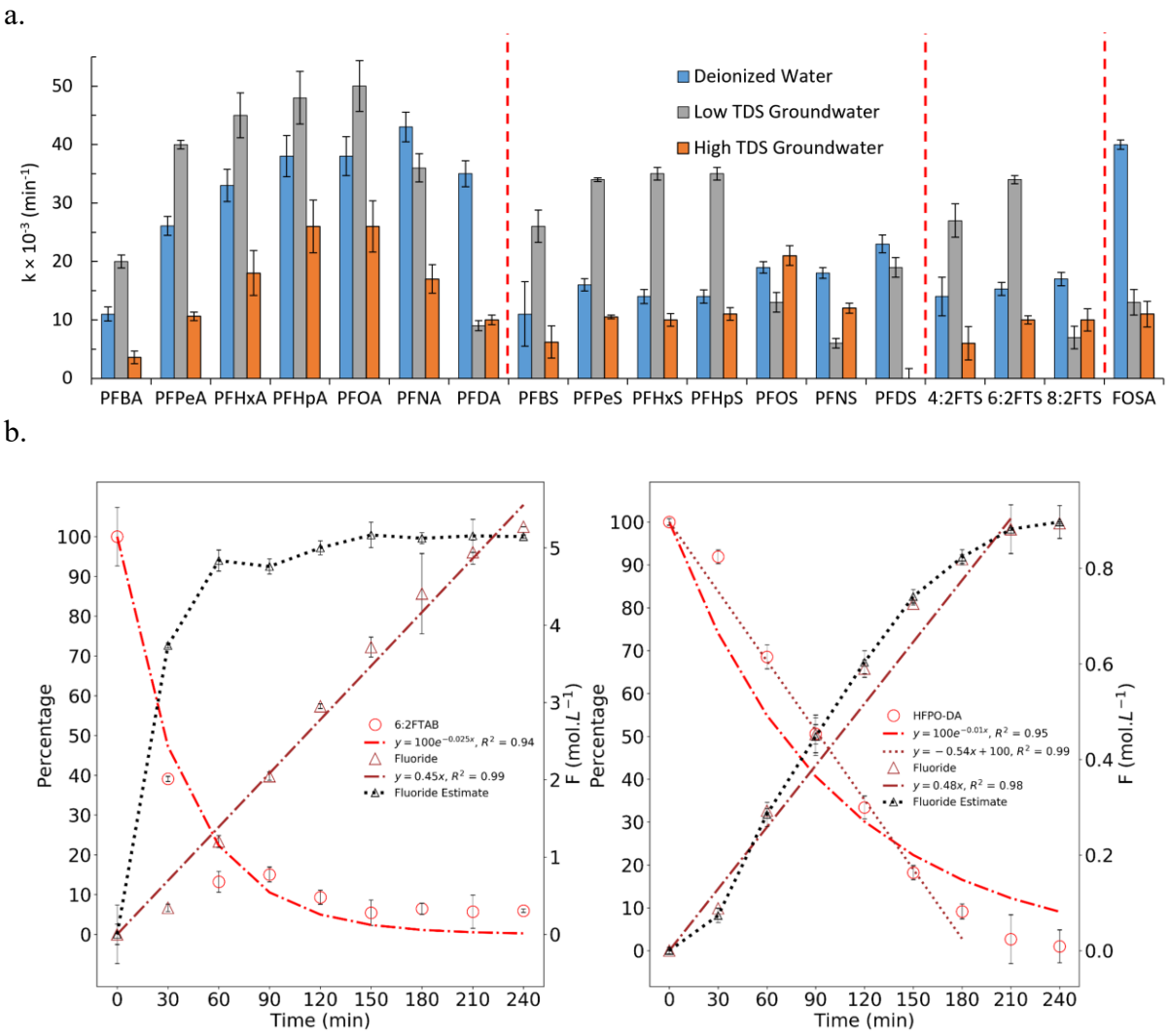

Figure 3.1: The degradation of PFASs in de-ionized water and groundwater by ultrasound. The degradation follows pseudo-first-order kinetics with degradation rates increasing with chain length. The degradation rates of PFSAs and short-chain PFASs (C < 8) were higher in the low TDS groundwater, while high TDS groundwater inhibits the degradation of PFASs. The experiments were performed for 240 minutes in Argon saturated atmosphere at 10 °C and the rates were calculated for the first 120 min based on the initial rate method. a. Comparison of pseudo-first-order removal rates (min^{-1}) of PFASs observed in the 700 kHz - 250 W open system (P_d = 1250 $W.L^{-1}$) for the 24Mix spiked deionized water, low TDS groundwater, and high TDS groundwater. Supplemental information can be found in Figure A 4 and Figure A 5. b. Defluorination of 6:2 FTAB and HFPO-DA in a 700 kHz - 1040 W closed system (P_d = 1040 $W.L^{-1}$). (△) represents measured fluoride, (□) represents the fluoride estimated based on the concentration of the PFAS compound, (○) represents the concentration of PFAS. HFPO-DA was degraded from 23 $mg.L^{-1}$ to 232 $\mu g.L^{-1}$ and 6:2 FTAB was degraded from 2 $mg.L^{-1}$ to 186 $\mu g.L^{-1}$ with 99% and 98% defluorination efficiency (concentration of fluoride measured/total fluorine in PFAS), respectively. The error bars represent the standard deviation of analytical triplicates.

longer-chain compounds, as the smaller chained compounds are less hydrophobic as a result have lower concentrations on the interface [31]. Low concentrations of ions might increase the transfer of PFASs from the aqueous phase to the sonication cavity interface by lowering the surface tension of the solution, thereby improving the acoustic degradation kinetics of PFASs [34, 37]. However, high salt concentrations, as observed in high TDS groundwater, might lead to neutralization of the charges on the ultrasonic cavities by the formation of an electrical double layer. The neutralization of charge allows attractive forces to overcome the electrostatic repulsion and cause the collapse or aggregation of the cavities [8]. Alternatively, charge neutralization of PFASs could enhance their hydrophobicity and therefore increase the mass transfer to the ultrasonic cavity. High salt and other organic compounds can also compete in consuming the destructive sonic energy and the reactive radicals generated during sonication, making them unavailable to act on the target compound [31, 34, 47]. The low removal kinetics in high TDS groundwater and the formation of precipitates were consistent in high TDS groundwater for sonication of the individual PFAS as well as the 24Mix.

The ionic strength, temperature, and surfactants can affect the surface tension of the solution, therefore affecting the ultrasonic degradation rates [34, 37]. Higher surface tension is detrimental for ultrasonic degradation rates as it negatively impacts the bubble size, bubble formation rate, bubble growth, and cavitation intensity [26, 39, 48, 49]. Alternatively, higher surface tension can also increase the mass transfer of PFASs to the bulk cavity hence, increasing the degradation rates [37, 42]. The initial losses observed for the 24Mix in the high TDS groundwater experiments can be attributed to bubbling out of the PFASs from the aqueous phase to the bulk gas-water interface during argon sparging (Figure A 4b). The longer chain PFASs being more hydrophobic than smaller chain compounds can partition to the gas-water interface more easily [5, 36]. The high salt concentration can further enhance the ‘salting out’ of PFASs from the

bulk aqueous phase [36, 47]. Costanza et al. have demonstrated that an increase in TDS results in the decrease of surface tension, thereby causing increased surface excess and phase separation of PFASs (PFOA and PFOS) [35]. Similarly, Schaefer et al. have also reported a decrease in surface tension for PFOS with an increase in aqueous NaCl concentration [36]. Reports of high concentrations of electrolytes increasing PFAS adsorption and increasing the tendency of PFASs to form hemi-micelles and aggregates, more prominently for long-chain PFASs have also been published [5]. The increase in the concentrations observed towards the end of the experiment could be attributed to the equilibrium shift caused by the acoustic degradation of PFASs and simultaneous precipitation of salts allowing the LNAPL PFASs to partition back into the aqueous bulk (Figure A 4b). High concentrations of long-chained PFASs have also been detected in seawater probably due to the neutralization of the charged headgroups. Interestingly, the water samples collected from the surface of the yellow sea Jiaozhou Bay, China had a prominently high concentration of PFUnDA, which was not observed in freshwater samples [50]. Similarly, a high concentration of PFASs was detected in the surface microlayer in sweater samples collected from South Bay, Livingston Island, Antarctica [51].

3.3.2 Removal of IDW and AFFF

The PFAS removal rates and the total moles removed were higher (76%) in the 700 kHz closed system (P_d = 1040 $W.L^{-1}$) than the 700 kHz open system (P_d = 1250 $W.L^{-1}$) for the degradation of IDW, despite the lower power density (Figure 3.2). The larger PFAS mass removal observed in the closed system can be attributed to faster PFAS degradation rates regardless of the larger treatment volume of IDW. No chlorate or perchlorate was generated during the defluorination of IDW in the 700 kHz closed system (P_d = 1040 $W.L^{-1}$) (Figure A 6). The IDW

water characteristics were similar to the high TDS groundwater characteristics (Table 3.2). A total of 41 PFAS species were examined for the treatment of concentrated IDW by 240 min of ultrasonic irradiation (Figure 3.2a and Figure A 7). In the 700 kHz open system (P_d = 1250 $W.L^{-1}$), 37 species show significant removal of PFASs. In summary, 12.4% degradation of PFOS, 69.7% degradation of PFOA, 38.6% degradation of PFBS, 46.6% degradation of PFBA, 45.9% degradation of 4:2 FTS, 82.9% degradation of PFPeA, 89.1% degradation of PFHxA, 80.1% degradation of PFHpA, 36.9% degradation of PFHxS, 6.9% degradation of PFHpS, 12.6% degradation of 8:2 FTS, 88.6% degradation of MeFPeSAA, 30.4% degradation of PFPeS, 91.9% degradation of PFNS, and 9.6% degradation of 6:2 FTS was observed. All the 41 PFAS species examined were significantly degraded when a 1000 mL undiluted IDW was treated in the 700 kHz - 1040 W closed system (P_d = 1040 $W.L^{-1}$). Collectively, 37.4% degradation of PFOS, 74% degradation of PFOA, 68.3% degradation of PFBS, 69.2% degradation of PFBA, 64.1% degradation of 4:2 FTS, 88.5% degradation of PFPeA, 91.2% degradation of PFHxA, 80.1% degradation of PFHpA, 50.7% degradation of PFHxS, 50.3% degradation of PFHpS, 38.0% degradation of 8:2 FTS, 80.2% degradation of MeFPeSAA, 61% degradation of PFPeS, 96.6% degradation of PFNS, and 19.7% degradation of 6:2 FTS was observed. The PFAS species with high starting concentrations, like PFBA, PFBS, PFHxS, PFHpS, 4:2 FTS, and 6:2 FTS, demonstrated zero-order kinetics. As demonstrated before (Figure A 2) at high concentrations, the diffusion of PFASs to the cavity interface limits the rates of acoustic degradation [20, 33, 42].

Traditionally, the treatment of PFAS-containing IDW is based on either separation processes like granular activated carbon and ion exchange, or disposal of the IDW and spent sorbents at hazardous waste landfill facilities or incineration [52]. Singh et al. [32] recently published a study on the destruction of low-concentration PFAS-IDW in a pilot-scale plasma

reactor with mean PFAS concentrations ranging from 0.04 $\mu g.L^{-1}$ to 179 $\mu g.L^{-1}$. The current work reports the removal of significantly higher concentrations of PFASs in the IDW (16 $\mu g.L^{-1}$ to 37 $mg.L^{-1}$) treated by ultrasound. The concentration of most PFASs identified was in low parts per million and compared to the concentrations listed in UCMR3, the detected concentrations were higher by a factor of 2.5×10^5 for PFOS, 1.3×10^4 for PFOA, 6.7×10^5 for PFHxS, and 4.4×10^4 for PFBS than the reporting levels. The PFASs defluorinated during sonication of IDW were significantly more than the 16 identified PFASs (Figure 3.2a), evident by the concentration of aqueous fluoride released (Figure A 6). The fluoride release detected during IDW sonication (61 $mg.L^{-1}$) was 43% higher than expected fluoride concentration, if calculated by the 16 identified PFAS species (35 $mg.L^{-1}$). The estimated moles of fluoride released (16 PFASs) was 1.84 mmol compared 3.22 ± 1.6 mmol detected by HPIC (Figure 3.2b).

The components of the AFFF influence the solubility of PFAS species affecting their concentration at the cavity-water interface and the degradation rates of PFASs. Similar to the sonication of 24Mix experiments, the AFFF diluted in the deionized water (1:12500) was treated in a 700 kHz - 250 W system (P_d = 1250 $W.L^{-1}$). Under the tested conditions, 33 species examined demonstrated significant degradation (Figure 3.3a and Figure A 8). In summary, PFPrS was degraded by 92%, PFOS degraded by 99.8%, PFOA degraded by 98%, PFBS degraded by 97.7%, PFBA degraded by 82%, PFPeA degraded by 61%, PFHxA degraded by 98%, PFHpA degraded by 97.5%, PFHxS degraded by 99.6%, PFPeS degraded by 99.6%, and PFHpS was degraded to below detection.

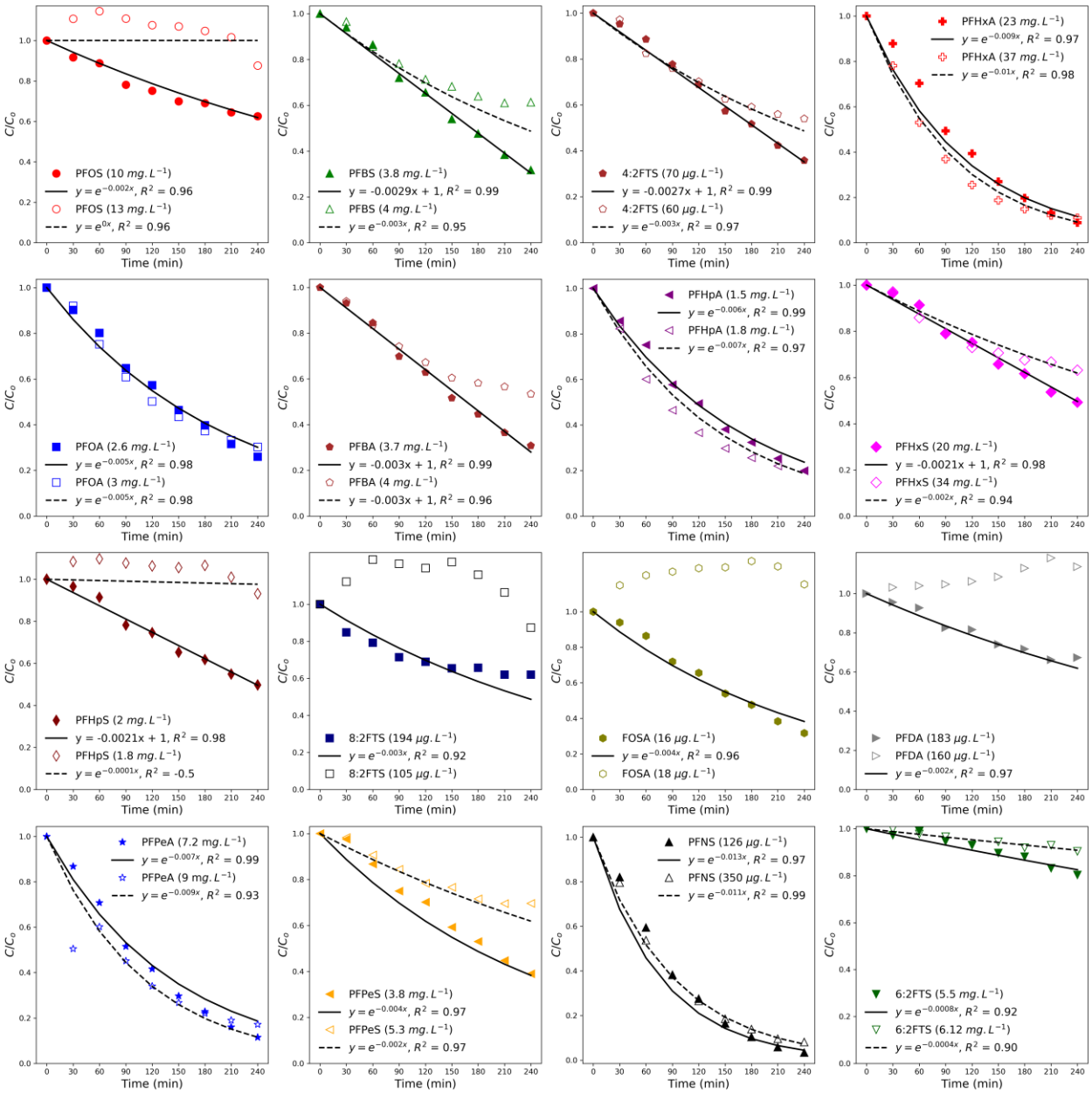
C/C0
Time (min)
PFOS (10 mg.L−1)
y = e−0.002x, R2 = 0.96
PFOS (13 mg.L−1)
y = e0x, R2 = 0.96
PFBS (3.8 mg.L−1)
y = -0.0029x + 1, R2 = 0.99
PFBS (4 mg.L−1)
y = e−0.003x, R2 = 0.95
4:2FTS (70 μg.L−1)
y = -0.0027x + 1, R2 = 0.99
4:2FTS (60 μg.L−1)
y = e−0.003x, R2 = 0.97
PFHxA (23 mg.L−1)
y = e−0.009x, R2 = 0.97
PFHxA (37 mg.L−1)
y = e−0.01x, R2 = 0.98
PFOA (2.6 mg.L−1)
y = e−0.005x, R2 = 0.98
PFOA (3 mg.L−1)
y = e−0.005x, R2 = 0.98
PFBA (3.7 mg.L−1)
y = -0.003x + 1, R2 = 0.99
PFBA (4 mg.L−1)
y = -0.003x + 1, R2 = 0.96
PFHpA (1.5 mg.L−1)
y = e−0.006x, R2 = 0.99
PFHpA (1.8 mg.L−1)
y = e−0.007x, R2 = 0.97
PFHxS (20 mg.L−1)
y = -0.0021x + 1, R2 = 0.98
PFHxS (34 mg.L−1)
y = e−0.002x, R2 = 0.94
PFHpS (2 mg.L−1)
y = -0.0021x + 1, R2 = 0.98
PFHpS (1.8 mg.L−1)
y = e−0.0001x, R2 = -0.5
8:2FTS (194 μg.L−1)
y = e−0.003x, R2 = 0.92
8:2FTS (105 μg.L−1)
FOSA (16 μg.L−1)
y = e−0.004x, R2 = 0.96
FOSA (18 μg.L−1)
PFDA (183 μg.L−1)
PFDA (160 μg.L−1)
y = e−0.002x, R2 = 0.97
PFPeA (7.2 mg.L−1)
y = e−0.007x, R2 = 0.99
PFPeA (9 mg.L−1)
y = e−0.009x, R2 = 0.93
PFPeS (3.8 mg.L−1)
y = e−0.004x, R2 = 0.97
PFPeS (5.3 mg.L−1)
y = e−0.002x, R2 = 0.97
PFNS (126 μg.L−1)
y = e−0.013x, R2 = 0.97
PFNS (350 μg.L−1)
y = e−0.011x, R2 = 0.99
6:2FTS (5.5 mg.L−1)
y = e−0.0008x, R2 = 0.92
6:2FTS (6.12 mg.L−1)
y = e−0.0004x, R2 = 0.90

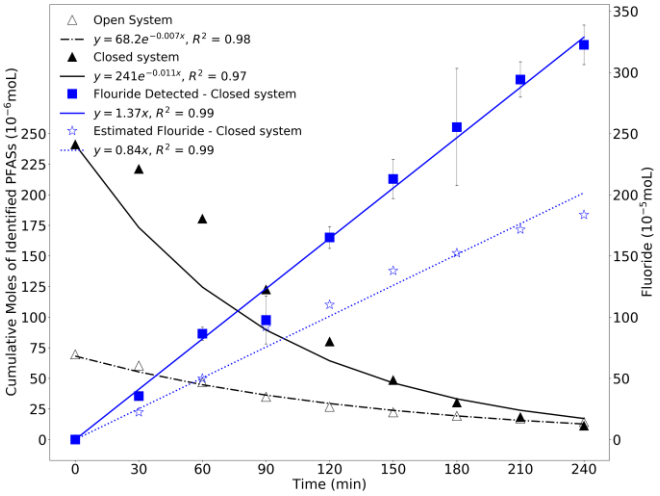
Open System
y = 68.2e−0.007x, R2 = 0.98
Closed system
y = 241e−0.011x, R2 = 0.97
Flouride Detected - Closed system
y = 1.37x, R2 = 0.99
Estimated Flouride - Closed system
y = 0.84x, R2 = 0.99
Cumulative Moles of Identified PFASs (10−6moL)
Fluoride (10−5moL)
Time (min)

Figure 3.2: Destruction of PFASs in concentrated investigation derived waste (IDW). The acoustic degradation rates and mass removal PFASs were higher in 700 kHz - 1040 W closed system (P_d = 1040 $W.L^{-1}$) as compared to 700 kHz - 250 W open system (Pd = 1250 $W.L^{-1}$) despite the lower power density. Fluoride detected (■) was 43% higher than the fluoride estimated to be released based on the 16 identified PFAS species (☆). The experiments were conducted for 240 minutes at 10 °C in Argon saturated environment. The rates were calculated for the first 120 min using the initial rate method. **a.** Sonication of IDW in a 700 kHz - 1040 W closed system (Pd = 1040 $W.L^{-1}$) and 700 kHz - 250 W open system (P_d = 1250 $W.L^{-1}$). The solid black line represents the kinetic model fitting for the experimental data (solid markers) in a 700 kHz - 1040 W closed system (P_d = 1040 $W.L^{-1}$) while the dotted black line represents the kinetic model fitting for the experimental data (empty markers) in a 700 kHz - 250 W open system (P_d = 1250 $W.L^{-1}$). The starting concentration of all PFASs in the IDW mixture is reported in parentheses. Degradation of more PFAS species is reported in Figure A 7. **b.** Defluorination and removal of PFAS moles during sonication of IDW. ■ - Moles of fluoride detected in the closed system, ☆ - moles of fluoride release estimated from 16 identified PFASs in the closed system, ▲ - PFAS mass removed in the closed system, △- PFAS mass removed in the open system. The concentrations ($mg.L^{-1}$) of fluoride, chlorate, and perchlorate are reported in Figure A 6.

Similar to this study, other studies have also demonstrated the defluorination of AFFF by ultrasound and reported that the AFFF components had little effect on the degradation of PFASs [8, 39, 42, 43, 53, 54]. In a mixture, the rates of mineralization are not generally affected by the concentration of PFASs for PFAS concentrations below the kinetics transition concentration [54]. Our data suggest that in the case of mixtures (Figure 3.2 and Figure 3.3), the competition might influence the rates but, if the concentrations of the species are lower than the kinetics transition concentration, the kinetics remain pseudo-first-order [20, 33, 42, 54, 55]. Interestingly, in this study, the first-order removal rates of sulfonates in the treated AFFF were found to be significantly higher than the rates of sulfonates removal observed in the deionized water for a 24 mix of PFASs treated under the same conditions (Figure 3.3b). However, the inverse was observed for the removal rates of carboxylates. Differences in the compositions of AFFF formulations might also influence the removal kinetics [54]. Adding surfactants to the PFAS sonication mixture has been shown to affect the mass transfer of PFASs to the ultrasonic cavity by electrostatic interactions [34]. The competition among the various AFFF constituents to partition to the cavity-water

interface might play a role in the removal rates of PFASs [53]. The competitive adsorption of species to the ultrasonic cavities has been reported to reduce the PFAS degradation rates [47]. The PFASs in AFFF account for only 1-5% of the total mass, therefore, while estimating the energy consumption during ultrasonic degradation of PFASs in mixtures like IDW and AFFF, the degradation of other organics should also be included in the calculations [53, 54].

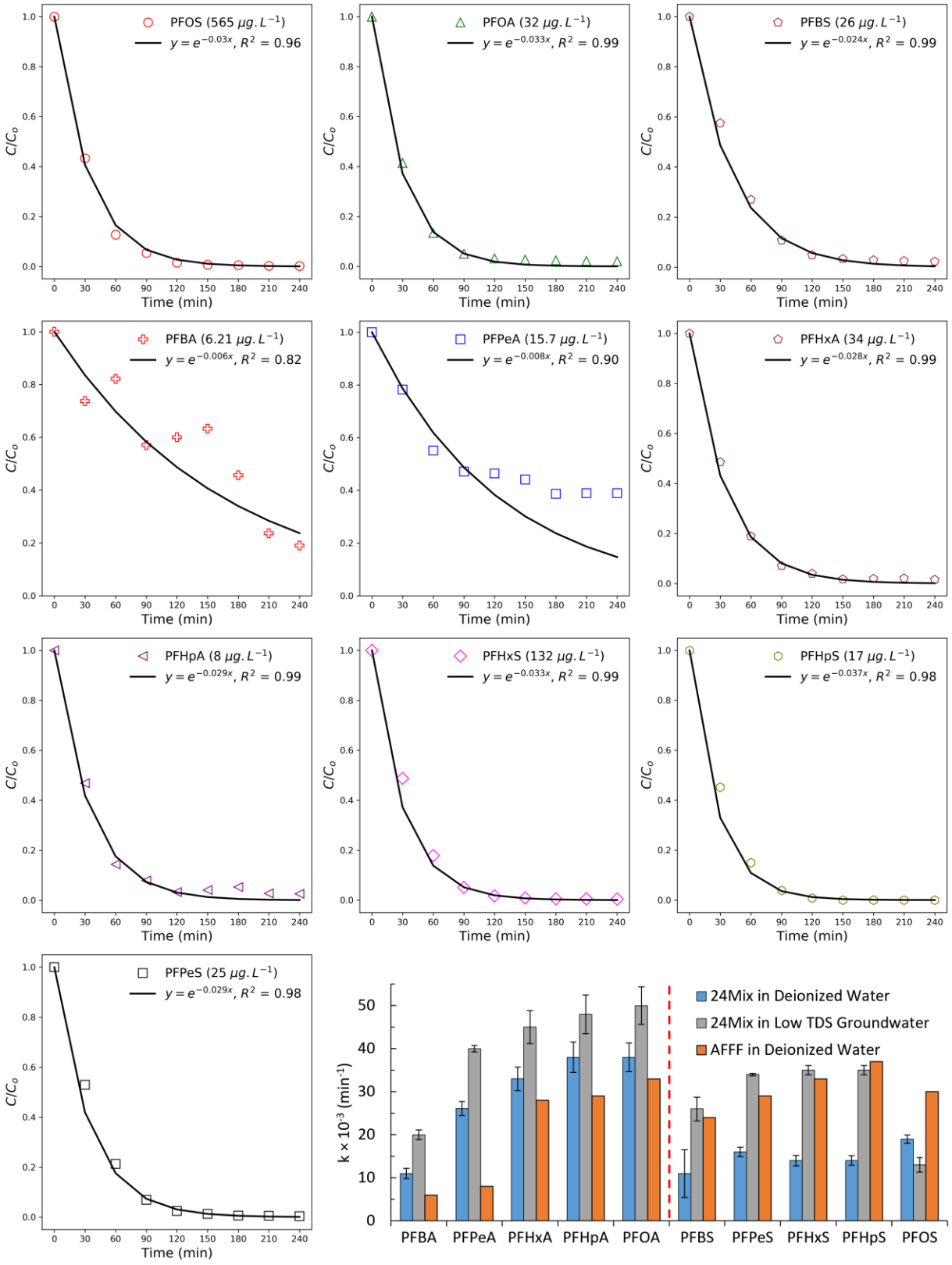
PFOS (565 μg.L⁻¹)
y = e^−0.03x, R² = 0.96
PFOA (32 μg.L⁻¹)
y = e^−0.033x, R² = 0.99
PFBS (26 μg.L⁻¹)
y = e^−0.024x, R² = 0.99
PFBA (6.21 μg.L⁻¹)
y = e^−0.006x, R² = 0.82
PFPeA (15.7 μg.L⁻¹)
y = e^−0.008x, R² = 0.90
PFHxA (34 μg.L⁻¹)
y = e^−0.028x, R² = 0.99
PFHpA (8 μg.L⁻¹)
y = e^−0.029x, R² = 0.99
PFHxS (132 μg.L⁻¹)
y = e^−0.033x, R² = 0.99
PFHpS (17 μg.L⁻¹)
y = e^−0.037x, R² = 0.98
PFPeS (25 μg.L⁻¹)
y = e^−0.029x, R² = 0.98
C/Co
Time (min)
k x 10⁻³ (min⁻¹)
24Mix in Deionized Water
24Mix in Low TDS Groundwater
AFFF in Deionized Water
PFBA
PFPeA
PFHxA
PFHpA
PFOA
PFBS
PFPeS
PFHxS
PFHpS
PFOS

Figure 3.3: Destruction of PFASs in AFFF spiked deionized water. The rates of removal for sulfonates in AFFF were significantly higher than those observed for a 24 mix of PFASs; vice versa for carboxylates. The highest rates of short-chained PFAS degradation were observed for the treatment of 24Mix in the low TDS groundwater. All experiments were performed in de-ionized water using a 700 kHz - 250 W open system (P_d = 1250 $W.L^{-1}$) for 240 minutes at 10 °C in Argon saturated environment. The rates were calculated for the first 120 min using the initial rate method. **a.** Pseudo-first-order removal of PFAS in AFFF sample (1:12500 dilution). The starting concentrations of PFASs before ultrasound irradiation are shown in parentheses. The solid black line represents the first-order kinetic model fitting for the experimental data (empty markers). The degradation of more PFAS species is reported in Figure A 8. **b.** Comparison of pseudo-first-order removal rates of PFASs in AFFF spiked deionized water, 24Mix-spiked deionized water, and 24Mix-spiked low TDS groundwater. The error bars represent the standard deviation.

3.3.3 Removal Rates of PFASs with Power Density and System Conditions

The removal rates of PFASs decreased with decreasing power density (increase in the treatment volume). To understand this relationship, degradation of PFOA, PFOS, PFBS, 6:2 FTS, FOSA, and 6:2 FTAB was conducted at different power densities in individual experiments (Figure 3.4a). In a 700 kHz - 1040 W closed system, the PFBS removal rate increased with an increase in the power density from 5200 $W.L^{-1}$ to 1040 $W.L^{-1}$, followed by a decrease in the removal rate with a further decrease in power density. Atomization of the bulk liquid was observed at a power density of 5200 $W.L^{-1}$ but not at 1040 $W.L^{-1}$, suggesting that the energy transferred to the liquid might be consumed in the atomization of water, thus reducing the rate of removal of PFBS. An increase in rates with an increase in power density is in agreement with Campbell et al. [39]. However, in this study, the power density was altered by changing the water treatment volume instead of changing the electrical power supplied. Interestingly, the observed relationship between the volume (power density) and PFAS degradation rates suggests that the ultrasonic cavitation energy fades with increasing distance from the transducer. The reduction in the relative pressure field with an increase in distance from the transducer was previously demonstrated by

Azar et al. [56]. Similarly, Tiehm et al. reported that maximum cavitation occurs closer to the transducer surface [57]. Transducer design and assembly are critical in increasing the cavitation intensity in the aqueous bulk. A comprehensive review of similar observations has been detailed by Gogate et al. [58].

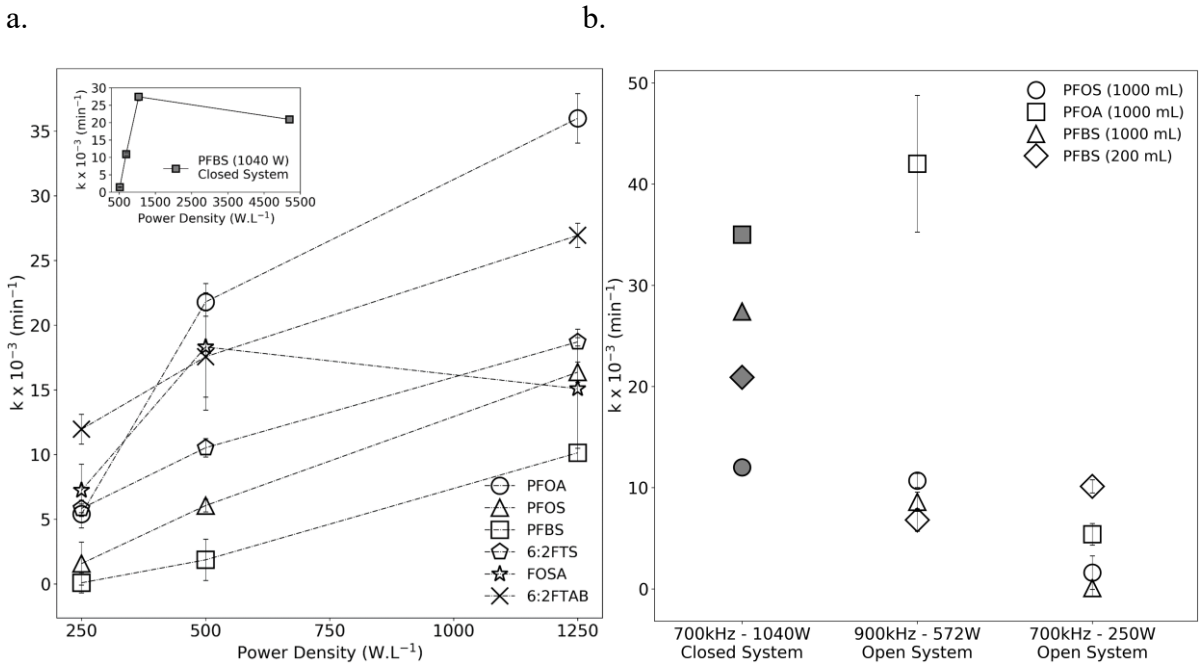

Figure 3.4: Variation in removal rates of PFASs with changing power density and system conditions. Pseudo-first-order removal rates (min^{-1}) of PFASs decreased with the decrease in power density. The rates of degradation were highest in the closed system as compared to the open systems. Rates of PFBS were higher at 700 kHz as compared to 900 kHz and vice versa for PFOA. Each data point represents experiments conducted independently over 240 minutes in an Argon-saturated environment at 10 °C. **a.** Comparison of degradation rates with the change in power density. The empty markers represent 700 kHz - 250 W open system while the solid markers represent 700 kHz - 1040 W closed system. **b.** Comparison of pseudo-first-order removal rates (min-1) of PFASs degradation by ultrasound in different system conditions. The solid markers represent a closed system while empty markers represent open system operation. The treatment volume is reported in parentheses. The error bars represent the standard deviation.

As observed for ultrasonic degradation of 24Mix (Figure A 5) and IDW (Figure 3.2a), the rates of degradation of individual PFASs in a closed system (P_d = 1040 $W.L^{-1}$) were found to be

significantly higher than those in the open system (P_d = 1250 $W.L^{-1}$) (Figure 3.4b). The PFBS degradation rate in a 700 kHz - 250 W open system (P_d = 250 $W.L^{-1}$) was insignificant. In the 900 kHz - 572 W open system (P_d = 572 $W.L^{-1}$), the PFBS degradation rate was 0.0086 ± 0.00096 min^{-1}, while the PFBS degradation rate observed in a 700 kHz - 1040 W closed system (P_d = 1040 $W.L^{-1}$) was 0.0274 min^{-1}. Similarly, in the 700 kHz - 250 W open system (P_d = 250 $W.L^{-1}$), the degradation rate of PFOS and PFOA were 0.0016 ± 0.0016 min^{-1} and 0.0053 ± 0.0010 min^{-1}. In the 900 kHz - 572 W open system (P_d = 572 $W.L^{-1}$), the rates were 0.0107 min^{-1} ± 0.0007 (PFOS) and 0.042 min^{-1} ± 0.0067 (PFOA), and in the 700 kHz - 1040 W closed system (P_d = 1040 $W.L^{-1}$), the rates of PFOS and PFOA were 0.012 min^{-1} and 0.035 min^{-1}, respectively (Figure 3.4b). The fluorocarbon chain produced by pyrolysis of the PFAS headgroup undergoes further pyrolytic reactions in the ultrasonic cavity generating smaller chain CF radicals [20]. The retention of the fluorochemical intermediates in the closed system, thus increasing the availability of CF radicals in the reaction, might explain the higher rates of degradation observed in a closed system compared to the open system. Furthermore, the pressurization of the system increases the mass transfer of fluorochemical intermediates from gas to liquid [41], increases the dissolved gas saturation in the liquid, and decreases the ultrasound cavitation threshold [26]. Consequently, the rates of ultrasonic PFAS degradation are increased. PFBS had higher rates of degradation at 700 kHz as compared to 900 kHz and vice versa for PFOA (Figure 3.4b). Similar observations have been reported by Campbell et al. [31]. The degradation rates peaked at 610 kHz for PFBS and PFBA because of an increase in mass transfer to the cavity-bulk interface and 358 kHz for PFOA and PFOS owing to the maximum number of cavitations per unit time [31].

3.3.4 Energy Consumption

Various studies, including the present work, have shown that ultrasonic treatment technology is capable of mineralizing PFASs in a complex mixture without the generation of shorter chain byproducts [42, 59]. First-order removal rates (k), required for calculating E_{EO}, vary with the chain length and functional group of PFASs. Therefore, the energy consumption for degradation of high concentration mixtures can be better described by E_{EM} instead of E_{EO} [31, 39, 60, 61]. This study estimated E_{EO} and E_{EM} values for AFFF, 24Mix, IDW, HFPO-DA, and 6:2 FTAB to compare their accuracy in evaluating the energy consumption in mixtures and high concentration experiments. However, only E_{EO} was calculated for low concentration single compound degradation by ultrasound (Table 3.5). Mineralization of 23 $mg.L^{-1}$ HFPO-DA consumed 203 $kWh.g^{-1}$ (E_{EM}) or 4.8 $MWh.m^{-3}.order^{-1}$ (E_{EO}) compared to 1.3 $MWh.m^{-3}.order^{-1}$ (E_{EO}) for degradation of 873 $\mu g.L^{-1}$ HFPO-DA. Similarly, the treatment of IDW consumed only 3 to 76 $kWh.g^{-1}$ (E_{EM}) compared to E_{EO} of 14 to 8 $MWh.m^{-3}.order^{-1}$ when estimated based on the 16 identified PFASs (Figure 3.2a). As reported above, the actual fluoride detected by IC was 43% higher than expected from the defluorination of the identified compounds (Figure 3.2b). Accounting for the removal of unidentified PFASs in energy estimates for the treatment of IDW will lower the energy consumed. Various unidentified organics that might have been degraded during ultrasonic treatment of IDW and AFFF, when accounted for in the energy calculations, might further decrease the estimated energy consumption. Evidently, E_{EM} is the more realistic estimation of energy consumption in the sonication of matrices with high PFAS load, especially for the mixture.

The energy demand associated with the ultrasonic degradation of PFASs observed in this study is comparable to previously published studies (Table 3.5) [9, 31, 32, 39, 42, 60, 62]. The energy consumption (E_{EO}) for PFAS sonication can be reduced by increasing the PFAS degradation rates and/or decreasing the power density (equation 3.5). Similarly, reducing E_{EM} requires decreasing the power and/or increasing the mass removed per unit time (equation 3.4). In contrast, the experiments in this study and by Campbell et al. [39] have shown that degradation rates increase with an increase in power density. Consequently, two basic techniques could be used to reduce the energy consumption for the ultrasonic treatment of PFASs. Firstly, optimizing the frequency of ultrasound to achieve maximum removal rate and secondly, altering the matrix chemistry, thereby increasing the energy translation efficiency from electrical to ultrasound cavitation and consequently increasing the degradation rates. Frequency optimization is compound-specific [31] and as a result, for mixtures and actual waters, the optimization of frequency will not be practical. Using single or multiple frequencies or changing the sonic field affects the radius and population of the cavities, in turn affecting the rates [39]. Energy losses during the conversion of electrical energy to ultrasonic cavitation are very high [9, 58, 62, 63]. Altering the matrix chemistry by changing the gaseous atmosphere, adjusting the pH, changing surface tension by adding salts and surfactants to the matrix [21, 34, 37, 46, 64], and combining ultrasonic treatment with other treatment processes like catalytic oxidation/reduction or electrolysis [42, 62, 65, 66] can significantly improve the energy transfer during sonication. During sonication, the temperature of the reaction mixture rose steadily to approximately 40 °C over the first 120 min, regardless of the recirculation of cold water (10 °C), and remained constant over the next 120 min for all experiments. Consequently, if the temperature control is not essential, the

cooling component can be removed, thereby reducing the energy consumption associated with cooling.

Table 3.5: Energy consumption for ultrasonic degradation. The calculations were performed using the appropriate treatment volume. 200 mL impacted water was treated in the open system while 1000 mL impacted water was treated in the closed system. a. Energy consumption for mixtures of PFASs and high concentration HFPO-DA.

Chemicals	System	C_i (µg.L^{-1})	E_{EM} (MWh.g^{-1})	E_{EO} (MWh.m^{-3}.order^{-1})
AFFF	700 kHz Open System (1250 W.L^{-1})	861.21 ± 43.06	5.9	2.18
IDW		120735.42 ± 6036.77	0.003	14.57
24Mix		215.63 ± 0.14	24.15	4.52
IDW	700 kHz Closed System (1040 W.L^{-1})	84089.22 ± 4204.46	0.076	8.8
HFPO-DA		23000 ± 180.04	0.203	4.8

b. Energy consumption for Individual PFASs.

Chemicals	System	C_i (µg.L^{-1})	k × 10^{-3} (min^{-1})	E_{EO} (MWh.m^{-3}.order^{-1})
PFOA	700 kHz Open System (1250 W.L^{-1})	140.26 ± 0.38	37 ± 1.92	1.28
PFOS		2.89 ± 0.11	16 ± 0.78	2.93
PFBS		10.53 ± 0.14	10 ± 0.64	4.75
6:2 FTS		5.04 ± 0.13	18 ± 0.32	2.67
FOSA		0.2 ± 0.008	15 ± 4.61	1.00
6:2 FTAB		7.2 ± 1.06	27 ± 0.94	1.65
HFPO-DA		867.15 ± 7.23	32 ± 3.09	1.31
PFOA	700 kHz Closed System (1040 W.L^{-1})	12.25	35	1.14
PFOS		16.78	12	3.33
PFBS		26.22	27	1.46
6:2 FTAB		2099.1 ± 146.94	25 ± 1.24	1.60
HFPO-DA		27425.66 ± 312.61	12 ± 0.27	3.33

c. E_{EO} was estimated for 600 mL volume for the data reported in Table 1 by Liang et al.[42].

Chemicals	System	C_i (µg.L^{-1})	k × 10^{-3} (min^{-1})	E_{EO} (MWh.m^{-3}.order^{-1})
PFBA	202 kHz (250 W.L^{-1})	100.6	7	3.81
PFHxS		92.0	12	2.22
PFHxA		100.5	19	1.40
PFBS	358 kHz (250 W.L^{-1})	89.7	18	1.48
PFBA		100.6	12	2.22
PFHxS		92.0	30	0.89
PFHxA		100.5	39	0.68
PFOA		99.4	41	0.65
PFOS		100.0	27	0.99
PFBS	610 kHz (250 W.L^{-1})	89.7	23	1.16
PFBA		100.6	14	1.57
PFHxS		92.0	22	1.21
PFHxA		100.5	36	0.74
PFBS	1060 kHz (250 W.L^{-1})	89.7	9	2.96
PFBA		100.6	8	3.33
PFHxS		92.0	12	2.22
PFHxA		100.5	22	1.21
PFOA	202 kHz (83 W.L^{-1})	99.4	20	0.44
PFOS		100.0	10	0.89
PFBA		100.6	7.2	1.23
PFBS		89.7	13	0.68
PFHxA		100.5	19	0.47
PFHxS		92.0	12	0.74
PFOA	610 kHz (333 W.L^{-1})	99.4	34	1.04
PFOS		100.0	20	1.78
PFBA		100.6	17	2.09
PFBS		89.7	17	2.09
PFHxA		100.5	36	0.99
PFHxS		92.0	22	1.61
PFOA	202 + 20 kHz (250 W.L^{-1})	99.4	27	0.99
PFOS		100.0	13	2.05
PFOA	610 + 20 kHz (250 W.L^{-1})	99.4	37	0.72
PFOS		100.0	21	1.27

3.3.5 Bio-Sono and Electro-Sono Treatment Trains

The treatment of AFFF was tested in a bio-sono treatment train and electro-sono treatment to evaluate the effect of the pretreatment on ultrasonic degradation. Similar to direct sonication experiments, the sonication of biologically treated (Figure A 9) and electrochemically treated (Figure A 10) AFFF solution demonstrated significant degradation of PFASs with pseudo-first-order degradation kinetics. The bio-sono treatment train was found to degrade 30% PFOA, 30% PFHpS, 60% AmPr-FPeSA, and 70% AmPr-FHxSA by incubating diluted AFFF with 1 $U.mL^{-1}$ laccase and 20 mM HBT for 30 days followed by > 90% degradation by sonolysis (Figure 3.5). The experimental details of the biological treatment of AFFF can be found in section 3.2.3. The pseudo-first-order sonolytic degradation rates of electrochemically treated AFFF were found to be significantly higher than those observed for sonolytic degradation of laccase + HBT treated AFFF (Figure 3.6). The lower degradation rates observed during the sonolysis of biologically treated AFFF can be attributed to competitive consumption of cavitation events by laccase, HBT, or other intermediates produced during the biological treatment.

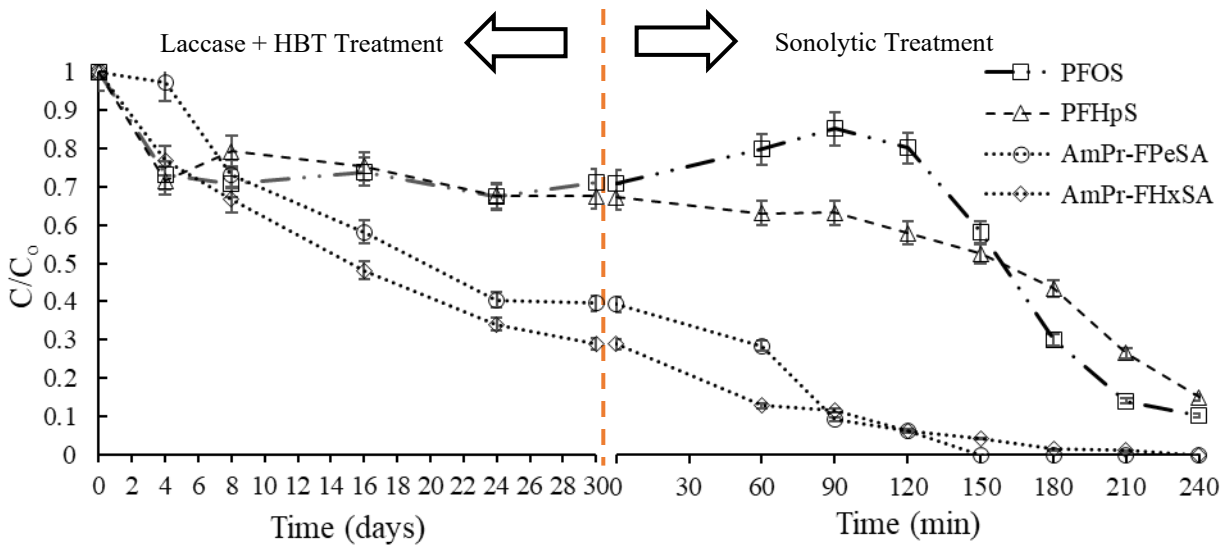

Figure 3.5: Sonolytic destruction of PFASs after biological treatment by 1 U.mL^{-1} laccase and 20 mM HBT (Section 3.2.3). Laccase + HBT system was able to degrade 30% PFOA and PFHpS in 30 days. The following sonolysis removed nearly 90% PFOA and PFHpS in 4 h. Similarly, more than 60% AmPr-FPeSA and AmPr-FHxSA were removed by laccase + HBT treatment followed by complete removal by 4 h sonication. The sonication experiments were performed in a 700 kHz - 250 W open system (P_d = 1250 W.L^{-1}) at 10 °C in Argon saturated environment. For the laccase + HBT experiment error bars represent experimental triplicates while error bars in the sonolytic experiment represent analytical triplicates.

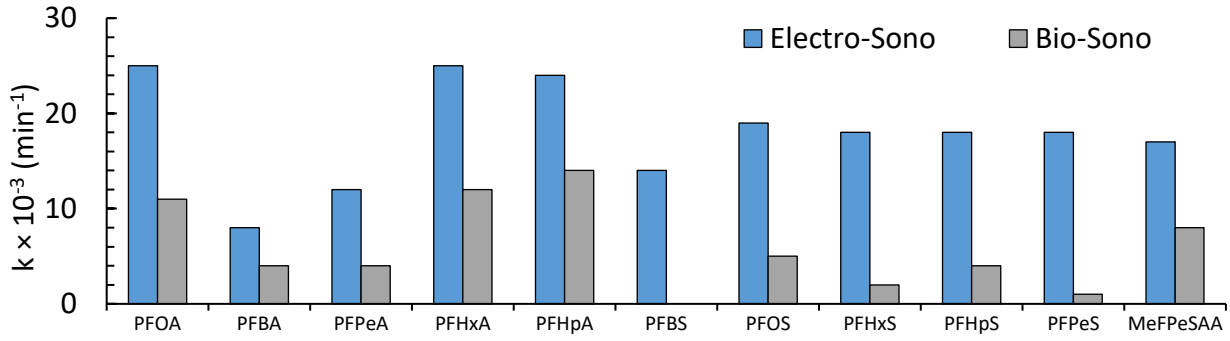

Figure 3.6: Comparison of pseudo-first-order removal rates of PFASs observed during the ultrasonic treatment of diluted AFFF initially treated electrochemically (blue bars) or by laccase + HBT system (grey bars). The rates were found to be higher for the electro-sono treatment train as compared to the bio-sono treatment train.

3.4 Conclusion

Efficient destructive technologies for PFASs are scarce and have limited field applicability. Despite the energy-intensive nature, ultrasound can be employed for the non-targeted treatment of PFASs in mixtures, AFFF, IDW, along with the treatment of various other classes of recalcitrant pollutants [31, 67]. This study demonstrates the effectiveness of ultrasound for the degradation and mineralization of legacy and novel PFASs, in real waters, complex mixtures, and high concentration IDW samples. The newer alternatives of legacy PFASs, like HFPO-DA, and zwitterionic species like 6:2 FTAB are efficiently mineralized by acoustic cavitation. The high-frequency ultrasound can also be used effectively to treat impacted groundwater. In low TDS groundwater, significant PFASs degradation (> 97%) was observed with 30% - 60% higher degradation rates for PFSAs and short-chained compounds (C < 8). However, the degradation rates of PFASs in high TDS groundwater were more than 50% lower than those in deionized water. High TDS groundwater and its constituents inhibit the degradation of PFASs by lowering the surface tension and assisting the formation of PFAS LNAPL at the bulk aqueous-gas interface. The acoustic irradiation of AFFF showed more than 97% degradation of the identified PFASs. In comparison to the rates observed for the treatment of 24Mix in similar conditions, the degradation rates for the treatment of diluted AFFF were 40% - 60% higher for PFSAs and 10% lower for most PFCAs. Compared to the open system operation of the reactor, closed system conditions demonstrated significantly higher removal rates across all matrices, owing to the increased availability of fluorocarbon intermediates in the reactions. Furthermore, for all PFAS tested, decreasing the power density decreased the degradation rates. The ultrasonic irradiation of high TDS IDW in a closed system also demonstrated mineralization of 230 µmol (89.4 mg) of cumulative identified PFAS mass using 76 $kWh.g^{-1}$ as compared to 55 µmol (15.9 mg) mass

removal using 3 $kWh.g^{-1}$ in an open system. Degradation of complex IDWs and impacted waters with high PFAS load by ultrasound might be more energy-efficient than treating low PFAS load. Treating such complex blends with ultrasound can make the matrix considerably cleaner and treatable for other downstream treatment technologies that are less energy-intensive but are otherwise not feasible. This study also provides insights into reactor design and system conditions which need further optimization to enable efficient utilization of ultrasonics in the field of water treatment. The destructive power of ultrasound can be more efficiently employed to treat high salinity - high concentration mixtures of PFASs like ion exchange and reverse osmosis brine, AFFF impacted groundwater, and IDWs.

Appendix A

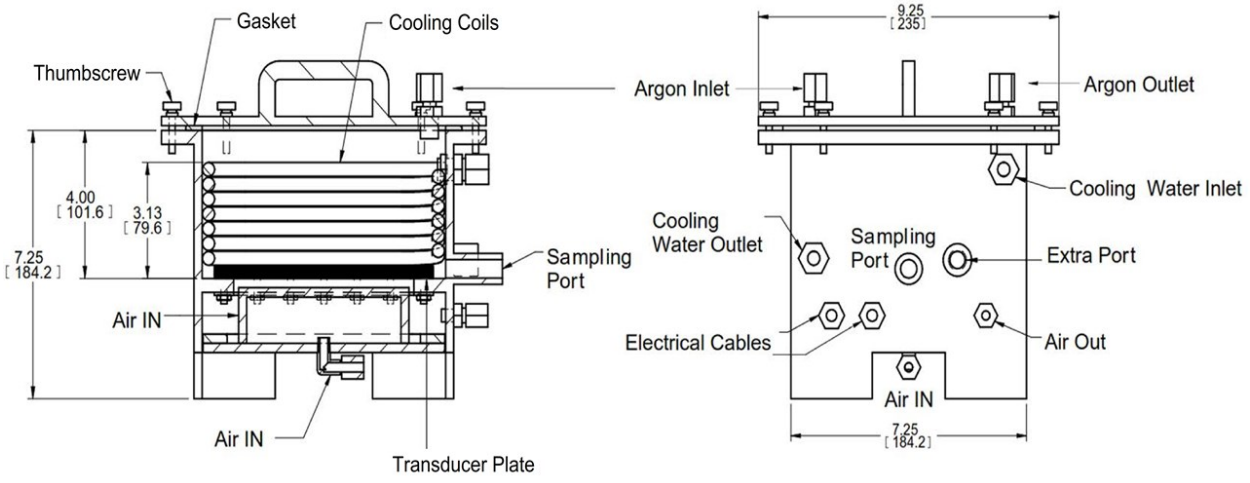

Figure A 1: Schematic of custom-made sealed polypropylene ultrasonic reactor (2 L) with PFAS-free components, equipped with piezoelectric (700 kHz or 900 kHz) transducer array. Temperature control was achieved by recirculating water through high-density polyethylene (0.25 in) or stainless-steel cooling coils. The dimensions are in inches [millimeters].

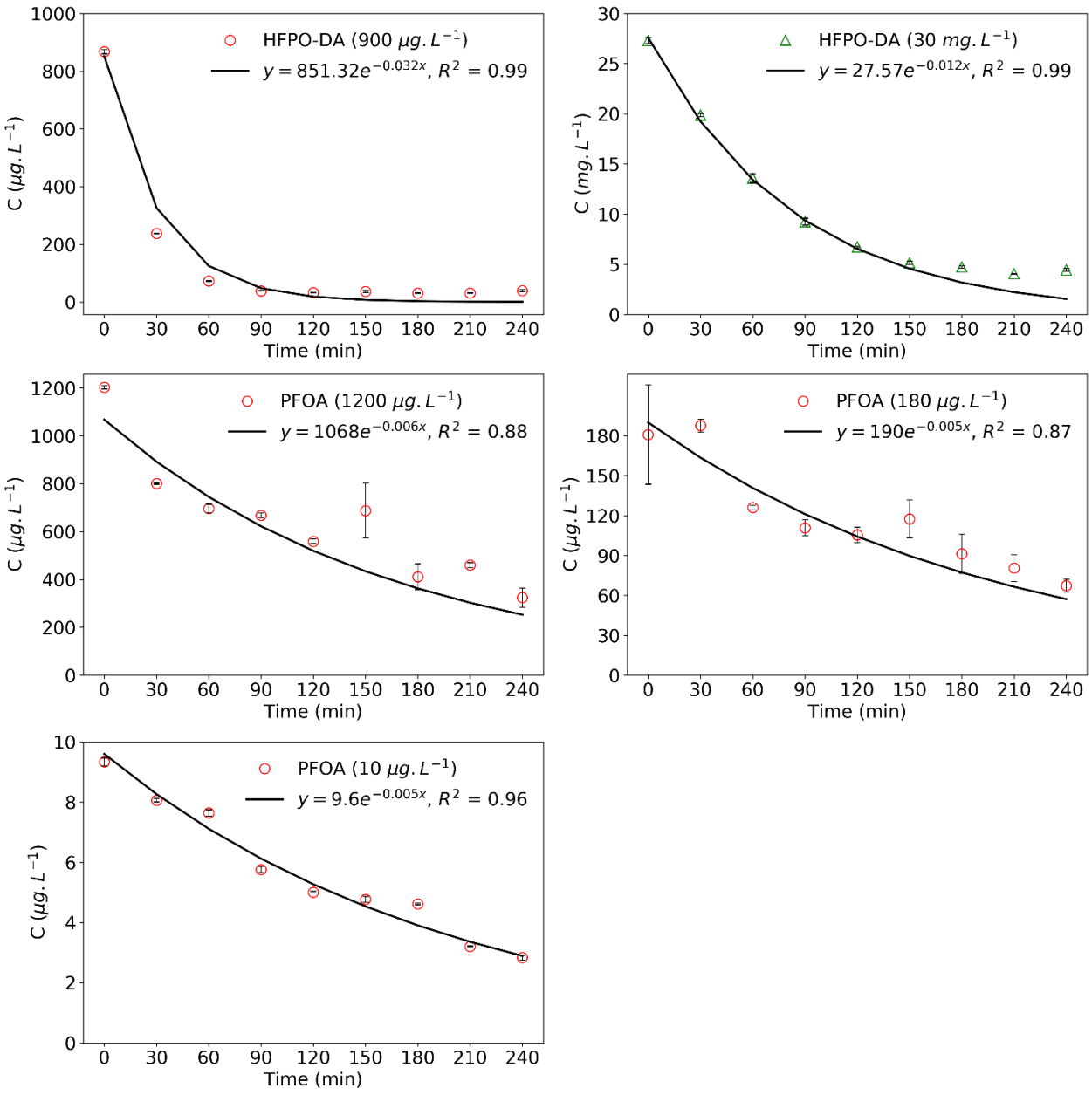

Figure A 2: Degradation of HFPO-DA and PFOA in independent experiments over 240 minutes by 700 kHz ultrasound in a 250 W open system. The HFPO-DA was treated in an argon saturated environment at a power density of 1250 $W.L^{-1}$ and PFOA was treated at a power density of 250 $W.L^{-1}$ (at 10 °C reactor temperature). The starting concentrations are shown in parenthesis and the error bars represent analytical triplicates. The solid line represents modeled pseudo-first-order kinetics, and the rates were calculated using the initial rate method.

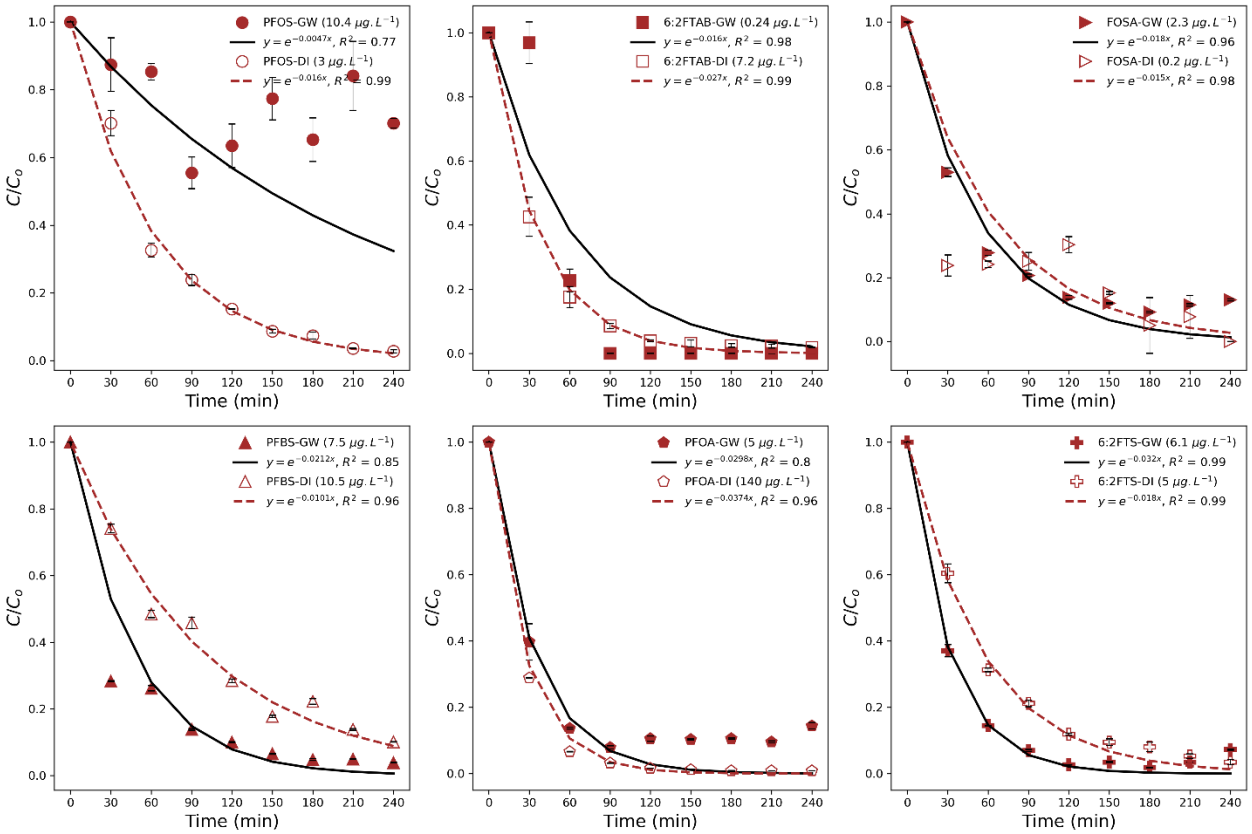

Figure A 3: Pseudo-first-order removal of PFASs in independent experiments over 240 minutes by 700 kHz - 250 W open system (P_d = 1250 W.L^{-1}) in low TDS groundwater (solid markers) and de-ionized water (empty markers). All the experiments were performed at 10 °C in argon saturated environment. The starting concentrations are shown in parenthesis and the error bars represent analytical triplicates. The first-order model fitting is presented by the solid black line for the low TDS groundwater (solid markers) and the dotted brown line for the deionized water (empty markers) and the rates were calculated using the initial rate method.

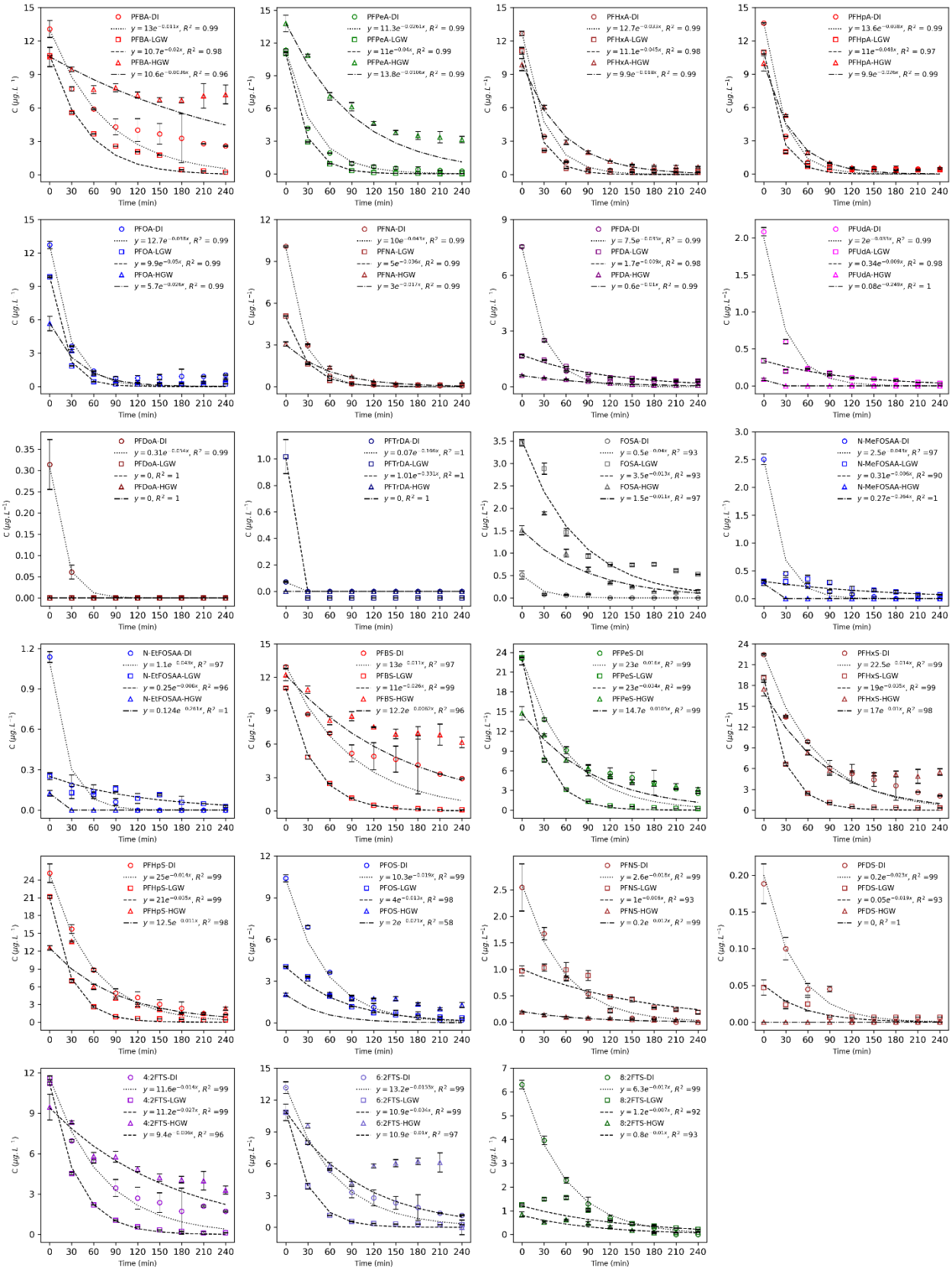
PFBA-DI
PFBA-LGW
PFBA-HGW
PFPeA-DI
PFPeA-LGW
PFPeA-HGW
PFHxA-DI
PFHxA-LGW
PFHxA-HGW
PFHpA-DI
PFHpA-LGW
PFHpA-HGW
PFOA-DI
PFOA-LGW
PFOA-HGW
PFNA-DI
PFNA-LGW
PFNA-HGW
PFDA-DI
PFDA-LGW
PFDA-HGW
PFUdA-DI
PFUdA-LGW
PFUdA-HGW
PFDoA-DI
PFDoA-LGW
PFDoA-HGW
PFTrDA-DI
PFTrDA-LGW
PFTrDA-HGW
FOSA-DI
FOSA-LGW
FOSA-HGW
N-MeFOSAA-DI
N-MeFOSAA-LGW
N-MeFOSAA-HGW
N-EtFOSAA-DI
N-EtFOSAA-LGW
N-EtFOSAA-HGW
PFBS-DI
PFBS-LGW
PFBS-HGW
PFPeS-DI
PFPeS-LGW
PFPeS-HGW
PFHxS-DI
PFHxS-LGW
PFHxS-HGW
PFHpS-DI
PFHpS-LGW
PFHpS-HGW
PFOS-DI
PFOS-LGW
PFOS-HGW
PFNS-DI
PFNS-LGW
PFNS-HGW
PFDS-DI
PFDS-LGW
PFDS-HGW
4:2FTS-DI
4:2FTS-LGW
4:2FTS-HGW
6:2FTS-DI
6:2FTS-LGW
6:2FTS-HGW
8:2FTS-DI
8:2FTS-LGW
8:2FTS-HGW
Time (min)

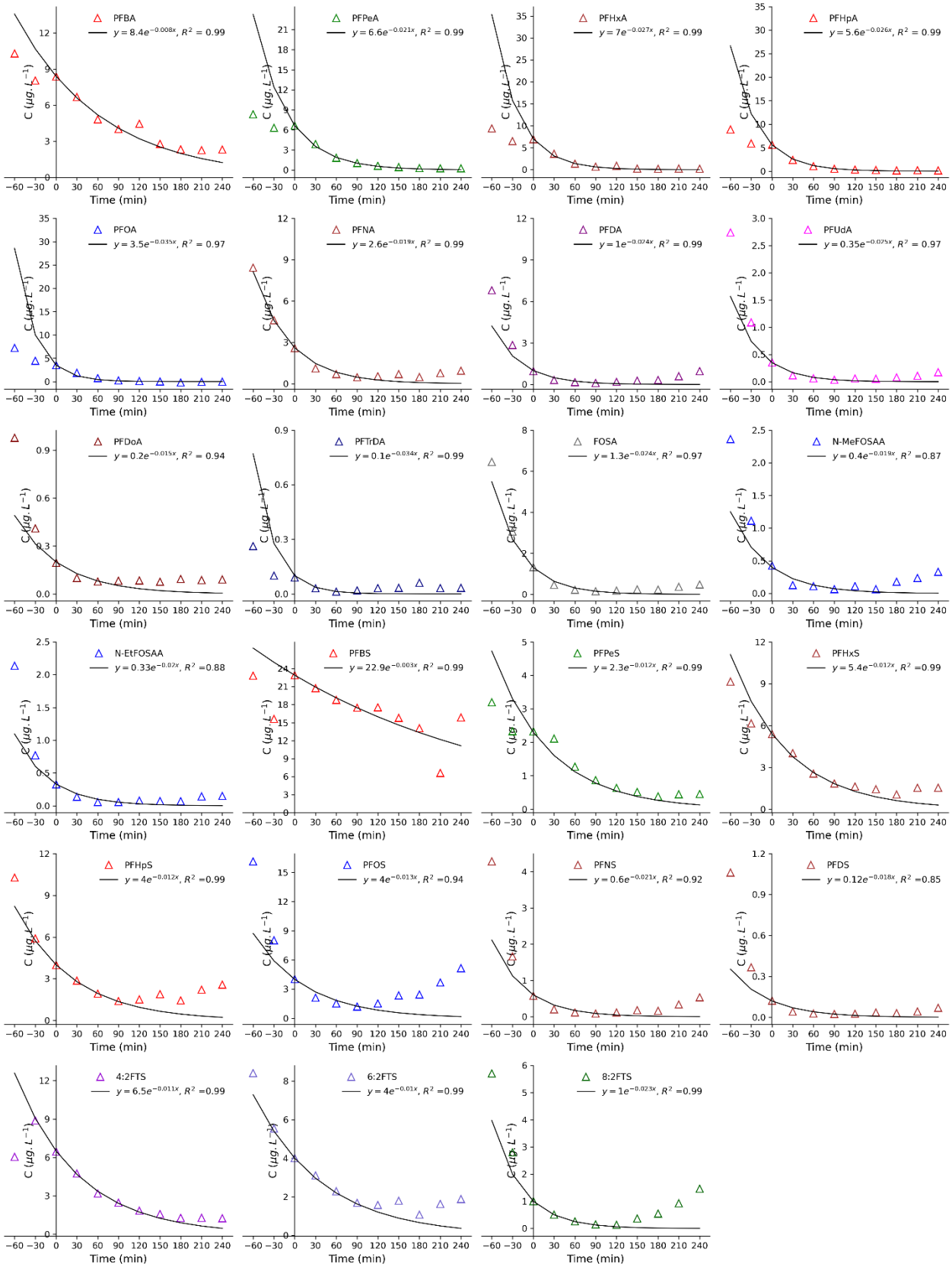
PFBA
$y = 8.4e^{-0.008x}$, $R^2 = 0.99$
PFPeA
$y = 6.6e^{-0.021x}$, $R^2 = 0.99$
PFHxA
$y = 7e^{-0.027x}$, $R^2 = 0.99$
PFHpA
$y = 5.6e^{-0.026x}$, $R^2 = 0.99$
PFOA
$y = 3.5e^{-0.035x}$, $R^2 = 0.97$
PFNA
$y = 2.6e^{-0.019x}$, $R^2 = 0.99$
PFDA
$y = 1e^{-0.024x}$, $R^2 = 0.99$
PFUdA
$y = 0.35e^{-0.025x}$, $R^2 = 0.97$
PFDoA
$y = 0.2e^{-0.015x}$, $R^2 = 0.94$
PFTrDA
$y = 0.1e^{-0.034x}$, $R^2 = 0.99$
FOSA
$y = 1.3e^{-0.024x}$, $R^2 = 0.97$
N-MeFOSAA
$y = 0.4e^{-0.019x}$, $R^2 = 0.87$
N-EtFOSAA
$y = 0.33e^{-0.02x}$, $R^2 = 0.88$
PFBS
$y = 22.9e^{-0.003x}$, $R^2 = 0.99$
PFPeS
$y = 2.3e^{-0.012x}$, $R^2 = 0.99$
PFHxS
$y = 5.4e^{-0.012x}$, $R^2 = 0.99$
PFHpS
$y = 4e^{-0.012x}$, $R^2 = 0.99$
PFOS
$y = 4e^{-0.013x}$, $R^2 = 0.94$
PFNS
$y = 0.6e^{-0.021x}$, $R^2 = 0.92$
PFDS
$y = 0.12e^{-0.018x}$, $R^2 = 0.85$
4:2FTS
$y = 6.5e^{-0.011x}$, $R^2 = 0.99$
6:2FTS
$y = 4e^{-0.01x}$, $R^2 = 0.99$
8:2FTS
$y = 1e^{-0.023x}$, $R^2 = 0.99$
C ($\mu g.L^{-1}$)
Time (min)

Figure A 4: Degradation kinetics of 24 different components of 24Mix in deionized water (DI), low TDS groundwater, and high TDS groundwater. The experiments were performed for 240 minutes in Argon saturated atmosphere at 10 °C. ○ - concentrations in deionized water, □ - concentrations in low TDS groundwater, and Δ - concentrations in high TDS groundwater. **a.** Pseudo-first-order removal of 24Mix in deionized water (DI), low TDS groundwater (LGW), and high TDS groundwater (HGW) using a 700 kHz - 250 W open system (P_d = 1250 $W.L^{-1}$). The error bars represent analytical triplicates. **b.** Pseudo-first-order removal of 24Mix in high TDS groundwater using 700 kHz - 1040 W closed system (P_d = 1040 $W.L^{-1}$). (See Figure 3.1 for comparison of rates)

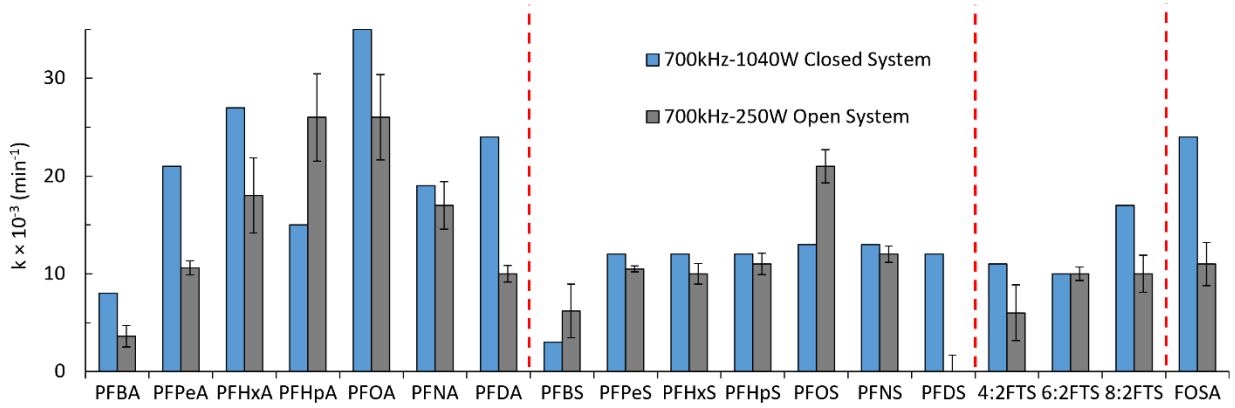

Figure A 5: Comparison of pseudo-first-order removal rates (min^{-1}) of PFASs observed in 700 kHz - 250 W open system (P_d = 1250 $W.L^{-1}$) with those observed in a 700 kHz - 1040 W closed system (P_d = 1040 $W.L^{-1}$) for the acoustic treatment of the 24Mix in high TDS groundwater. The removal rates were higher in the closed system despite the lower power density as compared to the open system. The error bars represent the standard deviation. (See Figure 3.1 for rates measured in different groundwater samples)

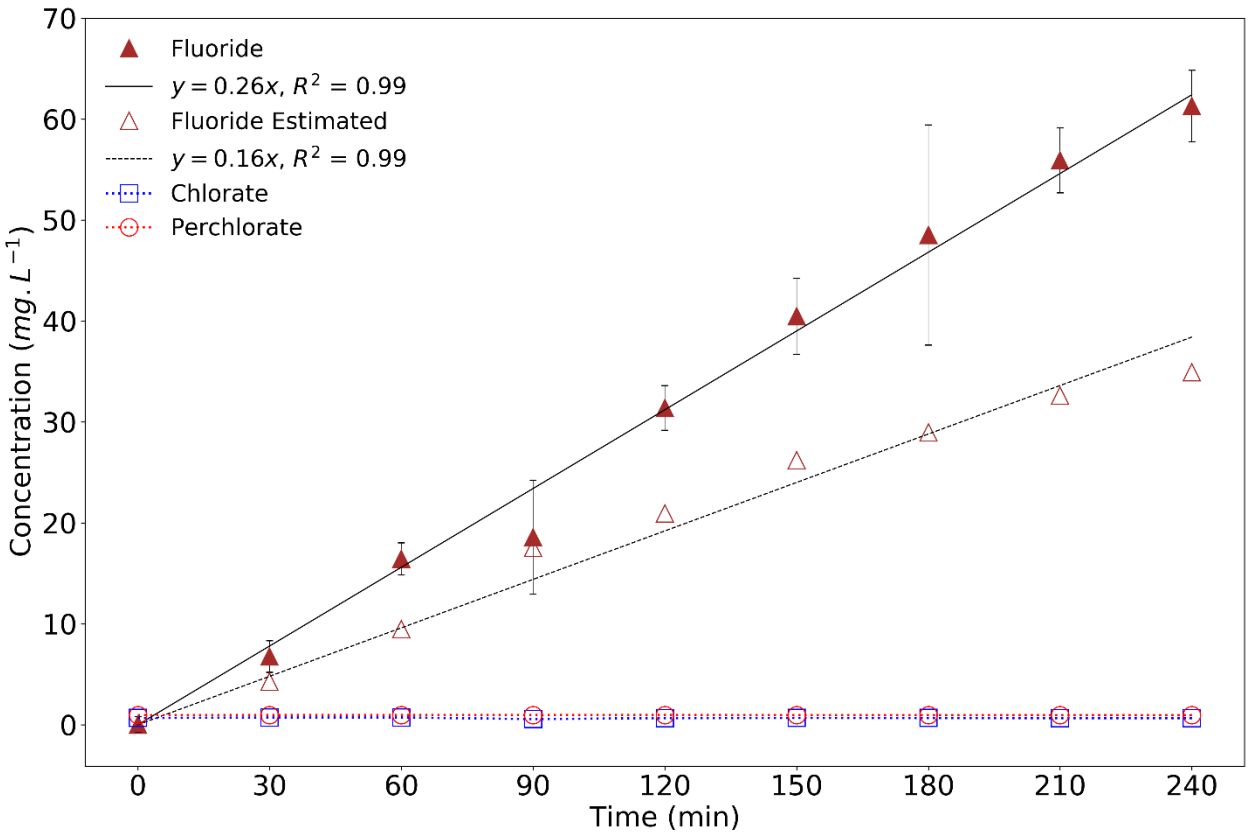

Figure A 6: Concentrations ($mg.L^{-1}$) of fluoride, chlorate and perchlorate detected during sonication of IDW in 700 kHz -1040 W closed system (P_d = 1040 $W.L^{-1}$). The experiment was conducted for 240 minutes at 10 °C in Argon saturated environment. (See Figure 3.2 for respective PFAS degradation and fluoride production in molar units)

a.

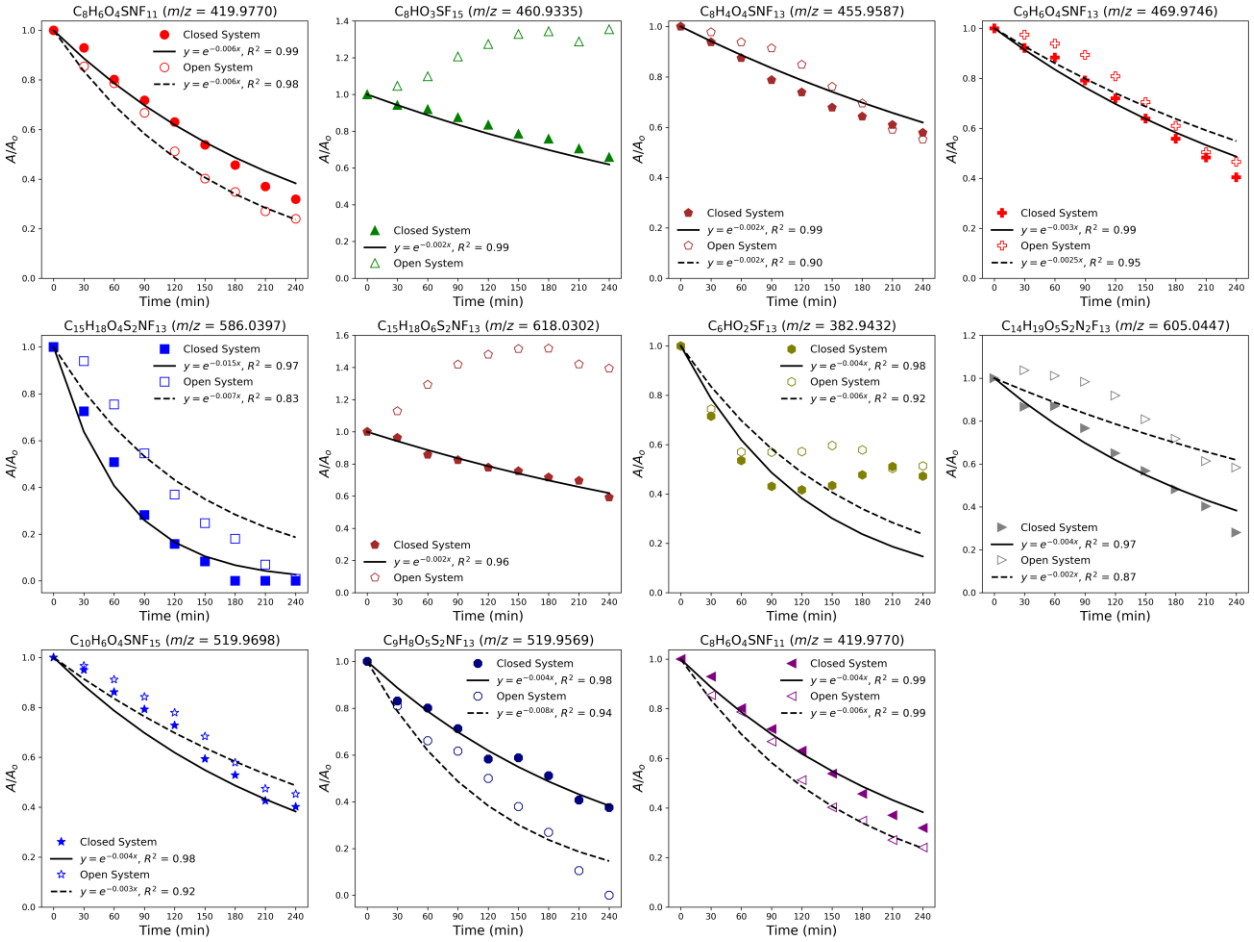
C8H6O4SNF11 (m/z = 419.9770)
Closed System
y = e−0.006x, R2 = 0.99
Open System
y = e−0.006x, R2 = 0.98
C8HO3SF15 (m/z = 460.9335)
Closed System
y = e−0.002x, R2 = 0.99
Open System
C8H4O4SNF13 (m/z = 455.9587)
Closed System
y = e−0.002x, R2 = 0.99
Open System
y = e−0.002x, R2 = 0.90
C9H6O4SNF13 (m/z = 469.9746)
Closed System
y = e−0.003x, R2 = 0.99
Open System
y = e−0.0025x, R2 = 0.95
C15H18O4S2NF13 (m/z = 586.0397)
Closed System
y = e−0.015x, R2 = 0.97
Open System
y = e−0.007x, R2 = 0.83
C15H18O6S2NF13 (m/z = 618.0302)
Closed System
y = e−0.002x, R2 = 0.96
Open System
C6HO2SF13 (m/z = 382.9432)
Closed System
y = e−0.004x, R2 = 0.98
Open System
y = e−0.006x, R2 = 0.92
C14H19O5S2N2F13 (m/z = 605.0447)
Closed System
y = e−0.004x, R2 = 0.97
Open System
y = e−0.002x, R2 = 0.87
C10H6O4SNF15 (m/z = 519.9698)
Closed System
y = e−0.004x, R2 = 0.98
Open System
y = e−0.003x, R2 = 0.92
C9H8O5S2NF13 (m/z = 519.9569)
Closed System
y = e−0.004x, R2 = 0.98
Open System
y = e−0.008x, R2 = 0.94
C8H6O4SNF11 (m/z = 419.9770)
Closed System
y = e−0.004x, R2 = 0.99
Open System
y = e−0.006x, R2 = 0.99
A/A0
Time (min)

b.

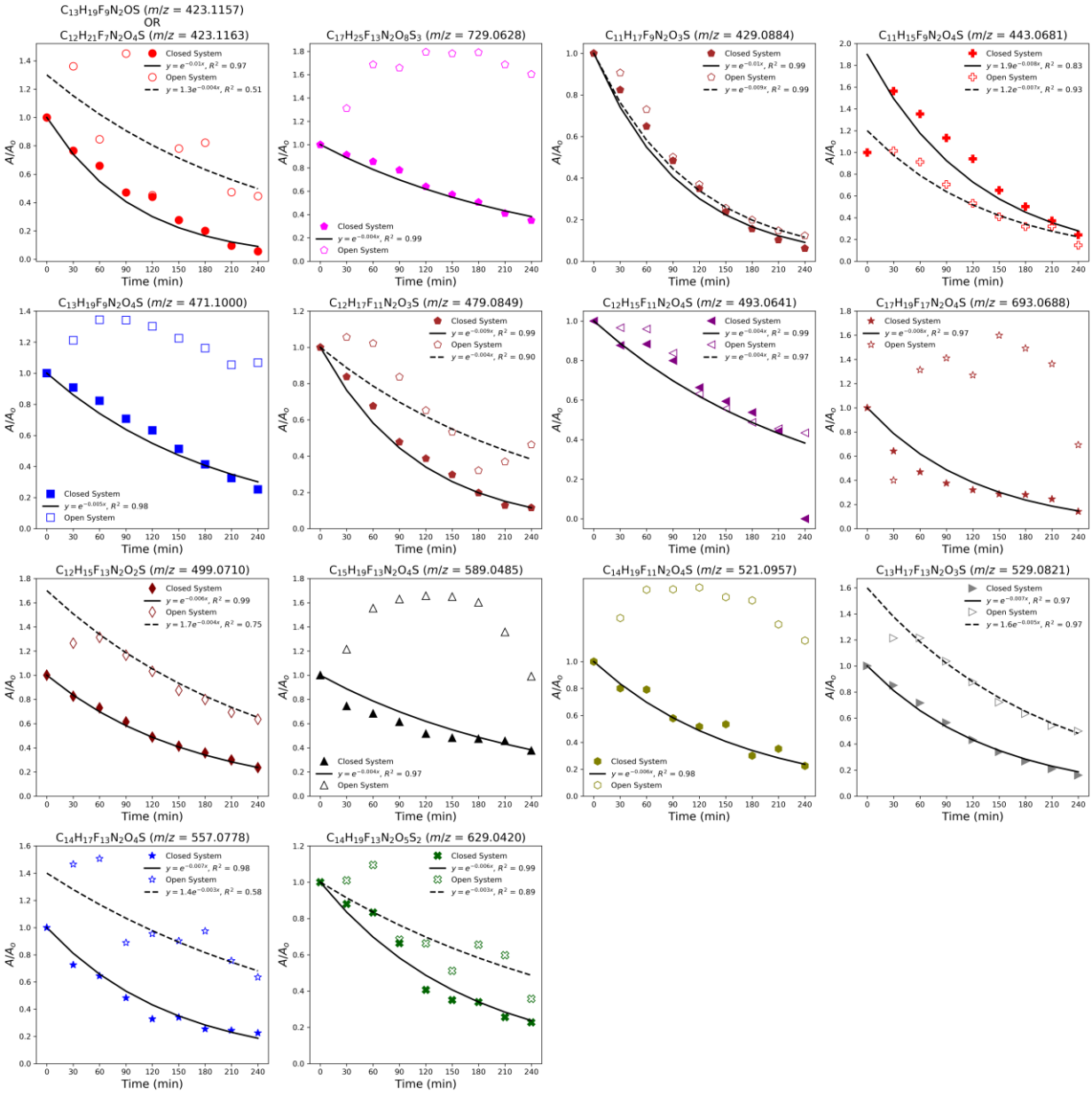

Figure A 7: Destruction of PFASs in concentrated investigation derived waste (IDW). The solid black line represents the kinetic model fitting for the experimental data (solid markers) in a 700 kHz - 1040 W closed system (P_d = 1040 $W.L^{-1}$) while the dotted black line represents the kinetic model fitting for the experimental data (empty markers) in a 700 kHz - 250 W open system (P_d = 1250 $W.L^{-1}$). The experiments were conducted for 240 minutes at 10 °C in Argon saturated environment. The rates were calculated for the first 120 min using the initial rate method. **a.** Relative decrease in the area (A/A_o) of PFASs detected in the negative electrospray ionization mode. **b.** Relative decrease in the area (A/A_o) of PFASs detected in the positive electrospray ionization mode. (See Figure 3.2 for measured concentrations of selected 16 PFASs)

a.

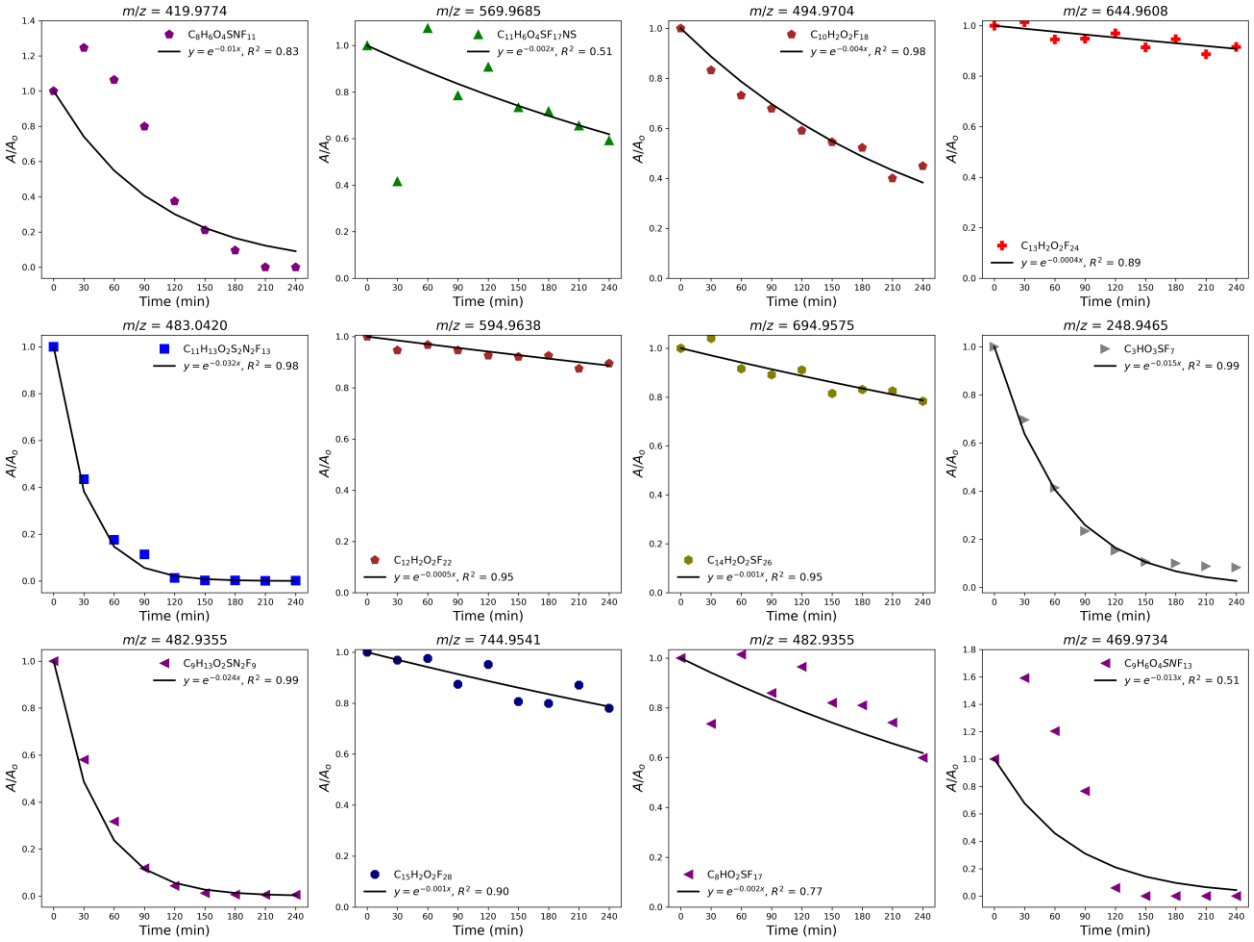
m/z = 419.9774
C8H6O4SNF11
y = e^-0.01x, R^2 = 0.83
m/z = 569.9685
C11H6O4SF17NS
y = e^-0.002x, R^2 = 0.51
m/z = 494.9704
C10H2O2F18
y = e^-0.004x, R^2 = 0.98
m/z = 644.9608
C13H2O2F24
y = e^-0.0004x, R^2 = 0.89
m/z = 483.0420
C11H13O2S2N2F13
y = e^-0.032x, R^2 = 0.98
m/z = 594.9638
C12H2O2F22
y = e^-0.0005x, R^2 = 0.95
m/z = 694.9575
C14H2O2SF26
y = e^-0.001x, R^2 = 0.95
m/z = 248.9465
C3HO3SF7
y = e^-0.015x, R^2 = 0.99
m/z = 482.9355
C9H13O2SN2F9
y = e^-0.024x, R^2 = 0.99
m/z = 744.9541
C15H2O2F28
y = e^-0.001x, R^2 = 0.90
m/z = 482.9355
C8HO2SF17
y = e^-0.002x, R^2 = 0.77
m/z = 469.9734
C9H6O4SNF13
y = e^-0.013x, R^2 = 0.51
A/A0
Time (min)

b.

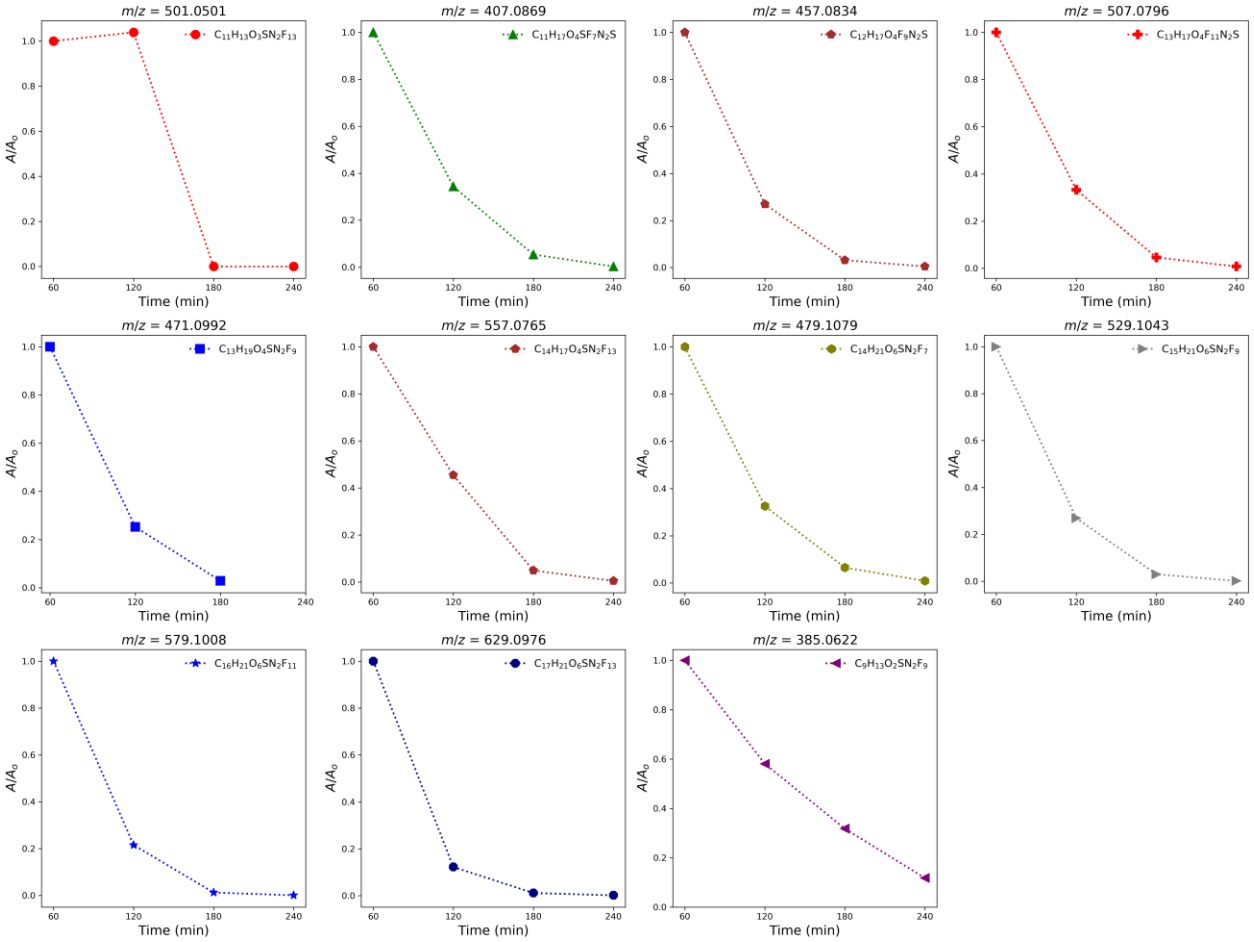

Figure A 8: Destruction of PFASs in AFFF spiked deionized water. The experiments were performed in a 700 kHz - 250 W open system (P_d = 1250 $W.L^{-1}$) for 240 minutes at 10 °C in Argon saturated environment. The rates were calculated for the first 120 min using the initial rate method. **a.** Relative decrease in the area (A/A_o) of PFASs detected in the negative electrospray ionization mode. **b.** Relative decrease in the area (A/A_o) of PFASs detected in the positive electrospray ionization mode. (See Figure 3.3 for measured concentrations of 10 selected PFASs)

a.

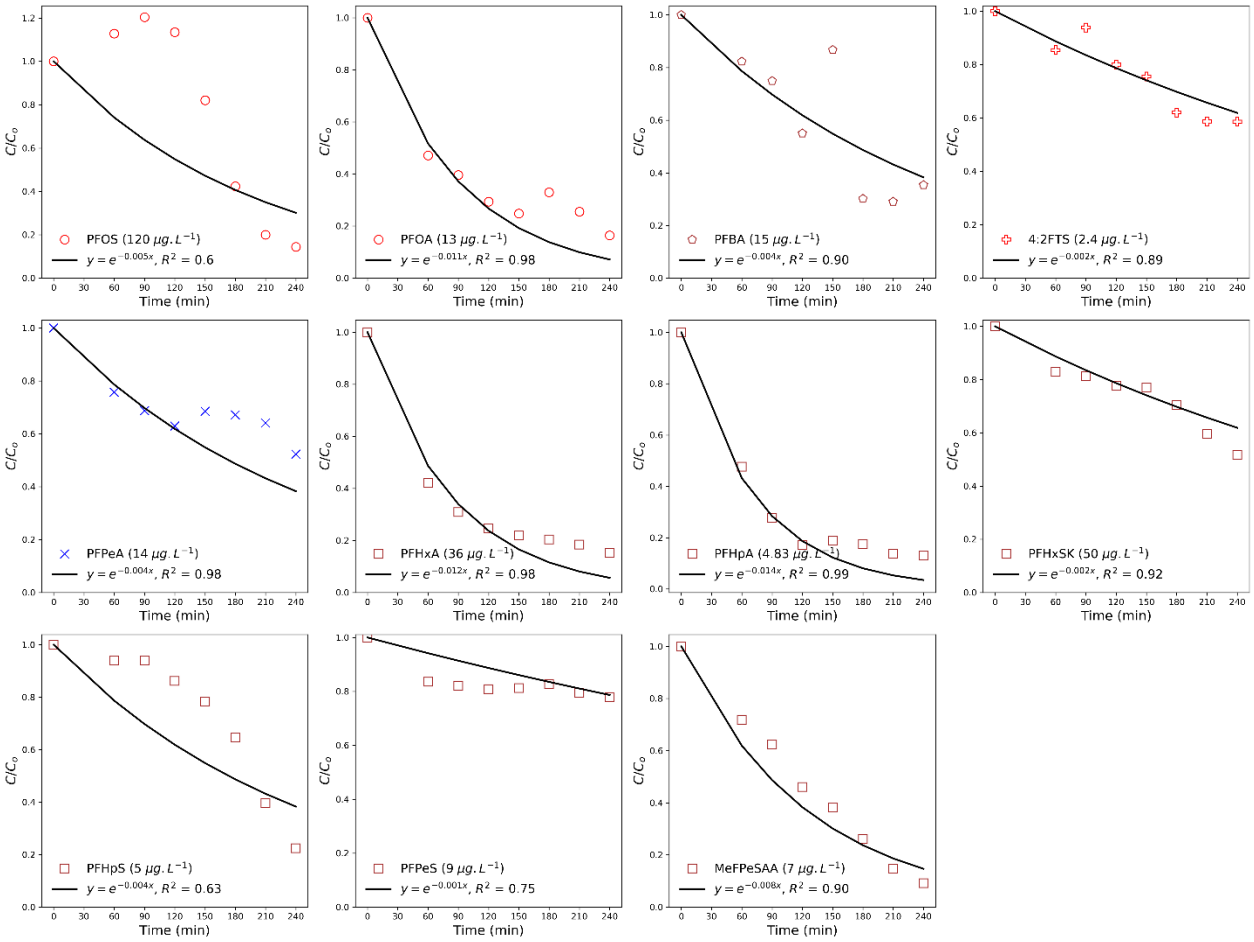
C/C_o
Time (min)
PFOS (120 μg.L⁻¹)
y = e^−0.005x, R² = 0.6
PFOA (13 μg.L⁻¹)
y = e^−0.011x, R² = 0.98
PFBA (15 μg.L⁻¹)
y = e^−0.004x, R² = 0.90
4:2FTS (2.4 μg.L⁻¹)
y = e^−0.002x, R² = 0.89
PFPeA (14 μg.L⁻¹)
y = e^−0.004x, R² = 0.98
PFHxA (36 μg.L⁻¹)
y = e^−0.012x, R² = 0.98
PFHpA (4.83 μg.L⁻¹)
y = e^−0.014x, R² = 0.99
PFHxSK (50 μg.L⁻¹)
y = e^−0.002x, R² = 0.92
PFHpS (5 μg.L⁻¹)
y = e^−0.004x, R² = 0.63
PFPeS (9 μg.L⁻¹)
y = e^−0.001x, R² = 0.75
MeFPeSAA (7 μg.L⁻¹)
y = e^−0.008x, R² = 0.90

b.

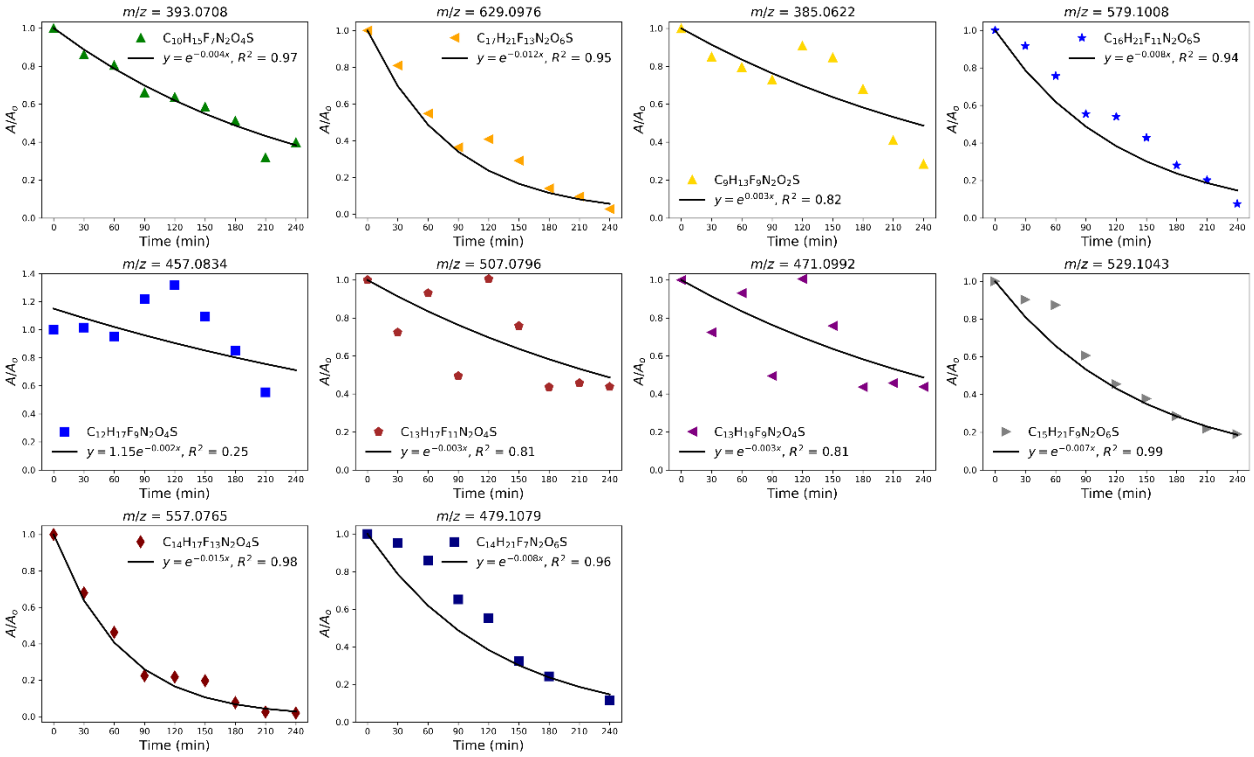
m/z = 393.0708
C10H15F7N2O4S
y = e−0.004x, R2 = 0.97
m/z = 629.0976
C17H21F13N2O6S
y = e−0.012x, R2 = 0.95
m/z = 385.0622
C9H13F9N2O2S
y = e0.003x, R2 = 0.82
m/z = 579.1008
C16H21F11N2O6S
y = e−0.008x, R2 = 0.94
m/z = 457.0834
C12H17F9N2O4S
y = 1.15e−0.002x, R2 = 0.25
m/z = 507.0796
C13H17F11N2O4S
y = e−0.003x, R2 = 0.81
m/z = 471.0992
C13H19F9N2O4S
y = e−0.003x, R2 = 0.81
m/z = 529.1043
C15H21F9N2O6S
y = e−0.007x, R2 = 0.99
m/z = 557.0765
C14H17F13N2O4S
y = e−0.015x, R2 = 0.98
m/z = 479.1079
C14H21F7N2O6S
y = e−0.008x, R2 = 0.96
A/Ao
Time (min)

c.

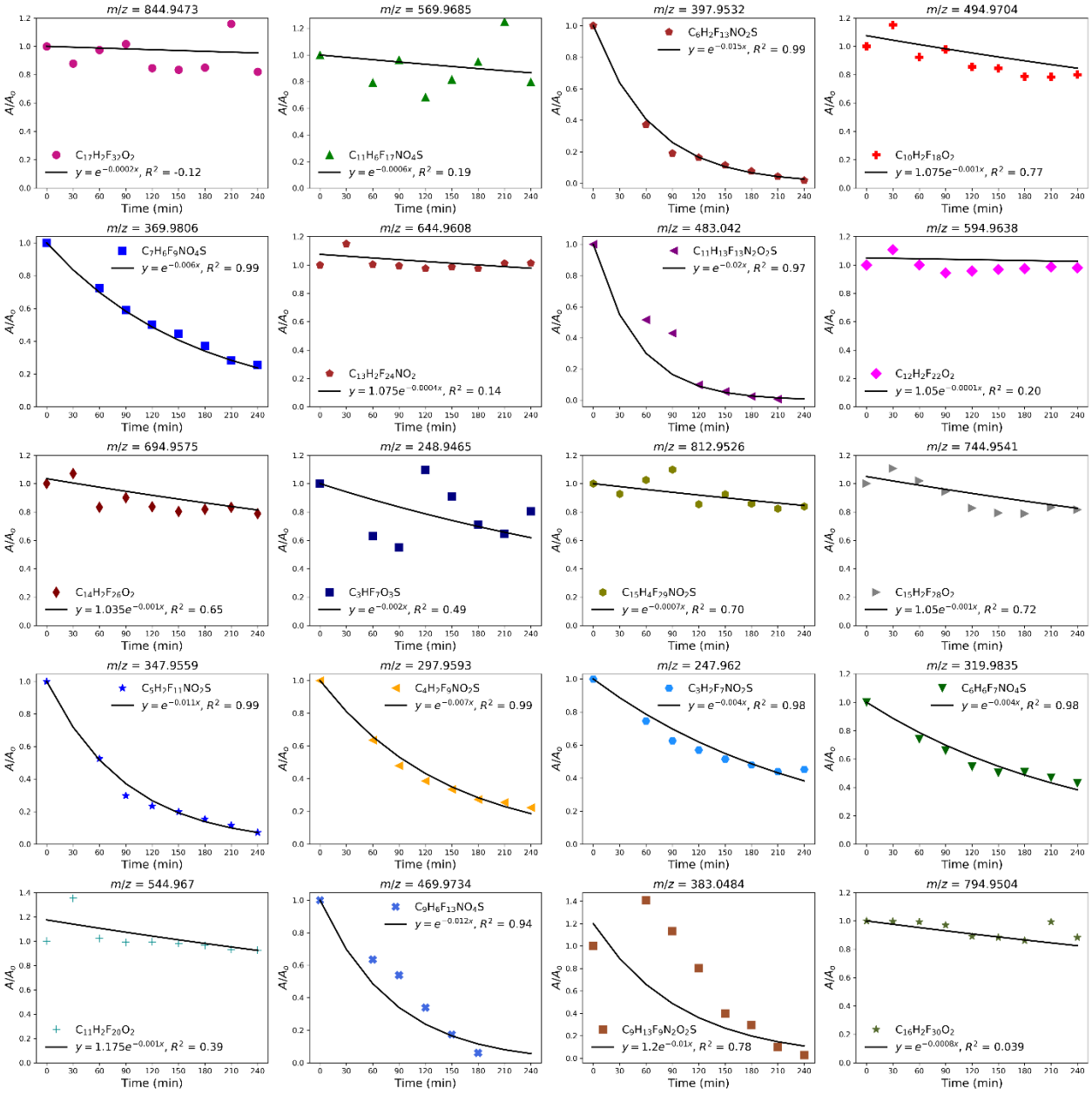

Figure A 9: Sonolytic destruction of PFASs after biological treatment by 1 U.mL^{-1} laccase and 20 mM HBT (Section 3.2.3). The experiments were performed in a 700 kHz - 250 W open system (P_d = 1250 W.L^{-1}) for 240 minutes at 10 °C in Argon saturated environment. The rates were calculated for the first 120 min using the initial rate method. **a.** Decrease in concentration of PFASs (C/C_o) **b.** Relative decrease in the area (A/A_o) of PFASs detected in the negative electrospray ionization mode. **c.** Relative decrease in the area (A/A_o) of PFASs detected in the positive electrospray ionization mode.

a.

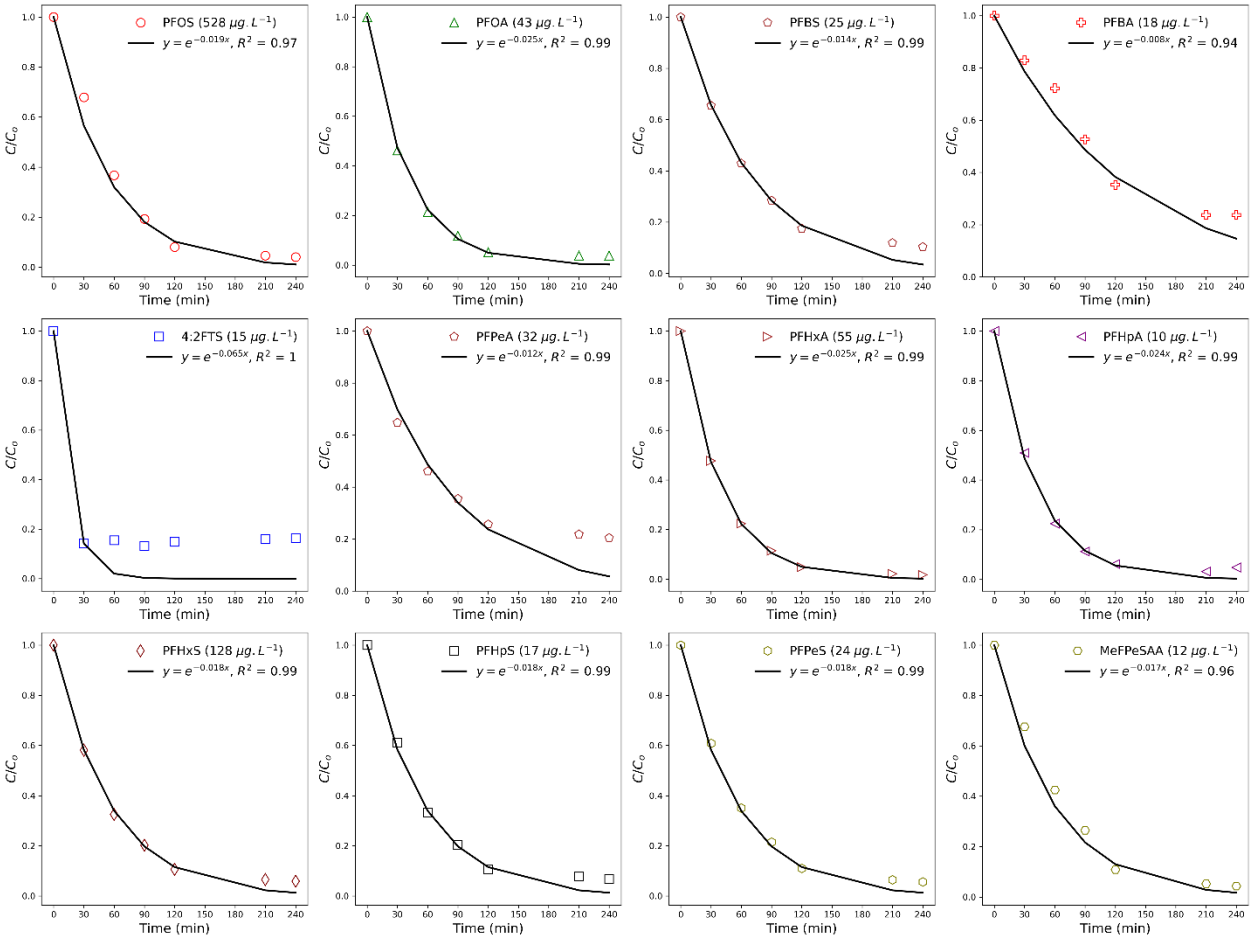
PFOS (528 μg. L⁻¹)
y = e^−0.019x, R² = 0.97
PFOA (43 μg. L⁻¹)
y = e^−0.025x, R² = 0.99
PFBS (25 μg. L⁻¹)
y = e^−0.014x, R² = 0.99
PFBA (18 μg. L⁻¹)
y = e^−0.008x, R² = 0.94
4:2FTS (15 μg. L⁻¹)
y = e^−0.065x, R² = 1
PFPeA (32 μg. L⁻¹)
y = e^−0.012x, R² = 0.99
PFHxA (55 μg. L⁻¹)
y = e^−0.025x, R² = 0.99
PFHpA (10 μg. L⁻¹)
y = e^−0.024x, R² = 0.99
PFHxS (128 μg. L⁻¹)
y = e^−0.018x, R² = 0.99
PFHpS (17 μg. L⁻¹)
y = e^−0.018x, R² = 0.99
PFPeS (24 μg. L⁻¹)
y = e^−0.018x, R² = 0.99
MeFPeSAA (12 μg. L⁻¹)
y = e^−0.017x, R² = 0.96
C/C0
Time (min)

b.

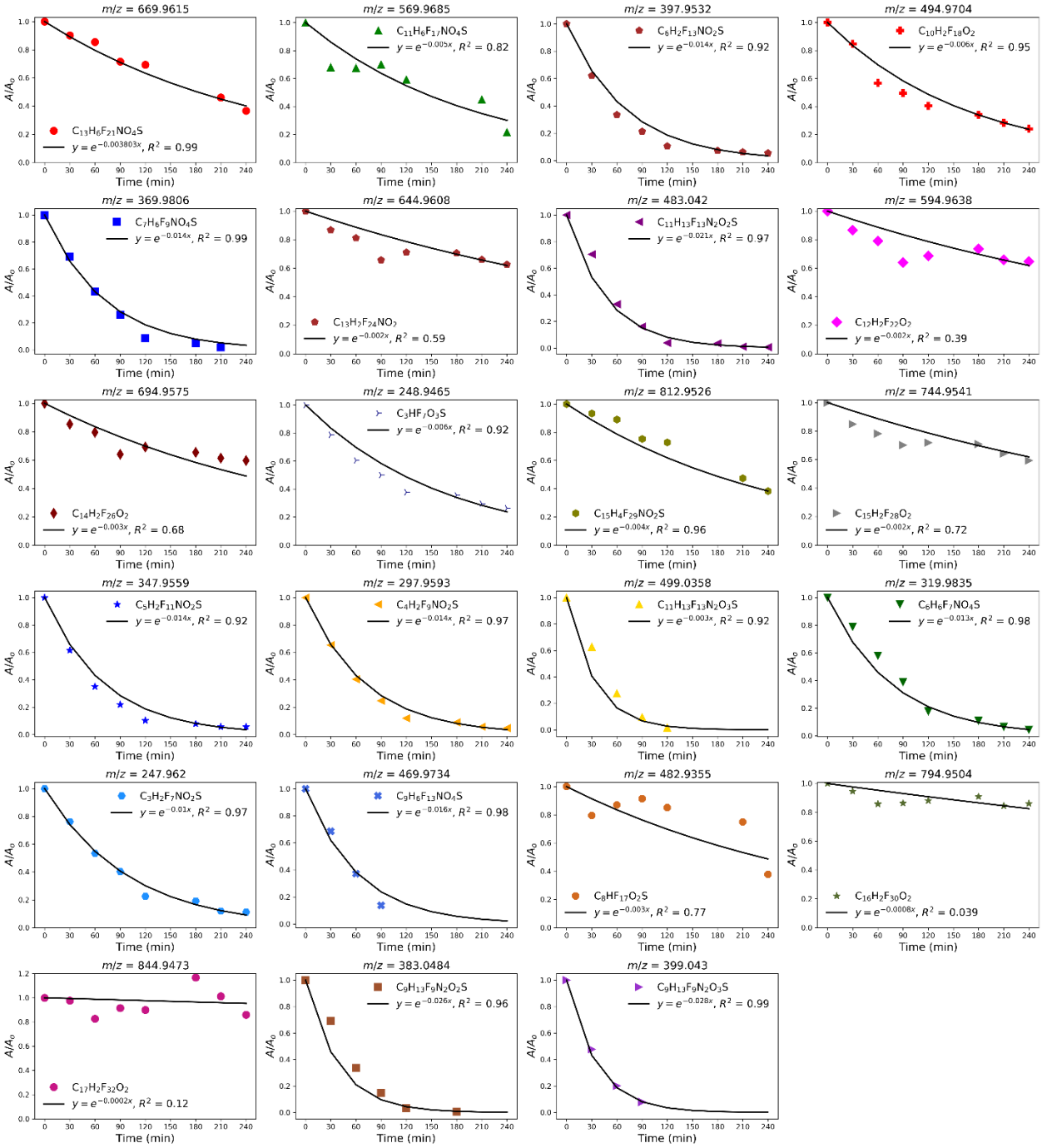
m/z = 669.9615
C13H6F21NO4S
y = e−0.003803x, R2 = 0.99
m/z = 569.9685
C11H6F17NO4S
y = e−0.005x, R2 = 0.82
m/z = 397.9532
C6H2F13NO2S
y = e−0.014x, R2 = 0.92
m/z = 494.9704
C10H2F18O2
y = e−0.006x, R2 = 0.95
m/z = 369.9806
C7H6F9NO4S
y = e−0.014x, R2 = 0.99
m/z = 644.9608
C13H7F24NO7
y = e−0.002x, R2 = 0.59
m/z = 483.042
C11H13F13N2O2S
y = e−0.021x, R2 = 0.97
m/z = 594.9638
C12H2F22O2
y = e−0.007x, R2 = 0.39
m/z = 694.9575
C14H2F26O2
y = e−0.003x, R2 = 0.68
m/z = 248.9465
C3HF7O3S
y = e−0.006x, R2 = 0.92
m/z = 812.9526
C15H4F29NO2S
y = e−0.004x, R2 = 0.96
m/z = 744.9541
C15H2F28O2
y = e−0.002x, R2 = 0.72
m/z = 347.9559
C5H2F11NO2S
y = e−0.014x, R2 = 0.92
m/z = 297.9593
C4H2F9NO2S
y = e−0.014x, R2 = 0.97
m/z = 499.0358
C11H13F13N2O3S
y = e−0.003x, R2 = 0.92
m/z = 319.9835
C6H6F7NO4S
y = e−0.013x, R2 = 0.98
m/z = 247.962
C3H2F7NO2S
y = e−0.01x, R2 = 0.97
m/z = 469.9734
C9H6F13NO4S
y = e−0.016x, R2 = 0.98
m/z = 482.9355
C8HF17O2S
y = e−0.003x, R2 = 0.77
m/z = 794.9504
C16H2F30O2
y = e−0.0008x, R2 = 0.039
m/z = 844.9473
C17H2F32O2
y = e−0.0002x, R2 = 0.12
m/z = 383.0484
C9H13F9N2O2S
y = e−0.026x, R2 = 0.96
m/z = 399.043
C9H13F9N2O3S
y = e−0.028x, R2 = 0.99
A/A0
Time (min)

c.

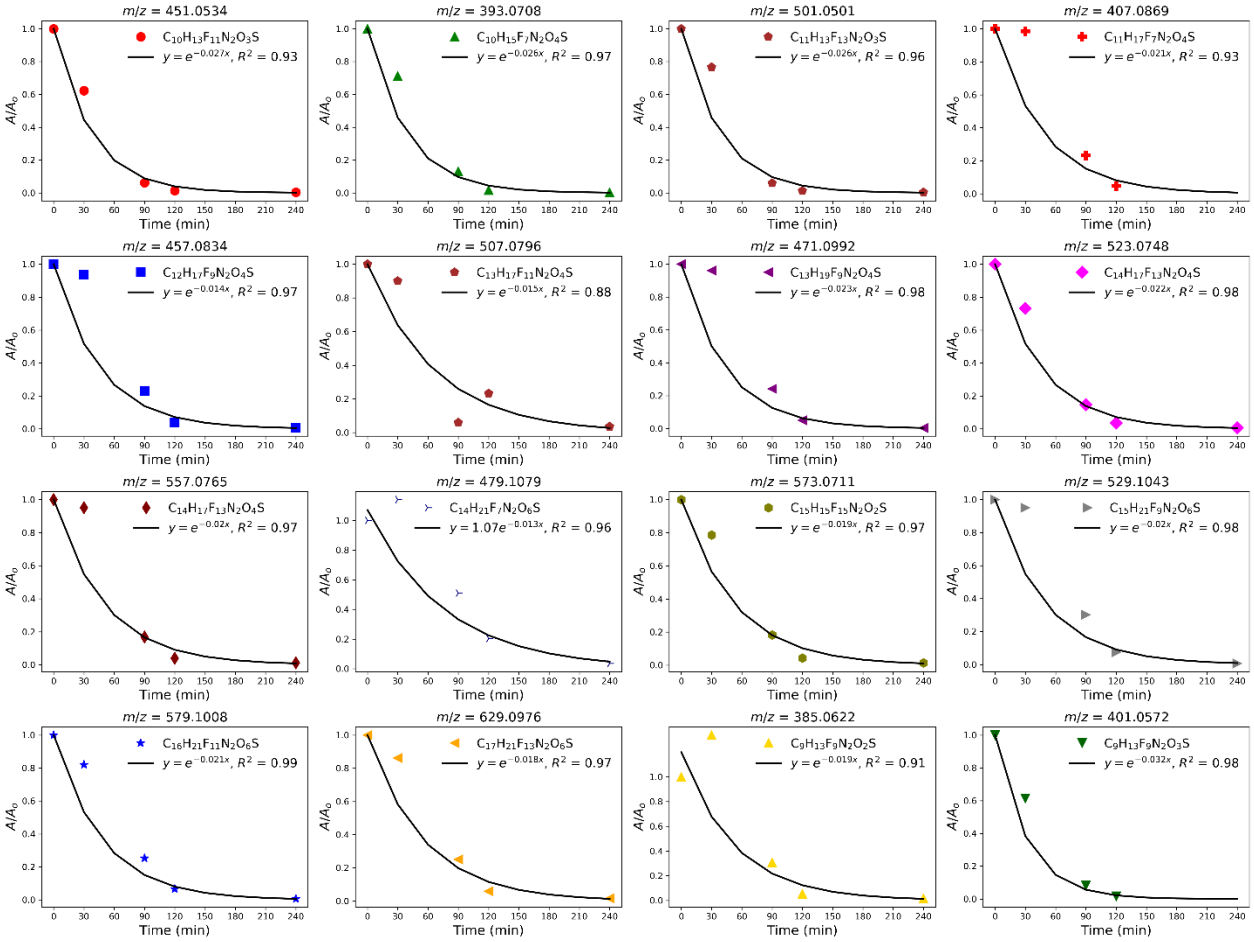

Figure A 10: Sonolytic destruction of PFASs after electrochemical treatment. The experiments were performed in a 700 kHz - 250 W open system (P_d = 1250 $W.L^{-1}$) for 240 minutes at 10 °C in Argon saturated environment. The rates were calculated for the first 120 min using the initial rate method. **a.** Decrease in concentration of PFASs (C/C_o) **b.** Relative decrease in the area (A/A_o) of PFASs detected in the negative electrospray ionization mode. **c.** Relative decrease in the area (A/A_o) of PFASs detected in the positive electrospray ionization mode.

References

1. USFDA. *Per and Polyfluoroalkyl Substances (PFASs)*. [Website] 2019 14 October 2019]; Available from: https://www.fda.gov/food/chemicals/and-polyfluoroalkyl-substances-pfas#targetText=There%20are%20nearly%205%2C000%20types,used%20and%20studied%20than%20others.
2. Sunderland, E.M., X.C. Hu, C. Dassuncao, A.K. Tokranov, C.C. Wagner, and J.G. Allen, *A review of the pathways of human exposure to poly- and perfluoroalkyl substances (PFASs) and present understanding of health effects.* Journal of Exposure Science & Environmental Epidemiology, 2019. **29**(2): p. 131-147.
3. Merino, N., Y. Qu, R.A. Deeb, E.L. Hawley, M.R. Hoffmann, and S. Mahendra, *Degradation and Removal Methods for Perfluoroalkyl and Polyfluoroalkyl Substances in Water.* Environmental Engineering Science, 2016. **33**(9): p. 615-649.
4. Rayne, S. and K. Forest, *Perfluoroalkyl sulfonic and carboxylic acids: a critical review of physicochemical properties, levels and patterns in waters and wastewaters, and treatment methods.* Journal of Environmental Science and Health Part A, 2009. **44**(12): p. 1145-99.
5. Li, F., J. Duan, S. Tian, H. Ji, Y. Zhu, Z. Wei, and D. Zhao, *Short-chain per- and polyfluoroalkyl substances in aquatic systems: Occurrence, impacts and treatment.* Chemical Engineering Journal, 2020. **380**.
6. Kah, M., D. Oliver, and R. Kookana, *Sequestration and potential release of PFAS from spent engineered sorbents.* Science of The Total Environment, 2020: p. 142770.
7. Lu, D., S. Sha, J. Luo, Z. Huang, and X. Zhang Jackie, *Treatment train approaches for the remediation of per- and polyfluoroalkyl substances (PFAS): A critical review.* Journal of Hazardous Materials, 2020. **386**: p. 121963.
8. Gole, V.L., A. Fishgold, R. Sierra-Alvarez, P. Deymier, and M. Keswani, *Treatment of perfluorooctane sulfonic acid (PFOS) using a large-scale sonochemical reactor.* Separation and Purification Technology, 2018. **194**: p. 104-110.
9. Nzeribe, B.N., M. Crimi, S. Mededovic Thagard, and T.M. Holsen, *Physico-Chemical Processes for the Treatment of Per- And Polyfluoroalkyl Substances (PFAS): A review.* Critical Reviews in Environmental Science and Technology, 2019. **49**(10): p. 866-915.
10. Dombrowski, P.M., P. Kakarla, W. Caldicott, Y. Chin, V. Sadeghi, D. Bogdan, F. Barajas-Rodriguez, and S.-Y.D. Chiang, *Technology review and evaluation of different chemical oxidation conditions on treatability of PFAS.* Remediation Journal, 2018. **28**(2): p. 135-150.
11. Wang, S., Q. Yang, F. Chen, J. Sun, K. Luo, F. Yao, X. Wang, D. Wang, X. Li, and G. Zeng, *Photocatalytic degradation of perfluorooctanoic acid and perfluorooctane sulfonate in water: A critical review.* Chemical Engineering Journal, 2017. **328**: p. 927-942.
12. Pica, N.E., J. Funkhouser, Y. Yin, Z. Zhang, D.M. Ceres, T. Tong, and J. Blotevogel, *Electrochemical Oxidation of Hexafluoropropylene Oxide Dimer Acid (GenX): Mechanistic Insights and Efficient Treatment Train with Nanofiltration.* Environmental Science & Technology, 2019. **53**(21): p. 12602-12609.
13. Horst, J., J. McDonough, I. Ross, M. Dickson, J. Miles, J. Hurst, and P. Storch, *Water treatment technologies for PFAS: the next generation.* Groundwater Monitoring Remediation, 2018. **38**(2): p. 13-23.

14. Horst, J., J. McDonough, I. Ross, and E. Houtz, *Understanding and Managing the Potential By-Products of PFAS Destruction.* Groundwater Monitoring and Remediation, 2020. **40**(2): p. 17-27.
15. Bentel, M.J., Y. Yu, L. Xu, Z. Li, B.M. Wong, Y. Men, and J. Liu, *Defluorination of Per- and Polyfluoroalkyl Substances (PFASs) with Hydrated Electrons: Structural Dependence and Implications to PFAS Remediation and Management.* Environmental Science & Technology, 2019. **53**(7): p. 3718-3728.
16. Cui, J., P. Gao, and Y. Deng, *Destruction of Per- and Polyfluoroalkyl Substances (PFAS) with Advanced Reduction Processes (ARPs): A Critical Review.* Environmental Science & Technology, 2020. **54**(7): p. 3752-3766.
17. Kim, T.H., S. Yu, Y. Choi, T.Y. Jeong, and S.D. Kim, *Profiling the decomposition products of perfluorooctane sulfonate (PFOS) irradiated using an electron beam.* Science of The Total Environment, 2018. **631-632**: p. 1295-1303.
18. Kim, T.-H., S.-H. Lee, H.Y. Kim, K. Doudrick, S. Yu, and S.D. Kim, *Decomposition of perfluorooctane sulfonate (PFOS) using a hybrid process with electron beam and chemical oxidants.* Chemical Engineering Journal, 2019. **361**: p. 1363-1370.
19. Wang, L., B. Batchelor, S.D. Pillai, and V.S.V. Botlaguduru, *Electron beam treatment for potable water reuse: Removal of bromate and perfluorooctanoic acid.* Chemical Engineering Journal, 2016. **302**: p. 58-68.
20. Vecitis, C.D., H. Park, J. Cheng, B.T. Mader, and M.R. Hoffmann, *Kinetics and mechanism of the sonolytic conversion of the aqueous perfluorinated surfactants, perfluorooctanoate (PFOA), and perfluorooctane sulfonate (PFOS) into inorganic products.* The Journal of Physical Chemistry A, 2008. **112**(18): p. 4261-70.
21. Leong, T., A. Muthupandian, and S. Kentish, *The Fundamentals of Power Ultrasound-A Review*. 2011.
22. Okitsu, K., T. Suzuki, N. Takenaka, H. Bandow, R. Nishimura, and Y. Maeda, *Acoustic multibubble cavitation in water: A new aspect of the effect of a rare gas atmosphere on bubble temperature and its relevance to sonochemistry.* The Journal of Physical Chemistry B, 2006. **110**(41): p. 20081-4.
23. Yasuda, K., H. Matsushima, and Y. Asakura, *Generation and reduction of bulk nanobubbles by ultrasonic irradiation.* Chemical Engineering Science, 2019. **195**: p. 455-461.
24. Suslick, K.S., *Mechanochemistry and sonochemistry: concluding remarks.* Faraday Discuss, 2014. **170**(0): p. 411-22.
25. Flint, E.B. and K.S. Suslick, *The temperature of cavitation.* Science, 1991. **253**(5026): p. 1397-9.
26. Mason, T.J. and T. Andreas, *Mason, Timothy J., and Andreas Tiehm. Advances in Sonochemistry: Ultrasound in Environmental Protection. Vol. 6. Elsevier*. Vol. 91. 2017. 399-404.
27. CDC. *Cleaning. Guideline for Disinfection and Sterilization in Healthcare Facilities* 2016 [cited 2020 10/2/2020]; Available from: https://www.cdc.gov/infectioncontrol/guidelines/disinfection/cleaning.html.
28. Mulţescu, R., D. Georgescu, P.A. Geavlete, and B. Geavlete, *Equipment and Instruments in Percutaneous Nephrolithotomy*, in *Percutaneous Surgery of the Upper Urinary Tract*. 2016. p. 3-24.

29. Niam, A.G. and L. Sucahyo, *Ultrasonic atomizer application for Low Cost Aeroponic Chambers (LCAC): a review.* IOP Conference Series: Earth and Environmental Science, 2020. **542**.
30. Frinking, P., T. Segers, Y. Luan, and F. Tranquart, *Three Decades of Ultrasound Contrast Agents: A Review of the Past, Present and Future Improvements.* Ultrasound in Medicine and Biology, 2020. **46**(4): p. 892-908.
31. Campbell, T.Y., C.D. Vecitis, B.T. Mader, and M.R. Hoffmann, *Perfluorinated surfactant chain-length effects on sonochemical kinetics.* The Journal of Physical Chemistry A, 2009. **113**(36): p. 9834-42.
32. Singh, R.K., N. Multari, C. Nau-Hix, R.H. Anderson, S.D. Richardson, T.M. Holsen, and S. Mededovic Thagard, *Rapid Removal of Poly- and Perfluorinated Compounds from Investigation-Derived Waste (IDW) in a Pilot-Scale Plasma Reactor.* Environmental Science & Technology, 2019. **53**(19): p. 11375-11382.
33. Shende, T., G. Andaluri, and R.P.S. Suri, *Kinetic model for sonolytic degradation of non-volatile surfactants: Perfluoroalkyl substances.* Ultrasonics Sonochemistry, 2019. **51**(September 2018): p. 359-368.
34. Lin, J.C., C.Y. Hu, and S.L. Lo, *Effect of surfactants on the degradation of perfluorooctanoic acid (PFOA) by ultrasonic (US) treatment.* Ultrasonics Sonochemistry, 2016. **28**: p. 130-135.
35. Costanza, J., M. Arshadi, L.M. Abriola, and K.D. Pennell, *Accumulation of PFOA and PFOS at the Air–Water Interface.* Environmental Science & Technology Letters, 2019. **6**(8): p. 487-491.
36. Schaefer, C.E., V. Culina, D. Nguyen, and J. Field, *Uptake of Poly- and Perfluoroalkyl Substances at the Air-Water Interface.* Environmental Science & Technology, 2019. **53**(21): p. 12442-12448.
37. Lin, J.C., S.L. Lo, C.Y. Hu, Y.C. Lee, and J. Kuo, *Enhanced sonochemical degradation of perfluorooctanoic acid by sulfate ions.* Ultrasonics Sonochemistry, 2015. **22**: p. 542-7.
38. Zhao, D., C. Ding, X. Xu, and M.R. Hoffmann, *Kinetics of perfluorooctane sulfonate and perfluorooctanoate degradation by ultrasound irradiation.* CIESC Journal, 2011.
39. Campbell, T. and M.R. Hoffmann, *Sonochemical degradation of perfluorinated surfactants: Power and multiple frequency effects.* Separation and Purification Technology, 2015. **156**(April): p. 1019-1027.
40. Casado, J., M.A. Lopez-Quintela, and F.M. Lorenzo-Barral, *The initial rate method in chemical kinetics: Evaluation and experimental illustration.* Journal of Chemical Education, 1986. **63**(5): p. 450-452.
41. Laugier, F., C. Andriantsiferana, A.M. Wilhelm, and H. Delmas, *Ultrasound in gas-liquid systems: effects on solubility and mass transfer.* Ultrasonics Sonochemistry, 2008. **15**(6): p. 965-72.
42. Cao, H., W. Zhang, C. Wang, and Y. Liang, *Sonochemical degradation of poly- and perfluoroalkyl substances - A review.* Ultrasonics Sonochemistry, 2020. **69**: p. 105245.
43. Fernandez, N.A., L. Rodriguez-Freire, M. Keswani, and R. Sierra-Alvarez, *Effect of chemical structure on the sonochemical degradation of perfluoroalkyl and polyfluoroalkyl substances (PFASs).* Environmental Science: Water Research & Technology, 2016. **2**(6): p. 975-983.

44. Wang, Z., M. MacLeod, I.T. Cousins, M. Scheringer, and K. Hungerbühler, *Using COSMOtherm to predict physicochemical properties of poly- and perfluorinated alkyl substances (PFASs).* Environmental Chemistry, 2011. **8**(4).
45. Ding, G. and W.J.G.M. Peijnenburg, *Physicochemical Properties and Aquatic Toxicity of Poly- and Perfluorinated Compounds.* Critical Reviews in Environmental Science and Technology, 2013. **43**(6): p. 598-678.
46. Cheng, J., C.D. Vecitis, H. Park, B.T. Mader, and M.R. Hoffmann, *Sonochemical degradation of perfluorooctane sulfonate (PFOS) and perfluorooctanoate (PFOA) in groundwater: kinetic effects of matrix inorganics.* Environmental Science & Technology, 2010. **44**(1): p. 445-50.
47. Cheng, J., C.D. Vecitis, H. Park, B.T. Mader, and M.R. Hoffmann, *Sonochemical degradation of peerfluorooctane sulfonate (PFOS) and perfluorooctanoate (PFOA) in landfill groundwater: environmental matrix effects.* Environmental Science & Technology, 2008. **42**(21): p. 8057-63.
48. Nejumal, K.K., P.R. Manoj, U.K. Aravind, and C.T. Aravindakumar, *Sonochemical degradation of a pharmaceutical waste, atenolol, in aqueous medium.* Environmental Science and Pollution Research, 2014. **21**(6): p. 4297-308.
49. Yang, G., J.-J. Zhu, K. Okitsu, Y. Mizukoshi, B.M. Teo, N. Enomoto, S.G. Babu, B. Neppolian, M. Ashokkumar, and S. Shaik, *Handbook of ultrasonics and sonochemistry*. 2016: Springer Singapore.
50. Han, T., L. Gao, J. Chen, X. He, and B. Wang, *Spatiotemporal variations, sources and health risk assessment of perfluoroalkyl substances in a temperate bay adjacent to metropolis, North China.* Environmental Pollution, 2020. **265**(Pt A): p. 115011.
51. Casas, G., A. Martinez-Varela, J.L. Roscales, M. Vila-Costa, J. Dachs, and B. Jimenez, *Enrichment of perfluoroalkyl substances in the sea-surface microlayer and sea-spray aerosols in the Southern Ocean.* Environmental Pollution, 2020. **267**: p. 115512.
52. Woodard, S., J. Berry, and B. Newman, *Ion exchange resin for PFAS removal and pilot test comparison to GAC.* Remediation Journal, 2017. **27**(3): p. 19-27.
53. Vecitis, C.D., Y. Wang, J. Cheng, H. Park, B.T. Mader, and M.R. Hoffmann, *Sonochemical degradation of perfluorooctanesulfonate in aqueous film-forming foams.* Environmental Science & Technology, 2010. **44**(1): p. 432-8.
54. Rodriguez-Freire, L., N. Abad-Fernandez, R. Sierra-Alvarez, C. Hoppe-Jones, H. Peng, J.P. Giesy, S. Snyder, and M. Keswani, *Sonochemical degradation of perfluorinated chemicals in aqueous film-forming foams.* Journal ofHazardous Materials, 2016. **317**: p. 275-283.
55. Moriwaki, H., Y. Takagi, M. Tanaka, K. Tsuruho, K. Okitsu, and Y. Maeda, *Sonochemical decomposition of perfluorooctane sulfonate and perfluorooctanoic acid.* Environmental Science & Technology, 2005. **39**(9): p. 3388-92.
56. Azar, L., *Cavitation in ultrasonic cleaning and cell disruption.* Controlled Environments, 2009: p. 14-17.
57. Tiehm, A. and U. Neis, *Ultrasound in environmental engineering. Papers*. Vol. 25. 1999: Society for the Development of Research and Development of Environmental Technologies at the Technical University of Hamburg-Harburg eV, Hamburg.
58. Gogate, P.R., P.A. Tatake, P.M. Kanthale, and A.B. Pandit, *Mapping of sonochemical reactors: review, analysis, and experimental verification.* AIChE Journal, 2002. **48**(7): p. 1542-1560.

59. James Wood, R., T. Sidnell, I. Ross, J. McDonough, J. Lee, and M.J. Bussemaker, *Ultrasonic degradation of perfluorooctane sulfonic acid (PFOS) correlated with sonochemical and sonoluminescence characterisation.* Ultrasonics Sonochemistry, 2020. **68**: p. 105196.
60. Trojanowicz, M., A. Bojanowska-Czajka, I. Bartosiewicz, and K. Kulisa, *Advanced Oxidation/Reduction Processes treatment for aqueous perfluorooctanoate (PFOA) and perfluorooctanesulfonate (PFOS) – A review of recent advances.* Chemical Engineering Journal, 2018. **336**: p. 170-199.
61. Bolton, J.R., K.G. Bircher, W. Tumas, and C.A. Tolman, *Figures-of-merit for the technical development and application of advanced oxidation technologies for both electric- and solar-driven systems (IUPAC Technical Report).* Pure and Applied Chemistry, 2001. **73**(4): p. 627-637.
62. Mahamuni, N.N. and Y.G. Adewuyi, *Advanced oxidation processes (AOPs) involving ultrasound for waste water treatment: a review with emphasis on cost estimation.* Ultrasonics Sonochemistry, 2010. **17**(6): p. 990-1003.
63. Kumar, A., P.R. Gogate, and A.B. Pandit, *Mapping the efficacy of new designs for large scale sonochemical reactors.* Ultrasonics Sonochemistry, 2007. **14**(5): p. 538-544.
64. Phan Thi, L.A., H.T. Do, and S.L. Lo, *Enhancing decomposition rate of perfluorooctanoic acid by carbonate radical assisted sonochemical treatment.* Ultrasonics Sonochemistry, 2014. **21**(5): p. 1875-80.
65. Hu, Y.B., S.L. Lo, Y.F. Li, Y.C. Lee, M.J. Chen, and J.C. Lin, *Autocatalytic degradation of perfluorooctanoic acid in a permanganate-ultrasonic system.* Water Research, 2018. **140**: p. 148-157.
66. Hori, H., Y. Nagano, M. Murayama, K. Koike, and S. Kutsuna, *Efficient decomposition of perfluoroether carboxylic acids in water with a combination of persulfate oxidant and ultrasonic irradiation.* Journal of Fluorine Chemistry, 2012. **141**: p. 5-10.
67. Wang, J., Z. Wang, C.L.Z. Vieira, J.M. Wolfson, G. Pingtian, and S. Huang, *Review on the treatment of organic pollutants in water by ultrasonic technology.* Ultrasonics Sonochemistry, 2019. **55**: p. 273-278.

Chapter 4

Field Demonstration: Large-scale Ultrasonic System for The Treatment of Per- and Polyfluoroalkyl Substances Impacted Groundwater.

Abstract

Per- and polyfluoroalkyl substances (PFASs) are a class of fluorinated surfactants used in countless applications. Potential human health risks posed by PFASs include endocrine disruptions and negative effects on the development of reproductive systems. Historical PFAS-containing AFFF release at fire training areas has impacted groundwater at many sites across the world. We tested the treatment of AFFF/PFAS impacted high salinity groundwater using a custom-built field scale reactor (59 L). The impacted groundwater had high dissolved solids concentrations (10200 $mg.L^{-1}$) due to seawater intrusion. The PFAS concentration in the reactor influent ranged from 54401 ± 2927 $ng.L^{-1}$ (PFHxS) to 26.5±7.6 $ng.L^{-1}$ (4:2 FTS) with 46660 ± 4236 $ng.L^{-1}$ PFOS and 37130 ± 7913 $ng.L^{-1}$ PFOA. The reactor carried out successful degradation of 15 PFASs (>90%) and 11 PFAS precursors, with 11 PFASs and 7 TOPs degraded to < 70 $ng.L^{-1}$ when impacted groundwater was irradiated by 700 kHz ultrasound. The rates of ultrasonic degradation were higher for PFCAs (compared to PFSAs), longer chain PFASs, and sonication at higher power densities. Investigation of the effect of reactor temperature (15 °C and 25 °C) on degradation kinetics demonstrated higher rates at higher temperatures. No disinfection byproducts (chlorate and perchlorate) and PFAS intermediates were detected during 8 h of sonication in all 6 operating conditions. The energy consumed during 8 h of sonication was 28.01 ± 0.47 kWh while the E_{EO} estimates for the treatment of 54 L, 33 L, and 22 L impacted groundwater were 599.51 ± 52.54 $kWh.m^{-3}.order^{-1}$, 797.25 ± 42.16 $kWh.m^{-3}.order^{-1}$, and 699.43 ± 3.30 $kWh.m^{-3}.order^{-1}$, respectively. There is a critical need for developing destructive and non-destructive technologies for the removal of PFASs from impacted environments. This study demonstrates the successful utilization of a large-scale ultrasonic reactor in the field for the treatment of PFAS impacted groundwater without production of disinfection byproducts or PFAS intermediates.

4.1 Introduction

PFASs have recently created much concern due to their detection in various environmental matrices and high resistance towards traditional treatment technologies. With increasing water recycling and reuse, the destructive technologies for remediation of PFAS impacted water have become increasingly important. The regulatory agencies have also started to introduce stringent regulations to mitigate the risks of PFASs impacting natural resources (Chapter 2).

Current treatment technologies are limited to the sorption or separation of PFASs with landfilling or incineration as the ultimate disposal/destruction alternative. The off-site transportation costs, chemical and reagent costs, and disposal costs could be significant contributors to the expenses involved in these technologies. Moreover, only a few PFAS destruction technologies, like plasma treatment, have been successfully demonstrated to be field-ready. However, these destructive technologies may have the downside of producing disinfection byproducts and short-chain intermediates [1-10]. The ultrasonic reactor can be used with relative ease for PFAS defluorination as it does not require technical expertise, specialized equipment, or additional reagents.

The ultrasonic bench-scale study demonstrated its effectiveness in PFAS mineralization in high salinity matrices with high PFAS load, including groundwater and investigation-derived waste, without generating disinfection byproducts, like chlorate and perchlorate. The acoustic treatment technology creates micro-nano cavities in the bulk liquid. Under the high acoustic pressure applied by high-frequency sound, the temperatures in these cavities can be over 5000 K. The high temperature leads to the pyrolysis of chemical bonds leading to complete mineralization of PFASs. The lab-scale study demonstrated the mineralization of 51 PFASs in IDW and

degradation of 41 PFASs in AFFF along with near stoichiometric fluoride recovery of HFPO-DA and 6:2 FTAB (Chapter 3).

This work evaluates the efficacy of the acoustic treatment technology at the field scale using a large-scale reactor for treating AFFF impacted groundwater. The field-scale reactor was designed as per the results obtained in the lab-scale study and incorporated into a mobile trailer for easy transport and testing at the desired site. We also assessed the formation of disinfection byproducts and evaluated the degradation of various PFAS precursors by ultrasound. The energy consumption estimates were also performed for the field scale demonstration.

4.2 Materials and Methods.

4.2.1 Chemicals

All labeled PFASs used as internal standards were obtained from Wellington Labs (Guelph, Ontario, Canada). LC-MS grade solvents and other reagents (ACS Grade) were purchased from Thermo Fisher Scientific (Waltham, MA) or Sigma-Aldrich (St. Louis, MO).

4.2.2 Site and Groundwater.

The site characterization and selection were performed by GSI Environmental Inc. The site had been used for testing and evaluation since 1945 (Figure 4.1). The site is approximately 1.5 acres and includes two fire training (or burn pits), one closed, and one active. The closed burn pit was used for firefighter training from the late 1950s to 1984. The active burn pit is still available for use as a fire training area, without AFFFs. The site has interbedded sands, silts, and clays, and the semi-perched aquifer extends from the water table (i.e., 0.6 m to 3 m) to approximately 26 m

to 41 m. The groundwater flow is to the northeast direction, during the dry season, and to the southwest direction, during the rainy season. The reversal of historical groundwater gradient, with the draw of groundwater from the aquifer systems, lead to seawater intrusion into the aquifers and high concentrations of total dissolved solids (TDS) (Table 4.1).

Table 4.1: Groundwater Characteristics.

Characteristic	Background Levels
Nitrate ($mg.L^{-1}$)	N.D.
Nitrite ($mg.L^{-1}$)	N.D.
Fluoride ($mg.L^{-1}$)	0.9
Chloride ($mg.L^{-1}$)	5283.7
Bromide ($mg.L^{-1}$)	17.4
Sulfate ($mg.L^{-1}$)	1955.5
Sodium ($mg.L^{-1}$)	3203.0
Aluminum ($mg.L^{-1}$)	N.D.
Magnesium ($mg.L^{-1}$)	581.6
Calcium ($mg.L^{-1}$)	1145.0
Manganese ($mg.L^{-1}$)	1.7
Iron ($mg.L^{-1}$)	0.05
TDS ($mg.L^{-1}$)	10200
pH	6.70
Specific Conductance ($\mu S.cm^{-1}$)	16000
TOC ($mg.L^{-1}$)	6.43

Figure 4.1: Site of the field demonstration of the Pilot-scale Ultrasonic Reactor for the treatment of PFAS impacted Groundwater.

4.2.3 Reactor Design and Operation.

The installation and operation of the reactor on the site were performed by GSI Environmental Inc. A customized sonolysis reactor was obtained from PCT Systems, Inc. (San Jose, CA). The reactor was made of stainless steel with a capacity of 59 L with dimensions of 101.60 cm (l) × 45.72 cm (w) × 12.7 cm (d). The ultrasound source is a collection of 48 - 700 kHz piezoelectrical transducers (2.54 cm × 12.70 cm) assembled in four quadrants, with a total piezo area of 1548 cm^2. (Figure 4.2). The reactor's rated operating power is 7200 W with a power intensity of approximately 9 $W.cm^{-2}$. The electrical power consumed during the sonication of PFASs was monitored using an inline power meter. Additionally, the reactor was equipped with a temperature sensor to measure the solution temperature, low-level switch, water level indicator, pressure gauge, and pressure relief valve to monitor the pressure conditions (≈ 1 atm) and stainless-steel cooling coils. A 5-ton cooling unit (220 V - 3Phase - 30 Amps) was used to circulate a water/alcohol refrigerant mixture through the cooling coils to control the reactor temperature. The design of the pilot-scale reactor was based on the findings of the laboratory study using a 2 L bench-scale reactor. The reactor was housed in a 4.27 m × 2.13 m trailer positioned on level ground on the paved area of the site under investigation. The groundwater was pumped from the extraction well through a 0.45 µm filter and stored in two polypropylene containers (1041 L each, 1.22 m × 1 m) till needed for treatment by the pilot-scale system. A portable generator was used to provide power (240 VAC) to the pilot-scale system. The reactor containing groundwater was purged with high purity argon for 30 min before, during, and after the operation of the reactor. A granular activated carbon (GAC) cartridge was installed on the headspace vent to capture any potential VOC or PFAS destruction bi-products emissions. The sonolysis experiments were performed for 8 h and each experiment was conducted once because of the time limitations. For every hour of

treatment, the ultrasound was on for 45 min on and off for 15 min. Different operational parameters like power density (122 $W.L^{-1}$, 203 $W.L^{-1}$, and 305 $W.L^{-1}$) and reactor temperature (15 °C and 25 °C), were tested in batches using the sonolysis reactor. The samples were collected every hour during the 15 min off phase.

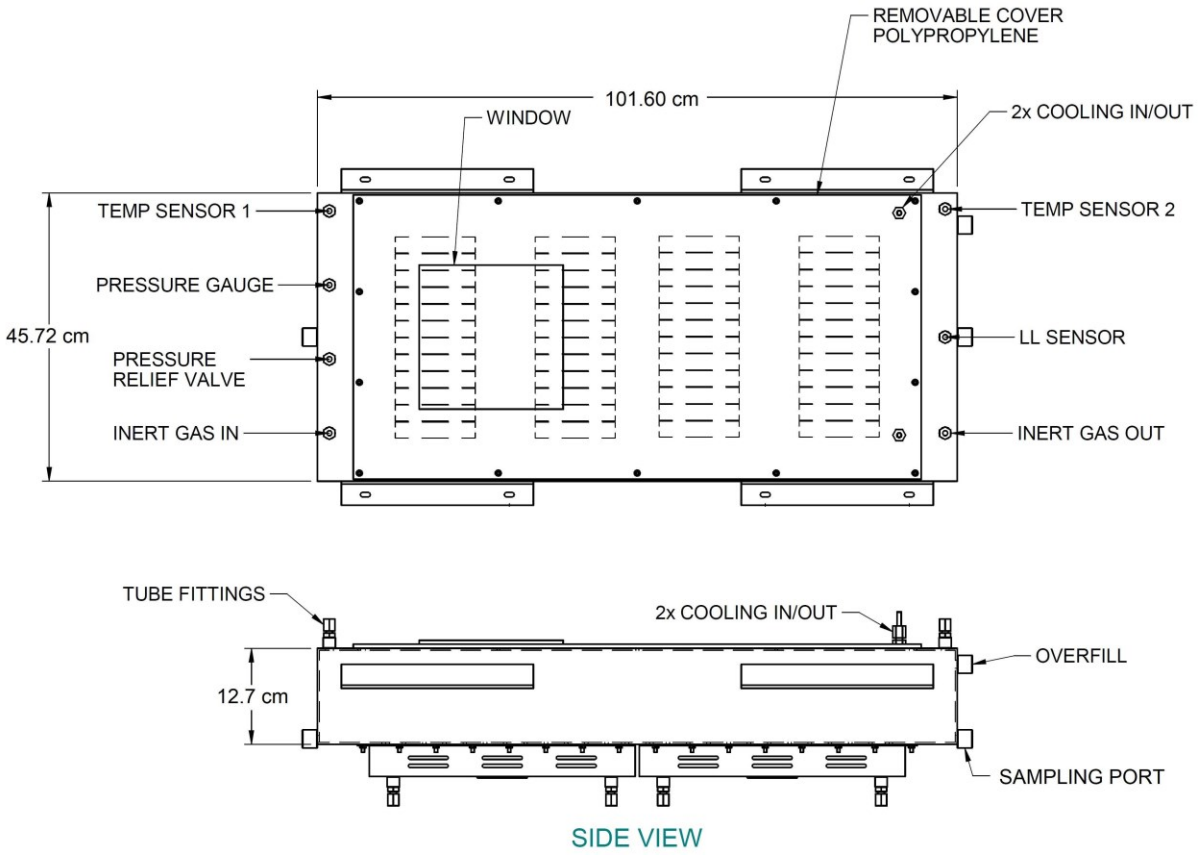

Figure 4.2: Schematic of stainless-steel ultrasonic field reactor (59 L) equipped with 700 kHz transducer array and stainless-steel (0.25 in) cooling coils. The dimensions are in centimeters.

4.2.4 Calculations.

The destruction of 15 PFASs and 11 PFAS precursors was monitored during the sonication of impacted groundwater. The pseudo-first-order rates were calculated using the initial rate method [11] and the kinetics were modeled as (equation 4.1)

$$\frac{dC_{PFAS}}{dt} = -k \times C_{PFAS} \quad (4.1)$$

The removal percentage was calculated by (equation 4.2)

$$\text{PFAS removal } (\%) = \frac{C_o - C}{C_o} \times 100 \quad (4.2)$$

where C_o is the initial PFAS concentration and C is the final PFAS concentration. The power density was calculated as (equation 4.3)

$$\text{Power Density} = \frac{I \times v}{V} \quad (4.3)$$

where I is the current drawn (A), v is the voltage (V), and V is the volume of water treated (L). The calorimetric power density is 62.2% of the electrical power and can be calculated as described by Laugier et al. [11]. The energy consumption was calculated as (equation 4.4 and equation 4.5).

$$E_{EM}(kWh.g^{-1}) = \frac{P \times t \times 10^3}{V(C_i - C_f)} \quad (4.4)$$

$$E_{EO}(kWh.m^{-3}.order^{-1}) = \frac{P \times t \times 10^3}{V \times \log(C_i/C_f)} \quad (4.5)$$

where E_{EM} is the energy consumed per mass removed ($kWh.g^{-1}$), E_{EO} is the energy consumed per order of magnitude removal ($kWh.m^{-3}.order^{-1}$), P is the rated power (kW), t is time (h), V is the volume (L), C_i is the initial cumulative PFAS concentration ($mg.L^{-1}$), C_f is the final cumulative PFAS concentration ($mg.L^{-1}$), and k is the pseudo-first-order rate constant (min^{-1}). The cumulative rate constant was calculated to estimate the energy consumed for the treatment of groundwater as equation 4.6.

$$\sum k = \frac{\ln\left(\sum C_i / \sum C_f\right)}{t} \qquad (4.6)$$

where Σk is cumulative removal rate (min^{-1}), t is time (min), ΣC_i is the initial cumulative PFAS concentration ($mg.L^{-1}$), ΣC_f is the final cumulative PFAS concentration ($mg.L^{-1}$). Cumulative PFAS mass removal was calculated as equation 4.7

$$\text{Cumulative PFAS Mass Removed} = \frac{(C_i^{PFAS} - C_f^{PFAS}) + (C_i^{TOP} - C_f^{TOP})}{10^6} \times V \qquad (4.7)$$

where C_i^{PFAS} is the initial cumulative PFAS concentration ($ng.L^{-1}$), C_f^{PFAS} is the final cumulative PFAS concentration ($mg.L^{-1}$), C_i^{TOP} is the initial cumulative TOP concentration ($ng.L^{-1}$), C_f^{TOP} is the final cumulative TOP concentration ($mg.L^{-1}$), and V is the volume of water treated (L).

4.2.5 Analytical Methods.

Water samples were spiked with 20 µL of 100 $ng.mL^{-1}$ internal standard solution (MPFAC-24ES, Wellington Labs, Guelph, Ontario, Canada), two grams of sodium chloride added, and then vortexed. Liquid-liquid extraction was performed with 2 mL of a 90% ethyl acetate/10% trifluoroethanol solution for 30 mins on a rotary mixer. Samples were centrifuged for 2 minutes at 3500 rpm and the upper organic phase was transferred to a clean vial. Solvent extraction was repeated, supernatants were combined, and then dried under nitrogen. Samples were resuspended by vortexing with 500 µL of methanol and then diluted with 500 µL of water. Final samples were transferred to sample vials with polypropylene insert and polypropylene caps for PFAS quantification.

The total oxidizable precursor (TOP) assay was performed in the original water sample containers to minimize sorption losses based on a previously published protocol with some modifications [12]. Potassium persulfate was added to a final concentration of 60 mM as dry powder to minimize sample dilution. Sodium hydroxide was added from a 5 M stock solution to a final concentration of 250 mM to ensure that the pH remained above 12 in the water samples for the entire duration of the oxidation. The samples were then transferred to a temperature-controlled water bath and treated at 85 °C for six hours. A pH adjustment at the end of the oxidative treatment was not necessary due to the subsequent liquid-liquid extraction of the samples as described above. The complete oxidative conversion of the quantified precursor compounds 4:2 FTS, 6:2 FTS, 8:2 FTS, and FOSA confirmed the effectiveness of our modified TOP assay protocol.

PFAS analysis was performed at Colorado State University, as discussed before (Chapter 3). PFASs in original water samples and TOP assay samples were analyzed on an Agilent 1290 liquid chromatograph coupled to an Agilent 6460 triple quadrupole mass spectrometer (LC/QqQ-MS), which was equipped with an electrospray ionization (ESI) source using Agilent Jet Stream Technology (Agilent, Santa Clara, CA). The analytes were separated on an Agilent Poroshell C18 column (2.1 mm x 100 mm, 2.7 µm particle size) at 40 °C. A sample volume of 15 µL was injected into a binary mixture of 5 mM ammonium acetate in water (A) and 5 mM ammonium acetate in methanol (B) at a flow rate of 0.4 $mL.min^{-1}$. The gradient used was 20% B for 1 minute, increasing to 45% B at 2 min, and finally increased to 100% B at 5 min. The ionization source conditions used were as follows: negative ESI, nebulizer of 15 psi, gas flow of 4 L/min at 230 °C, sheath gas flow of 12 $L.min^{-1}$ at 350 °C, nozzle voltage of 500 V, and capillary voltage at 3500 V. Analytes were identified by comparison of retention times with analytical standards, individual MRM mass transitions, and with MS/MS ion ratios. Peaks matching retention

within 5% and with ion ratios at 20% of the standard ratio were considered acceptable for identification. The data collection and processing were performed by using Agilent MassHunter Quantitative software (v B.07.01). Quantitation was performed with linear regression using calibration curves from 0.01-250 $ng.mL^{-1}$. To minimize system-related interferences or background, an Agilent Eclipse Plus C18 column (4.6 mm × 50 mm, 5 µm particle size) was installed as a delay column, immediately after the binary pump and prior to the injection port. The mobile phase degasser was bypassed allowing the mobile phase to enter the binary pump directly and avoiding contact with plastic filters. All plastic tubing in the LC/MS system was replaced with PEEK tubing and plastic frits were replaced with stainless steel. All sample vials were polypropylene with polypropylene caps. Five injections of pure methanol were made prior to sample analysis to determine if any system background analyte levels were present. With these system changes, background levels for each analyte were not detected in blank samples.

For the quantification of fluoride, chlorate, and perchlorate, filtered samples (0.22 µm filtered) were injected onto an ion chromatograph (Dionex Integrion HPIC, Thermo Fisher Scientific) equipped with an IonPac™ AG16 Guard Column (4 mm × 50 mm) and Dionex™ IonPac™ AS16 Analytical Column (250 m × 4.0 mm ID) operated at 30 °C. Chromatographic separation of anions was achieved by running a gradient of aqueous hydroxide mobile phase ramping from 0.5 mM to 55 mM at a flow rate of 1 $mL.min^{-1}$ for a total run time of 35 min. Anions were detected using a conductivity detector with elution patterns confirmed by standards. The detection limit for all three anions was 0.007 $mg.L^{-1}$.

4.3 Results and Discussion.

4.3.1 Acoustic Destruction of PFASs.

The treatment of groundwater by 700 kHz ultrasound in the pilot-scale reactor demonstrated the destruction of 15 investigated PFASs (Figure 4.3) and total oxidizable precursors (TOPs) for 11 investigated TOP categories (Figure 4.4) for all tested conditions. The acoustic destruction of PFASs and TOPs followed pseudo-first-order kinetics. The degradation rates of 15 investigated PFASs, and the initial and final concentrations are reported in (Table 4.2). Similar data are reported for TOPs in (Table 4.3). Interestingly, despite the variations in precursor chain-length, the rate of decrease in TOP concentrations, observed in this study, followed a trend similar to that of the terminal PFASs for chain length and headgroup. Additionally, the degradation rates of TOPs were higher for TOPs with higher starting concentrations. In general, as reported in previous studies, the degradation rates increased with an increase in chain length, and for the same chain length ($C > 4$), the rates of PFCAs were higher than PFSAs (Chapter 3). The air-water partitioning coefficient of PFASs (K_{aw}) decreases with decreasing chain length, thereby reducing the degradation rates. For example, the degradation rates of PFBS were higher than PFBA (Figure 4.6) as PFBA is more hydrophilic due to a shorter carbon chain ($C = 3$), and as a result, has lower availability on the cavity bulk interface [13]. Compared to carboxylates, higher surface activity, higher steric hindrance of the headgroup [14], and stronger C-S bond of sulfonates [15] are some of the causes for slower ultrasonic degradation of sulfonates. However, lower rates of PFOS degradation compared to PFHpS can be attributed to the interaction of PFOS with a high concentration of dissolved solids. K_{aw} of PFASs increases with increasing salt concentration, causing higher partition of PFASs to the bulk-air interface, thereby making them unavailable in

reaction at the ultrasonic cavity. The change in partitioning coefficient is prominent for longer chain PFASs due to their higher hydrophobicity. The high salt concentration can neutralize the electrostatic forces and therefore enhance the hydrophobic properties of PFASs.

For the same reactor temperature, the degradation rates increased with an increasing power density for all PFASs and TOPs. The rates observed at 305 $W.L^{-1}$ were 33% - 66% higher than those observed for 203 $W.L^{-1}$. Similarly, the rates were 22% - 75% higher for 203 $W.L^{-1}$ as compared to 122 $W.L^{-1}$. At 305 $W.L^{-1}$ (T = 25 °C), 11 out of 15 investigated PFASs were degraded to below 70 $ng.L^{-1}$ and 14 out of 15 were degraded to below 200 $ng.L^{-1}$ including PFOA (22.8 $ng.L^{-1}$), PFHpS, PFPeA, PFBS, PFPeS and PFHxS (Table 4.2). Similarly, 10 out of 11 investigated TOPs were degraded to below 200 $ng.L^{-1}$ (Table 4.3). Interestingly, compared to 15 °C, for the same power density, the degradation rates of PFAS and TOP were higher at 25 °C. Suri et al. have also reported increasing rates with increasing bulk temperature for PFOA and PFOS [16]. Contrary to this work, some studies have reported increasing the bulk temperature negatively impacts the PFAS degradation rates by decreasing the surface tension and lowering the availability of PFAS in the ultrasonic cavity [17, 18], while Wood et al. suggest that the bulk temperature does not have much effect on PFAS degradation rates [19]. During the time frame of a cavity imploding (µs), mixing in the bulk liquid is nominal. As a result, the availability of PFASs on the cavity will remain nearly constant [13]. However, the lower surface tension caused by higher bulk temperature may increase PFASs mobility, and combined with high salt concentration, the enhanced hydrophobic interactions among PFAS molecules might increase their availability in the reaction. Furthermore, lower surface tension increases the number and the size of cavities [16], thereby increasing the surface area available for PFAS adsorption. Increased adsorbed PFAS concentration might also explain the increase in degradation rate with temperature.

Table 4.2: Degradation of 15 PFAS species for the treatment of AFFF impacted groundwater, performed at 305 $W.L^{-1}$, 203 $W.L^{-1}$, and 122 $W.L^{-1}$ (treatment volume = 22 L, 33 L, and 54 L) and 25 °C or 15 °C. The treatment of groundwater was performed using a large-scale ultrasonic reactor by 700 kHz ultrasound in a closed system for 480 minutes in Argon saturated environment. The rates were calculated for the first 120 min using the initial rate method.

		122 $W.L^{-1}$ (V_T = 54 L)			203 $W.L^{-1}$ (V_T = 33 L)			305 $W.L^{-1}$ (V_T = 22 L)		
	PFASs	C_i ($ng.L^{-1}$)	C_f ($ng.L^{-1}$)	$k\times10^{-3}$ (min^{-1})	C_i ($ng.L^{-1}$)	C_f ($ng.L^{-1}$)	$k\times10^{-3}$ (min^{-1})	C_i ($ng.L^{-1}$)	C_f ($ng.L^{-1}$)	$k\times10^{-3}$ (min^{-1})
T = 25 °C	PFBA	3570.6	1548.1	1.8	3454.8	1283.3	2.7	3596.2	172.6	6.8
	PFPeA	11024.0	1368.3	4.0	10154.2	933.9	6.5	10603.8	36.5	12.0
	PFBS	7838.9	1594.6	3.0	7584.5	1264.5	5.0	7739.4	61.3	10.0
	4:2 FTS	26.5	7.7	2.0	16.7	ND	0.0	27.7	ND	11.0
	PFHxA	28761.7	1107.1	7.0	26432.4	827.2	9.0	21085.7	6.6	17.0
	PFPeS	9687.5	1155.8	4.0	6896.6	608.8	6.0	7704.8	19.0	10.0
	PFHpA	6009.9	276.5	6.0	6115.7	181.0	9.0	5876.6	ND	17.0
	PFHxS	51073.9	6386.1	4.0	46929.2	6315.4	4.0	58222.3	133.9	12.0
	6:2 FTS	4656.4	428.3	4.0	6054.2	352.8	7.0	5186.7	3.9	14.0
	PFOA	37130.5	1428.8	7.0	32991.6	950.0	9.0	30285.2	22.8	17.0
	PFHpS	4854.3	348.9	6.0	3141.7	278.2	6.0	3523.6	21.5	13.0
	PFOS	42424.4	7688.0	3.0	39907.7	5928.8	5.0	46709.0	2693.4	9.0
	PFNA	498.7	64.7	5.0	470.2	33.8	7.0	448.1	ND	11.0
	8:2 FTS	949.2	134.0	3.0	903.2	83.9	6.0	1083.5	76.8	9.0
	FOSA	31.7	7.8	1.0	30.9	6.9	4.0	34.5	ND	6.0
T = 15 °C	PFBA	3414.7	1946.3	1.2	3540.8	1045.3	2.5	3290.6	314.8	6.0
	PFPeA	9869.5	2425.9	3.0	9936.7	691.3	5.0	9891.4	83.6	9.0
	PFBS	7933.2	2515.6	2.0	7624.4	863.8	4.0	7135.6	143.3	7.0
	4:2 FTS	34.1	6.4	4.0	25.0	ND	3.0	27.3	ND	7.0
	PFHxA	19905.5	2685.8	4.0	26995.5	547.6	7.0	19645.4	55.1	10.0
	PFPeS	15836.0	2693.1	3.0	8183.9	437.6	6.0	12815.6	131.0	7.0
	PFHpA	6505.0	807.1	4.0	6207.9	129.7	7.0	6059.6	18.8	10.0
	PFHxS	54400.8	13146.5	2.0	47644.0	4883.9	3.0	55361.2	415.3	6.0
	6:2 FTS	5619.9	1189.5	3.0	4493.9	265.1	4.0	4710.0	42.4	8.0
	PFOA	29217.0	4173.5	3.0	31931.9	648.8	7.0	28300.7	85.4	10.0
	PFHpS	3454.2	803.0	3.0	3806.2	214.4	7.0	3364.7	22.7	8.0
	PFOS	46660.1	13710.1	2.0	43894.4	4477.6	5.0	42412.4	1961.9	6.0
	PFNA	473.4	107.7	3.0	442.4	28.3	5.0	425.8	ND	8.0
	8:2 FTS	1160.9	238.6	3.0	1009.2	56.3	6.0	938.5	49.7	8.0
	FOSA	49.5	21.0	1.0	30.6	5.5	3.0	56.3	ND	6.0

Table 4.3: Degradation of Total Oxidizable Precursors (TOPs) for 11 PFAS species during the treatment of AFFF impacted groundwater, performed at 305 $W.L^{-1}$, 203 $W.L^{-1}$, and 122 $W.L^{-1}$ (treatment volume = 22 L, 33 L, and 54 L) and 25 °C or 15 °C. The treatment of groundwater was performed using a large-scale ultrasonic reactor by 700 kHz ultrasound in a closed system for 480 minutes in Argon saturated environment. The rates were calculated for the first 120 min using the initial rate method.

	TOPs	122 $W.L^{-1}$ (V_T = 54 L)			203 $W.L^{-1}$ (V_T = 33 L)			305 $W.L^{-1}$ (V_T = 22 L)		
		C_i ($ng.L^{-1}$)	C_f ($ng.L^{-1}$)	$k\times10^{-3}$ (min^{-1})	C_i ($ng.L^{-1}$)	C_f ($ng.L^{-1}$)	$k\times10^{-3}$ (min^{-1})	C_i ($ng.L^{-1}$)	C_f ($ng.L^{-1}$)	$k\times10^{-3}$ (min^{-1})
T = 25 °C	PFBA	7679.5	1864.4	3.0	7584.8	1581.3	4.0	6988.4	184.3	8.0
	PFPeA	14903.2	1651.0	5.0	13117.1	1198.0	6.0	13511.3	62.2	12.0
	PFBS	8524.6	1808.6	3.0	7966.2	1324.3	5.0	8264.7	66.3	10.0
	PFHxA	41941.0	1418.0	7.0	43251.9	1416.4	9.0	35113.1	115.9	26.0
	PFPeS	17973.9	824.0	5.0	7972.4	706.0	6.0	8845.2	38.2	12.0
	PFHpA	7769.3	345.0	7.0	6464.4	222.1	9.0	6899.2	49.2	12.0
	PFHxS	62621.5	7526.3	4.0	54336.6	5945.3	6.0	59103.7	137.1	13.0
	PFOA	39678.3	1389.3	7.0	28488.5	959.4	9.0	34602.9	62.6	14.0
	PFHpS	3406.8	358.9	5.0	2683.2	274.9	6.0	2930.6	35.2	10.0
	PFOS	46151.1	8716.7	3.0	48435.4	7394.6	5.0	47094.9	2880.9	6.0
	PFNA	478.2	ND	4.0	469.0	55.7	6.0	459.0	ND	50.0
T = 15 °C	PFBA	6979.1	2731.2	2.0	7287.5	1317.5	3.0	8297.1	380.6	6.0
	PFPeA	12174.8	3350.7	3.0	12555.1	903.4	5.0	13455.5	113.8	10.0
	PFBS	8208.9	2655.0	2.0	7807.5	971.1	4.0	8012.9	160.7	8.0
	PFHxA	40199.6	4543.6	5.0	41945.5	885.9	7.0	49505.7	136.6	12.0
	PFPeS	7901.9	1938.0	3.0	7736.6	527.8	5.0	8361.1	80.9	10.0
	PFHpA	6048.7	852.4	4.0	6263.7	197.4	7.0	6222.2	34.6	11.0
	PFHxS	57423.8	15709.5	3.0	55345.6	4565.0	4.0	54312.7	477.4	10.0
	PFOA	27327.1	4455.2	4.0	29111.1	775.8	7.0	28525.6	121.0	10.0
	PFHpS	2908.7	714.5	3.0	2885.7	245.1	5.0	3225.6	42.7	9.0
	PFOS	49924.1	15982.8	2.0	48682.1	6506.8	4.0	59101.5	2406.8	7.0
	PFNA	464.0	106.0	3.0	469.0	52.5	4.0	470.0	ND	21.0

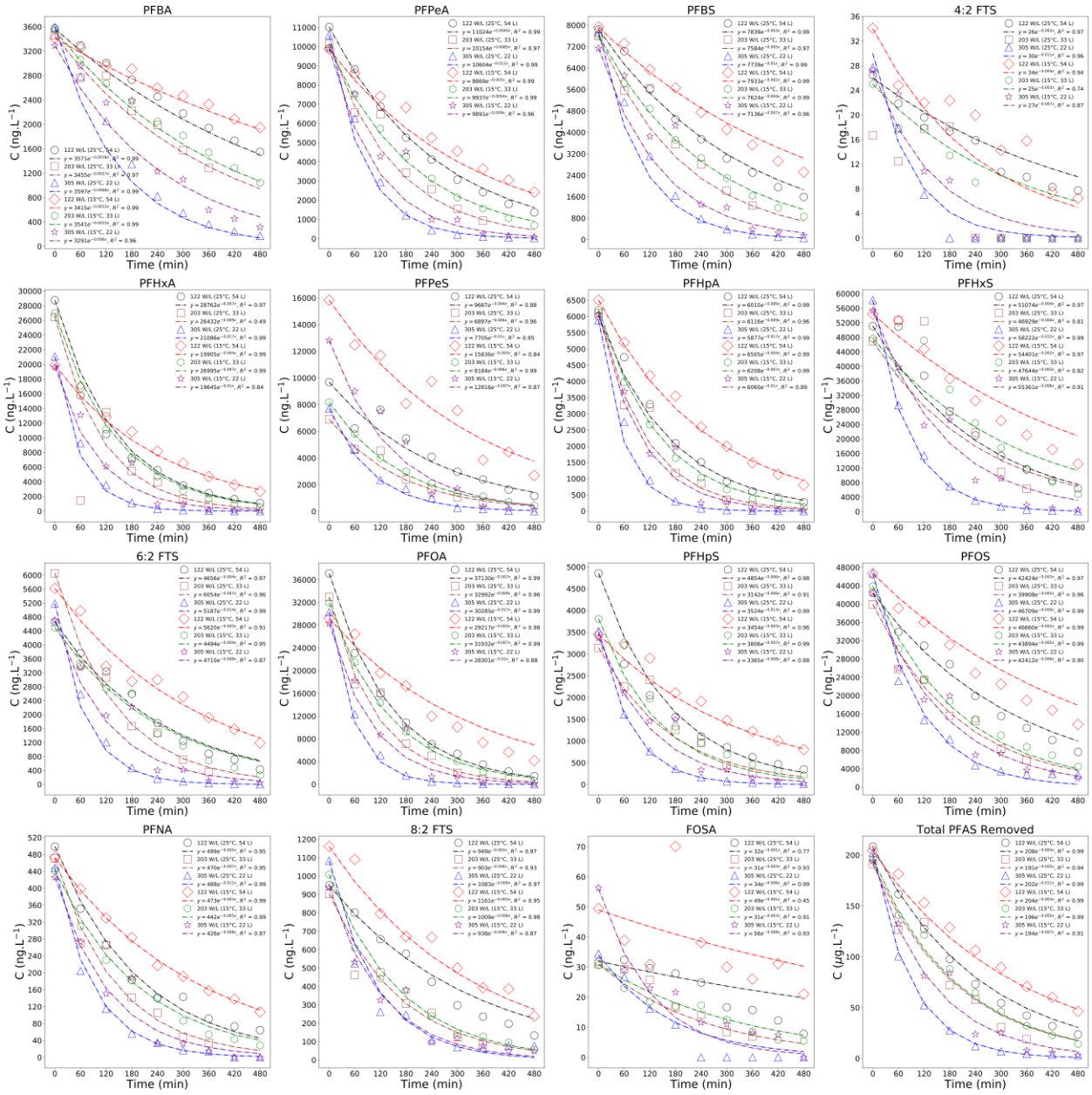

Figure 4.3: Decrease in relative concentration (C/C_o) of 15 PFAS species and cumulative mass removal of 15 PFASs for the treatment of AFFF impacted groundwater, performed at 305 $W.L^{-1}$, 203 $W.L^{-1}$, and 122 $W.L^{-1}$ (treatment volume = 22 L, 33 L, and 54 L) and 25 °C or 15 °C. The treatment of groundwater was performed using a large-scale ultrasonic reactor by 700 kHz ultrasound in a closed system for 480 minutes in Argon saturated environment. The rates were calculated for the first 120 min using the initial rate method. The dotted lines represent the first-order kinetic model fitting for the experimental data at different testing conditions (temperature and power densities)

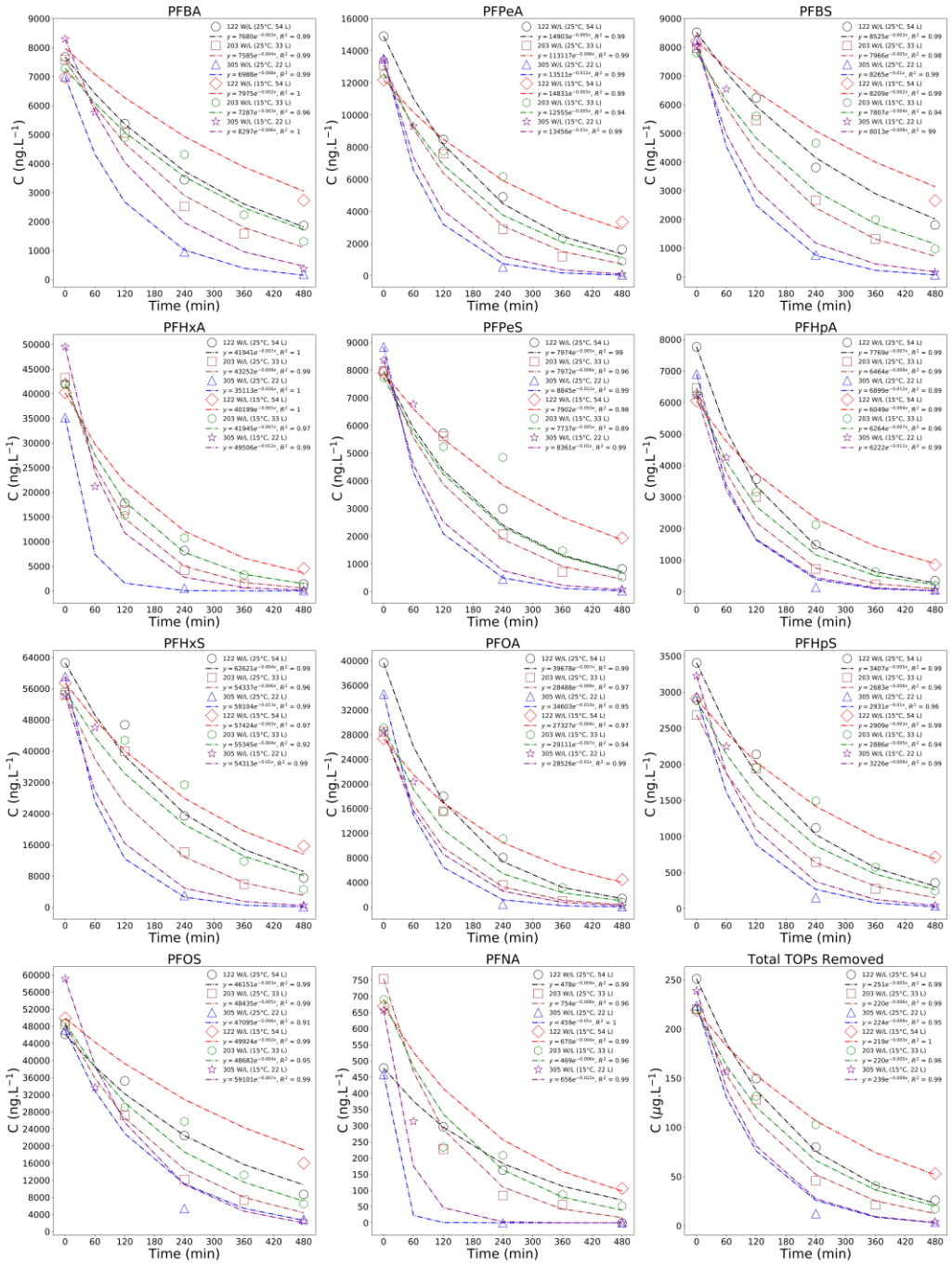

Figure 4.4: Decrease in relative concentration (C/C_o) of Total Oxidizable Precursors (TOPs) for 11 PFAS species and cumulative mass removal of 11 TOPs for the treatment of AFFF impacted groundwater, performed at 305 $W.L^{-1}$, 203 $W.L^{-1}$, and 122 $W.L^{-1}$ (treatment volume = 22 L, 33 L, and 54 L) and 25 °C or 15 °C. The treatment of groundwater was performed using a large-scale ultrasonic reactor by 700 kHz ultrasound in a closed system for 480 minutes in Argon saturated environment. The rates were calculated for the first 120 min using the initial rate method. The dotted lines represent the first-order kinetic model fitting for the experimental data at different testing conditions (temperature and power densities)

A few studies have tested the destruction of PFASs in environmental samples. The salinity of groundwater tested in this study is comparable to that of seawater and comparative to other studies on the destruction of PFASs in environmental samples [10, 20-23]. For example, the conductivity of landfill leachate, treated by 0.5 L plasma reactor, and IDW, treated by 4 L plasma reactor, ranges from 5.8 $mS.cm^{-1}$ - 21.5 $mS.cm^{-1}$ and 22 × 10^{-3} $mS.cm^{-1}$ - 26.3 $mS.cm^{-1}$, respectively [20, 21], while the conductivity of impacted groundwater, in this study, is 16 $mS.cm^{-1}$. The field demonstration of the plasma-based reactor for the treatment of PFAS impacted groundwater did not discuss the groundwater characteristics [10]. Previously Gole et al. [24] monitored the sonication of PFOS, in ultra-pure water, based on the release of fluoride and sulfate ions in a field-scale reactor (91 L). However, this study is the first evidence of large-scale ultrasonic treatment of impacted groundwater in the field, demonstrating the destruction of 15 PFAS and 11 PFAS precursors. Moreover, the effect of power density and temperature has not been previously demonstrated in the field testing of ultrasonic reactors. The power density was altered by changing the volume of the impacted water. The decrease in degradation rates with power density can be attributed to the decay of acoustic pressure and cavitation intensity with increasing distance from the ultrasound source. Farther from the source of ultrasound, the cavities become increasingly weaker and sparse in the bulk liquid leading to lower degradation rates. Rates observed in the field-scale reactor are generally lower than those observed in the lab-scale study because of lower power density (Chapter 3). Interestingly, the rates of degradation observed in the field reactor at 305 $W.L^{-1}$ are comparable to those observed in the lab reactor at 3.5-fold higher power density (1040 $W.L^{-1}$) (Figure 4.5), especially for PFSAs. Furthermore, in the lab-scale experiment, the concentrations of some longer chain PFASs were found to increase towards the end of the experiment, while this was not observed for the field scale reactor. PFSAs are reported

to be more surface-active than PFCAs [13] and ultrasonic treatment is also reported to increase the surface activity of PFASs [25]. Therefore, lower power density may reduce the agitation of the mixture (compared to higher power density), thereby reducing the separation of PFSAs to the bulk air-water interface, increasing their availability at the cavity-water interface.

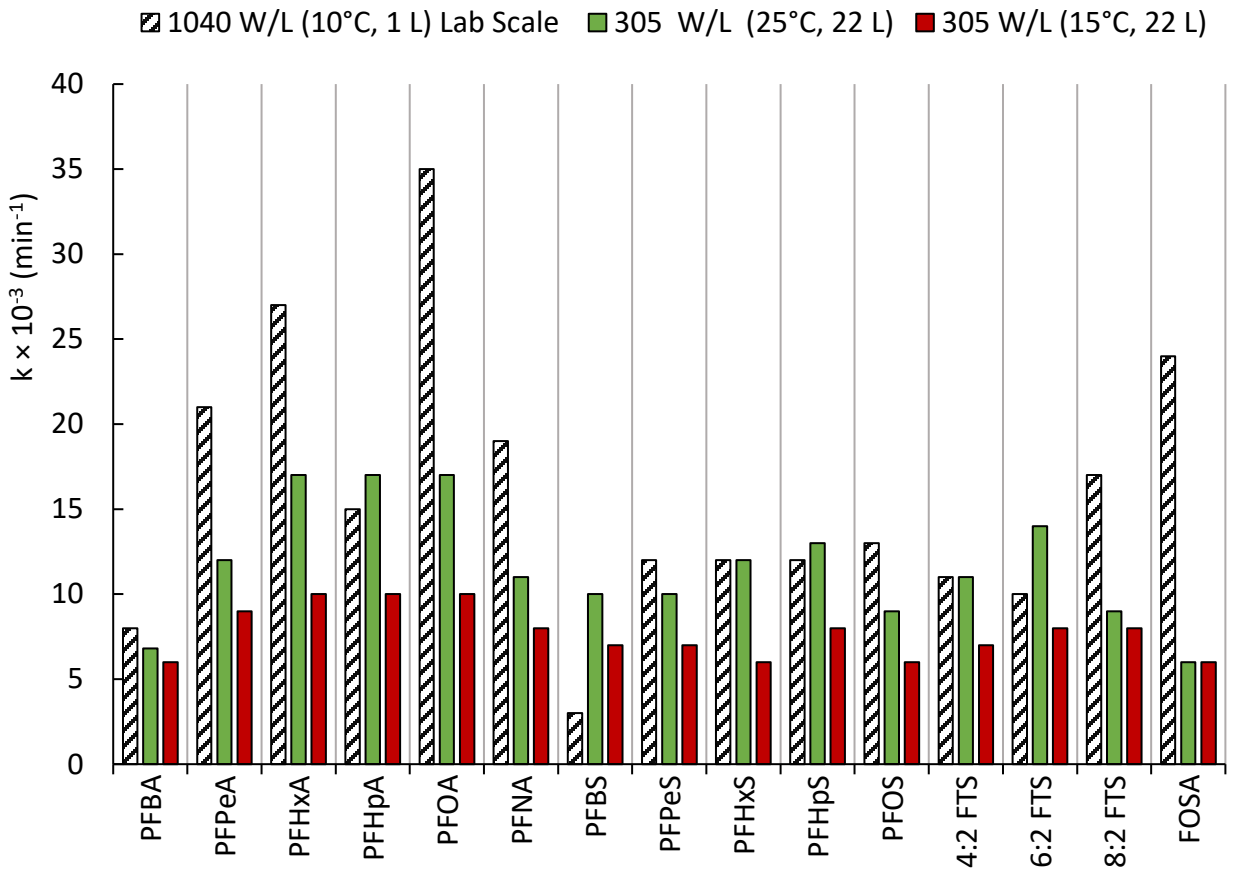

Figure 4.5: Comparison of pseudo-first-order degradation rates of PFASs in the lab-scale reactor (shaded bars) with those observed in the field-scale reactor at 25 °C (green bars) and 15 °C (red bars). The rates in the field reactor at 25 °C were comparable to the lab-scale reactor.

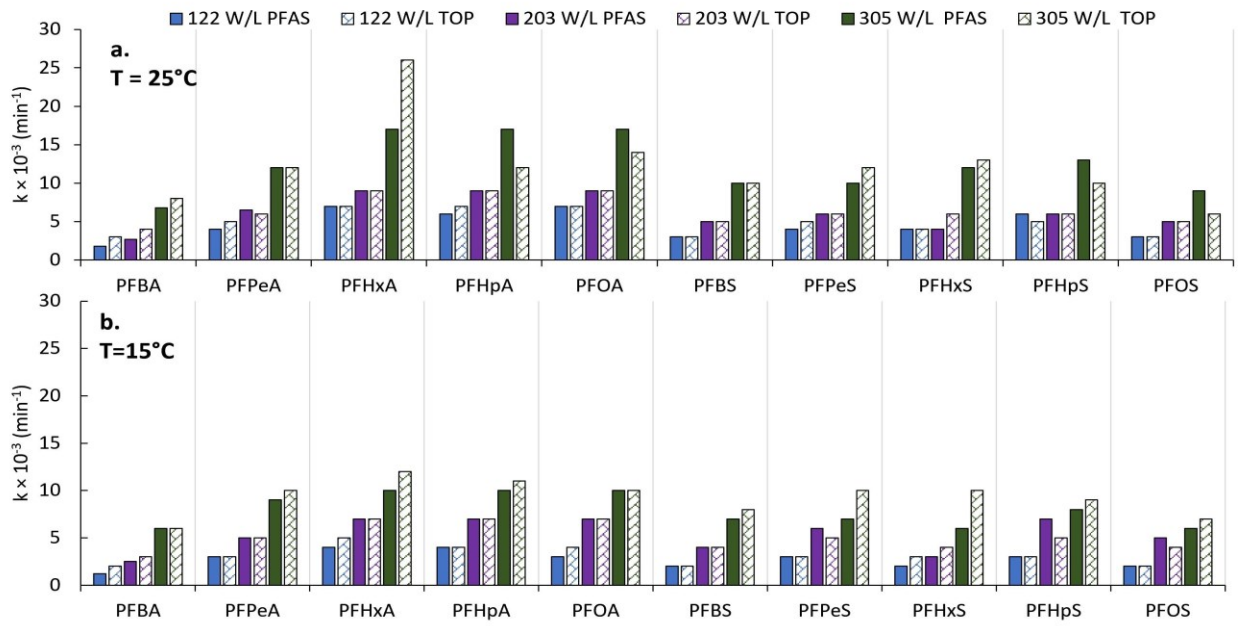

Figure 4.6: Comparison of pseudo-first-order removal rates of PFASs and TOPs during sonication of groundwater by pilot-scale reactor. The rates were higher at 25 °C (**a.**) compared to 15 °C (**b.**)

The concentrations of perchlorate (below detection, < 7 µg.L^{-1}), chlorate (16.85 mg.L^{-1}), chloride (5267.95 mg.L^{-1}) , and sulfate (5102.92 mg.L^{-1}) remained constant at background levels during sonication of PFAS impacted groundwater. The nitrite concentration increased for the first 2 h (background level = 0.01 mg.L^{-1}), followed by a steady decrease for the remaining duration while nitrate concentration increased consistently. The formation of nitrate and nitrite during sonication, followed by an eventual decrease in nitrite concentration, has been reported in the literature. The reaction of nitrogen with oxygen in the imploding ultrasonic cavities produces nitrate and nitrite. The hydroxyl radical is also generated during the implosion of the ultrasonic cavities. The hydroxyl radical can further oxidize nitrite to nitrate, explaining the observed reduction in nitrite concentration [26, 27]. For lower power densities (122 W.L^{-1} and 203 W.L^{-1}), the fluoride concentrations remained nearly constant at baseline levels (0.9 mg.L^{-1}). However, an approximately 20% decrease in fluoride concentration was observed for sonication at 305 W.L^{-1}

(Figure 4.7). The release of fluoride by the destruction of PFASs during sonication of impacted groundwater was not discernible as the background fluoride levels (0.9 $mg.L^{-1}$) in the groundwater were higher than the fluoride released. The decrease in fluoride concentration may be attributed to its removal by precipitates formed during sonication. The formation of precipitates was also observed in the lab-scale study conducted using the same groundwater (Chapter 3). Moreover, sonication is known to form nanomaterials from ions present in the sonicated solutions [28].

4.3.2 Energy Consumption in PFAS Sonolysis.

The average energy consumption recorded using the inline energy meter during 8 h acoustic treatment of the AFFF impacted groundwater, in six tested conditions, was 28.01 ± 0.47 kWh with an average electric load of 3.5 ± 0.10 kW. The cost of electricity for 8 h operation of the reactor was only $3.14 ($0.12/ kWh [10]). The estimated E_{EO} for ultrasonic treatment of AFFF impacted groundwater ranged from 547 $kWh.m^{-3}.order^{-1}$ for 22.15 mg PFAS mass (including TOPs) removal at 122 $W.L^{-1}$ (T = 25 °C) to 839 $kWh.m^{-3}.order^{-1}$ for 12.25 mg PFAS mass removal at 203 $W.L^{-1}$ (T = 25 °C). Interestingly, the E_{EM} values for the removal of PFAS mass (including TOPs) ranged from 1.29 $MWh.g^{-1}$ (22.15 mg removal at 122 $W.L^{-1}$, 25 °C) to 2.98 $MWh.g^{-1}$ (9.22 mg removal at 305 $W.L^{-1}$, 25 °C). Larger mass removal (22.15 mg) was observed for lower power density (122 $W.L^{-1}$) owing to the larger volume of groundwater treated. However, higher removal rates and the lowest final concentration of PFASs (Table 4.2 and Table 4.3) were observed for treatment at 305 $W.L^{-1}$ followed by 203 $W.L^{-1}$ and 122 $W.L^{-1}$. The lowest mass removal (9.22 mg) was observed for a power density of 305 $W.L^{-1}$ (T = 25 °C) (Table 4.4).

E_{EO} is calculated based on the pseudo-first-order degradation rates, which are highly dependent on the type of PFASs (Chapter 3). Selecting the degradation rate of a particular PFAS

species for E_{EO} estimation is also not suitable as it raises the question of correct selection and neglects the removal of precursors or other high concentration PFAS species. Therefore, Σk was calculated to estimate E_{EO} for the impacted groundwater (equation 4.6). The energy density in the field-scale study was 1.3 $kWh.L^{-1}$ (for treatment at 305 $W.L^{-1}$), while 4-fold higher (5.6 $kWh.L^{-1}$) was consumed in the lab-scale treatment of IDW (Chapter 3). Similarly, the cumulative PFASs concentration removal during the sonication of groundwater in the field-scale study, including precursors, was (0.4 $mg.L^{-1}$) 135-fold lower compared to the treatment of IDW in the lab-scale study (54.5 $mg.L^{-1}$). Therefore, the estimated E_{EM} (equation 4.4) for the field-scale treatment of groundwater (2.98 $MWh.g^{-1}$) was approximately 34-fold higher compared to the lab-scale treatment of IDW (76 $kWh.g^{-1}$) (Figure 4.8). Moreover, as the mass removal decreases the E_{EM} values increase (Figure 4.9b). Neglecting the TOP removal decreases the estimated PFAS mass removal from 0.4 $mg.L^{-1}$ to 0.2 $mg.L^{-1}$ thereby doubling the E_{EM} (Table 4.4). Therefore, the E_{EM} estimation is more realistic for the treatment of solutions with high PFAS load, like IDW, while E_{EO} should be estimated for low PFAS load solutions like groundwater. For example, E_{EO} for the treatment of groundwater at 305 $W.L^{-1}$ (T = 25 °C) was 696 $kWh.m^{-3}.order^{-1}$ for removal of 0.4 $mg.L^{-1}$ (or 9.22 mg) PFAS mass, including precursors, at a cumulative rate of 0.0086 min^{-1}, while E_{EO} for the same experiment calculated by neglecting the precursor mass removal was 222 $kWh.m^{-3}.order^{-1}$ for 0.2 $mg.L^{-1}$ (or 4.4 mg) PFASs mass removed at same cumulative rate. Moreover, the energy estimates (E_{EO} and E_{EM}) consistently increased with an increasing power density (Figure 4.9a). E_{EM} increases at a higher rate as compared to E_{EO} because increasing power density translates to lower treatment volume and lower cumulative mass removal. The E_{EO} estimates increase with increasing power density at a slower rate as increasing the power density also increases the cumulative rate constant (Figure 4.10).

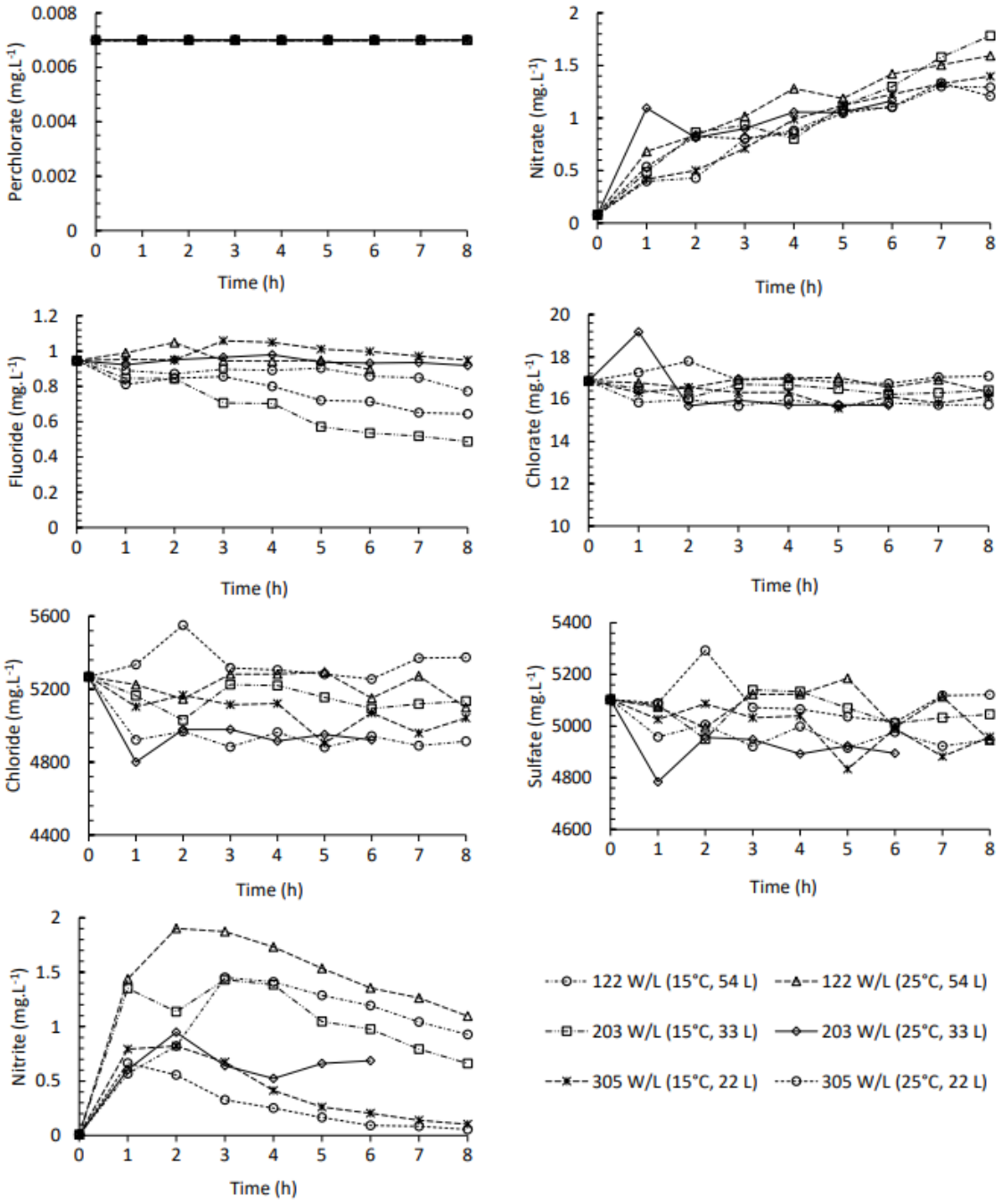

Figure 4.7: Concentrations of perchlorate, fluoride, chloride, nitrite, nitrate, chlorate, and sulfate during the treatment of AFFF impacted groundwater, performed at 305 $W.L^{-1}$, 203 $W.L^{-1}$, and 122 $W.L^{-1}$ (treatment volume = 22 L, 33 L, and 54 L) and 25 °C or 15 °C. The treatment of groundwater was performed using a large-scale ultrasonic reactor (rated power 7200 W) by 700 kHz ultrasound in a closed system for 480 minutes in Argon saturated environment. The concentration of chlorate and per-chlorate remained constant at background levels.

Table 4.4: Performance characteristics of the field-scale reactor for the treatment of AFFF impacted groundwater including the removal of TOP (+TOP) and excluding the removal of TOPs (-TOP).

			+TOP		-TOP	
Power Density ($W.L^{-1}$)	Volume (L)	Performance Characteristics	T = 25 °C	T = 15 °C	T = 25 °C	T = 15 °C
122	54	Cumulative $k \times 10^3$ (min^{-1})	4.65	3.02	4.54	3.09
		E_{EM} ($MWh.g^{-1}$)	1.29	1.63	2.86	3.35
		E_{EO} ($kWh.m^{-3}.order^{-1}$)	546.97	652.05	559.10	822.93
		Energy Consumed (kWh)	28.60			
		Mass Removed (mg)	22.15	17.50	9.99	8.54
203	33	Cumulative $k \times 10^3$ (min^{-1})	4.85	5.39	4.8	5.45
		E_{EM} ($MWh.g^{-1}$)	2.29	2.21	4.93	4.68
		E_{EO} ($kWh.m^{-3}.order^{-1}$)	839.41	755.08	847.33	746.54
		Energy Consumed (kWh)	28.00			
		Mass Removed (mg)	12.25	12.68	5.68	5.99
305	22	Cumulative $k \times 10^3$ (min^{-1})	8.60	8.51	8.61	8.48
		E_{EM} ($MWh.g^{-1}$)	2.98	2.93	6.27	6.53
		E_{EO} ($kWh.m^{-3}.order^{-1}$)	696.13	702.74	695.26	705.82
		Energy Consumed (kWh)	27.44			
		Mass Removed (mg)	9.22	9.38	4.38	4.20

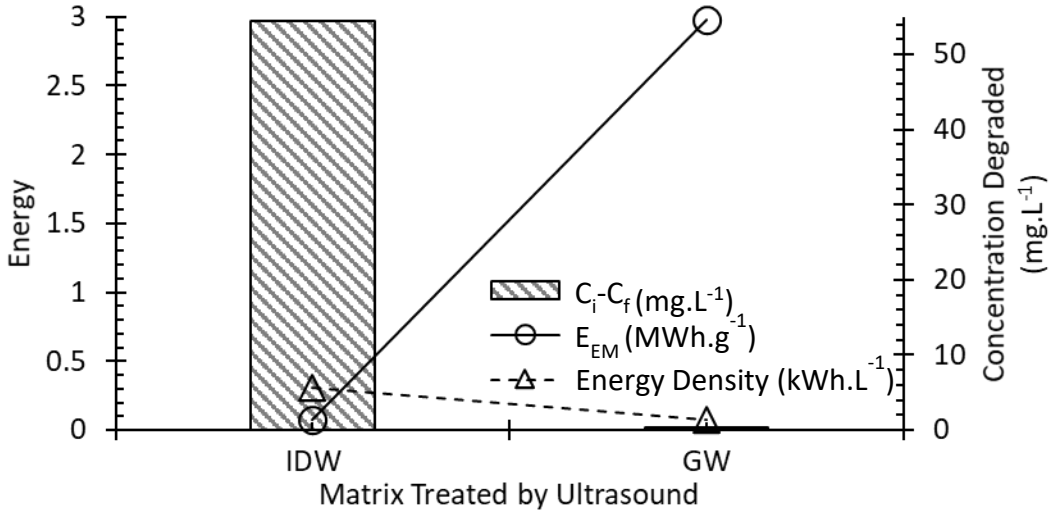

Figure 4.8: Comparison of E_{EM} for IDW treatment in the lab-scale reactor with E_{EM} for treatment of groundwater (305 $W.L^{-1}$, 25 °C) by the field-scale reactor. The E_{EM} ($\frac{energy\ density}{concentration\ degraded}$) is lower for the treatment of solution with higher mass removal by ultrasound.

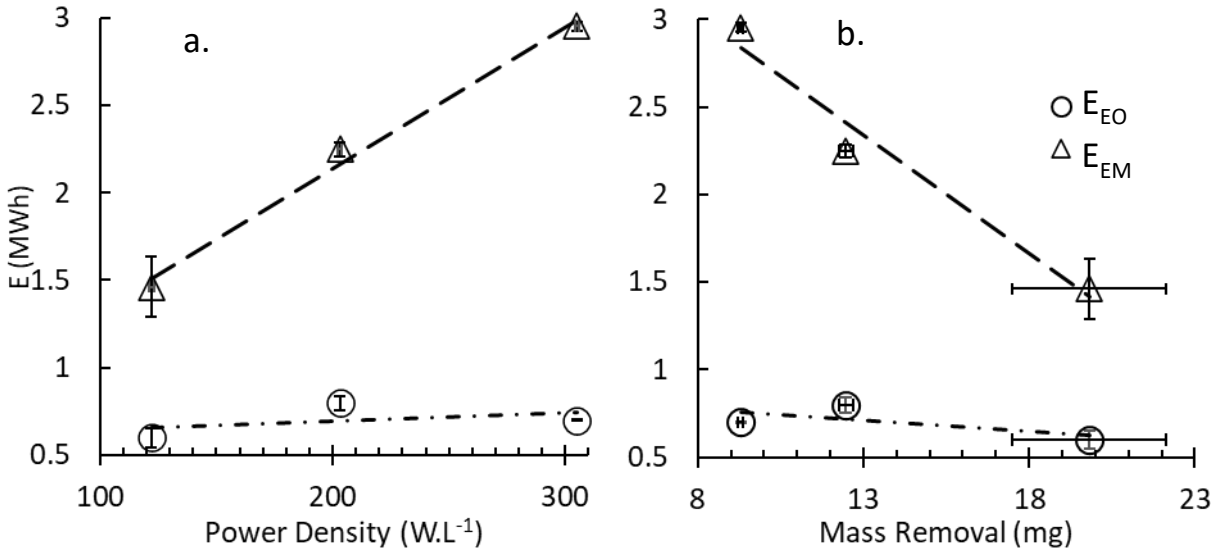

Figure 4.9: Comparison of E_{EM} with E_{EO} for the sonication of AFFF impacted groundwater with the power density and mass removal. The error bars represent variation with temperature (25 °C and 15 °C).

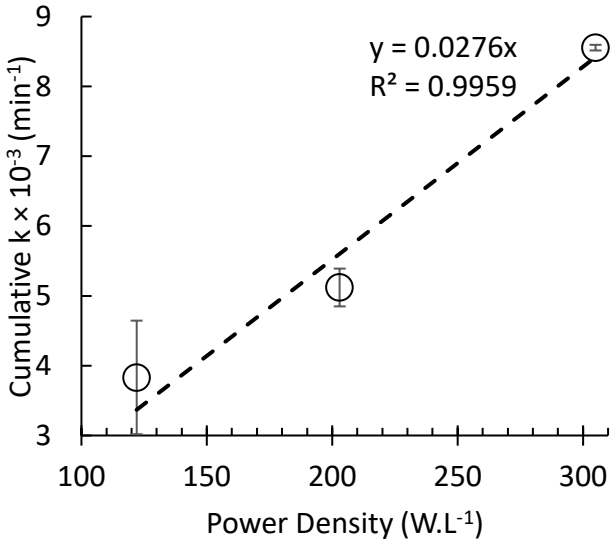

Figure 4.10: Variation in cumulative removal (Σk) rate with power density for the sonication of AFFF impacted groundwater. The error bars represent variation in Σk with temperature (25 °C and 15 °C).

4.4 Conclusion

The custom-built field scale ultrasonic reactor was successful in treating AFFF impacted high salinity groundwater. This study is the first instance of field scale demonstration of ultrasound to degrade AFFF impacted groundwater. A total of 15 PFASs and 11 PFAS precursors were degraded (50% - 99%) at power densities of 122 $W.L^{-1}$, 203 $W.L^{-1}$, and 305 $W.L^{-1}$. The pseudo-first-order degradation kinetics was followed by PFASs and TOP in all tested conditions. The rates of degradation were generally 10% - 40% higher at 25 °C than at 15 °C. For the same chain length, the sulfonates had lower degradation rates, and for the same headgroup, the longer-chain compounds were degraded faster. The degradation rates were influenced by the salinity of the groundwater affecting the surface activity of PFASs. The degradation rates of TOPs generally increased with increasing carbon length and were higher for carboxylates than sulfonates. However, the degradation rates of TOPs were also higher for TOPs with higher starting concentrations. No intermediate PFAS species were detected, and the chlorate and perchlorate concentrations remained at background levels in all tested conditions for 8 h of sonication. 699.43 ± 3.3 $kWh.m^{-3}.order^{-1}$ (E_{EO}) was consumed at 305 $W.L^{-1}$ to deliver the fastest removal rates and lowest final concentrations (< 70 ng/L for 11 PFASs and 7 TOPs). However, maximum mass removal, 19.82 ± 2.32 mg (122 $W.L^{-1}$) consumed only 599.51 ± 52.5 $kWh.m^{-3}.order^{-1}$ (E_{EO}). These results support the consideration of ultrasonic treatment for the mineralization of PFASs in AFFF impacted real waters with high salinity and PFAS load. Acoustic treatment of AFFF impacted water for PFAS destruction might be more energy-efficient than treating a matrix impacted with single/low concentration PFASs. Moreover, an auxiliary cooling unit is not needed as increased bulk temperatures enhance the degradation kinetics, thereby further decreasing the energy consumption. Further testing of the acoustic treatment technology with different PFAS impacted

waters and wastewater is needed to discern its applicability at an industrial scale. However, the advantages like the ease of operation, nominal chemical and disposal costs, and non-selective complete mineralization of PFASs without the production of short-chain intermediates or disinfection by-products make it a better alternative to other PFAS treatment technologies.

References

1. Nzeribe, B.N., M. Crimi, S. Mededovic Thagard, and T.M. Holsen, *Physico-Chemical Processes for the Treatment of Per- And Polyfluoroalkyl Substances (PFAS): A review.* Critical Reviews in Environmental Science and Technology, 2019. **49**(10): p. 866-915.
2. Pica, N.E., J. Funkhouser, Y. Yin, Z. Zhang, D.M. Ceres, T. Tong, and J. Blotevogel, *Electrochemical Oxidation of Hexafluoropropylene Oxide Dimer Acid (GenX): Mechanistic Insights and Efficient Treatment Train with Nanofiltration.* Environmental Science & Technology, 2019. **53**(21): p. 12602-12609.
3. Horst, J., J. McDonough, I. Ross, M. Dickson, J. Miles, J. Hurst, and P. Storch, *Water treatment technologies for PFAS: the next generation.* Groundwater Monitoring Remediation, 2018. **38**(2): p. 13-23.
4. Horst, J., J. McDonough, I. Ross, and E. Houtz, *Understanding and Managing the Potential By-Products of PFAS Destruction.* Groundwater Monitoring and Remediation, 2020. **40**(2): p. 17-27.
5. Bentel, M.J., Y. Yu, L. Xu, Z. Li, B.M. Wong, Y. Men, and J. Liu, *Defluorination of Per- and Polyfluoroalkyl Substances (PFASs) with Hydrated Electrons: Structural Dependence and Implications to PFAS Remediation and Management.* Environmental Science & Technology, 2019. **53**(7): p. 3718-3728.
6. Cui, J., P. Gao, and Y. Deng, *Destruction of Per- and Polyfluoroalkyl Substances (PFAS) with Advanced Reduction Processes (ARPs): A Critical Review.* Environmental Science & Technology, 2020. **54**(7): p. 3752-3766.
7. Kim, T.H., S. Yu, Y. Choi, T.Y. Jeong, and S.D. Kim, *Profiling the decomposition products of perfluorooctane sulfonate (PFOS) irradiated using an electron beam.* Science of The Total Environment, 2018. **631-632**: p. 1295-1303.
8. Kim, T.-H., S.-H. Lee, H.Y. Kim, K. Doudrick, S. Yu, and S.D. Kim, *Decomposition of perfluorooctane sulfonate (PFOS) using a hybrid process with electron beam and chemical oxidants.* Chemical Engineering Journal, 2019. **361**: p. 1363-1370.
9. Wang, L., B. Batchelor, S.D. Pillai, and V.S.V. Botlaguduru, *Electron beam treatment for potable water reuse: Removal of bromate and perfluorooctanoic acid.* Chemical Engineering Journal, 2016. **302**: p. 58-68.
10. Nau-Hix, C., N. Multari, R.K. Singh, S. Richardson, P. Kulkarni, R.H. Anderson, T.M. Holsen, and S. Mededovic Thagard, *Field Demonstration of a Pilot-Scale Plasma Reactor for the Rapid Removal of Poly- and Perfluoroalkyl Substances in Groundwater.* ACS ES&T Water, 2021.

11. Laugier, F., C. Andriantsiferana, A.M. Wilhelm, and H. Delmas, *Ultrasound in gas-liquid systems: effects on solubility and mass transfer.* Ultrasonics Sonochemistry, 2008. **15**(6): p. 965-72.
12. Houtz, E.F. and D.L. Sedlak, *Oxidative Conversion as a Means of Detecting Precursors to Perfluoroalkyl Acids in Urban Runoff.* Environmental Science & Technology, 2012. **46**(17): p. 9342-9349.
13. Campbell, T.Y., C.D. Vecitis, B.T. Mader, and M.R. Hoffmann, *Perfluorinated surfactant chain-length effects on sonochemical kinetics.* The Journal of Physical Chemistry A, 2009. **113**(36): p. 9834-42.
14. Kah, M., D. Oliver, and R. Kookana, *Sequestration and potential release of PFAS from spent engineered sorbents.* Science of The Total Environment, 2021. **765**: p. 142770.
15. Shende, T., G. Andaluri, and R.P.S. Suri, *Kinetic model for sonolytic degradation of non-volatile surfactants: Perfluoroalkyl substances.* Ultrasonics Sonochemistry, 2019. **51**(September 2018): p. 359-368.
16. Shende, T., G. Andaluri, and R. Suri, *Frequency-dependent sonochemical degradation of perfluoroalkyl substances and numerical analysis of cavity dynamics.* Separation and Purification Technology, 2021. **261**: p. 118250.
17. Cao, H., W. Zhang, C. Wang, and Y. Liang, *Sonochemical degradation of poly- and perfluoroalkyl substances - A review.* Ultrasonics Sonochemistry, 2020. **69**: p. 105245.
18. Lin, J.C., S.L. Lo, C.Y. Hu, Y.C. Lee, and J. Kuo, *Enhanced sonochemical degradation of perfluorooctanoic acid by sulfate ions.* Ultrasonics Sonochemistry, 2015. **22**: p. 542-7.
19. James Wood, R., T. Sidnell, I. Ross, J. McDonough, J. Lee, and M.J. Bussemaker, *Ultrasonic degradation of perfluorooctane sulfonic acid (PFOS) correlated with sonochemical and sonoluminescence characterisation.* Ultrasonics Sonochemistry, 2020. **68**: p. 105196.
20. Singh, R.K., E. Brown, S. Mededovic Thagard, and T.M. Holsen, *Treatment of PFAS-containing landfill leachate using an enhanced contact plasma reactor.* Journal of Hazardous Materials, 2020.
21. Singh, R.K., E. Brown, S. Mededovic Thagard, and T.M. Holsen, *Treatment of PFAS-containing landfill leachate using an enhanced contact plasma reactor.* Journal of Hazardous Materials, 2021. **408**: p. 124452.
22. Cheng, J., C.D. Vecitis, H. Park, B.T. Mader, and M.R. Hoffmann, *Sonochemical degradation of perfluorooctane sulfonate (PFOS) and perfluorooctanoate (PFOA) in groundwater: kinetic effects of matrix inorganics.* Environmental Science & Technology, 2010. **44**(1): p. 445-50.
23. Cheng, J., C.D. Vecitis, H. Park, B.T. Mader, and M.R. Hoffmann, *Sonochemical degradation of peerfluorooctane sulfonate (PFOS) and perfluorooctanoate (PFOA) in landfill groundwater: environmental matrix effects.* Environmental Science & Technology, 2008. **42**(21): p. 8057-63.
24. Gole, V.L., A. Fishgold, R. Sierra-Alvarez, P. Deymier, and M. Keswani, *Treatment of perfluorooctane sulfonic acid (PFOS) using a large-scale sonochemical reactor.* Separation and Purification Technology, 2018. **194**: p. 104-110.
25. Vecitis, C.D., H. Park, J. Cheng, B.T. Mader, and M.R. Hoffmann, *Enhancement of Perfluorooctanoate and Perfluorooctanesulfonate Activity at Acoustic Cavitation Bubble Interfaces.* Journal of Physical Chemistry C, 2008. **112**(43): p. 16850-16857.

26. Kwedi-Nsah, L.M. and T. Kobayashi, *Sonochemical nitrogen fixation for the generation of NO^{2-} and NO^{3-} ions under high-powered ultrasound in aqueous medium*, in *Ultrasonics Sonochemistry*. 2020, Elsevier B.V. p. 105051.
27. Supeno and P. Kruus, *Sonochemical formation of nitrate and nitrite in water.* Ultrasonics Sonochemistry, 2000. **7**(3): p. 109-113.
28. Hu, Y.B., S.L. Lo, Y.F. Li, Y.C. Lee, M.J. Chen, and J.C. Lin, *Autocatalytic degradation of perfluorooctanoic acid in a permanganate-ultrasonic system.* Water Research, 2018. **140**: p. 148-157.

Chapter 5

Engineered Laccase: Peptide (INT) fused enzyme for Vault Packaging.

Abstract

Laccase from *Trametes versicolor* is a ligninolytic multicopper oxidase and is a promising candidate for biodegradation of recalcitrant chemicals. Free enzymes last for a short duration due to their instability in environmental and reaction conditions, as a result, frequent replenishment is required to achieve the desired target. This chapter seeks to address this limitation by engineering the laccase secreted by the white-rot fungus *T. versicolor* and packaging it into biological nanocages called vaults. Vault nanoparticles have been studied in detail and are being used for the targeted therapeutic delivery for cancer treatment. Our studies of vault-packaged manganese peroxidase have shown to increase enzyme stability, and activity thereby reducing the enzyme requirements significantly for biodegradation of phenolic and nitroaromatic compounds. This paper attempts to provide laccase isozyme sequence standardization and records the secretion and detection of laccase A, C, and D category isozymes produced by *T. versicolor* in the Tisma medium. To enable the selective packaging of the detected laccase isozymes into the vault nanoparticles, laccase messenger RNA (mRNA) was extracted from *T. versicolor* and engineered to introduce INT peptide. The expression of the engineered laccase (eLac) was performed by using the Baculovirus Expression System (BVES) in Sf9 insect cells cultured in SF-900 II serum-free media. Based on the isozyme categories and INT fusion, five configurations of eLac were studied (LDI, LAI, ILA, ILD, and MLDGI) out of which MLDGI was found to have the best activity. The extracellular secretion of the active laccase (MLDGI) was enhanced by the honeybee melittin secretion signal while, a long Glycine-Serine (5 × GGSG) linker bridging the INT peptide and laccase protein, ensured that the activity of laccase is not affected by the fusion of the INT peptide. The activity of vault-packaged MLDGI (VMLDGI) was severely dependent on the amount of copper in the MLDGI expressing Sf9 culture medium. The vault-packaged laccase was able to

catalyze the oxidation of a battery of substrates like 2,2-azinobis (3-ethylbenzothiazo-line-6-sulfonic acid (ABTS), guaiacol, catechol, 1-naphthol, 2,6-dichlorohydroquinone, and was able to retain nearly 100% activity after 7 days of incubation at 30 ºC with 1-hydroxybenzotriazole. This paper presents the packaging of laccase (MLDGI – 90 kDa) as the largest protein to be packaged in vault nanoparticles while retaining its catalytic activity. Vault-packaged laccase degraded 60% NTO at 5 U L^{-1} laccase activity while degradation of NTO by unpackaged laccase was insignificant.

5.1 Introduction

The wood-rotting fungi and their enzymes have great potential in the world of environmental bioremediation because of their ability to mineralize the largest biological polymers like lignin and various chemicals causing public health concern [1]. The wood-rotting fungi like *Trametes versicolor* and its extracellular ligninolytic enzyme, laccase, have been studied for a long time in a wide range of applications like pulp and paper, probiotics and gut health, textile manufacturing, food and alcohol production, biosensors, and synthesis of therapeutics for cancer treatment, etc. [2-7]. Laccases have been extensively studied and reviewed and were first discovered in plants in 1883, followed by the discovery in fungi (1896) and bacteria [8]. The plant laccases are difficult to purify, and most of the bacterial laccases are intracellular, as a result, the fungal laccases have a practical advantage and have been studied in greater detail [9, 10]. Laccase from *T. versicolor* is one of the highest redox potential laccases (785 mV). Like most of the laccases, it can oxidize the compounds with higher redox potentials, which are not direct substrates, using the laccase-mediator system [11]. These mediator compounds can be synthetic

or natural, phenolic, azo, hydroxamic acids, and oxime compounds, which are oxidized by laccase to produce radical species that can further assist in the transformation of the target compounds.

The increasing interest in laccase-mediated biodegradation and biosynthesis because of its non-specific and wide spectrum applicability prompts the enhancement and protection of the enzymes using encapsulation technologies [12-22]. Vault nanoparticle is a ribonucleoprotein that has been studied for more than 30 years for its ability to package and deliver therapeutics while keeping them active and protected in the blood or different buffer environments [23-25]. The ligninolytic enzyme, manganese peroxidase (MnP) from the fungus *Phanerochaete chrysosporium* has been previously packaged in the vault nanoparticles. Vault-packaged MnP has shown better stability and catalytic activity compared to the natural MnP in reaction with phenolic compounds and nitroaromatic explosives [26-28].

Presented in this study is the vault packaging of laccase from *Trametes versicolor,* along with the categorization and identification of laccase isozymes produced by the fungus. The study also records the packaging of the longest enzyme (90 kDa) to be packaged in vaults. A flexible linker connecting the INT domain and laccase protein along with the supplementation of copper in the expressing insect cell culture allowed the protein-peptide fusion to regain catalytic activity. The vault-packaged laccase successfully oxidized various known laccase substrates in independent reactions. The lyophilized vault-packaged enzyme after resuspension in phosphate buffer (0.1 M, pH 6) retained nearly 80% activity for 7 days in reaction with 1-hydroxybenzotriazole.

5.2 Material and Methods

5.2.1 Expression of Laccase in Tisma Medium by *Trametes versicolor*

The fungus *Trametes versicolor* was grown at 30 ºC for 10 days on YMG agar plates containing 4 $g.L^{-1}$ yeast extract, 10 $g.L^{-1}$ malt extract, 4 $g.L^{-1}$ glucose, and 16 $g.L^{-1}$ agar. The plates were then stored at 4 ºC till needed. The expression of laccase was performed by cultivating the fungus in sterile 100 mL Tisma medium [29] for 6 days in cotton stoppered 500 mL Erlenmeyer flasks at 30 ºC and 150 rpm. Guaiacol (0.4 $g.L^{-1}$) was added after 48 h of growth to induce laccase expression. The liquid fungal culture medium (Tisma medium) was composed of 10 $g.L^{-1}$ glucose, 0.3 $g.L^{-1}$ peptone, 0.5 $g.L^{-1}$ yeast extract, 0.8 $g.L^{-1}$ KH_2PO_4, 0.2 $g.L^{-1}$ Na_2HPO_4, 0.057 $g.L^{-1}$ $CaCl_2.2H_2O$, 0.5 $g.L^{-1}$ $MgSO_4.7H_2O$, 0.25 $g.L^{-1}$ citric acid, 0.1% Tween 80, 0.035 $g.L^{-1}$ $FeSO_4.7H_2O$, 0.007 $g.L^{-1}$ $MnSO_4.H_2O$, 0.011 $g.L^{-1}$ $ZnSO_4.7H_2O$, 0.002 $g.L^{-1}$ H_3BO_3, 0.00035 $g.L^{-1}$ KI and 0.00064 $g.L^{-1}$ $CuSO_4$.

5.2.2 Laccase Activity Assay

To measure laccase activity, 0.1 mL 2,2-azinobis (3-ethylbenzothiazo-line-6-sulfonic acid ABTS (20 mM) was mixed with 0.880 mL, 100 mM phosphate buffer (pH 6) [30]. The activity assay was initiated by zeroing the absorbance of the mixture followed by the addition of 0.02 mL enzyme solution. The rate of change of absorbance at 420 nm was measured every 2 sec over 1-min. Equation 5.1 was used to calculate the enzyme activity,

$$\text{Activity}(\text{U.L}^{-1}) = \frac{\Delta A \times V_T \times 10^6}{\xi \times b \times V_{en}} \qquad (5.1)$$

where $U.L^{-1}$ is units of enzyme activity per liter, DA is the rate of absorbance change at 420 nm (min^{-1}), V_T is the total volume (L), ξ is the molar extinction coefficient of ABTS at 420 nm (36000 $L.mol^{-1}.cm^{-1}$), V_{en} is enzyme volume (L), and b is path length (cm). One unit of enzyme activity is defined as the amount of enzyme needed to produce 1 µmol of product per minute. All enzyme activity assays were measured on the NanoDrop 2000c spectrophotometer.

5.2.3 Identification and Extraction of Laccase Isozyme cDNA from *Trametes versicolor*

Literature search and NCBI database were used to identify possible isozymes of laccase secreted by *T. versicolor* grown in Tisma medium. Laccase cDNA sequences were grouped into five different categories, namely A to E based on both, the mRNA nucleotide sequence and the resulting enzyme's amino acid sequence. Five cloning primer pairs, one for each isozyme category and a positive control primer pair, based on the conserved copper binding region of the blue copper oxidase as designed by Dabson et al. [31], were used for identification and amplification of laccase cDNA. The PCR primers were designed using primer3plus (Table 5.1).

Table 5.1: Primers designed for laccase cDNA amplification using TPCR

Category	Direction	Primer Sequence
A	Forward	ATG GGT CTG CAG CGA TTC
	Reverse	TCA CTG GTT AGC CTC GCT C
B	Forward	ATG GGC AGG GTC TCA TCT CT
	Reverse	TTA GAG GTC GGA TGA GTC AAG A
C	Forward	ATG TCG AGG TTT CAC TCT CTT CTC
	Reverse	TTA CTG GTC GCT CGG GTC
D	Forward	ATG GGC AAG TTT CAC TCT TTT G
	Reverse	TCA GAG GTC GGA CGA GTC C
E	Forward	ATG ACT GGG CTC CGT CTT CT
	Reverse	ATG ATT GAG AAA ATG GTT GAC G
Control	Forward	ATT GGC ACG GCT TCT TCC
	Reverse	GAT CTG GAT GGA GTC GAC

The fungal biomass expressing laccase isozymes was harvested by centrifuging the liquid fungal culture at 3000 × g for 5 min in 50 mL vials after the maximum laccase activity was observed in the culture. The collected biomass was then divided into approximately 100 mg sections and lysed using a bead beater in 2 mL screw cap vials. The lysis mixture consisted of 1 g zirconia-silica beads (100 µm diameter), 350 µL lysis buffer (5% SDS, 10 mM EDTA, and 200 mM tris-Cl (pH 7.5)) and 1 mL phenol. The cells were lysed by heating the mixture at 65 ºC for 2 min and bead beating for 2 min, followed by one more round of heating for 8 min and bead beating for 2 min [32]. The lysate was then used to extract total nucleic acids using the Phenol: Chloroform: Isoamyl Alcohol (25:24:1) (PCA method) [33]. The purity of the lysate and its nucleic acid concentration was analyzed using a Spectrophotometer (NanoDrop 2000c) according to the manufacturer's instructions. Further, the lysate was treated with DNase using TURBO DNA-free Kit (Life Technologies) followed by reverse transcription of the laccase messenger RNA (mRNA) using EasyScript Plus cDNA Synthesis Kit (Lambda Biotech). The reverse-transcribed laccase isozyme cDNA was then amplified using respective primer pairs, synthesized for each isozyme category.

The DNA amplification was performed in Veriti Thermal Cycler (Applied Biosystems) using a touchdown polymerase chain reaction (TPCR) [34] to allow multiplexing and high amplicon yield of isozyme cDNA. The TPCR cycle ran for a total of 35 cycles, starting at the annealing temperatures 4 ºC higher than those predicted. For the first 20 cycles, the temperature was reduced by a gradient of 0.7 ºC per cycle and then held constant for the remaining cycles. The denaturation step was performed at 95 ºC for 1 min, followed by an annealing step for 30 min and an extension step for 1 min 30 sec. The last extension step was run for 7 minutes to ensure complete synthesis of partially synthesized cDNA fragments if any. The PCR mix comprised of 1 µM

forward primer, 1 µM reverse primer, 1 µL DNA template (< 250 ng), and 25 µL Go Taq Promega Master Mix (2x) supplemented with nuclease-free water to a final volume of 50 µL.

5.2.4 Molecular Cloning for Synthesis of Insect Cell Expression Vector

The PCR amplified isozyme cDNA was cloned using the TOPO-TA cloning kit in Mach1T1 *E. coli* (Invitrogen). The cloned plasmids containing the inserts were then extracted from the positive colonies using Monarch Plasmid Miniprep Kit (New England Biolabs, Ipswich, MA, USA). The extracted plasmids were sequence-verified, to rule out false positives, before fusing the laccases' cDNA with INT cDNA cloning into the pFastBac1 vector. Further, the BVES carrier plasmids were synthesized using a Gibson assembly [35] kit supplied by New England Biolabs, which allowed for a quick fusion of multiple DNA fragments. Four different BVES carrier plasmids (pLDI, pILD, pLAI, and pILA) were created to account for the different configurations for INT peptide fusion with the laccase isozymes (Figure 5.3). These constructs were created with the native secretion signals of the laccase isozymes to enable the secretion of the protein in Sf9 culture. A fifth carrier plasmid (pMLDGI) was also assembled by modifying the pLDI to introduce the glycine-serine linker (5 × GGSG) between the laccase D isozyme and INT peptide (Figure 5.3). Laccase's native secretion signal was also replaced with honeybee melittin secretion signal in MLDGI (Table 5.2). The secretion signal and 5 × GGSG were introduced during the Gibson assembly using the designed primers. The primers for assembling BVES carrier plasmids were designed using the Gibson assembly wizard at Benchling.com and cross verified with primer3plus (Table 5.3). The PCR amplification of the DNA fragments was performed using the Q5® High-Fidelity 2X Master Mix (New England Biolabs, Ipswich, MA, USA) according to the TPCR protocol as described above.

Table 5.2: GGSG linker and secretion signal DNA sequences for MLDGI carrier plasmid.

Glycine-serine Linker	DNA sequence - GGTGGTTCTGGTGGTGGTTCTGGTGGTGGTTCTGGTGGTGGTTCTGGTGGTGGTTCTGGT Peptide sequence - GGSG GGSG GGSG GGSG GGSG
Honeybee melittin secretion signal	ATGAAATTCTTAGTCAACGTTGCCCTTGTTTTTATGGTCGTATACATTTCTTACATCTATGCG

Table 5.3: Primers for Gibson assembly of different BVES carrier plasmids. pMLDGI, pLDI, pILD, pLAI, and pILA

pMLDGI	
Primer A	TGTATACGACCATAAAAACAAGGGCAACGTTGACTAAGAATTTCATCTAGTGAGCTCGTCGACGTAGGCCTTTG
Primer C	TCAACGTTGCCCTTGTTTTTATGGTCGTATACATTTCTTACATCTATGCGGGCGCCATTGGGCCCGT
Primer F	ACCAGAACCACCACCAGAACCACCACCAGAACCACCGAGGTCGGACGAGTCCAAAGCATCG
Primer G	GGTGGTTCTGGTGGTGGTTCTGGTGGTGGTTCTGGTTGCACACAACACTGGCAGGATGC
pLDI	
pFB1-D2D REV	GACGTTCACAAAAGAGTGAAACTTGCCCATCTAGTGAGCTCGTCGACGTA
D2D FWD	TTCAAAGGCCTACGTCGACGAGCTCACTAGATGGGCAAGTTTCACTCTTTTGT
D2D REV	AGCATCCTGCCAGTGTTGTGTGCAGCTAGCGAGGTCGGACGAGTCCAAA
INT-D2D FWD	GATGCTTTGGACTCGTCCGACCTCGCTAGCTGCACACAACACTGGCAG
INT-D2D REV	AGACTGCAGGCTCTAGATTCGAAAGCGGCCTTAGCCTTGACTGTAATGGAGGA
pFB1-INT FWD	CATAGAGTCCTCCATTACAGTCAAGGCTAAGGCCGCTTTCGAATCTAGAG
pILD	
pFB1-D-REV	GACTAAGGGCGACGACGTTCACAAAAGAGTGAAACTTGCCCATTGAGCTCGTCGACGTAGGCC
INT-D-FWD	GAACGTCGTCGCCCTTAGTCTTTCTTTGAGCGGTCGTGTGTTCTGCACACAACACTGGCAGG
INT-D-REV	GTCGGTGACGGGCCCAATGGCGCCGCTAGCGCCTTGACTGTAATGGAGGACTCTATG
CAT_D-D2D FWD	AGAGTCCTCCATTACAGTCAAGGCGCTAGCGGCGCCATTGGGCCCGTCAC
CAT_D-D2D REV	CTCTAGATTCGAAAGCGGCCTCAGAGGTCGGACGAGTCCAAAGCATCG
pFB1-D-FWD	TACGATGCTTTGGACTCGTCCGACCTCTGAGGCCGCTTTCGAATCTAGAGCC
pLAI	
pFB1-A2A REV	GACGAGGAAGCTGAATCGCTGCAGACCCATCTAGTGAGCTCGTCGACGTA
A2A FWD	TTCAAAGGCCTACGTCGACGAGCTCACTAGATGGGTCTGCAGCGATTCAG
A2A REV	AGCATCCTGCCAGTGTTGTGTGCAGCTAGCCTGGTTAGCCTCGCTCAGC
INT-A2A FWD	GACGGGCTGAGCGAGGCTAACCAGGCTAGCTGCACACAACACTGGCAG
INT-A2A REV	AGACTGCAGGCTCTAGATTCGAAAGCGGCCTTAGCCTTGACTGTAATGGAGGA
pFB1-INT FWD	CATAGAGTCCTCCATTACAGTCAAGGCTAAGGCCGCTTTCGAATCTAGAG
pILA	
pFB1-A-REV	CGAGAGCAAGGGTGACGAGGAAGCTGAATCGCTGCAGACCCATTGAGCTCGTCGACGTAGGCC
INT-A-FWD	CAGCTTCCTCGTCACCCTTGCTCTCGTCGCCCGCTCTCTTGCATGCACACAACACTGGCAGGA
INT-A-REV	GAGGCTCGCCGCGGGCCCGATGGCGCTAGCGCCTTGACTGTAATGGAGGACTCTATGA
CAT_A-A2A FWD	AGAGTCCTCCATTACAGTCAAGGCGCTAGCGCCATCGGGCCCGCGG
CAT_A-A2A REV	AGACTGCAGGCTCTAGATTCGAAAGCGGCCTCACTGGTTAGCCTCGCTCAGCCCG
pFb1-A-FWD	TACGACGGGCTGAGCGAGGCTAACCAGTGAGGCCGCTTTCGAATCTAGAGCC

Following the assembly of DNA fragments, the plasmids were transfected in DH5alpha *E. coli*, and the positive colonies were selected using ampicillin resistance and blue-white screening. The positive colonies were then verified using colony PCR (m13 primers) followed by extraction and sequencing of the carrier plasmids to rule out the false positives or errors in cloning. DH10Bac *E. coli* were then chemically transformed using the BVES carrier plasmids, and the positive colonies were screened and selected using blue-white screening and ampicillin resistance. The extracted bacmids were verified for successful recombination of INT fused isozyme cDNA by colony PCR (m13 primers) as well as Sanger sequencing.

5.2.5 Expression of Engineered laccase (eLac) and Empty Recombinant Vaults

Transfection of Sf9 cells was performed using the carrier plasmids, according to the Bac-to-Bac manual (Invitrogen). Post transformation, the Sf9 cells were incubated at 27 ºC for 4 days to produce recombinant baculovirus. The baculovirus stock was then amplified once and used for optimizing the expression of engineered laccase by varying the inoculation volume. The samples were collected every 24 h and stored at -80 ºC until required for SDS-PAGE and Western blot. Sf9 cells expressing the proteins were cultured in Erlenmeyer flasks equipped with 0.2 µm filters. The expression cultures consisting of SF-900 II serum-free media and 2×10^6 cells.mL^{-1} were incubated for 96 h at 120 rpm and 27 ºC. The expression optimization experiments were performed in 125 mL flasks containing 25 mL culture. Post-optimization, the eLac was expressed in 2 L flasks containing 600 mL culture. Similarly, empty recombinant vaults were expressed in Sf9 cells using the optimized amount of the respective amplified recombinant baculovirus stock.

5.2.6 Verification of Expression and Packaging in Empty Recombinant Vaults

The expression and packaging of eLac were verified by SDS-PAGE and western blot using an AnyKD Mini-PROTEAN Precast Gel. The protein samples were diluted using a 2x Laemmli buffer containing β-mercaptoethanol and heated for 10 min at 100 ºC, before loading in the precast gel. The electrophoresis was run for 1 h in SDS PAGE running buffer (25 mM tris, 192 mM glycine, 0.1% SDS, pH 8.3) at 100 V. The gels were then stained using Coomassie blue or processed further for western blot.

The Western blot was performed by transferring the proteins from the polyacrylamide gel to an Immun-Blot PVDF membrane (Bio-Rad Laboratories, Hercules, CA, USA) using electrophoresis at 100 V for 1 h in Western blot transfer buffer (25 mM tris, 190 mM glycine, 20% methanol). Membrane blocking was then performed by incubating the membrane for 30 min in 2.5% milk in TBST buffer (20 mM tris, pH 7.5, 150 mM NaCl, 0.1% Tween 20). The membrane was imaged after incubation at 4 ºC with the anti-INT or anti-MVP antibody overnight, followed by the secondary antibody for 2 h at room temperature.

The packaging of engineered laccase isozymes (eLac) was performed in one of the two ways, first, by lysing the Sf9 cells expressing Major Vault Protein (MVP) along with the Sf9 cells expressing engineered laccase (eLac) isozyme (LL method) and second, by mixing the empty recombinant vaults with the Sf9 culture supernatant containing the secreted enzyme (LS method) (Figure 5.1). The Sf9 cell pellet expressing the protein of interest (POI) was lysed and homogenized by douncing the pellet suspension 10-20 times in 5 mL of lysis buffer per gram of cell. The lysis buffer contained 50 mM tris (pH 7.7), 70 mM NaCl, 0.5 mM $MgCl_2$, 1% Triton

X100, 1 mM dithiothreitol (DTT), 1 mM phenylmethylsulfonyl fluoride (PMSF) and 1% protease inhibitor cocktail (Sigma 8849). The Sf9 cell pellets expressing MVP and eLac were lysed together in the case of the LL packaging method. Following lysis, the cell debris was removed by centrifuging the lysate at 20,000 × g (4 ºC, 20 min) followed by centrifuging the clear lysate at 100,000 × g (4 ºC, 60 min) to pellet out the total protein. The total protein pellet was then resuspended in 4.5 mL lysis buffer per gram of cell pellet, containing 1 M ammonium acetate. The mixture was then incubated in shaking at 4 ºC for 1 h, to salt out the packaged vaults. The salted-out vaults were then pelleted by centrifuging at 20,000 × g at 4 ºC for 20 min. The vault pellet was then resuspended in the resuspension buffer, containing 50 mM tris (pH 7.7), 70 mM NaCl, and 0.5 mM $MgCl_2$. Further, the mixture was centrifuged at 13,000 × g to remove co-precipitated ribosomal proteins.

In the case of the LS method, the empty vaults and engineered laccase (eLac) in the supernatant were incubated together in 1:5 weight ratios of the expressing cell pellets at 4 ºC for 1 h. The packaged vaults were pelleted by centrifuging the mixture at 100,000 × g (4 ºC, 60 min) and resuspended in the resuspension buffer. The packaging of MLDGI in recombinant vaults produced in *Pichia pastoris* was also performed by the LS method.

In some cases, the packaged vault suspensions were further purified using a sucrose gradient (60-20%) column. The sucrose column containing the sample was centrifuged at 90,000 × g at 4 ºC for 16 h. Further, the 40-50% sucrose fractions containing packaged vaults were pooled together and centrifuged at 100,000 × g (4 ºC, 60 min) to pellet the vaults and then resuspended in the resuspension buffer. The samples were then verified for packaging by western blot as described above or by imaging on an electron microscope. All ultra-centrifuging (> 20,000 × g) was

performed on Beckman Coulter ultracentrifuge using a Ti45 fixed angled rotor. The sucrose gradient was performed on the SW25.1 swinging bucket rotor.

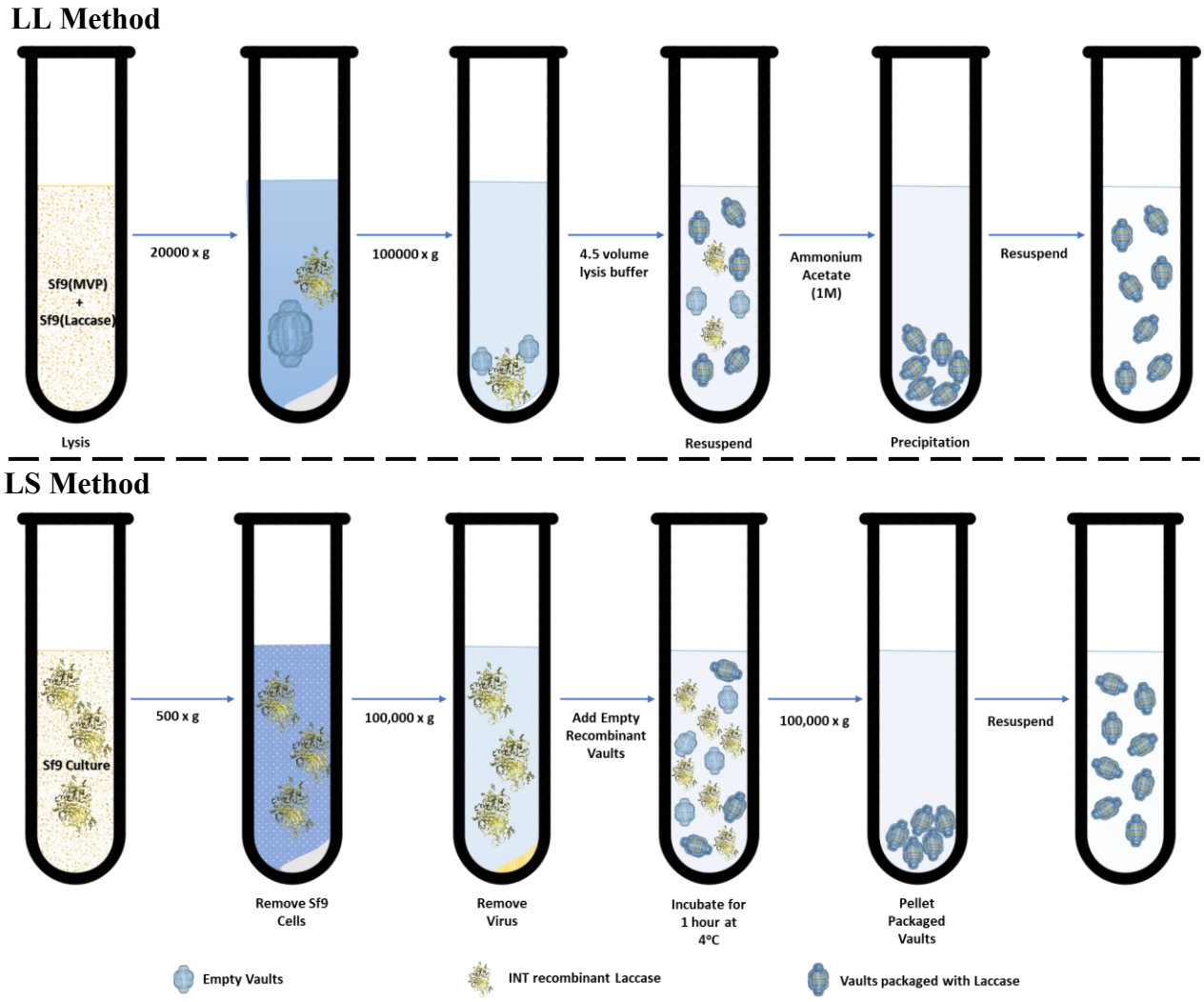

Figure 5.1**:** Vault Packaging procedures for engineered laccase. LL method – packaging in vaults by lysing the Sf9 cells expressing Major Vault Protein (MVP) along with the Sf9 cells expressing engineered laccase isozyme. LS method - packaging in vaults by mixing the empty recombinant vaults with the Sf9 culture supernatant containing the secreted engineered laccase isozyme.

The production of empty recombinant vaults expressed by Sf9 cells was done by processing only the Sf9 cells expressing the MVP protein as described above in the LL method. The yeast recombinant vaults were produced by growing the recombinant yeast cells in YPD medium at 30ºC

for 32 h and 200 rpm in Erlenmeyer flasks. The recombinant cells were collected by centrifuging the culture at 3000 × g at 4 ºC for 5 min. The cell pellet was resuspended in 3 mL lysis buffer A, per gram of cell pellet, containing 50 mM Na_3PO_4 (pH 7.4), 1 mM EDTA, 5% glycerol, 1 mM DTT, 1 mM PMSF, and 1X protease inhibitor cocktail (Sigma P8215). The cells were then lysed for 5 min in a beat beater using 4 g, 0.5 mm glass beads per gram of cells. The lysate was then separated from the beads by centrifuging the mixture at 3000 × g at 4 ºC for 5 min followed by washing of the beads thrice, with 1 mL lysis buffer per gram of cells and centrifugation at 3000 × g (4 ºC, 5 min) to recover the remaining lysate. The lysate was then clarified by pelleting the cell debris at 20,000 × g at 4 ºC for 20 min. The clear supernatant was centrifuged at 100,000 × g (4 ºC, 60 min) to pellet out the extracted proteins followed by resuspension of the protein pellet in 3.5 mL lysis buffer B per gram of cells (50 mM tris (pH 7.7), 70 mM NaCl, 0.5 mM $MgCl_2$, 1% Triton X100, 1 mM DTT, 1 PMSF, and 1% protease inhibitor cocktail (Sigma P8215)). The mixture was then homogenized using a douncer followed by adding 1M $NH_4CH_3CO_2$ and incubating the mixture for at 4 ºC 30 min in shaking to salt out the vaults. The salted-out vaults were treated as described above.

The lyophilization of VMLDGI was performed by adding trehalose (10 mg. mL^{-1}) to 1 mL vault solution and flash freezing the sample at -40 ºC using dry ice and ethanol bath. The freeze-drying was performed overnight using a VirTis DBT benchtop lyophilizer at -85 ºC and 200 millitorr vacuum. Samples were then stored at -20 ºC and later resuspended in the desired buffer as required.

5.2.7 Copper titration for Vault-packaged MLDGI activity.

The activity of vault-packaged laccase was optimized by adding copper salts to the Sf9 protein expression culture. $CuCl_2$ and $CuSO_4$ were added in a concentration range of 0.5 μM to 500 μM at different stages of Sf9 culture growth starting from time zero (at the start of viral infection) to 76 h of growth. Post expression, the supernatant containing the secreted enzyme was evaluated for activity by ABTS microplate assay. The relative activity was compared by analyzing the enzyme-catalyzed oxidation of ABTS (colorless) to ABTS+ (green color). A white microplate was incubated at room temperature and the enzyme reactions were started by adding the packaged/unpackaged enzyme (10 μL) solution to 190 μL bi-phosphate buffer (0.1 M, pH 6) containing 2 mM ABTS. The appearance of the green color was monitored for the desired duration.

5.2.8 Verification of the Vault-packaged Laccase Activity and NTO Degradation.

The activity of vault packaged LDI, ILD, LAI, and ILA was evaluated using the microplate assay by monitoring the change in absorbance of ABTS at 420 nm on a Promega plate reader. The reactions were performed in triplicates and were started by adding 10 μL of the packaged enzyme to 190 μL ABTS (2 mM) solution in 0.1 M bi-phosphate buffer (pH 6). The ABTS solution without the enzyme was also analyzed to account for the absorbance of the reaction mixture. The activity was calculated as stated before.

Similarly, the activity of VMLDGI was evaluated by monitoring the change in absorbance of ABTS (420 nm), guaiacol (465 nm), 1-naphthol (530 nm), 2,6-dichlorohydroquinone (323 nm), and catechol (480 nm and 287 nm) using a spectrophotometer (NanoDrop 2000c). The reaction

mixture consisted of 990 µL substrate (2 mM) solution in 0.1 M bi-phosphate buffer (pH 6). The catalytic reaction was initiated by adding a 10 µL enzyme solution to the ABTS solution after zeroing its absorbance at 420 nm.

5.2.9 NTO Degradation by Vault-packaged Laccase.

To evaluate the potential of the vault-packaged laccase (VMLDGI) for degradation of NTO. 5 $U.L^{-1}$ VMLDGI and natural laccase were incubated with 2 mM HBT in 50 mL polypropylene tubes. Empty vaults condition was used as a control experiment to account for the removal of NTO by the vault particles without laccase. All reactions were performed in triplicates to ensure statistical significance of the results and incubated in shaking incubators at 150 rpm at 30 °C. At the desired time point, the reactions were quenched by adding an equal volume of methanol to denature the enzymes.

All collected samples were stored at -20 °C till needed for analysis on HPLC-UV. All samples were filtered using 0.2 µm nylon filters before injection in the HPLC. The analysis was performed on HP 1050 HPLC equipped with Hypercarb column 150 mm x 4.6 mm x 5 µm. NTO was detected at 312 nm and was eluted after 9.5 minutes at 1 mL min^{-1} using 65% H_2O and 15% acetonitrile with 0.1% trifluoroacetic acid (TFA) according to the previously published method [36].

5.3 Results

5.3.1 Expression of Laccase in Tisma medium by *Trametes versicolor*

The activity of laccase in *T. versicolor* culture was monitored for 10 days by ABTS activity assay as described above. Laccase activity in the culture supernatant was detected after the addition of guaiacol on the 2nd day of fungal growth. Peak activity was detected on the 6th day of fungal growth in the Tisma medium (Figure 5.2a). Additionally, lowering the guaiacol concentration by half, doubled the laccase activity however, increasing or decreasing it further negatively impacted the laccase activity in the culture (data are not shown).

5.3.2 Identification and Extraction of Laccase Isozyme cDNA from *Trametes versicolor*

The literature search for laccase produced by *T. versicolor* resulted in the identification of twenty-one different laccase cDNA sequences that were previously reported and registered in the NCBI database (Table 5.4). In this study, these sequences were grouped in five different categories as explained above, which resulted in the identification of three isozymes, simultaneously secreted by *T. versicolor* cultured in the Tisma medium. The identity of laccase isozymes was confirmed by the control primers as well as the category-specific primers (Figure 5.2b).

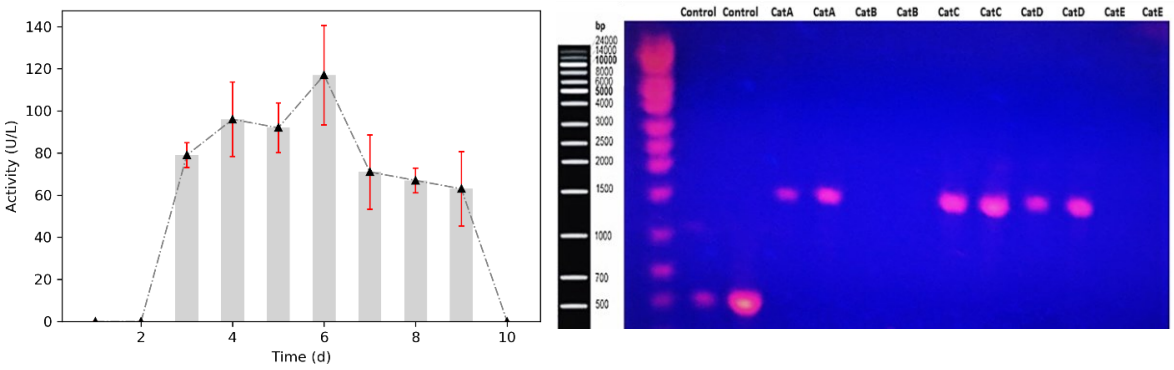

Figure 5.2**: a.** Laccase Activity from *Trametes versicolor* in Tisma culture. The activity (U/L) was determined using the ABTS assay, by measuring the change in absorbance at 420 nm for 5 mins. Activity estimation was done in triplicates and is represented as the mean activity ± standard deviation. **b.** Identification and amplification of laccase isozymes expressed by *T. versicolor* in Tisma medium. Three out of the five isozymes were detected in the same culture. Control primer was used to identify the presence of laccase based on the conserved copper binding region with an expected amplicon size of approximately 600 bp. CatA - Category A isozyme detected using Category A primer with a resultant amplicon size of 1560 bp. CatC - Category C isozyme detected using Category C primer with a resultant amplicon size of 1563 bp. CatD - Category D isozyme detected using Category D primer with a resultant amplicon size of 1584 bp. CatB - No amplicon detected at the expected amplicon size of 1563 bp using the category-specific primer. CatE - No amplicon detected at the expected amplicon size of 1574 bp using the category-specific primer. The amplicons were further verified by sanger sequencing.

Table 5.4: List of laccase isozymes grouped into five categories.

Category	Names in Literature	NCBI GeneBank#	Coding Region	NCBI Protein ID
A	lccA	JQ828930 (1560 bp)	1560 bp	AFM31222.1
	lac1	AY049275 (2408 bp)		AAL00887.1
	lccI	U44430 (1895 bp)		AAC49828.1
	lcc1	Y693776 (1560 bp)		AAW29420.1
	Laccase Protein	FJ469151 (1625 bp)		ACK77785.1
	lac2	AB212732 (1560 bp)		BAD98306.1
	TvLac1	XM_008034546 (1659 bp)		XP_008032737.1
B	TvLac4	XM_008037774 (1563 bp)	1563 bp	XP_008035965.1
	lac3	AB212733 (1563 bp)		BAD98307.1
	klc2	AM422387 (1784 bp)		CAM12361.1
	lcc1	X84683 (2800 bp)		CAA59161.1
C	lcc2	Y18012.1 (1563bp)	1563 bp	CAA77015.1
	lac1	AB212731 (1563 bp)		BAD98305.1
	laccase III	AY081188 (3936 bp)		AAL93622.1
	lac1	AF414109 (1563 bp)		AAL07440.1

	CVL3	D13372 (2684 bp)		BAA22153.1
D	lccIV	U44431 (2561 bp)	1584 bp	AAC49829.1
	lac4	AB212734 (1584 bp)		BAD98308.1
	CVLG1	D84235.1 (3099 bp)		BAA23284.1
E	lac5	AB539566 (1828 bp)	1574 bp	BAL42810.1
	TvLac2	XM_008038707 (1686 bp)		XP_008036898.1

5.3.3 Molecular Cloning for Synthesis of Insect Cell Expression Vector

The isozyme A and D sequences amplified from *T. versicolor* were found to be 95% and 99% in confirmation to the UniProt recorded sequences Q12717 and I6QS85 (Figure B 1). However, a stop codon was introduced in the middle of the isozyme C sequence, resulting in the expression of a truncated protein. Successfully cloned isozymes (laccase A and D) with different configurations of INT peptide fusion resulted in the synthesis of five different BVES carrier plasmids. The plasmids with INT sequence fused to the N terminus of laccase A or D are pLAI (6824 bp), pLDI (6848 bp), and pMLDGI (6895 bp). Similarly, pILD (6844 bp) and pILA (6820 bp) are the plasmids with INT sequences fused to the C terminus of laccase D or A, respectively (Figure 5.3).

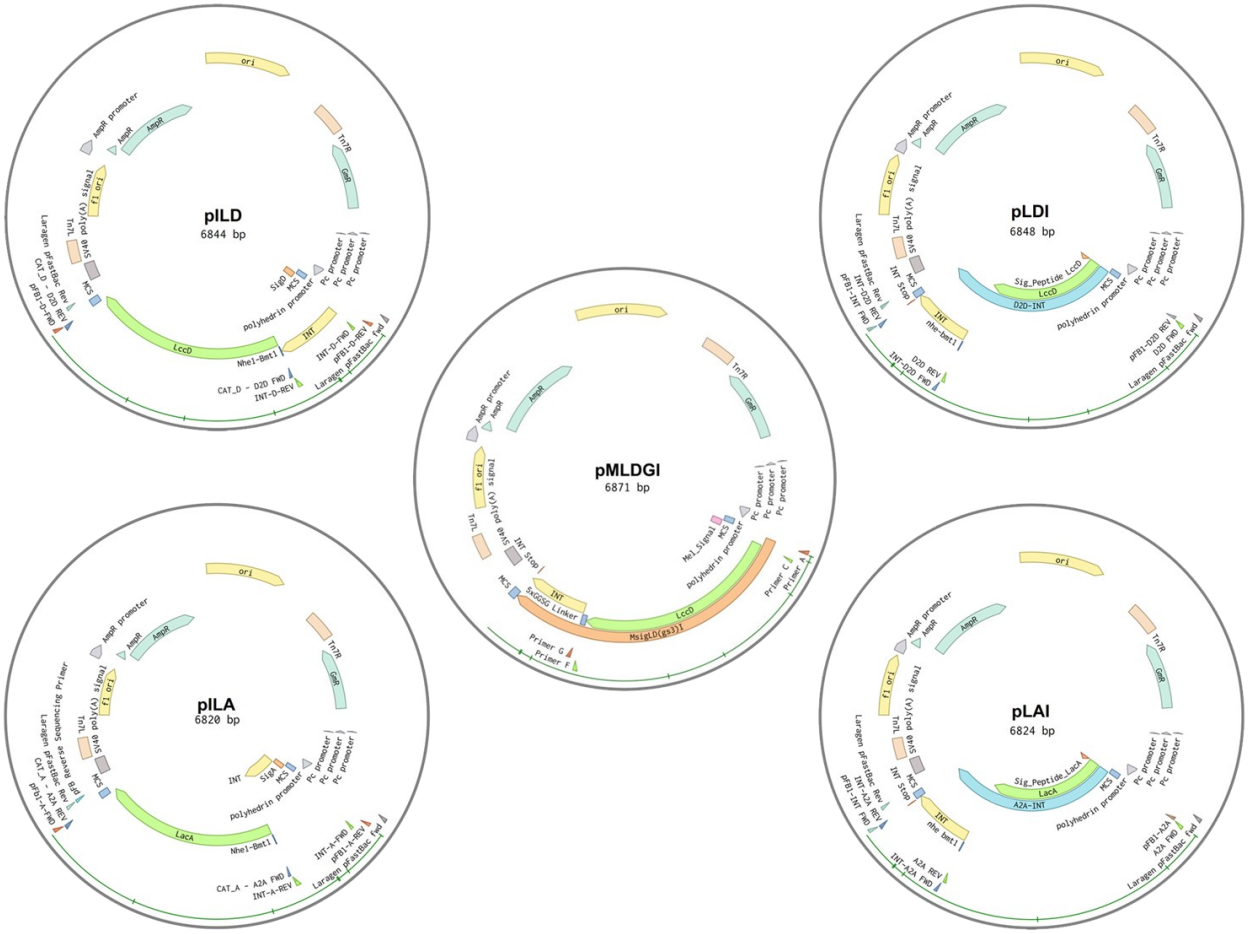

Figure 5.3: Plasmids maps for BVES carrier plasmids. pLDI (6848 bp) - map of the plasmid with INT sequence fused to the N terminus of laccase D as the gene of interest. pLAI (6824 bp) - map of the plasmid with INT sequence fused to the N terminus of laccase A as the gene of interest. pMLDGI (6895 bp) - map of the plasmid with INT sequence linked to the N terminus of laccase D with honeybee melittin secretion signal using a 5 x GSGG flexible linker as the gene of interest. pILD (6844 bp) - map of the plasmid with INT sequence fused to the C terminus of laccase D as the gene of interest. pILA (6820 bp) - map of the plasmid with INT sequence fused to the C terminus of laccase A as the gene of interest.

5.3.4 Expression and Vault Packaging of Engineered Laccase.

The eLac proteins were found to be approximately 90 kDa, on SDS-PAGE which is nearly 20 kDa heavier than the theoretical estimate of 76 kDa. Optimization of eLac expression by the

corresponding recombinant baculoviral infected Sf9 cells resulted in the highest expression after 96 h (LDI and ILD) and 96 h (MLDGI) (Figure 5.4).

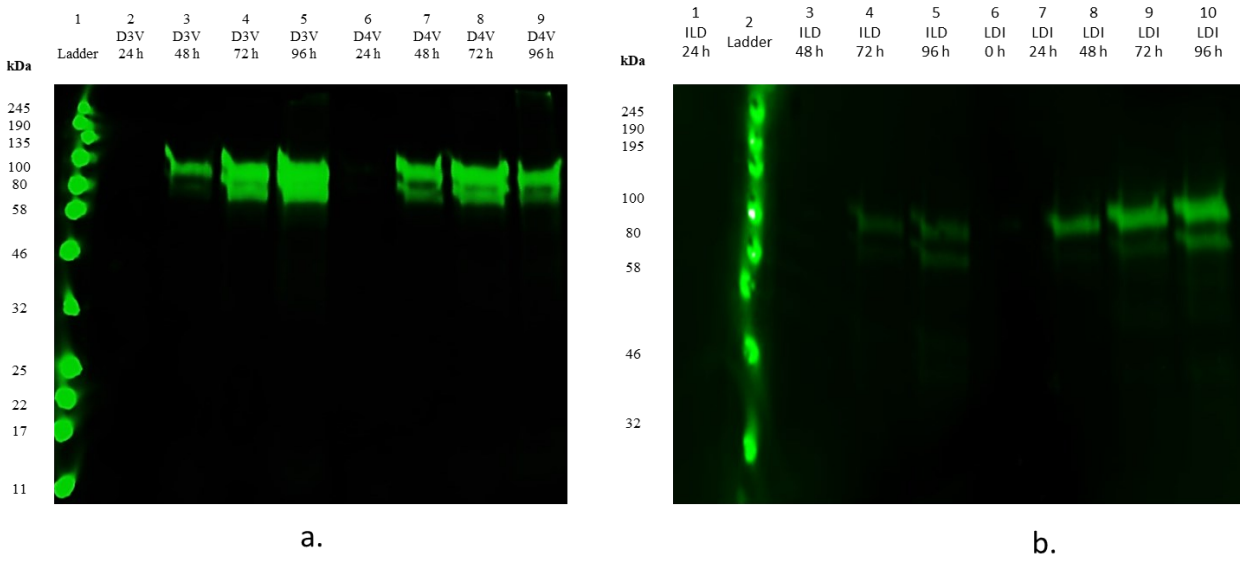

Figure 5.4: Western Blot (WB) of engineered laccase proteins using an anti-INT antibody. **a.** Verification of the presence of MLDGI after infection with recombinant baculovirus. D3V - virus harvested after 3 days of baculoviral amplification in Sf9 insect cells. D4V - virus harvested after 4 days of baculoviral amplification in Sf9 insect cells. Samples were collected after every 24 hours post-infection with the amplified virus for the WB analysis. The MLDGI band of approximately 90 kDa was obtained. Expression of MLDGI started 24 h post-expression and maximum expression of MLDGI was obtained for Sf9 insect cells infected for 96 h by the 3 days amplified virus. **b.** Verification of expression of eLac. ILD- INT domain attached to N-terminal of laccase protein. LDI -INT domain attached to C-terminal of laccase protein. Samples were collected after every 24 hours post-infection with the amplified virus for the WB analysis. The LDI expression appeared 24 h post-infection and the maximum expression was observed after 96 h, whereas expression of ILD was insignificant. A protein size of approximately 90 kDa was obtained.

Packaging of MLDGI in vaults was verified by detecting the MVP protein along with the MLDGI in the same VMLDGI sample. The MVP was detected using an anti-MVP antibody and was found to be near 100 kDa marker on the protein ladder in agreement with previously published studies. Similarly, an anti-INT antibody detected the MLDGI protein slightly lower than the 100 kDa mark. The packaging was further confirmed by EM imaging of the same sample (Figure 5.5).

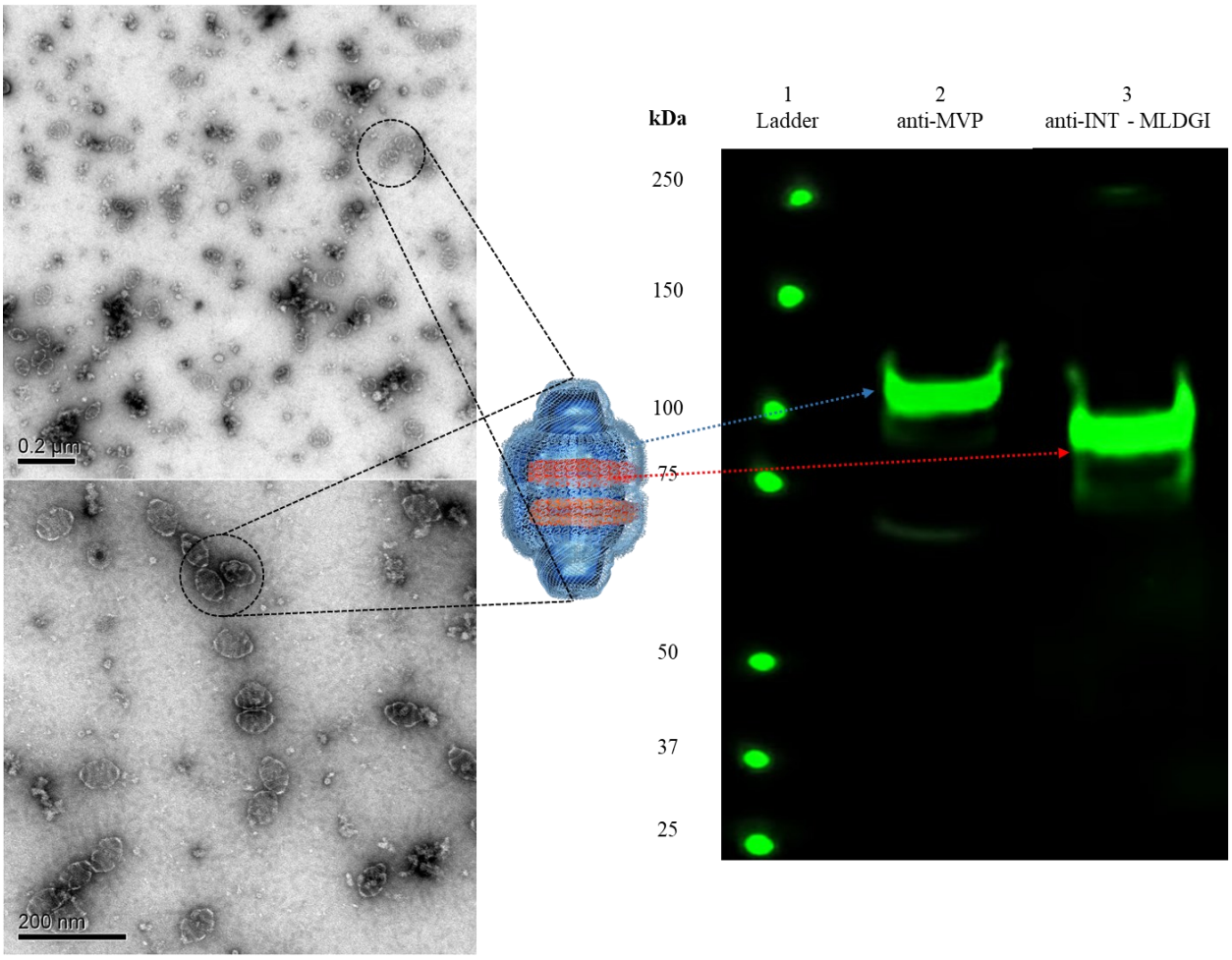

Figure 5.5: Electron Microscopic Image and Western Blot of Vault packaged Laccase. Packaging of Laccase (~90 kDa) in vaults (>100 kDa) was verified with respective antibodies in the same sample. The barrel-shaped vault structure can be seen intact in the micrograph and the ABTS activity assay of the sample, along with the western blotting with anti-INT and anti-MVP antibodies confirmed the packaging and activity of MLDGI

5.3.5 Engineered and Vault-packaged Laccase Activity.

Among all five proteins, the MLDGI protein showed the best activity. The eLac expressed in the SF-900 II serum-free media was found to be inactive. However, the addition of copper in the protein-expressing cultures resulted in activating the expressed MLDGI. The titration of copper did not have a significant effect on the activity of LDI, ILD, LAI, and ILA proteins.

The optimization of MLDGI activity was performed by adding $CuCl_2$ or $CuSO_4$ to the expressing Sf9 culture. ABTS oxidation was not observed when either of the copper salts of concentrations 0.5 µM and 5 µM was added at time zero (start of the culture). Similar results were observed when 50 µM and 200 µM $CuSO_4$ were added at time zero. However, the addition of 50 µM $CuCl_2$ developed some green color due to the oxidation of ABTS by MLDGI/VMLDGI. The green color development increased with the increase in the concentration of $CuCl_2$ to 200 µM (Figure B 2). Further increasing the concentration of copper from 200 µM to 500 µM increased the enzyme activity but, adding more than 500 µM copper appeared to have a negative impact (Figure 5.6). Similarly, when the salts were added at different times (18 h, 24 h, 30 h, 42 h, 48 h, etc.) post baculoviral inoculation of Sf9 culture, the activity of the enzyme increased. The highest activity was achieved after adding $CuCl_2$ 48 h post-inoculation however, increasing the time of adding copper, any further, reduced the enzyme activity. The protein expression was not affected by the addition of copper, as observed by western blot (Figure 5.6).

The activity of MLDGI increased considerably and retained longer after packaging in vaults. Performing the multiple rounds of vault packaging using the MLDGI supernatant increased the yield of VMLDGI production (Figure B 3a). The LDI protein was found active for two days on incubation with ABTS, only after packaging using the LL method (vsLDI-LL) and sucrose purification. The increase in absorbance along with the appearance of a green color corresponding to the oxidation of ABTS to ABTS+ was observed, after four hours of vsLDI-LL incubation with ABTS. However, the increase in absorbance for the blank and vsILD-LL was insignificant. The LDI and ILD proteins packaged by the LS method showed no activity (data not shown). The packaging of LDI and ILD was confirmed by SDS-PAGE gel stained with Coomassie blue. MVP band was detected at 100 kDa, and eLac was detected at 90 kDa (Figure B 4). The expression of

LAI and ILA proteins was low, and the proteins were found to be inactive even after vault packaging and sucrose purification of packaged enzymes.

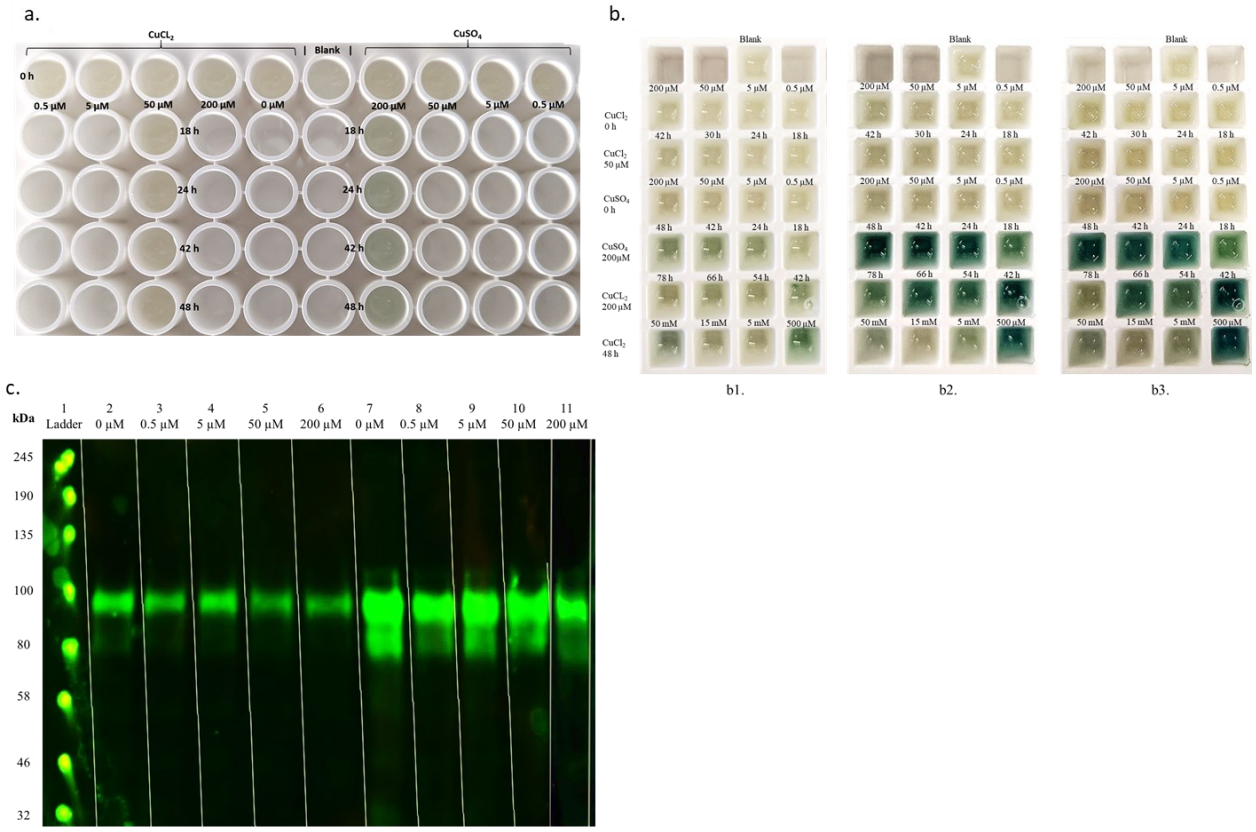

Figure 5.6: **a.** MLDGI (10 µL) incubation with 2 mM ABTS solution (190 µL) at room temperature. The Sf9 culture expressing MLDGI was supplemented with different concentrations of $CuCl_2$/$CuSO_4$ added at different times. **b.** VMLDGI (10 µL) incubation with 2 mM ABTS solution (190 µL) at room temperature. The Sf9 culture expressing MLDGI was supplemented with different concentrations of $CuCl_2$/$CuSO_4$ added at different times. From right to left – **b1.** after 10 min incubation. **b2.** after 2 h incubation. **b3.** after 5 h incubation, **c.** Effect of copper concentrations on MLDGI expression. Wells 2-6 show the expression of MLDGI and 7-11 show the bands after vault-packaging of the respective protein from wells 2-6. The Sf9 culture expressing MLDGI was supplemented with different concentrations of $CuCl_2$, 48 h post-infection with the optimized baculovirus. The western blot was performed using the anti-INT antibody. The effect of copper on the expression of MLDGI was found to be insignificant which can also be seen in the VMLDGI bands. The bands in wells 7-11 are thicker as compared to 2-6 because the enzyme is concentrated in a smaller volume.

5.3.6 Verification of Vault-packaged MLDGI Catalytic Activity and Stability.

Vault-packaged MLDGI was found to be nearly three orders of magnitude more active than vsLDI-LL when incubated with ABTS (2 mM). The catalytic activity of VMLDGI was first evaluated by incubating it for 3 h with a 2 mM ABTS solution as described before (Figure 5.7). The activity was retained after the VMLDGI was lyophilized and resuspended in 0.1 M bi-phosphate buffer (pH 6) and PBS buffer. The phosphate resuspended VMLDGI retained nearly 100% activity (5.5 $U.L^{-1}$) and was found to be stable when incubated for 7 days at 30 ºC, 150 rpm while, after additional 7 days of incubation (Figure B 3b). Further testing was performed by incubating VMLDGI with different known laccase substrates (2 mM) in 0.1 M bi-phosphate buffer (pH 6) for 3 h. The oxidation was monitored at 465 nm for guaiacol, 530 nm for 1-naphthol, 323/340 nm for 2,6-dichlorohydroquinone, and 287/480 nm for catechol (Figure 5.8).

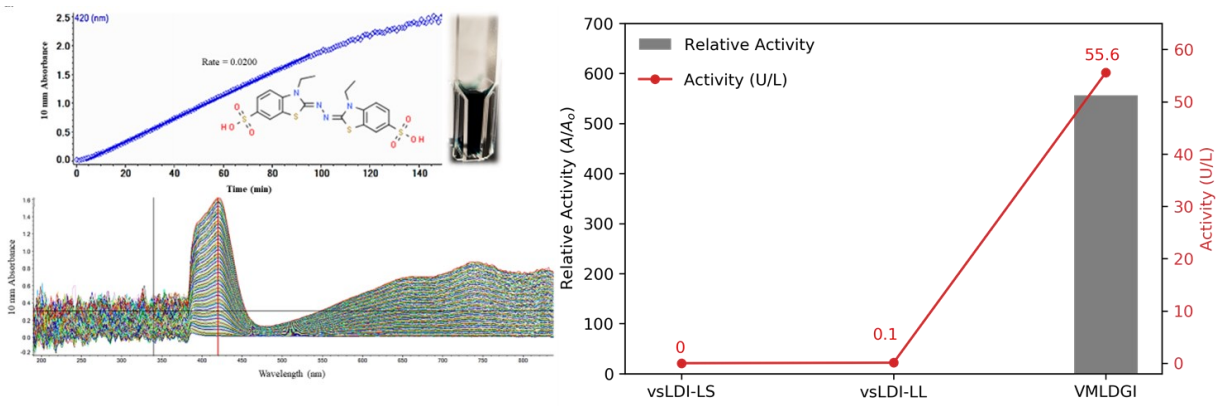

Figure 5.7: Comparison of ABTS activity measured at 420 nm for different vault-packaged laccase configurations. The red curve shows the absolute activity ($U.L^{-1}$) of the sample while the gray bars represent the relative activity (A/A_o) of the samples in different conditions. The VMLDGI was found to have three orders of magnitude higher activity as compared to the other configurations of the vault-packaged laccase.

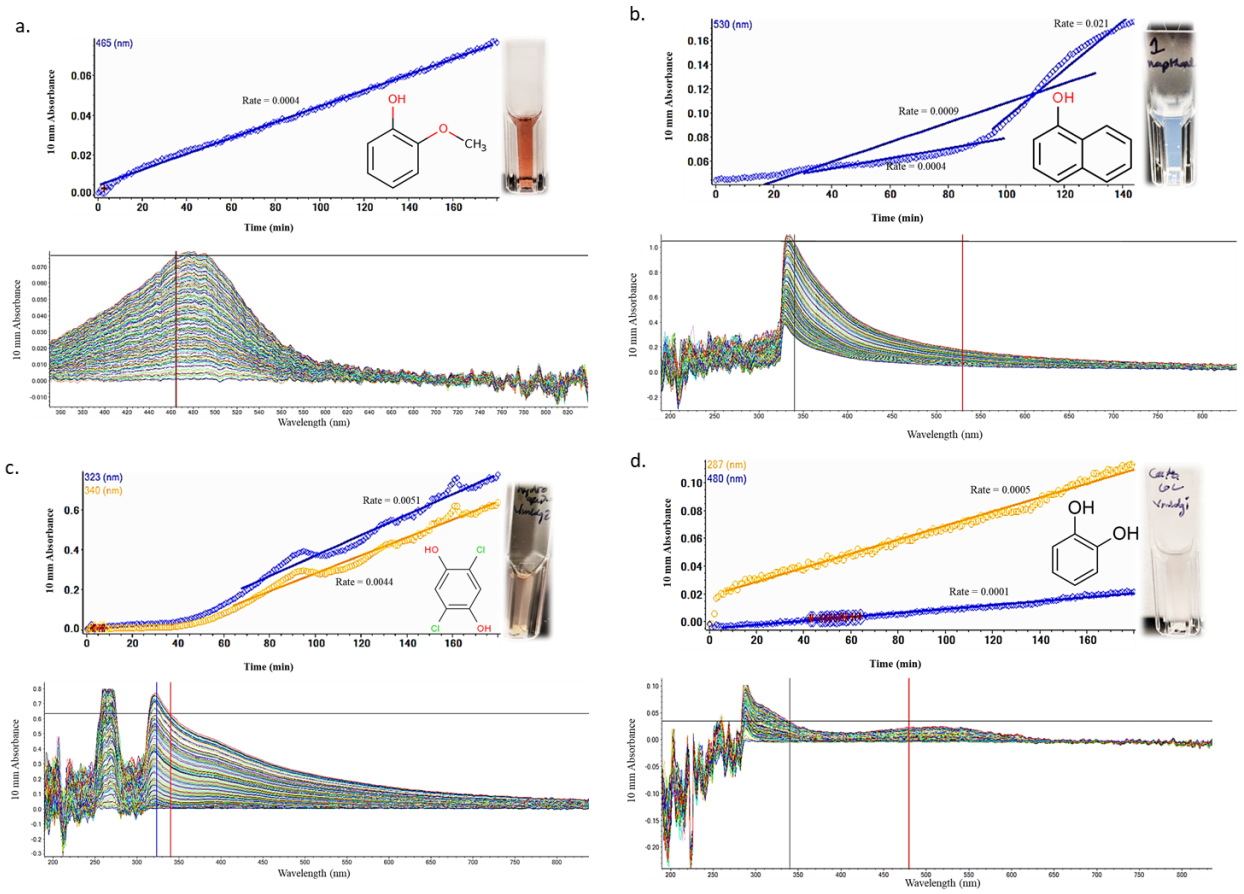

Figure 5.8: Oxidation of substrates catalyzed by vaults-package laccase (VMLGI) monitored for 3 h. The development of color in the cuvette corresponds to the increase in absorbance over time and the change in absorbance spectra because of the oxidation of the laccase-specific substrate catalyzed by VMLDGI. **a.** Guaiacol (465 nm). **b.** 1-Napthol (530 nm). **c.** Hydrochloroquinone (340 nm/323 nm). **d.** Catechol (287 nm/480 nm). The rate of change in absorbance is displayed on the curve.

5.3.7 NTO Degradation by Vault-packaged Laccase.

5 $U.L^{-1}$ vault-packaged laccase (VMLDGI) was able to catalyze the degradation of 60% NTO with 2 mM HBT in 96 h. The degradation of NTO by empty vaults and 5 $U.L^{-1}$ laccase was insignificant (Figure 5.9).

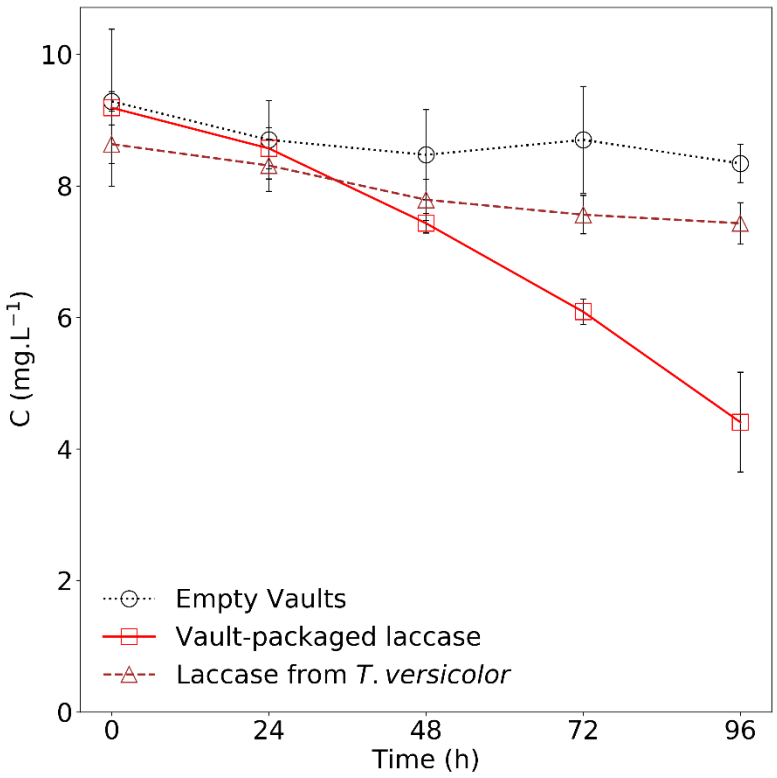

Figure 5.9: Degradation of NTO by vault-packaged laccase. 60% (10 mg L^{-1}- 4 mg L^{-1}) NTO was degraded 5 $U.L^{-1}$ laccase in 96 h while no degradation was observed for empty vaults and 5 $U.L^{-1}$ native laccase from *T. versicolor*. Empty vaults did not contain laccase and were used to account for the removal of NTO by major vault protein. The reactions were performed in 0.2 M phosphate buffer (pH 6) and incubated in triplicates at 150 rpm at 30 °C. Error bars represent experimental triplicates.

5.4 Discussion

Laccases are among the most widely studied enzymes for use as biocatalysts. Their applications include chemical synthesis, polymerization, textile bleaching, pulp, and paper production, food processing, advanced water and wastewater treatment by dye decolorization, enzymatic degradation of pharmaceutical and personal care products, xenobiotics, endocrine disruptors, olefin plastics, etc. In recent years, laccases have also been shown to display

antiproliferative properties against various cancer cell lines along with reverse transcriptase inhibitory activity for HIV [21, 37-39]. As a result, laccase has been widely engineered and expressed heterologously to increase its production and catalytic activity. The heterologous expression of laccases has been performed in prokaryotic as well as eukaryotic organisms. Expression hosts include plant cell lines like tobacco and corn but, fungal systems like *Pichia pastoris, Saccharomyces cerevisiae* is prolific. Expression in prokaryotic organisms has been mostly unsuccessful [2, 40]. Selective mutation of laccase, fusion with peptides, and chimerization of enzymes with laccase can increase its activity and secretion by heterologous hosts along with providing additional catalytic properties to laccase [40-44]. Previously, in one study, the expression of worm laccase has been performed in *Spodoptera frugiperda* (Sf9) cells [45]. In this study, we use the Sf9 insect cell line as the expression host for laccase derived from the fungi *T. versicolor* and fuse with INT peptide to enable the selective packaging of laccase into the vault nanoparticles while retaining its activity.

Biocatalytic properties of *T. versicolor* derived laccase, like the requirement of oxygen as a cofactor instead of hydrogen peroxide, near-neutral pH optimum, and broad-spectrum catalytic applications make it an ideal candidate for packaging in vault nanoparticle. Vault packaging of laccase is a step forward to enhance its applicability in biologically catalyzed water and wastewater treatment, especially as a post-tertiary treatment option for unselective biodegradation of untreated xenobiotics. Previously, we have shown that the packaging of manganese peroxidase (MnP) enzyme produced by the wood-rotting fungi *P. chrysosporium* in the vault nanoparticles improved the biodegradation of munition compounds like Amino-Nitro Toluene (ANT) and Diamino Toluene (DAT) [26] as well as phenolic compounds [28]. The biodegradation of bisphenols by vault-packaged MnP also showed a lower toxicity profile as compared to natural MnP [27].

Packaging of enzymes in vault nanoparticles have also been shown to increase enzyme stability in reaction conditions [26-28]. As a result, it is hypothesized that the packaging of laccase would have similar inferences. The natural vault particle contains vault-associated poly(ADP-ribose) polymerase (VPARP) bound the MVP shell and retains its activity after the natural vault particle is assembled and purified. The VPARP is a 193 kDa protein [46] which includes a 19 kDa MVP interaction domain called INT. MLDGI being a 90 kDa protein, can also be packaged inside the recombinant vaults. Before MLDGI, the heaviest protein packaged in recombinant vaults was 61(+19) kDa firefly luciferase protein [47, 48].

Previously published studies suggested the expression of multiple laccase isozymes by *T. versicolor.* Some of these are expressed constitutively, and can also be induced by some aromatic compounds, like guaiacol and gallic acid [49-51]. Many different laccase isozymes, synthesized by *T. versicolor,* have been reported in the literature and registered on NCBI. Similar sequences have been registered under different names. This paper attempts to systematize the laccase isozyme database by grouping them into five categories, based on the similarity in nucleotide and amino acid sequences (Table 5.4). The categorization enabled the identification of the type of isozymes produced in a single culture and multiplexing of laccase mRNA amplification for further experimentation. Hence, this study also provides experimental evidence for the expression of multiple laccase isozymes at the same time in a single fungal culture. Three different laccase category cDNA were amplified by TPCR and cross-verified by primers designed to detect conserved copper regions [31] as well as through sequencing. The total nucleic acid was extracted from the fungal biomass when maximum laccase activity was registered in the culture (Figure 5.2). A touchdown PCR (TPCR) was performed using the category-specific primers, instead of conventional PCR, to allow multiplexing and ensure higher amplicon yield (Table 5.1). The

category C isozyme was found to have a stop codon introduced mid-sequence. As a result, only category A (UniProt# Q12717) and category D (UniProt# I6QS85) (Figure B 1) isozymes were selected for packaging in vaults. The introduction of the stop codon can be attributed to a sequencing error or replication error caused during Taq polymerase catalyzed TPCR amplification. Further experimentation on the variation of isozyme expression with the culture growth was out of the scope of this study. Post amplification of the enzyme cDNAs, the INT cDNA was attached to the laccase cDNA (including the native secretion signals) to ensure selective packaging of the laccase protein in the vault nanoparticles. This resulted in two possibilities: firstly, the catalytic activity of the laccase protein could be affected if the INT peptide was attached to the C terminus of laccase. This is because the type I copper of the active site is extremely close to the C terminus and many studies have reported the importance of C-terminus peptide in laccase proteins [40, 44, 52, 53]. Secondly, INT peptide could lose its MVP binding activity if the INT peptide was attached to the N terminus of laccase thereby putting its C terminus in the middle of the fusion protein. In the natural vault particle, the N terminus of the INT peptide is bound to the C terminus of VPARP [54]. To test these possibilities, four BVES carrier plasmids, namely, pLAI, pLDI, pILA, and pILD (Figure 5.3) were synthesized, using the Gibson Assembly protocol to fuse INT, laccase, and pFASTBac1 vector in different configurations. The three DNA fragments were PCR amplified using the primers designed to contain the overlapping base pair sequence (Table 5.3). The Gibson Assembly protocol for DNA assembly is broadly accepted and has been extensively used to create multiple DNA assemblies [35, 55].

Laccase protein is a multiple copper oxidase and has four copper-binding sites [56]. The catalytic mechanism of laccase is highly dependent on the presence of copper, as a result, laccase cannot reach its maximum activity in a copper-exhausted state [57]. When laccase is produced in

its original host like *T. versicolor* the mechanism to incorporate copper is already present in the host organism, however, in the case of heterologous expression, the ability of the new host to incorporate copper, during protein production becomes essential, along with the availability of the macronutrient. It has been shown that the expression of laccase in the original host improves with the increase in copper concentration to an extent after which, the copper toxicity results in lower cell growth [58]. In the case of the Sf9 expression of MLDGI, the addition of copper did not induce its production. The observation could be related to the fact that some isozymes produced by the original host are inducible, whereas, in the case of Sf9 only one isozyme was expressed, and the transfected expression cassette did not have copper inducible machinery. The MLDGI expression level was verified by varying the amount of copper present in the expression culture and normalizing the expression to the number of cells (Figure 5.6).

The fusion proteins LDI, LAI, ILD, and ILA, when expressed by Sf9 cells, did not show any activity even after copper titration in the Sf9 expression culture. However, LDI protein showed some activity over long periods of incubations but only after packaging in vaults and sucrose purification (Figure B 4). Some interaction between the INT peptide and laccase protein in the fusion proteins is evident, as all configurations were rendered inactive due to the fusion, irrespective of the INT peptide location. Furthermore, stronger MVP and INT binding as compared to INT and laccase interaction, resulting in freeing the active site of laccase, could be the cause for vsLDI activity. It was safe to assume that the INT peptide did not lose its MVP binding activity when it was attached to the N terminus of laccase in ILD and ILA proteins as the fusion proteins got packaged in vault nanoparticles. As a result, the LDI protein fusion was selected for further experimentation and improvements. The pMLDGI carrier plasmid was created by fusing the INT cDNA to the N terminus of laccase D cDNA along with a flexible linker (5 × GGSG) between

them. The C terminus of laccase D was also modified to replace the native secretion signal with the honeybee melittin secretion signal (Table 5.2) to allow enhanced secretion by Sf9 cells [59]. The glycine serine linker peptides have been extensively studied as flexible linkers. They have been shown to reduce the interference in fusion proteins leading to an increase in stability and proper protein folding [60]. Similar linkers have been used in previously published studies and are also registered on different databases like the International Genetically Engineered Machine (iGEM) registry [61-64]. Following the Gibson assembly of the DNA fragments, expression of the MLDGI protein in copper titrated Sf9 cultures, and vault packaging of the protein, three orders of magnitude increase in the activity of the packaged fusion protein was observed when compared to vsLDI-LL (Figure 5.7). As mentioned above, the VMLDGI was synthesized by packaging the MLDGI protein secreted in the culture by 2 x 10^6 cells/ml Sf9 cells, and vsLDI-LL was synthesized by packaging the intracellular LDI using the LL method for the same cell count. However, the VMLDGI should be compared with vsLDI-LS, because the synthesis method for both the enzymes is the same. The MLDGI showed significant activity even without packaging into vault nanoparticles (Figure 5.6a), which were not observed in other eLac. This supports the conclusion that the introduction of the long and flexible Gly-Ser linker reduced the interaction of INT with the laccase isozymes. This observation is also supported by the fact that multiple rounds of packaging could be performed from the same supernatant, because of the reduced interaction between the two peptides more fusion protein was available for packaging per vault (Figure B 3a).

A VMLDGI sample was lyophilized to test whether the vault packaged enzymes retained their activity post resuspension in different conditions (Figure B 3b). Due to lyophilization, the vaults packaged enzymes could be applied at varying concentrations, and in different buffers, hence, lyophilization improves their applicability in remediation systems and facilitates its long-

term storage. This study is the first recorded lyophilization of the vault packaged enzymes with successful retention of activity after resuspension. The UV-vis absorbance spectra of VMLDGI oxidizing ABTS were found to be identical to the spectra of natural laccase catalyzed oxidation of ABTS. This outcome suggests that laccase retained its properties after packaging in vaults. This observation was further verified by monitoring the oxidation of known laccase substrates like guaiacol, catechol, 1-naphthol, and 2,6-dichlorohydroquinone by VMLDGI (Figure 5.8).

In this study, the vault-packaged laccase and HBT (2mM) were found to degrade 60% NTO in 96 h at 5 $U.L^{-1}$ laccase activity while unpackaged *T. versicolor* native laccase at the same activity and HBT was not able to demonstrate any significant degradation (Figure 5.9). Despite the low enzyme activity (5 $U.L^{-1}$), the increased local concentration of laccase inside the vaults and the sacrificial protection imparted by major vault protein may be the reason for the longest active life of the packaged enzyme, while the unpackaged enzyme was quickly inactivated in the reaction environment [65, 66]. Various vehicles have been investigated for the encapsulation of enzymes to increase enzyme longevity and applicability, but vault nanoparticles have the advantage of being naturally occurring non-hazardous protein nanostructures [26]. The applicability of vault-packaged enzymes in bioremediation has been investigated by other studies. However, this work demonstrates the applicability of vault-packaged laccase for biodegradation. Similar to this work, studies on vault-packaged MnP, for biodegradation of nitroaromatic explosives and phenolic/biphenolic compounds, demonstrated that the packaged enzyme had better degradation efficiency, active life, and the toxicological profile of degradation by-products compared to the native unpackaged enzyme [26-28, 67]. These properties of vault-package enzymes provide a practical advantage for the use of both vault-packaged MnP and vault-packaged laccase, together or individually, for the treatment of munitions contaminated water but the addition of this

technology to wastewater treatment systems and stormwater biofilters must be further analyzed. Nonetheless, our results suggest that the ligninolytic enzyme (vault-packaged or native) can be used for ex-situ or in-situ remediation of NTO contaminated water.

Appendix B

Figure B 1: Comparison of laccase D and A with UniProt registered sequence ID: **a.** UniProt # Q12717. The sequence match of the laccase D with Q12717 was found to be 99%. **b.** UniProt # I6QS85. The sequence match of the laccase A with 16QS85 was found to be 95%. The red highlights represent the mismatches.

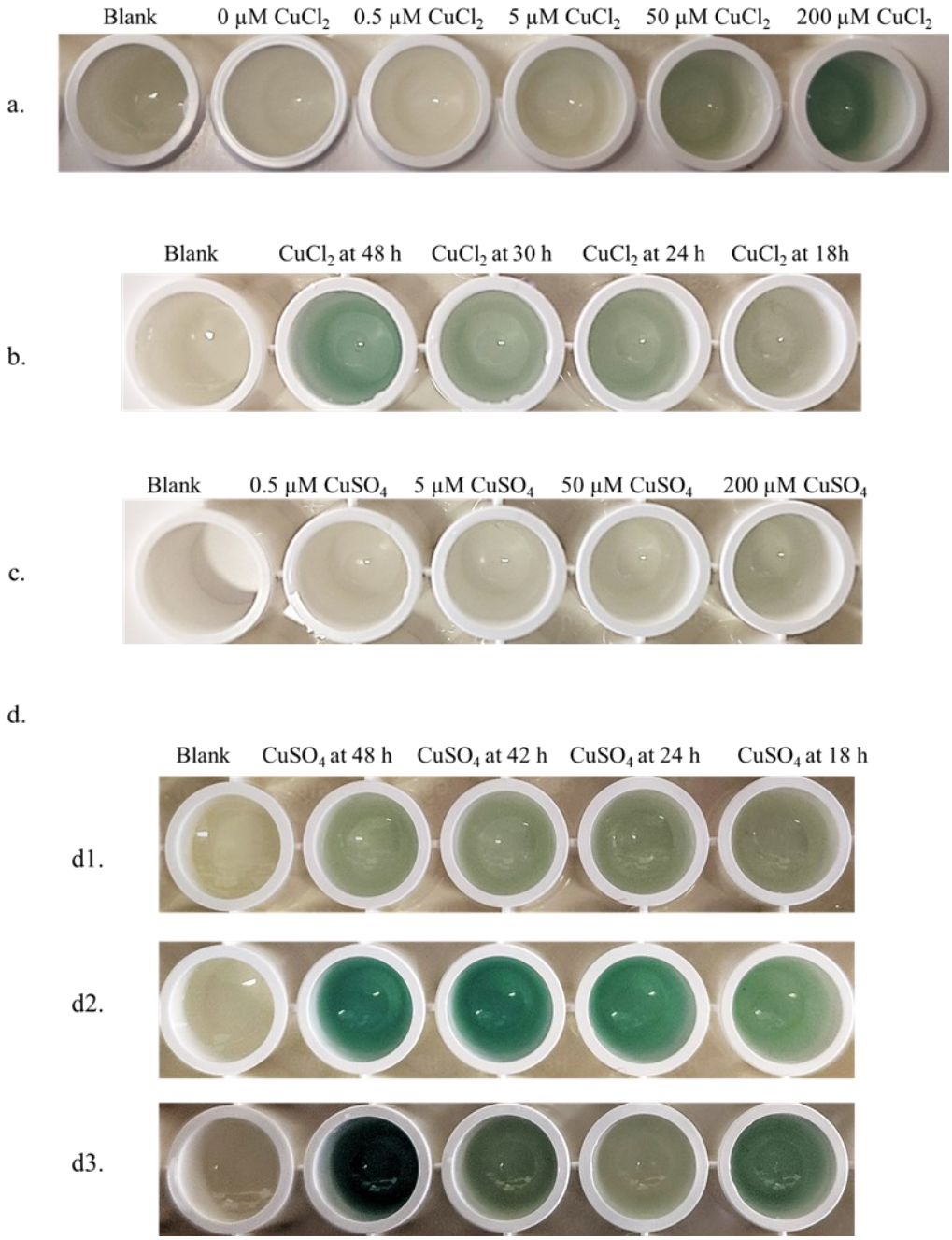

Figure B 2**:** Copper titration to estimate the optimal activity of VLMDGI. The assay was performed by incubating VMLDGI (20 µL) with 2 mM ABTS solution (180 µL) at room temperature. **a.** Varying concentrations of $CuCl_2$ added at the start of the expression culture (t = 0). **b.** 50 µM $CuCl_2$ added different times (18 h, 24 h, 30 h, 48 h) after the start of the expression culture. **c.** Varying concentrations of $CuSO_4$ were added at the start of the expression culture (t = 0). **d.** oxidation of ABTS by VMLDGI synthesized by titrating 200 µM $CuSO_4$ at different times (18 h, 24 h, 42 h, 48 h) after the start of the expression culture after 10 min incubation (d1), after 1 h incubation (d2), and after 24 h incubation (d3)

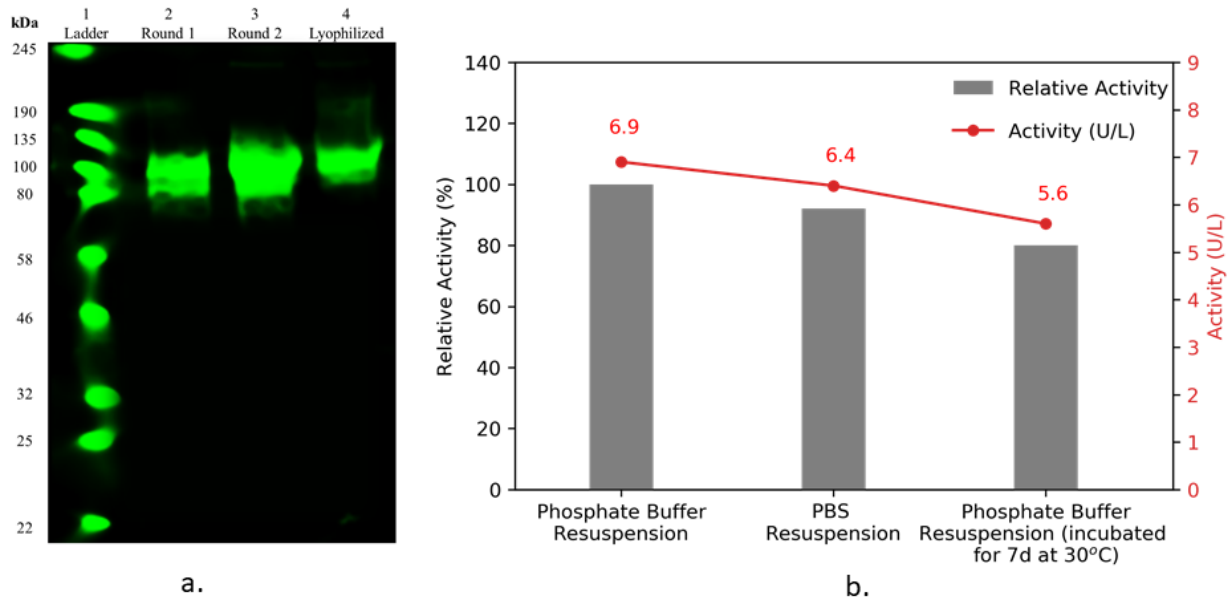

Figure B 3: **a.** Multiple rounds of MLDGI packaging from SF9 culture and presence of VMLDGI post resuspension of the lyophilized sample. Round 1 represents the first round of packaging and Round 2 represents the second round of packaging from the supernatant of Round 1. Lyophilized represents the detection of VMLDGI after the lyophilized sample was resuspended in the phosphate buffer. The Sf9 culture expressing MLDGI was supplemented with 500 µM $CuCl_2$, 48 h post-infection with the optimized baculovirus. The western blot was performed using the anti-INT antibody. **b.** The red curve shows the absolute activity (U/L) of the sample while the gray bars represent the relative activity (%) of the samples in different conditions. The lyophilized VMLDGI was resuspended in respective buffers to estimate the activity using the ABTS assay in a cuvette for a period of 1 h. About 80% of the initial activity was retained after 7 days incubation at 30 ºC for the phosphate buffer resuspended sample.

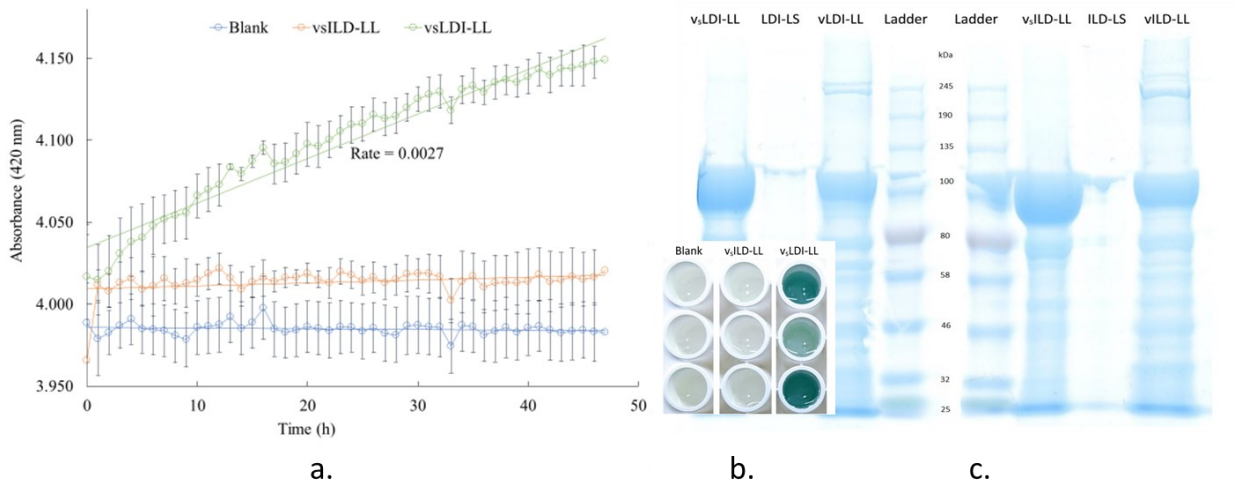

Figure B 4: a. Oxidation of ABTS by vault packaged eLac. An increase in absorbance indicates the sustained activity of packaged laccase enzyme. The ABTS assay was performed using a microplate and absorbance was monitored at 420 nm. Error bars represent triplicates and are represented as the mean absorbance ± standard deviation. b. SDS-PAGE gel stained with Coomassie blue. MVP band (100 kDa) eLac (90 kDa), c. Vault packaged INT laccase isozymes ABTS activity assay. vsLDI-LL - sucrose purified vault packaged laccase D-INT (LL method); LDI-LS -vault packaged laccase D-INT (LS method); LDI-LL - vault packaged laccase D-INT without sucrose purification (LL method); vsILD-LL - sucrose purified vault packaged INT-laccase D (LL method); ILD-LS - vault packaged INT-laccase D (LS method); ILD-LS - vault packaged INT-laccase D (LS method) without sucrose purification. Blank – no enzyme control.

References

1. Harms, H., D. Schlosser, and L.Y. Wick, *Untapped potential: exploiting fungi in bioremediation of hazardous chemicals.* Nature Reviews Microbiology, 2011. **9**(3): p. 177-92.
2. Roca-Lema, D., O. Martinez-Iglesias, C. Fernandez de Ana Portela, A. Rodriguez-Blanco, M. Valladares-Ayerbes, A. Diaz-Diaz, A. Casas-Pais, C. Prego, and A. Figueroa, *In Vitro Anti-proliferative and Anti-invasive Effect of Polysaccharide-rich Extracts from Trametes Versicolor and Grifola Frondosa in Colon Cancer Cells.* International Journal of Medical Sciences, 2019. **16**(2): p. 231-240.
3. Islam, S.M.R. and T.J. Siddiqua, *Functional foods in cancer prevention and therapy: Recent epidemiological findings*, in *Functional Foods in Cancer Prevention and Therapy*, Y. Kabir, Editor. 2020, Academic Press. p. 405-433.
4. Blagodatski, A., M. Yatsunskaya, V. Mikhailova, V. Tiasto, A. Kagansky, and V.L. Katanaev, *Medicinal mushrooms as an attractive new source of natural compounds for future cancer therapy.* Oncotarget, 2018. **9**(49): p. 29259-29274.
5. Hsieh, T.C. and J.M. Wu, *Cell growth and gene modulatory activities of Yunzhi (Windsor Wunxi) from mushroom Trametes versicolor in androgen-dependent and androgen-insensitive human prostate cancer cells.* International Journal of Oncology, 2001. **18**(1): p. 81-8.
6. Bolli, A., P. Galluzzo, P. Ascenzi, G. Del Pozzo, I. Manco, M.T. Vietri, L. Mita, L. Altucci, D.G. Mita, and M. Marino, *Laccase treatment impairs bisphenol A-induced cancer cell proliferation affecting estrogen receptor alpha-dependent rapid signals.* IUBMB Life, 2008. **60**(12): p. 843-52.
7. Rodriguez Couto, S. and J.L. Toca Herrera, *Industrial and biotechnological applications of laccases: a review.* Biotechnology Advances, 2006. **24**(5): p. 500-13.
8. Call, H.P. and I. Mücke, *History, overview and applications of mediated lignolytic systems, especially laccase-mediator-systems (Lignozym®-process).* Journal of Biotechnology, 1997. **53**(2-3): p. 163-202.
9. Dwivedi, U.N., P. Singh, V.P. Pandey, and A. Kumar, *Structure–function relationship among bacterial, fungal and plant laccases.* Journal of Molecular Catalysis B: Enzymatic, 2011. **68**(2): p. 117-128.
10. Sharma, P., R. Goel, and N. Capalash, *Bacterial laccases.* World Journal of Microbiology and Biotechnology, 2006. **23**(6): p. 823-832.
11. Morozova, O.V., G.P. Shumakovich, S.V. Shleev, and Y.I. Yaropolov, *Laccase-mediator systems and their applications: A review.* Applied Biochemistry and Microbiology, 2007. **43**(5): p. 523-535.
12. S. R, Y., S. B. P, U. T. H, and K. B. M, *Laccase Biosensor: Green Technique for Quantification of Phenols in Wastewater.* Oriental Journal of Chemistry, 2018. **34**(2): p. 631-637.
13. Widsten, P. and A. Kandelbauer, *Laccase applications in the forest products industry: A review.* Enzyme and Microbial Technology, 2008. **42**(4): p. 293-307.
14. Strong, P.J. and H. Claus, *Laccase: A Review of Its Past and Its Future in Bioremediation.* Critical Reviews in Environmental Science and Technology, 2011. **41**(4): p. 373-434.

15. Slagman, S., H. Zuilhof, and M.C.R. Franssen, *Laccase-Mediated Grafting on Biopolymers and Synthetic Polymers: A Critical Review.* Chembiochem, 2018. **19**(4): p. 288-311.
16. Senthivelan, T., J. Kanagaraj, and R.C. Panda, *Recent trends in fungal laccase for various industrial applications: An eco-friendly approach - A review.* Biotechnology and Bioprocess Engineering, 2016. **21**(1): p. 19-38.
17. Rangabhashiyam, S., N. Anu, and N. Selvaraju, *The Significance of Fungal Laccase in Textile Dye Degradation - A Review.* Research Journal of Chemistry and Environment, 2013. **17**(6): p. 88-95.
18. Nasir, M., R. Hashim, O. Sulaiman, N.A. Nordin, J. Lamaming, and M. Asim, *Laccase, an Emerging Tool to Fabricate Green Composites: A Review.* Bioresources, 2015. **10**(3): p. 6262-6284.
19. Liu, H., X. Wu, J. Sun, and S. Chen, *Stimulation of Laccase Biocatalysis in Ionic Liquids: A Review on Recent Progress.* Current Protein & Peptide Science, 2018. **19**(1): p. 100-111.
20. Kudanga, T., G.S. Nyanhongo, G.M. Guebitz, and S. Burton, *Potential applications of laccase-mediated coupling and grafting reactions: a review.* Enzyme and Microbial Technology, 2011. **48**(3): p. 195-208.
21. Bilal, M., T. Rasheed, F. Nabeel, H.M.N. Iqbal, and Y. Zhao, *Hazardous contaminants in the environment and their laccase-assisted degradation - A review.* Journal of Environmental Management, 2019. **234**: p. 253-264.
22. Barrios-Estrada, C., M. de Jesus Rostro-Alanis, B.D. Munoz-Gutierrez, H.M.N. Iqbal, S. Kannan, and R. Parra-Saldivar, *Emergent contaminants: Endocrine disruptors and their laccase-assisted degradation - A review.* Science of The Total Environment, 2018. **612**: p. 1516-1531.
23. Champion, C.I., V.A. Kickhoefer, G. Liu, R.J. Moniz, A.S. Freed, L.L. Bergmann, D. Vaccari, S. Raval-Fernandes, A.M. Chan, L.H. Rome, and K.A. Kelly, *A vault nanoparticle vaccine induces protective mucosal immunity.* PLoS One, 2009. **4**(4): p. e5409.
24. Casanas, A., P. Guerra, I. Fita, and N. Verdaguer, *Vault particles: a new generation of delivery nanodevices.* Current Opinion in Biotechnology, 2012. **23**(6): p. 972-7.
25. Kar, U.K., M.K. Srivastava, A. Andersson, F. Baratelli, M. Huang, V.A. Kickhoefer, S.M. Dubinett, L.H. Rome, and S. Sharma, *Novel CCL21-vault nanocapsule intratumoral delivery inhibits lung cancer growth.* PLoS One, 2011. **6**(5): p. e18758.
26. Lothe, A.G., S.S. Kalra, M. Wang, E.E. Mack, C. Walecka-Hutchison, V.A. Kickhoefer, L.H. Rome, and S. Mahendra, *Vault packaged enzyme mediated degradation of amino-aromatic energetic compounds.* Chemosphere, 2020. **242**: p. 125117.
27. Wang, M., Y. Chen, V.A. Kickhoefer, L.H. Rome, P. Allard, and S. Mahendra, *A Vault-Encapsulated Enzyme Approach for Efficient Degradation and Detoxification of Bisphenol A and Its Analogues.* ACS Sustainable Chemistry & Engineering, 2019. **7**(6): p. 5808-5817.
28. Wang, M., D. Abad, V.A. Kickhoefer, L.H. Rome, and S. Mahendra, *Vault Nanoparticles Packaged with Enzymes as an Efficient Pollutant Biodegradation Technology.* ACS Nano, 2015. **9**(11): p. 10931-40.
29. Tisma, M., P. Znidarsic-Plazl, D. Vasic-Racki, and B. Zelic, *Optimization of laccase production by Trametes versicolor cultivated on industrial waste.* Applied Biochemistry and Biotechnology, 2012. **166**(1): p. 36-46.

30. Robles, A., R. Lucas, G.A. de Cienfuegos, and A. Galvez, *Phenol-oxidase (laccase) activity in strains of the hyphomycete Chalara paradoxa isolated from olive mill wastewater disposal ponds.* Enzyme and Microbial Technology, 2000. **26**(7): p. 484-490.
31. Collins, P.J. and A. Dobson, *Regulation of Laccase Gene Transcription in Trametes versicolor.* Applied and environmental microbiology, 1997. **63**(9): p. 3444-50.
32. Johnson, D.R., P.K. Lee, V.F. Holmes, and L. Alvarez-Cohen, *An internal reference technique for accurately quantifying specific mRNAs by real-time PCR with application to the tceA reductive dehalogenase gene.* Applied and environmental microbiology, 2005. **71**(7): p. 3866-71.
33. Rio, D.C., M. Ares, Jr., G.J. Hannon, and T.W. Nilsen, *Purification of RNA by SDS solubilization and phenol extraction.* Cold Spring Harbor Protocols, 2010. **2010**(6): p. pdb prot5438.
34. Korbie, D.J. and J.S. Mattick, *Touchdown PCR for increased specificity and sensitivity in PCR amplification.* Nature Protocols, 2008. **3**(9): p. 1452-6.
35. Gibson, D.G., L. Young, R.Y. Chuang, J.C. Venter, C.A. Hutchison, 3rd, and H.O. Smith, *Enzymatic assembly of DNA molecules up to several hundred kilobases.* Nature Methods, 2009. **6**(5): p. 343-5.
36. Koutsospyros, A., J. Pavlov, J. Fawcett, D. Strickland, B. Smolinski, and W. Braida, *Degradation of high energetic and insensitive munitions compounds by Fe/Cu bimetal reduction.* Journal of Hazardous Materials, 2012. **219-220**: p. 75-81.
37. Kim, M., S.C. Jee, J.S. Sung, and A.A. Kadam, *Anti-proliferative applications of laccase immobilized on super-magnetic chitosan-functionalized halloysite nanotubes.* International Journal of Biological Macromolecules, 2018. **118**(Pt A): p. 228-237.
38. Kunamneni, A., F.J. Plou, A. Ballesteros, and M. Alcalde, *Laccases and their applications: a patent review.* Recent Patents on Biotechnology, 2008. **2**(1): p. 10-24.
39. Charles Guest, T. and S. Rashid, *Anticancer Laccases: A Review.* Journal of Clinical & Experimental Oncology, 2016. **05**(01).
40. Piscitelli, A., C. Pezzella, P. Giardina, V. Faraco, and S. Giovanni, *Heterologous laccase production and its role in industrial applications.* Bioengineered bugs, 2010. **1**(4): p. 252-62.
41. Ribeiro, L.F., G.P. Furtado, M.R. Lourenzoni, A.J. Costa-Filho, C.R. Santos, S.C. Nogueira, J.A. Betini, L. Polizeli Mde, M.T. Murakami, and R.J. Ward, *Engineering bifunctional laccase-xylanase chimeras for improved catalytic performance.* Journal of Biological Chemistry, 2011. **286**(50): p. 43026-38.
42. Ravalason, H., I. Herpoel-Gimbert, E. Record, F. Bertaud, S. Grisel, S. de Weert, C.A. van den Hondel, M. Asther, M. Petit-Conil, and J.C. Sigoillot, *Fusion of a family 1 carbohydrate binding module of Aspergillus niger to the Pycnoporus cinnabarinus laccase for efficient softwood kraft pulp biobleaching.* Journal of Biotechnology, 2009. **142**(3-4): p. 220-6.
43. Paananen, A., D. Ercili-Cura, M. Saloheimo, R. Lantto, and M.B. Linder, *Directing enzymatic cross-linking activity to the air–water interface by a fusion protein approach.* Soft Matter, 2013. **9**(5): p. 1612-1619.
44. Mate, D.M. and M. Alcalde, *Laccase engineering: from rational design to directed evolution.* Biotechnology Advances, 2015. **33**(1): p. 25-40.

45. Dittmer, N.T., M.J. Gorman, and M.R. Kanost, *Characterization of endogenous and recombinant forms of laccase-2, a multicopper oxidase from the tobacco hornworm, Manduca sexta.* Insect Biochemistry and Molecular Biology, 2009. **39**(9): p. 596-606.
46. Kickhoefer, V.A., A.C. Siva, N.L. Kedersha, E.M. Inman, C. Ruland, M. Streuli, and L.H. Rome, *The 193-kD vault protein, VPARP, is a novel poly(ADP-ribose) polymerase.* Journal of Cell Biology, 1999. **146**(5): p. 917-28.
47. Kickhoefer, V.A., Y. Garcia, Y. Mikyas, E. Johansson, J.C. Zhou, S. Raval-Fernandes, P. Minoofar, J.I. Zink, B. Dunn, P.L. Stewart, and L.H. Rome, *Engineering of vault nanocapsules with enzymatic and fluorescent properties.* Proceedings of the National Academy of Sciences, 2005. **102**(12): p. 4348-52.
48. Rome, L.H. and V.A. Kickhoefer, *Development of the vault particle as a platform technology.* ACS Nano, 2013. **7**(2): p. 889-902.
49. Revankar, M.S. and S.S. Lele, *Increased production of extracellular laccase by the white rot fungus Coriolus versicolor MTCC 138.* World Journal of Microbiology and Biotechnology, 2006. **22**(9): p. 921-926.
50. Piscitelli, A., P. Giardina, V. Lettera, C. Pezzella, G. Sannia, and V. Faraco, *Induction and transcriptional regulation of laccases in fungi.* Current Genomics, 2011. **12**(2): p. 104-12.
51. Prieto, A., M. Moder, R. Rodil, L. Adrian, and E. Marco-Urrea, *Degradation of the antibiotics norfloxacin and ciprofloxacin by a white-rot fungus and identification of degradation products.* Bioresource Technology, 2011. **102**(23): p. 10987-95.
52. Becker, D., S. Varela Della Giustina, S. Rodriguez-Mozaz, R. Schoevaart, D. Barcelo, M. de Cazes, M.P. Belleville, J. Sanchez-Marcano, J. de Gunzburg, O. Couillerot, J. Volker, J. Oehlmann, and M. Wagner, *Removal of antibiotics in wastewater by enzymatic treatment with fungal laccase - Degradation of compounds does not always eliminate toxicity.* Bioresource Technology, 2016. **219**: p. 500-509.
53. Sato, Y., B. Wuli, R. Sederoff, and R. Whetten, *Molecular Cloning and Expression of Eight Laccase cDNAs in Loblolly Pine (Pinus taeda)*.* Journal of Plant Research, 2001. **114**(2): p. 147-155.
54. Kickhoefer, V.A., A.C. Siva, N.L. Kedersha, E.M. Inman, C. Ruland, M. Streuli, and L.H. Rome, *The 193-kD vault protein, VPARP, is a novel poly(ADP-ribose) polymerase.* The Journal of cell biology, 1999. **146**: p. 917-928.
55. Thomas, S., N.D. Maynard, and J. Gill, *DNA library construction using Gibson Assembly®.* Nature Methods, 2015. **12**(11): p. i-ii.
56. Agrawal, K., V. Chaturvedi, and P. Verma, *Fungal laccase discovered but yet undiscovered.* Bioresources and Bioprocessing, 2018. **5**(1).
57. Arregui, L., M. Ayala, X. Gomez-Gil, G. Gutierrez-Soto, C.E. Hernandez-Luna, M. Herrera de Los Santos, L. Levin, A. Rojo-Dominguez, D. Romero-Martinez, M.C.N. Saparrat, M.A. Trujillo-Roldan, and N.A. Valdez-Cruz, *Laccases: structure, function, and potential application in water bioremediation.* Microbial Cell Factories, 2019. **18**(1): p. 200.
58. Gomaa, O.M. and O.A. Momtaz, *Copper induction and differential expression of laccase in Aspergillus flavus.* Brazilian Journal of Microbiology, 2015. **46**(1): p. 285-92.
59. Tessier, D.C., D.Y. Thomas, H.E. Khouri, F. Laliberte, and T. Vernet, *Enhanced secretion from insect cells of a foreign protein fused to the honeybee melittin signal peptide.* Gene, 1991. **98**(2): p. 177-83.

60. Chen, X., J.L. Zaro, and W.C. Shen, *Fusion protein linkers: property, design and functionality.* Advanced Drug Delivery Reviews, 2013. **65**(10): p. 1357-69.
61. Li, E., A. Pedraza, M. Bestagno, S. Mancardi, R. Sanchez, and O. Burrone, *Mammalian cell expression of dimeric small immune proteins (SIP).* Protein Engineering, 1997. **10**(6): p. 731-6.
62. Rice, J.J., A. Schohn, P.H. Bessette, K.T. Boulware, and P.S. Daugherty, *Bacterial display using circularly permuted outer membrane protein OmpX yields high affinity peptide ligands.* Protein Science, 2006. **15**(4): p. 825-36.
63. Gehl, C., D. Kaufholdt, D. Hamisch, R. Bikker, J. Kudla, R.R. Mendel, and R. Hansch, *Quantitative analysis of dynamic protein-protein interactions in planta by a floated-leaf luciferase complementation imaging (FLuCI) assay using binary Gateway vectors.* The Plant Journal, 2011. **67**(3): p. 542-53.
64. Cheung, L.S., M. Kanwar, M. Ostermeier, and K. Konstantopoulos, *A hot-spot motif characterizes the interface between a designed ankyrin-repeat protein and its target ligand.* Biophysical Journal, 2012. **102**(3): p. 407-16.
65. Kickhoefer, V.A., Y. Garcia, Y. Mikyas, E. Johansson, J.C. Zhou, S. Raval-Fernandes, P. Minoofar, J.I. Zink, B. Dunn, P.L. Stewart, and L.H. Rome, *Engineering of vault nanocapsules with enzymatic and fluorescent properties.* Proceedings of the National Academy of Sciences of the United States of America, 2005. **102**(12): p. 4348.
66. Chakraborti, S., T.-Y. Lin, S. Glatt, and J.G. Heddle, *Enzyme encapsulation by protein cages.* RSC Advances, 2020. **10**(22): p. 13293-13301.
67. Wang, M., *Peroxidase Enzymes Packaged in Vaults as an Innovative Bioremediation Technology*. 2015, UCLA.

Chapter 6

Fungal-mediated Degradation of Nitrotriazolone: Implications on Design of Stormwater Biofilters

Abstract

Nitrotriazolone (NTO), a highly water-soluble insensitive munition constituent (MC), can be present in surface runoff in range sites and can pose groundwater risk unless treated using stormwater treatment systems. However, bacterial removal of NTO requires an anaerobic followed by aerobic processes, thereby making it difficult to design a stormwater treatment system where aerobic conditions are generally prevalent. In contrast to bacteria, fungi have the potential to remove munition constituents in aerobic conditions. Yet, the potential of fungi to remove NTO has not been evaluated. Using two species of wood-rotting fungi, *Phanerochaete chrysosporium* and *Trametes versicolor*, we demonstrated that both fungi could remove at least 85% of NTO within 96 h in batch reactors, but the removal processes by both fungi differed. While biosorption contributed to 40% of NTO removal by *P. chrysosporium*, the same process was insignificant when *T. versicolor* was used. By exposing NTO solution to extracellularly secreted ligninolytic enzymes, manganese peroxidase (MnP), and laccase, we found that neither enzyme at an activity of 1 U mL^{-1} catalyzed NTO degradation. However, 1 U mL^{-1} laccase in the presence of 2 mM hydroxybenzotriazole (HBT), a model mediator, degraded more than 90% NTO after 48 h, indicating that a mediator is essential for extracellular degradation of NTO by *T. versicolor*. Overall, the results suggest that a fungal-augmented stormwater treatment system can effectively degrade NTO in aerobic conditions, thereby eliminating the need of maintaining anaerobic conditions in stormwater biofilters.

6.1 Introduction

Nitrotriazolone (NTO) is one of the components of the IMX-101 formulation developed as a substitute to 1,3,5-Trinitro-1,3,5-triazinane or RDX, which could explode spontaneously [1]. Unlike RDX, NTO is highly water-soluble (12000 mg L^{-1}), thereby increasing the risk of the contaminated plume migrating farther from the range sites. At range sites, NTO from scattered explosive residues can dissolve in stormwater runoff and infiltrates through subsurface soil to groundwater, and increase health risk via drinking water wells. NTO exposure could cause testicular toxicity and oligospermia in rats [2, 3]. NTO and its reduced form aminiotriazolone (ATO) can pose ecological risk [4]. Thus, it is critical to design adequate treatment systems to minimize groundwater pollution. Because range sites are large and the runoff from the sites is considered a non-point source, point-source treatment technologies using electrochemical[5], photocatalytic, and advanced oxidation processes [6, 7] can be cost-prohibitive, and designing wastewater treatment plant [8-12] to treat runoff is not practical. Alternatively, nature-based stormwater treatment systems such as biofilters could be used to implement at the range sites.

Biofilters are passive treatment units where stormwater is captured in a depressed area with plants and infiltrates through subsurface soil. The soil is mixed with sand and amendments to increase infiltration and pollutant removal [13]. The filter media adsorb the pollutant and facilitate biodegradation of pollutants by microorganisms including bacteria and fungi [14]. As stormwater is typically saturated with oxygen, the aerobic condition is prevalent in the filter layer [15]. Consequently, biofilters are often ineffective at removing pollutants such as nitrate, which often requires anaerobic conditions [16]. To induce anaerobic conditions, biofilters design is improved by installing a submerged layer with a carbon source such as wood chips [17, 18]. However,

maintaining a submerged layer is challenging at range sites where the condition is typically dry and rainfall events can be sporadic, resulting in ineffective removal of contaminants [16]. Thus, an alternative design that does not require maintaining an anaerobic condition in biofilters should be explored.

Unlike chemical treatment, biodegradation of organic pollutants is inexpensive and is an integral part of biofilter design [19]. NTO is biodegraded by bacterial/mixed cultures derived from contaminated sites and wastewater treatment plants [8-12, 20]. In these systems, bacterial communities first reduce the nitro group in NTO to amino group, forming aminotriazolone (ATO) before aerobic oxidation of ATO. In contrast, fungi can biodegrade other nitroaromatic explosives in aerobic conditions because of their ability to reduce nitro-group inside the cell [21]. For instance, *Phanerochaete chrysosporium* mineralizes dinitrotoluene (DNT) within 24 days [22] starting with the intracellular reduction of DNT to its amino derivatives amino-nitro toluene (ANT) and diaminotoluene (DAT). Similarly, *Trametes versicolor* has also been found to degrade TNT and its derivatives while inducing the production of laccase [23]. After the formation of amino derivatives intracellularly, the fungi produce extracellular ligninolytic enzymes such as manganese peroxidase (MnP) and laccase, which can further oxidize the reduced derivatives of nitro explosive compounds [24, 25]. These wood-rotting fungi can naturally present at high concentrations in biofilters, where woodchips and plant detritus are used as amendments [26]. Thus, further study is needed to examine the potential of fungi to remove NTO from contaminated runoff.

One previous study showed that three fungi *Beauveria bassiana*, *Rhizopus arrhizus*, and *Cylindrocarpon radicicola* could reduce NTO [8], but the relative importance of processes by which fungi can remove NTO is unclear. Fungi can remove organic contaminants including nitroaromatic compounds by any combination of three broadly categorized processes: biosorption,

extracellular enzymic degradation, and internal (co)metabolism [27]. In the late 1990s, fungi were thoroughly investigated for biosorption of heavy metals, such as zinc, nickel, cadmium, and chromium [28]. Biosorption is facilitated by the high surface area, a high density of functionalized proteins, polysaccharides, and chitin on fungal cell walls. Previously, *P. chrysosporium* was also demonstrated to sorb DNT and ANT and has been reported to remove phenolic compounds and dyes through biosorption [29, 30]. Fungal enzymes can catalyze the degradation of a wide gamut of recalcitrant compounds including dyes, polycyclic aromatic hydrocarbons (PAHs) munition constituents, pharmaceutical, and personal care products, xenobiotics, endocrine disruptors, and olefin plastics. The versatility of fungal biodegradation is partly due to the non-substrate-specific extracellularly secreted ligninolytic enzymes (oxidoreductases and peroxidases). The ligninolytic enzymes assist fungi in mining nutrients by decomposing complex natural polymers. The mixed-function cell-bound/intracellular enzymes such as P450s and reductases further enhance their (co)metabolic capabilities. The cell-bound nitro reductases are suspected to reduce the nitro-aromatic explosives to their amino derivatives thereby making them easily oxidizable by microorganisms [27, 31-33]. Moreover, for certain enzymes including laccase, the catalytic spectrum can be extended by the use of mediator compounds [34]. All these processes could help NTO removal by fungi. However, the relative importance of biosorption and enzyme degradation on NTO removal is not clear. The understanding relative importance of these processes would help design stormwater treatment systems to efficiently remove legacy and novel munition constituents from runoff from range sites.

Enzymatic bioremediation can overcome the dependence of the treatment processes on the microorganism and alleviate the concerns of introducing pathogens in the environment. However, the applicability of the biocatalysts in environmental bioremediation is limited by their short active

life in reaction environments. As a result, a large number of enzymes may be required to achieve the desired results. To prevent enzymes from inactivation and enhance the efficiency of degradation at low enzyme activities, vault nanoparticles can be used to package enzymes. Previously, manganese peroxidase (MnP) packaged in vaults was demonstrated to have increased degradation efficiency and active life for the degradation of nitroaromatic explosives and phenolic/biphenolic compounds [29, 35-37]. Thus, further study is needed to examine the potential of the vault-packaged enzyme on the degradation of NTO, so that they can be potentially used to deliver an enzyme to hotspots in the contaminated subsurface.

This study aims to examine the biodegradation of NTO by two white wood-rotting fungi, *P. chrysosporium,* and *T. versicolor*, to identify the role of ligninolytic enzymes involved, and to quantify the relative importance of biosorption and enzymic degradation on the removal of NTO. We hypothesize that fungi can degrade NTO via ligninolytic enzymes, laccase or MnP, secreted by *T. versicolor* or *P. chrysosporium,* respectively. To test the hypothesis, we conducted a series of batch experiments and quantify the contribution of each process on NTO removal.

6.2 Materials and Methods

6.2.1 Chemicals

The NTO used in this study was obtained from AccuStandard Inc. (New Haven, CT). The chemicals used in the culture medium preparation were obtained from Sigma-Aldrich (St. Louis, MO) or Thermo Fisher Scientific (Waltham, MA) with ACS grade or higher purity (> 98%).

6.2.2 Degradation of NTO by Fungal Cultures.

P. chrysosporium and *T. versicolor* were cultivated and maintained on appropriate agar plates as mentioned elsewhere [38, 39] for 10 days at 37 °C and 30 °C, respectively. The mycelium from the agar plates was transferred by scraping using a sterile inoculation loop and suspended in the appropriate culture medium to make a stock spore suspension. The suspension was filtered through a 0.45 µm mixed cellulose ester (MCE) membrane to separate fungal mycelium from spores. Post-filtration, the spore count was performed using a hemocytometer [40]. The biodegradation of NTO by *P. chrysosporium* was tested in a modified Kirk medium [22] to induce the production of MnP. Similarly, the NTO degradation by *T. versicolor* was tested in the Tisma medium to produce laccase [38]. The culture medium (25 mL) was inoculated to a spore count of 10^4 spores mL^{-1} using the appropriate filtered spore suspension. The experiments were performed in 125 mL baffled flasks equipped with 0.2 µm air filters and incubated for 4 days at 30 °C and 150 rpm. The desired concentration of nitrotriazolone (NTO) was added after 4 days of fungal growth, and 200 µL samples were collected every 24 h. The 0 h samples were collected immediately after the addition of the substrate on day 4 of fungal growth. The collected samples were quenched by adding an equal volume of methanol. The samples were then filtered through a 0.2 µm nylon filter to remove fungal biomass and spores. The killed control was prepared by autoclaving the fungal culture before the addition of NTO to test for adsorption of NTO on fungal biomass. Abiotic controls with no fungal inoculation were prepared to account for matrix effects. All reactions were kept in similar conditions and in triplicate to ensure the statistical significance of the data.

6.2.3 Degradation of NTO by Purified MnP, Laccase, and Vault-packaged Laccase

To evaluate the role of extracellularly secreted ligninolytic enzymes in the degradation of NTO, *P. chrysosporium* was cultivated in the Kirk medium without NTO to produce MnP. The culture supernatant containing the secreted MnP was filtered through glass wool when the maximum enzyme activity was observed, whereas purified laccase from *T. versicolor* was purchased from Sigma Aldrich (St. Louis, MO). 200 µL enzymatic degradation reactions, with purified enzymes, were performed in 2 mL, 96-well polypropylene plate sealed with a silicone mat. Enzyme-free controls and mediator controls were also kept in identical conditions to account for the removal of NTO by interaction with the mediator compounds. For MnP catalyzed reactions, the reaction mixture consisted of 1 $U.mL^{-1}$ MnP in 50 mM malonate buffer (pH 4.5), 0.1 mM $MnCl_2$, 10 $mg.L^{-1}$ NTO, and the reaction was initiated by adding 0.2 mM H_2O_2. Similarly, for the laccase and laccase mediator system, the reaction mixture consisted of 1 $U.mL^{-1}$ laccase in 0.1 M phosphate buffer (pH 6) and 10 (or 320) $mg.L^{-1}$ NTO. To evaluate the effect of the mediator, 2 mM HBT was used as a model mediator in a parallel reactor setup. The laccase catalyzed reactions were initiated by adding laccase and were kept open to air for 15 min every day to provide the oxygen required for catalysis. An identical setup was used to evaluate the potential of the vault-packaged laccase (VMLDGI) for degradation of NTO with 2 mM HBT used as a laccase mediator. The activity of laccase or VMLDGI in these experiments was 5 $U.L^{-1}$, and the empty vaults condition was used as a control experiment to account for the removal by the vault particles without laccase. All reactions were performed in triplicates to ensure statistical significance of the results and incubated in shaking incubators at 150 rpm at 30 °C. At the desired time point, the reactions were quenched by adding an equal volume of methanol to denature the enzymes.

6.2.4 Enzyme Activity Assay

To measure MnP activity [22, 41], 0.125 mL sample was mixed with 0.025 mL 20 mM $MnCl_2$ and 0.25 mL 50 mM malonate buffer (pH 4.5). After absorbance has been zeroed, 0.025 mL 4 mM H_2O_2 was added to start the assay, and change in absorbance was monitored at 270 nm (ξ = 11,590 $L.mol^{-1}.cm^{-1}$) over 1 minute. To measure laccase activity [42], 0.1 mL ABTS (20 mM) was mixed with 0.880 mL 100 mM phosphate buffer (pH 6). After absorbance was zeroed, 0.02 mL was enzyme solution was added to start the assay, and absorbance change measured every 2 seconds over 1 minute (ξ = 36000 $L.mol^{-1}.cm^{-1}$). Enzyme activity was calculated using equation 6.1

$$\text{Activity}(U.L^{-1}) = \frac{\Delta A \times V_T \times 10^6}{\xi \times b \times V_{en}} \qquad (6.1)$$

where, U L^{-1} units of enzyme activity per L, ΔA is the rate of absorbance change (min^{-1}), V_T is the total volume (L), ξ is molar extinction coefficient in ($L\ mol^{-1}\ cm^{-1}$), V_{en} is enzyme volume (L), and b is path length (cm). One unit of enzyme activity is defined as the amount of enzyme needed to produce 1 µmol of product per minute. All enzyme activity assays were measured in a NanoDrop 2000c spectrophotometer.

6.2.5 Analytical Methods

All collected samples were stored at -20 °C till needed for analysis on HPLC-UV. All samples were filtered using 0.2 µm nylon filters before injection in the HPLC. The analysis was performed on HP 1050 HPLC equipped with Hypercarb column 150 mm x 4.6 mm x 5 µm. NTO was detected at 312 nm and was eluted after 9.5 minutes at 1 mL min^{-1} using 65% H_2O and 15%

acetonitrile with 0.1% trifluoroacetic acid (TFA) according to the previously published method [7].

6.3 Results

6.3.1 Degradation of NTO by Fungal Cultures

Both fungi significantly removed (≥ 70%) NTO by the end of 4 days of incubation (Figure 6.1). *P. chrysosporium* decreased the NTO concentration from 10 to 1 $mg.L^{-1}$, while the killed *P. chrysosporium* control removed 40% of NTO (Figure 6.1a). Similarly, *T. versicolor* removed around 70% of NTO in 4 days, whereas killed *T. versicolor* control did not remove NTO significantly (Figure 6.1b). The degradation of NTO by *T. versicolor* was also tested at 5 initial NTO concentrations ranging between 10 $mg.L^{-1}$ to 370 $mg.L^{-1}$ (Figure 6.2), and the observed degradation rates were fitted to the Michaelis-Menton kinetics model. The V_{max} was estimated to be 3.5 $mg.L^{-1}.h^{-1}$ and K_m was estimated to be 15.7 $mg.L^{-1}$. The degradation of NTO appeared to follow zero-order degradation kinetics for the tested concentration range. The decay rates of the negative control were subtracted from the degradation rates of NTO degradation to calculate the observed degradation rates (V).

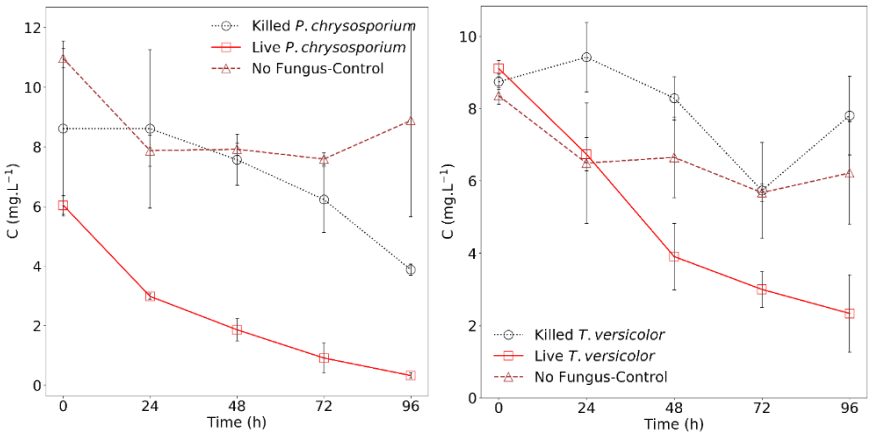

Figure 6.1: Degradation of NTO by (a) *Phanerochaete chrysosporium* and (b) *Trametes versicolor*. Biosorption of NTO was significant on *P. chrysosporium* biomass but insignificant on *T. versicolor* biomass. **Live *P. chrysosporium*** - reactors with live *P. chrysosporium*. **Killed *P. chrysosporium*** - reactors containing autoclaved fungal biomass to estimate biosorption. **No Fungus-Control** - abiotic control reactors with no fungus. **Live *T. versicolor*** - reactors with live *T. versicolor*. **Killed *T. versicolor*** - reactors containing autoclaved fungal biomass to estimate biosorption. Error bars represent experimental triplicates.

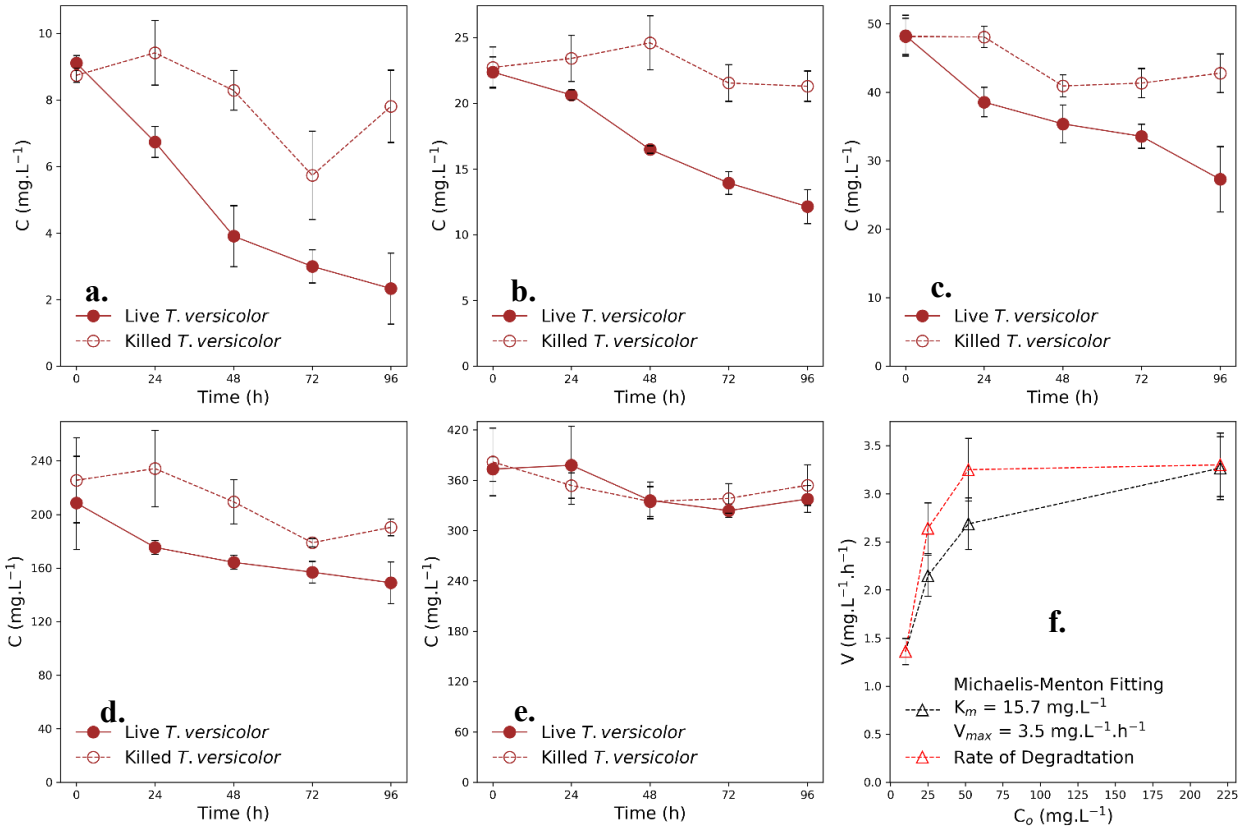

Figure 6.2: Degradation of NTO by *T. versicolor* was tested at (a) 10 mg.L^{-1}, (b) 20 mg.L^{-1}, (c) 50 mg L^{-1}, (d) 220 mg.L^{-1}, and (e) 370 mg.L^{-1}. (f) the observed degradation rates were modeled using the Michaelis-Menton Kinetics K_m and V_{max} were estimated to be 15.7 mg.L^{-1} and 3.5 mg.L^{-1}.h^{-1}, respectively. Note different ranges in the y-axis indicating a difference in NTO concentration. **Live *T. versicolor*** - reactors with live *T. versicolor*. **Killed *T. versicolor*** - reactors containing autoclaved fungal biomass to estimate biosorption. Error bars represent experimental triplicates

6.3.2 Degradation of NTO by Purified MnP and Laccase

Approximately 90% NTO was removed by 1 U.mL^{-1} laccase and 2 mM HBT in 48 h (Figure 6.3a). Approximately 40% NTO was removed when 320 mg L^{-1} NTO was incubated with

1 U.mL^{-1} laccase and 2 mM HBT in 96 h (Figure C 1). However, no significant removal was observed over 96 h when NTO was incubated with only *T. versicolor* derived laccase or with *P. chrysosporium* derived MnP (Figure 6.3b). Similar results were observed for the degradation of amino-nitro toluene (ANT) by laccase and laccase HBT system (Figure C 2).

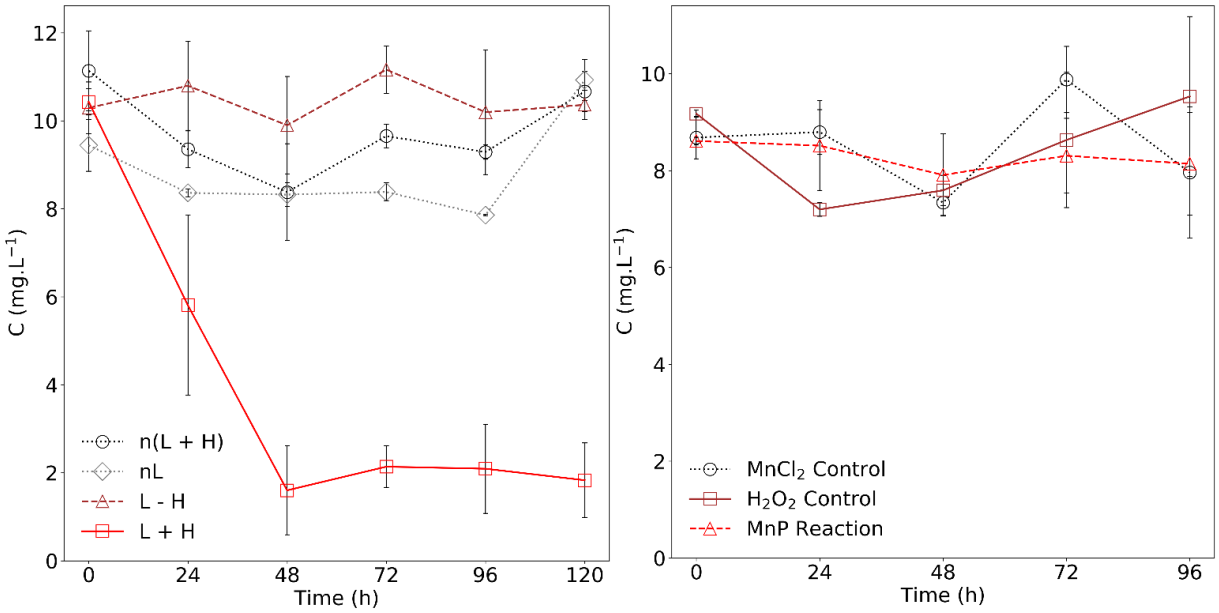

Figure 6.3: Degradation of NTO by ligninolytic enzymes. (a) Laccase (from *T. versicolor*) + 2mM HBT and (b) Incubation of NTO with MnP from *P. chrysosporium*. **n(L + H)** – reactors with NTO with no laccase and HBT. **nL** – reactors with NTO and 2 mM HBT without laccase. **L - H** – reactors with NTO and 1 U mL^{-1} laccase HBT. **L + H** – reactors with NTO, 1 U mL^{-1} laccase, and 2 mM HBT. **MnCl$_2$ control** – reactors with MnCl$_2$ without MnP and H$_2$O$_2$. **H$_2$O$_2$ control** – reactors with 1 U mL^{-1} MnP and MnCl$_2$ without H$_2$O$_2$. **MnP Reaction** – reactors with 1 U mL^{-1} MnP, H$_2$O$_2$, and MnCl$_2$. Error bars represent experimental triplicates

6.4 Discussion

6.4.1 Aerobic degradation of NTO by *Phanerochaete chrysosporium* and *Trametes versicolor*.

Our results demonstrate that both *P. chrysosporium* and *T. versicolor* could degrade NTO in aerobic conditions, and *T. versicolor* was less efficient than *P. chrysosporium* in removing NTO. However, about 40% NTO was removed by the killed *P. chrysosporium* suggesting significant biosorption of NTO on fungal biomass (Figure 6.1). NTO removal by killed *T. versicolor* was insignificant suggesting minimal biosorption on *T. versicolor* biomass. The percentage removal of NTO by *T. versicolor* decreased with an increase in initial NTO concentration. For instance, no degradation was observed when 370 $mg.L^{-1}$ of NTO was incubated with *T. versicolor,* which can be attributed to the increased toxicity leading to the inactivation or growth inhibition of *T. versicolor* (Figure 6.2). The elevated levels of nitroaromatic compounds such as NTO may inhibit the production of an enzyme while also being toxic to microorganisms causing inactivation and loss of functionality – both factors that could explain the lower degradation rates at high NTO levels.

The bacterial degradation of NTO has been studied in recent publications [9-11, 43], while this study is the first instance of fungal degradation of NTO in aerobic conditions. The bacterial degradation of NTO requires anaerobic conditions for the initial conversion of NTO to its reduced amine derivative, ATO, followed by aerobic conditions for further degradation [8, 10]. Moreover, the NTO degradation pathway was published independently, by Campion et al.[43] and Krzmarzick et al. [9] suggest that the reduction of NTO to ATO is the essential first step for microbial biodegradation of NTO, while the transformation of NTO in mammals is performed by

P450s. Similarly, our results of NTO degradation by fungi in aerobic conditions suggest a degradation mechanism involving cell-bound/intracellular enzymes. The reduction of the nitro group by cell-bound fungal P450s and/or aromatic nitro reductases is reported in literature for the degradation of munitions by fungi [27, 28, 44]. Moreover, the substitution of the nitrogen salts in the fungal (*T. versicolor*) culture by NTO as a substitute nitrogen source demonstrated no degradation of NTO, bolstering the involvement of intracellular enzymes in degradation of NTO by fungi. The zero-order degradation kinetics followed by *T. versicolor* (Figure 6.2) demonstrates that intracellular mechanisms are involved in the transformation of NTO and/or the transport rate of NTO from the culture into the cells control the rates of degradation.

Fungi are known to (co)metabolize organic pollutants and some aliphatic or aromatic compounds with the help of a range of extracellular oxidoreductases with relatively nonspecific activities [27]. Previously, *P. chrysosporium* has been demonstrated to convert the nitro explosives to their amino derivatives intracellularly, followed by further degradation of metabolites by ligninolytic enzymes such as MnP [29, 45]. Similarly, *T. versicolor* was also demonstrated to degrade TNT with increased laccase production during the degradation [23]. In this study, the fungal cultivation cultures were selected to provide nutrient limiting conditions and induce the production of MnP and laccase. The ligninolytic enzymes are secreted by the fungi in the exponential growth phase. Therefore, MnP activity in modified Kirk medium peaks at around 5-6 days [22], and laccase activity in Tisma medium is typically maximum at the 6^{th} day of growth [38]. Supplementing NTO on day 4 of culture growth ensured optimal fungal growth and production of desired enzymes by avoiding any NTO induced toxicity during the initial growth phase [23]. The synergy between bacteria and fungi is necessary for most environments to promote suitable microbiome growth and plant health. The incorporation of the fungi in the bacterial

microcosm could effectively mineralize the munitions in an aerobic environment by overcoming the limitations of anaerobic nitro-reduction by bacteria or the use of physicochemical treatment processes.

6.4.2 Degradation of NTO by Purified MnP and Laccase

The ligninolytic enzymes secreted by fungi can be used to degrade NTO, but the degradation depends on the type of enzyme. Our results showed that reactors containing laccase without mediator could not degrade the NTO, but the co-existence of laccase and a mediator degraded NTO in 48 h. In the laccase HBT system, the degradation appeared to flatline after 48 h plausibly, due to the exhaustion of HBT or inactivation of laccase (Figure 6.3). The degradation of NTO by purified enzymes was observed for only the laccase HBT system and not by laccase or MnP, supplementing our observation of the involvement of intracellular enzymes in fungal degradation of NTO. Various mediator compounds such as hydroxybenzotriazole (HBT), 2,2'-azino-bis(3-ethylbenzothiazoline-6-sulfonic acid) (ABTS) and 2,2,6,6-tetramethyl-1-piperidinyloxyl (TEMPO), N-hydroxyphthalimide (HPI), violuric acid (VA), and N-hydroxyacetanilide (HAA), and other inexpensive humic substances found in the natural organic matter are well known to widen laccase's catalytic range [46]. Although our results informed the biodegradation of NTO, the production of ATO during the fungal degradation of NTO and its subsequent enzymatic or fungal degradation remains to be tested. However, laccase, MnP, and fungi have been previously shown to mineralize azo, azoxy, acylated, and phenolic derivatives of legacy munition constituents indicating potential mineralization of ATO and other intermediates [23, 24, 28, 47-49].

6.5 Conclusions and Environmental Implications

This study showed fungal-mediated removal of NTO under aerobic conditions and provided insights on the removal mechanisms, particularly the relative importance of intra/extracellular enzymes and biosorption processes. Specifically, the data demonstrate that both *P. chrysosporium* and *T. versicolor* removed at least 70% NTO in aerobic conditions over 96 h, but 40% removal by *P. chrysosporium* was due to biosorption. However, biosorption on *T. versicolor* biomass was negligible. The degradation of NTO by both fungi was mainly catalyzed by intracellular enzymes as MnP and laccase alone did not remove NTO. The presence of the mediator (HBT) was essential for NTO removal by laccase which removed >80% NTO (10 $mg.L^{-1}$) in 48 h. The USA produced 3130 metric tons of nitroamine explosives in 2006, and in 2002, 6.2 metric tons of explosive compounds were released in the US soils from explosive testing sites [50]. Although limited toxicological evidence is available for NTO, most munition constituents are toxic to humans and wildlife alike. The high solubility and toxicity of NTO increase contaminant transport and poses a threat to the environment. Bioremediation can be a cost-effective treatment strategy for munitions contaminated waters and has been demonstrated to remediate legacy munitions [51]. Limited literary evidence exists in support of pure culture-mediated biodegradation of NTO, especially with fungi. This study extends strategies for biodegradation of munition constituents to the realm of fungi with two wood-rotting fungi, *P. chrysosporium*, and *T. versicolor*, degrading NTO aerobically in contrast to sequential anaerobic-aerobic bacterial degradation demonstrated by previous studies. The biodegradation of NTO by fungal cells and fungi secreted ligninolytic enzymes can be a greener alternative to energy intensive nonbiological advance oxidation processes. Furthermore, a fungi-augmented biofilter could be effective to treat the watershed runoff contaminated by NTO because of its aerobic degradation. However, further

studies are necessary to identify the conditions (e.g., hydraulic retention time, geo-media type, and biofilter design) where the implementation of fungi to biofilters would make NTO removal a feasible technology for stormwater treatment.

Appendix C

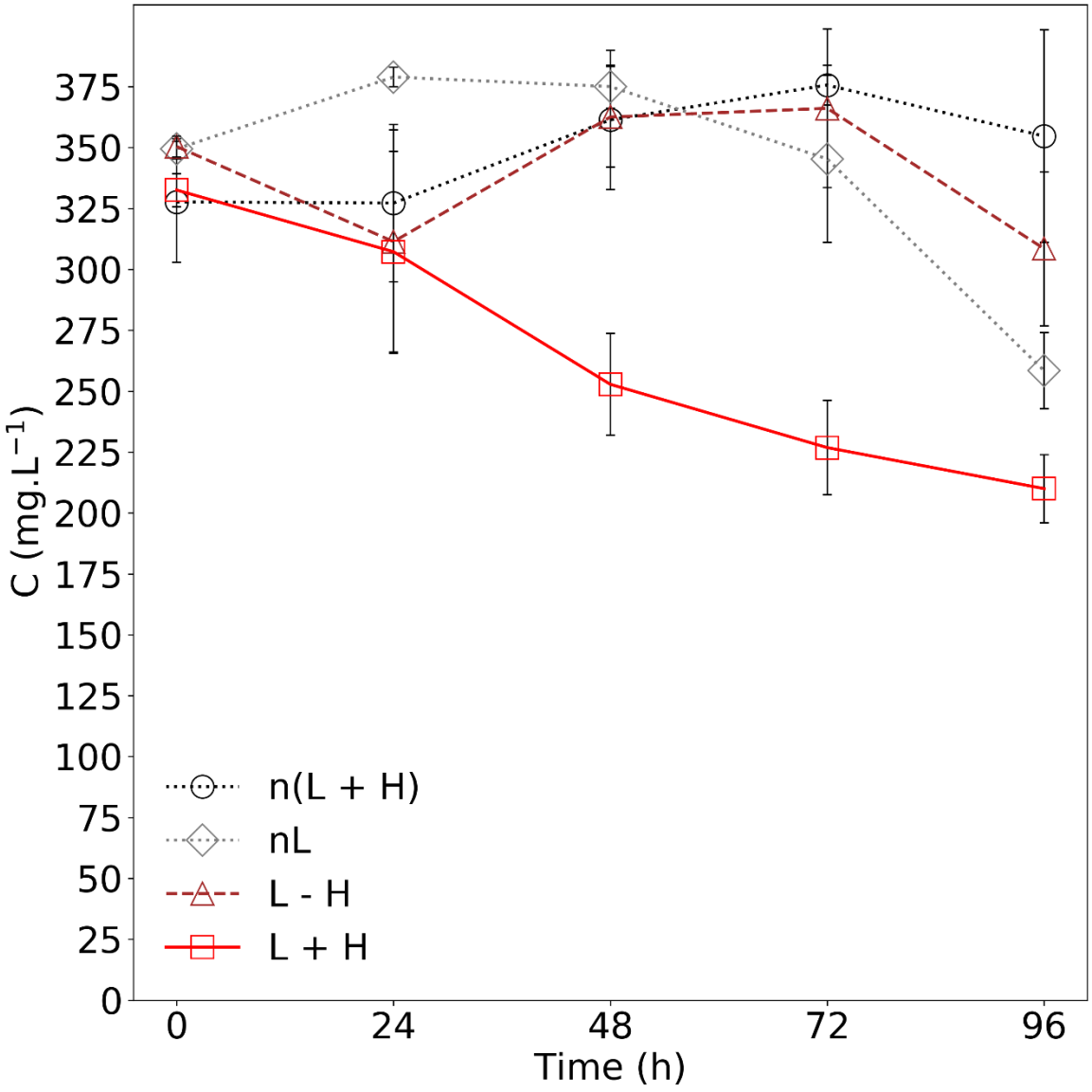

Figure C 1: Degradation of 320 mg.L^{-1} NTO by extracellularly secreted *T. versicolor* laccase (1 U.mL^{-1}) and HBT (2 mM). n(L + H) - Negative laccase and HBT control. nL - Negative laccase control. L - H - reactors with laccase only. L + H - reactors with 1 U.mL^{-1} laccase and 2 mM HBT.

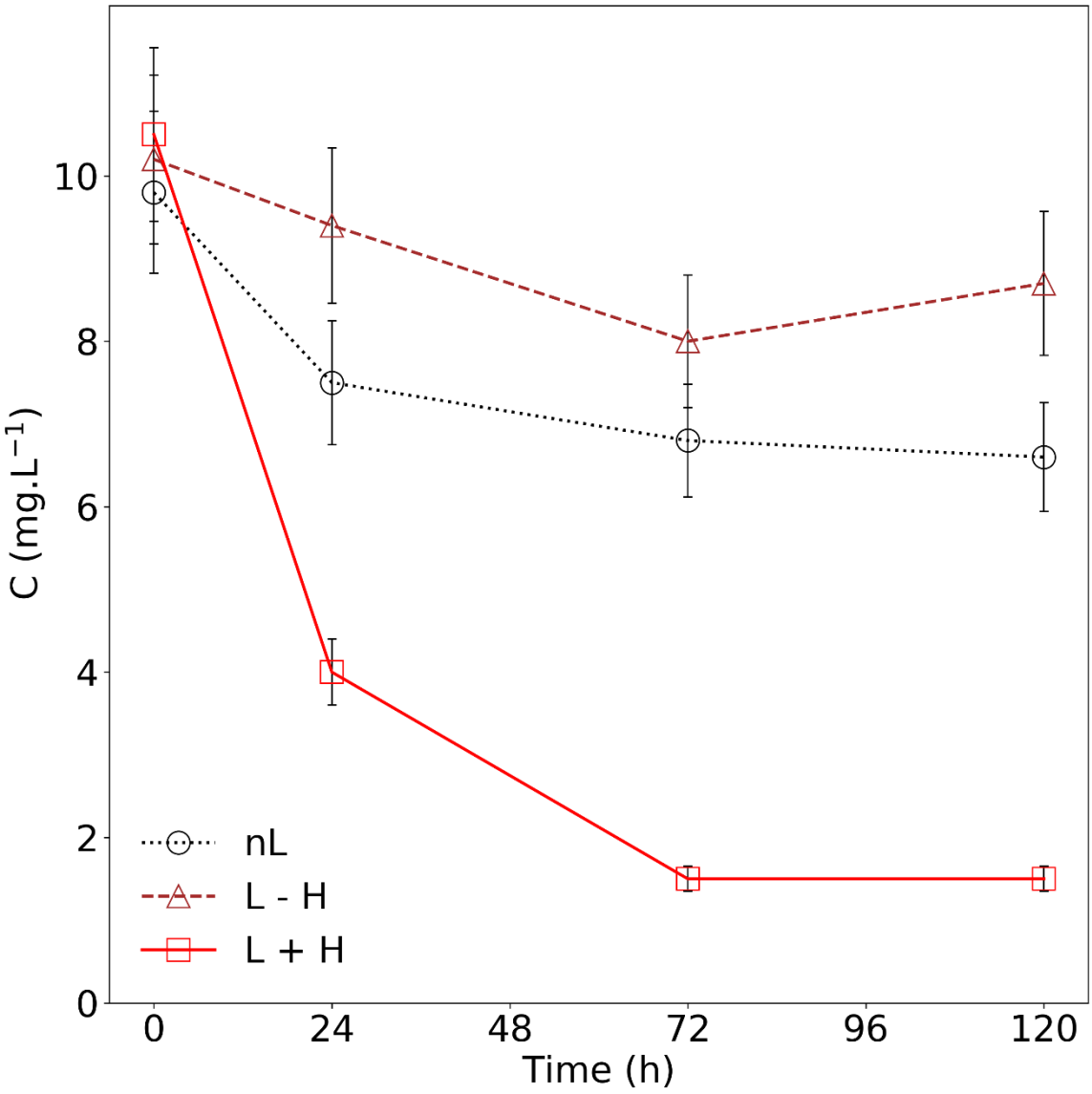

Figure C 2 Degradation of 10 mg.L^{-1} amino-nitro toluene (ANT) by extracellularly secreted *T. versicolor* laccase (1 U.mL^{-1}) and HBT (2 mM). n(L + H) - Negative laccase and HBT control. nL - Negative laccase control. L - H - reactors with laccase only. L + H - reactors with 1 U.mL^{-1} laccase and 2 mM HBT.

References

1. Lotufo, G.R., G. Rosen, W. Wild, and G. Carton. *Summary Review of the Aquatic Toxicology of Munitions Constituents, ERDC/EL TR-13-8*. 2013.
2. Lent, E.M., L.C. Crouse, A.M. Jackovitz, E.E. Carroll, and M.S. Johnson, *An extended one-generation reproductive toxicity test of 1,2,4-Triazol-5-one (NTO) in rats.* Journal of Toxicology and Environmental Health, Part A, 2016. **79**(24): p. 1159-1178.
3. Lent, E.M., A.M. Narizzano, K.A. Koistinen, and M.S. Johnson, *Chronic oral toxicity of 3-nitro-1,2,4-triazol-5-one (NTO) in rats.* Regulatory Toxicology and Pharmacology, 2020. **112**: p. 104609.
4. Madeira, C.L., J.A. Field, M.T. Simonich, R.L. Tanguay, J. Chorover, and R. Sierra-Alvarez, *Ecotoxicity of the insensitive munitions compound 3-nitro-1,2,4-triazol-5-one (NTO) and its reduced metabolite 3-amino-1,2,4-triazol-5-one (ATO).* Journal of Hazardous Materials, 2018. **343**: p. 340-346.
5. Cronin, M.P., A.I. Day, and L. Wallace, *Electrochemical remediation produces a new high-nitrogen compound from NTO wastewaters.* Journal of Hazardous Materials, 2007. **149**(2): p. 527-31.
6. Le Campion, L., C. Giannotti, and J. Ouazzani, *Photocatalytic degradation of 5-nitro-1,2,4-triazol-3-one NTO in aqueous suspension of TiO2. Comparison with Fenton oxidation.* Chemosphere, 1999. **38**(7): p. 1561-70.
7. Koutsospyros, A., J. Pavlov, J. Fawcett, D. Strickland, B. Smolinski, and W. Braida, *Degradation of high energetic and insensitive munitions compounds by Fe/Cu bimetal reduction.* Journal of Hazardous Materials, 2012. **219-220**: p. 75-81.
8. Le Campion, L., A. Vandais, and J. Ouazzani, *Microbial remediation of NTO in aqueous industrial wastes.* FEMS Microbiol LettFEMS Microbiology Letters, 1999. **176**(1): p. 197-203.
9. Krzmarzick, M.J., R. Khatiwada, C.I. Olivares, L. Abrell, R. Sierra-Alvarez, J. Chorover, and J.A. Field, *Biotransformation and Degradation of the Insensitive Munitions Compound, 3-Nitro-1,2,4-triazol-5-one, by Soil Bacterial Communities.* Environmental Science & Technology, 2015. **49**(9): p. 5681-8.
10. Madeira, C.L., S.A. Speet, C.A. Nieto, L. Abrell, J. Chorover, R. Sierra-Alvarez, and J.A. Field, *Sequential anaerobic-aerobic biodegradation of emerging insensitive munitions compound 3-nitro-1,2,4-triazol-5-one (NTO).* Chemosphere, 2017. **167**: p. 478-484.
11. Eberly, J.O., K.J. Indest, D.E. Hancock, C.M. Jung, and F.H. Crocker, *Metagenomic analysis of denitrifying wastewater enrichment cultures able to transform the explosive, 3-nitro-1,2,4-triazol-5-one (NTO).* Journal of Industrial Microbiology and Biotechnology, 2016. **43**(6): p. 795-805.
12. Wallace, L., M.P. Cronin, A.I. Day, and D.P. Buck, *Electrochemical method applicable to treatment of wastewater from nitrotriazolone production.* Environmental Science & Technology, 2009. **43**(6): p. 1993-8.
13. Grebel, J.E., S.K. Mohanty, A.A. Torkelson, A.B. Boehm, C.P. Higgins, R.M. Maxwell, K.L. Nelson, and D.L. Sedlak, *Engineered Infiltration Systems for Urban Stormwater Reclamation.* Environmental Engineering Science, 2013. **30**(8): p. 437-454.

14. Tirpak, R.A., A.N. Afrooz, R.J. Winston, R. Valenca, K. Schiff, and S.K. Mohanty, *Conventional and amended bioretention soil media for targeted pollutant treatment: A critical review to guide the state of the practice.* Water Research, 2021. **189**: p. 116648.
15. Payne, E.G.I., T.D. Fletcher, P.L.M. Cook, A. Deletic, and B.E. Hatt, *Processes and Drivers of Nitrogen Removal in Stormwater Biofiltration.* Critical Reviews in Environmental Science and Technology, 2014. **44**(7): p. 796-846.
16. Valenca, R., H. Le, Y. Zu, T.M. Dittrich, D.C.W. Tsang, R. Datta, D. Sarkar, and S.K. Mohanty, *Nitrate removal uncertainty in stormwater control measures: Is the design or climate a culprit?* Water Research, 2021. **190**: p. 116781.
17. Kim, H., E.A. Seagren, and A.P. Davis, *Engineered Bioretention for Removal of Nitrate from Stormwater Runoff.* Water Environment Research, 2003. **75**(4): p. 355-367.
18. Berger, A.W., R. Valenca, Y. Miao, S. Ravi, S. Mahendra, and S.K. Mohanty, *Biochar increases nitrate removal capacity of woodchip biofilters during high-intensity rainfall.* Water Research, 2019. **165**: p. 115008.
19. LeFevre, G.H., R.M. Hozalski, and P.J. Novak, *The role of biodegradation in limiting the accumulation of petroleum hydrocarbons in raingarden soils.* Water Research, 2012. **46**(20): p. 6753-6762.
20. Madeira, C.L., O. Menezes, D. Park, K.V. Jog, J.K. Hatt, S. Gavazza, M.J. Krzmarzick, R. Sierra-Alvarez, J.C. Spain, K.T. Konstantinidis, and J.A. Field, *Bacteria Make a Living Breathing the Nitroheterocyclic Insensitive Munitions Compound 3-Nitro-1,2,4-triazol-5-one (NTO).* Environmental Science & Technology, 2021. **55**(9): p. 5806-5814.
21. Aburto-Medina, A., M. Taha, E. Shahsavari, and A.S. Ball, *Degradation of the Dinitrotoluene Isomers 2,4- and 2,6-DNT: Appraising the Role of Microorganisms*, in *Enhancing Cleanup of Environmental Pollutants*. 2017, Springer International Publishing: Cham. p. 5-20.
22. Wariishi, H., K. Valli, and M.H. Gold, *Manganese(II) oxidation by manganese peroxidase from the basidiomycete Phanerochaete chrysosporium. Kinetic mechanism and role of chelators.* Journal of Biological Chemistry, 1992. **267**(33): p. 23688-95.
23. Cheong, S., S. Yeo, H.G. Song, and H.T. Choi, *Determination of laccase gene expression during degradation of 2,4,6-trinitrotoluene and its catabolic intermediates in Trametes versicolor.* Microbiological Research, 2006. **161**(4): p. 316-20.
24. Dietrich, D., W.J. Hickey, and R. Lamar, *Degradation of 4,4'-dichlorobiphenyl, 3,3',4,4'-tetrachlorobiphenyl, and 2,2',4,4',5,5'-hexachlorobiphenyl by the white rot fungus Phanerochaete chrysosporium.* Applied and environmental microbiology, 1995. **61**(11): p. 3904-9.
25. Lamar, R.T., *The role of fungal lignin-degrading enzymes in xenobiotic degradation.* Current Opinion in Biotechnology, 1992. **3**(3): p. 261-266.
26. Wolfand, J.M., G.H. LeFevre, and R.G. Luthy, *Metabolization and degradation kinetics of the urban-use pesticide fipronil by white rot fungus Trametes versicolor.* Environmental Science Processes & Impacts, 2016. **18**(10): p. 1256-1265.
27. Harms, H., D. Schlosser, and L.Y. Wick, *Untapped potential: exploiting fungi in bioremediation of hazardous chemicals.* Nature Reviews Microbiology, 2011. **9**(3): p. 177-92.
28. Arora, D.K., *FungaI BiotechnoIogy in Agricultural, Food, and Environmental AppIications*. 2003: CRC Press. 471.

29. Lothe, A.G., S.S. Kalra, M. Wang, E.E. Mack, C. Walecka-Hutchison, V.A. Kickhoefer, L.H. Rome, and S. Mahendra, *Vault packaged enzyme mediated degradation of amino-aromatic energetic compounds.* Chemosphere, 2020. **242**: p. 125117.
30. Sintakindi, A. and B. Ankamwar, *Fungal biosorption as an alternative for the treatment of dyes in waste waters: a review.* Environmental Technology Reviews, 2021. **10**(1): p. 26-43.
31. Bilal, M., T. Rasheed, F. Nabeel, H.M.N. Iqbal, and Y. Zhao, *Hazardous contaminants in the environment and their laccase-assisted degradation - A review.* Journal of Environmental Management, 2019. **234**: p. 253-264.
32. Kunamneni, A., F.J. Plou, A. Ballesteros, and M. Alcalde, *Laccases and their applications: a patent review.* Recent Patents on Biotechnology, 2008. **2**(1): p. 10-24.
33. Alexander, D.G.S., D. Annadurai, A. Bajpai, H.G. Brink, M.A.A. Coetzee, R. Dhanker, R. Dubey, A. Dwivedi, D. Gupta, Hemansi, T. Hussain, J. Immanuel Suresh, A. Jasu, N. Jennifer Michellin Kiruba, A. Jillani, B.N. Johri, A. Joseph Thatheyus, S. Joshi, A. Judith, S.S. Kamble, I. Kamika, T.K. Kasonga, H. Khatoon, V. Kumar, R. Kumaran, D. Lahiri, M.M. M. de Wet, S. Mishra, M.N.B. Momba, M. Nag, M. Naseem, R. Paliwal, S. Parmar, R. Raghuwanshi, J.P.N. Rai, T. Ramesh, D. Ramya, B. Ranawat, S.K. Rath, D. Rathore, R.R. Ray, J.K. Saini, F. Shah, M.P. Shah, A.K. Shankhwar, H. Sharma, P. Sharma, P.K. Srivastava, A. Sundaramanickam, M. Thangaraj, A.J. Thatheyus, P. Tyagi, S. Uniyal, J.O. Unuofin, M. Verma, P.C. Verma, and R. Yamunadevi, *List of Contributors*, in *Fungi Bio-Prospects in Sustainable Agriculture, Environment and Nano-technology*, V.K. Sharma, M.P. Shah, S. Parmar, and A. Kumar, Editors. 2021, Academic Press. p. xv-xviii.
34. Morozova, O.V., G.P. Shumakovich, S.V. Shleev, and Y.I. Yaropolov, *Laccase-mediator systems and their applications: A review.* Applied Biochemistry and Microbiology, 2007. **43**(5): p. 523-535.
35. Wang, M., D. Abad, V.A. Kickhoefer, L.H. Rome, and S. Mahendra, *Vault Nanoparticles Packaged with Enzymes as an Efficient Pollutant Biodegradation Technology.* ACS Nano, 2015. **9**(11): p. 10931-40.
36. Wang, M., *Peroxidase Enzymes Packaged in Vaults as an Innovative Bioremediation Technology*. 2015, UCLA.
37. Wang, M., Y. Chen, V.A. Kickhoefer, L.H. Rome, P. Allard, and S. Mahendra, *A Vault-Encapsulated Enzyme Approach for Efficient Degradation and Detoxification of Bisphenol A and Its Analogues.* ACS Sustainable Chemistry & Engineering, 2019. **7**(6): p. 5808-5817.
38. Tisma, M., P. Znidarsic-Plazl, D. Vasic-Racki, and B. Zelic, *Optimization of laccase production by Trametes versicolor cultivated on industrial waste.* Applied Biochemistry and Biotechnology, 2012. **166**(1): p. 36-46.
39. Tien, M. and T.K.K. Kirk, *Lignin peroxidase of Phanerochaete chrysosporium.* Methods in Enzymology, 1988. **161**: p. 238-249.
40. Sambrook, J. and D.W. Russell, *Estimation of cell number by hemocytometry counting.* CSH Protoc, 2006. **2006**(1): p. pdb.prot4454.
41. Petruccioli, M., M. Frasconi, D. Quaratino, S. Covino, G. Favero, F. Mazzei, F. Federici, and A. D'Annibale, *Kinetic and redox properties of MnP II, a major manganese peroxidase isoenzyme from Panus tigrinus CBS 577.79.* Journal of Biological Inorganic Chemistry, 2009. **14**(8): p. 1153-63.

42. Robles, A., R. Lucas, G.A. de Cienfuegos, and A. Galvez, *Phenol-oxidase (laccase) activity in strains of the hyphomycete Chalara paradoxa isolated from olive mill wastewater disposal ponds.* Enzyme and Microbial Technology, 2000. **26**(7): p. 484-490.
43. Le Campion, L., M. Delaforge, J.P. Noel, and J. Ouazzani, *Metabolism of 14C-labelled 5-nitro-1,2,4-triazol-3-one (NTO): comparison between rat liver microsomes and bacterial metabolic pathways.* Journal of Molecular Catalysis B: Enzymatic, 1998. **5**(1): p. 395-402.
44. Rylott, E.L., R.G. Jackson, J. Edwards, G.L. Womack, H.M.B. Seth-Smith, D.A. Rathbone, S.E. Strand, and N.C. Bruce, *An explosive-degrading cytochrome P450 activity and its targeted application for the phytoremediation of RDX.* Nature Biotechnology, 2006. **24**(2): p. 216-219.
45. Valli, K., B.J. Brock, D.K. Joshi, and M.H. Gold, *Degradation of 2,4-dinitrotoluene by the lignin-degrading fungus Phanerochaete chrysosporium.* Applied and environmental microbiology, 1992. **58**(1): p. 221-8.
46. Lloret, L., G. Eibes, G. Feijoo, M.T. Moreira, and J.M. Lema, *Degradation of estrogens by laccase from Myceliophthora thermophila in fed-batch and enzymatic membrane reactors.* Journal of Hazardous Materials, 2012. **213-214**: p. 175-83.
47. Tseng, N.S.-l., *Feasibility of Biodegradation of Polyfluoroalkyl and Perfluoroalkyl Substances.* 2012.
48. Riva, S., *Laccases: blue enzymes for green chemistry.* Trends Biotechnol, 2006. **24**(5): p. 219-26.
49. Fernando, T., J.A. Bumpus, and S.D. Aust, *Biodegradation of TNT (2,4,6-trinitrotoluene) by Phanerochaete chrysosporium.* Applied and environmental microbiology, 1990. **56**(6): p. 1666-71.
50. Mahbub, P. and P.N. Nesterenko, *Application of photo degradation for remediation of cyclic nitramine and nitroaromatic explosives.* RSC Advances, 2016. **6**(81): p. 77603-77621.
51. Niedźwiecka, J.B. and K.T. Finneran, *Combined biological and abiotic reactions with iron and Fe(iii)-reducing microorganisms for remediation of explosives and insensitive munitions (IM).* Environmental Science: Water Research & Technology, 2015. **1**(1): p. 34-39.

Chapter 7

Conclusions and Perspectives

7.1 Summary

This research methodically evaluated the destruction of per- and polyfluoroalkyl substances (PFASs) using high-frequency ultrasound and demonstrated its applicability at the field scale. The biodegradation of PFASs and nitrotriazolone (NTO) by wood-rotting fungi and their extracellular ligninolytic enzymes was also investigated while probing the capability of vault packaging to enhance the application of *Trametes versicolor* derived laccase in reaction environments.

The second chapter provided a brief review of the current literature on per- and polyfluoroalkyl substances (PFASs) in treated wastewater and surface runoff around the world with respect to water recycling and reuse. The current regulations around PFASs, the toxicity of PFASs, and the limitations of novel technologies for the destruction of PFASs are also discussed along with a review of current analytical methods for the detection of PFASs. This work reveals that the conventional water treatment plants are ineffective in the removal of PFASs and that the fate and transport of PFASs in the wastewater treatment plant and the environment are highly dependent on their absorption on solids/biomass. The short-chain and novel PFASs are also increasingly detected around the world due to the shift in usage from legacy PFASs, like PFOS and PFOA, to the novel PFASs. The review suggests a critical need for destructive treatment technologies for the remediation of water recycling and reuse source streams.

The third chapter described efficient defluorination of legacy and novel PFASs in high and low TDS groundwaters, complex mixtures, AFFF, and high concentration IDW samples. High-frequency ultrasound was able to demonstrate stoichiometric defluorination of HFPO-DA (GenX), novel PFASs, and zwitterionic 6:2 FTAB. Compared to deionized water, the acoustic treatment of

24Mix of PFASs showed 30% - 60% higher degradation rates for PFSAs and short-chained compounds (C < 8) observed in low TDS groundwater compared to 50% lower degradation rates in high salinity groundwater. However, significant PFASs degradation (> 97%) was observed in both, deionized water, and low TDS groundwater, while the high TDS groundwater and its constituents were demonstrated to inhibit the degradation of PFASs. The work also demonstrated that a high concentration of dissolved solids in the treatment matrix can lower the degradation kinetics of PFASs by lowering the surface tension, increasing hydrophobic properties, and enhancing the transfer of PFASs to the bulk aqueous-gas interface. Similarly, comparing the rates observed for the treatment of 24Mix in deionized water, the degradation rates for the treatment of AFFF in deionized water were 40% - 60% higher for PFSAs and 10% lower for most PFCAs with > 97% degradation of most PFASs. The operating condition of the reactor was also optimized for better degradation of PFASs. Closed system operation of the reactor increased the availability of fluorocarbon intermediates, and therefore demonstrated significantly higher removal rates across all matrices as compared to the open system operation. Furthermore, the results demonstrate that degradation rates are higher for the operation of the reactor at a lower treatment volume due to the diminished intensity and density of transient cavitation events with increasing distance from the source of ultrasound. PFASs in high TDS IDW were mineralized in a closed system demonstrating mineralization of 89.4 mg of identified PFAS mass using only 76 $kWh.g^{-1}$ without the generation of any disinfection byproducts or short-chain intermediates. This work suggests that ultrasonic treatment of the impacted waters by defluorination of PFASs is energetically viable and favorable for large-scale application.

The fourth chapter described the acoustic treatment of AFFF impacted groundwater at a fire training site in California. This study is the first report of field-scale demonstration of

ultrasonic treatment technology for the removal of PFASs. For all tested conditions and 8 h of sonication, no intermediate PFAS species were detected along with no increase in the chlorate and perchlorate concentrations from the background levels. The observed energy consumption was similar to other destructive technologies for PFAS removal. Only 699.43 ± 3.3 $kWh.m^{-3}.order^{-1}$ (E_{EO}), was consumed at 305 $W.L^{-1}$ to deliver the fastest removal rates and lowest final concentrations (< 70 ng/L for 11 PFASs and 7 PFAS-TOPs). Similarly, only 599.51 ± 52.5 $kWh.m^{-3}.order^{-1}$ (E_{EO}) was consumed for maximum mass removal of 19.82 ± 2.32 mg (122 $W.L^{-1}$). The cost of energy consumed for the ultrasonic removal of PFASs during an eight-hour operation was only $3.14. Overall, the field-scale reactor was able to demonstrate 50% - 99% removal of 15 PFASs and 11 PFAS-TOPs depending on the power density. Furthermore, 10% - 40% higher degradation rates were observed at a bulk temperature of 25 °C than at 15 °C depending on the type of PFAS. Similar to the observations in Chapter 3, for the same chain length, the sulfonates had lower degradation rates, and for the same headgroup, the longer-chain compounds were degraded faster. The degradation rates were also influenced by the salinity of the groundwater affecting the surface activity of PFASs. The ultrasonic treatment of PFASs presents an exciting frontier for the remediation of PFAS impacted water without producing toxic and unwanted byproducts.

The fifth chapter described the identification of laccase isozymes produced by *Trametes versicolor*, packaging of enzyme in vault nanoparticles, and the applicability of vault packaged laccase in environmental remediation. The packaging of laccase in vault nanoparticles was attempted to address the problem of instability of natural enzymes in environmental and reaction conditions as a major hindrance in the application of enzymatic bioremediation. The sequence standardization of laccase isozyme and their detection in the Tisma medium revealed simultaneous

production of three isozymes by *T. versicolor*. The fusion of INT domain with Laccase cDNA (MLDGI), extracted from *T. versicolor* producing laccase, required incorporating a flexible linker to retain the activity of laccase. Furthermore, the addition of 500 µM $CuCl_2$ after 48 h of culturing in the Sf9 culture expressing MLDGI produced the maximum activity which was enhanced after packaging in vaults. The vault-packaged laccase (VMLDGI) demonstrated activity with substrates like ABTS, guaiacol, catechol, 1-naphthol, 2,6- dichlorohydroquinone and was able to retain nearly 100% activity after 7 days of incubation at 30 ºC with 1-hydroxybenzotriazole. The VMLDGI also demonstrated degradation of 60% NTO at 5 $U.L^{-1}$ in 96 h with 2mM HBT. This work presents the packaging of the largest protein (90 kDa) to date in recombinant vault nanoparticles while retaining its catalytic activity and preliminary evidence of its applicability in bioremediation.

The sixth chapter described the biodegradation of nitrotriazolone (NTO) as model insensitive munition by wood-rotting fungi, *Trametes versicolor,* and *Phanerochaete chrysosporium,* and their ligninolytic enzymes, laccase and manganese peroxidase (MnP). NTO poses a threat to the environment due to the increased transport caused by its high water solubility. The results demonstrate that both fungi were able to remove at least 70% NTO in aerobic conditions over 96 h. The removal by *P. chrysosporium* included biosorption (40%), while no biosorption on *T. versicolor* biomass was observed. The investigation revealed that the degradation of NTO by fungi was primarily intracellular. MnP did not catalyze the removal of NTO while laccase in the presence of the mediator (HBT) was able to remove >80% NTO in 48h. The extensive testing of munitions at training sites releases a large number of munition constituents therefore, the stormwater from explosive testing sites is bound to contain munition constituents. This work presents proof of concept for incorporation of fungi in biofilters for the treatment of

watershed runoff contaminated with munition constituents, like NTO, owing to the aerobic treatment conditions.

Overall, this research presents high-frequency ultrasound as an effective and energetically viable treatment technology for PFAS-impacted water without the production of toxic intermediates or byproducts. Moreover, mycoremediation using wood-rotting fungi, and immobilized ligninolytic enzymes is presented as a potentially economical long-term treatment option for contaminants like munition constituents, which are commonly found at munitions testing and fire training sites around the world. This work highlights the importance of using multiple technologies for the treatment of waters containing various contaminants and utilizing both physicochemical and biological treatment strategies for comprehensive environmental remediation.

7.2 Significance of the Research

This research presents the following insights into the removal of PFASs and nitrotriazolone using ultrasound and fungi-mediated biodegradation.

1. PFASs are expected to impact water recycling and reuse sources as they are detected in treated wastewater and surface runoff throughout the world and traditional treatment plants are inefficient in removing PFASs. Therefore, new PFAS destructive technologies are needed to ensure effective remediation.
2. High-frequency ultrasound is capable of mineralizing PFASs in various matrices, including, AFFF-impacted high and low salinity groundwater, and highly concentrated investigation

derived waste, without the production of short-chain intermediates or other disinfection byproducts like chlorate and perchlorate.

3. The majority of cavitation events occur closer to the ultrasonic source, therefore, an ultrasonic reactor for remediation of PFAS-impacted water should be designed to minimize the height of the water column from the source of ultrasound and the reactor should be operated in closed system conditions to allow for retention of reactive species from the gaseous headspace.
4. The ultrasonic treatment of PFASs is more energy efficient for the treatment of high PFAS load matrices compared to the treatment of diluted single compound solutions as ultrasound can non selectively treat PFAS mixtures, at the same supplied power, irrespective of the relative concentration of PFAS species.
5. Fungi, *Trametes versicolor,* and *Phanerochaete chrysosporium,* and the laccase mediator system can biodegrade nitrotriazolone (NTO) in aerobic conditions overcoming the limitation of sequential anaerobic and aerobic environment for degradation of NTO by bacteria. This makes fungi ideal candidates for the treatment of stormwater runoff from active munition testing sites, in cohorts with bacteria or independently.
6. Vault packaging can locally concentrate and enhance the active life of laccase allowing it to catalyze substrates at very low activity. To ensure enzyme activity in vault-packaged laccase, the supplementation of copper in the expression culture and a long flexible linker separating laccase from the INT domain is critical.
7. Five different laccase isozymes are produced by *Trametes versicolor* out of which at least three isozymes are produced in Tisma medium spiked with guaiacol.

7.3 Future Research Directions and Recommendations

7.3.1 In-situ and Wide Spectrum Applicability of Ultrasound

This work developed the ultrasonic treatment reactor for the defluorination of PFAS-impacted water and demonstrated its applicability in the ex-situ treatment of groundwater. However, another logical way forward would be to consider implementing in-situ ultrasonic treatment for destruction of PFASs and other contaminants. Evolving this technology for in-situ applications will further reduce the costs associated with the pumping of water. One potential method of deploying ultrasound for the treatment of groundwater would be designing probes with the cylindrical assembly of the transducer elements that can be lowered into the water table, permeable reactive barrier, or a groundwater reservoir/well with desired hydraulic retention time for treatment of PFASs. The design of these wells/reservoirs should be such that the thickness of water in contact with the source of ultrasound can be minimized, and the well headspace gas can be recirculated into the treatment matrix.

Although current work only demonstrates the use of ultrasound to treat PFASs in water, evidence for the treatment of various other contaminants including biological entities in liquid or solid matrices also exists. Therefore, testing the ultrasonic treatment of emerging contaminants like insensitive munitions, in mixtures or otherwise, wastewater, ion exchange, and reverse osmosis brines, contaminated soils, and cleaning of materials contaminated with antibiotic-resistant strains of bacteria, fungi, and novel viruses like Ebola, HIV, and SARS-CoV-2 is also warranted. Furthermore, due to the ability of ultrasound to degrade a multitude of contaminants

non-electively, when adopted at an industrial scale, the energy efficiency of ultrasonic treatment of water is expected to increase making it more practical.

The results of this work show that matrix constituents can have synergic or detrimental effects on ultrasonic degradation kinetics. However, deeper investigation to understand the mechanisms involved in affecting the degradation kinetics, effects of cations on ultrasonic degradation, and discovery of synergic matrix constituents are required to improve the performance of the technology. Combining ultrasonic treatment with other advanced reductive treatment technologies like persulphate or UV catalysis may also improve the overall degradation efficiency. Further research into increasing the number of transient cavitation events capable of developing the desired high pressure and temperature conditions while reducing the input power is required. Additionally, exploration of different piezoelectric materials and waveforms improving the efficiency of converting electrical energy to acoustic energy is also needed to reduce the energy demands associated with ultrasonic treatment technology.

7.3.2 Biodegradation of Emerging Contaminants by Fungi

While the results of this research provide preliminary evidence for the degradation of NTO by ligninolytic fungi and enzymes, it has also revealed the need for better-cultivating methods that can ensure the long-term growth of fungi and production of ligninolytic enzymes. The biodegradation of some xenobiotics, such as PFASs, requires long treatment times which can be as high as a few months, therefore a constant supply of nutrients is needed to sustain fungal activity and growth allowing the complete potential for degradation. Liquid culture for biodegradation experiments can only support the growing conditions for a few days after which the nutrients are depleted, leading to stagnant conditions in the culture. Therefore, the nutrients should be

replenished periodically either by adding reagents as a dry powder or the fungi should be cultivated using a solid-state fermentation or submerged fermentation technique containing lignocellulosic substrates like barley barn. Solid-state fermenters with lignocellulosic support as growth substrates can replicate the natural conditions required to sustain the growth of filamentous fungi while ensuring high production of ligninolytic enzymes for longer durations. Furthermore, these fermenters can be more practical for the in-situ application of fungal bioremediation technology. Additional research to discern the applicability of solid-state fermenters for bioremediation should be conducted.

The degradation of NTO by fungi should be further studied to discern the mechanisms involved in the removal of NTO, especially with regard to the production of amino derivatives during NTO degradation. Consequently, the investigation into the degradation of ATO by fungi or ligninolytic enzymes and the eventual mineralization of NTO is needed. Additional research on the design of a stormwater biofilter containing fungi for the degradation of munition constituents in stormwater runoff is needed. The selection of a biofilter media containing lignocellulosic substrates is critical for growth of fungi, production of ligninolytic enzymes, and ensuring optimal remediation conditions.

The amount of laccase required for degradation of contaminants can be high due to the inactivation of enzymes in reaction conditions. Although the vault packaging of laccase explored in this work demonstrated improved stability at low activity in reaction with NTO, further investigation into the stability of vault packaged laccase in various environmental buffers is needed. Moreover, improving the packaging efficiency of laccase into vaults can also affect its stability due to the large size of MLDGI (≈90 kDa). Further studies on the degradation of other

contaminants comparing the performance of vault-packaged laccase with natural laccase are also warranted.